INCLUDING DISPERSION IN AN EQUATION OF STATE COMPOSITIONAL SIMULATOR

BY

HIDEAKI TAKEDA, B.S.P.E.

THESIS

Presented to the Faculty of the Graduate School of

The University of Texas at Austin

in Partial Fulfillment

of the Requirements

for the Degree of

MASTER OF SCIENCE IN ENGINEERING

THE UNIVERSITY OF TEXAS AT AUSTIN

December, 1985

INCLUDING DISPERSION IN AN EQUATION OF STATE COMPOSITIONAL SIMULATOR

APPROVED:

_____

_____

TO

H. K.

ACKNOWLEDGEMENTS

I would like to express my sincere appreciation to my supervising proffessors, Dr. Larry W. Lake and Dr. Kamy Sepehrnoori, for their persistent guidance and valuable comments through this study.

I also acknowledge Kent Thele who originally coded this simulator and enabled me to extend it.

Finally, I thank Teikoku Oil Co., Ltd. (TOC) Japan who gave me an opportunity to complete this work, and especially my colleagues in Reservoir and Production Engineering Department in TOC for their encouragement during this study.

Hideaki Takeda
The University of Texas at Austin
Austin, Texas
September 5, 1985

ABSTRACT

One of the state-of-the-art, equation of state, compositional simulators, the Young and Stephenson formulation, was improved to model physical dispersion as the first step of a series of modifications.

The physical dispersion term was implemented as generally as possible since it was treated explicitly.

Numerical dispersion is usually at least an order of magnitude larger than physical dispersion and masks its real effect on an EOR process. Hence, to reduce numerical dispersion, two versions of two-point upstream weighting and Chaudhari's technique were tested and compared.

Through several test cases, Chaudhari's technique was discarded due to its inability to model small physical dispersion.

Using two-point upstream weighting, various application runs, including 1-D, 2-D areal, and 2-D cross-sectional geometries, were made to investigate the effect of longitudinal and transverse dispersion on a miscible displacement process.

TABLE OF CONTENTS

LIST OF TABLES

LIST OF FIGURES

CHAPTER I

INTRODUCTION

There are two aspects in the development and improvement of a reservoir simulator. They are:

1. How accurately the complicated physical phenomena can be described in a mathematical model, and
2. How fast and efficiently the stated mathematical problems (equations) can be solved numerically.

Usually, these are not compatible, and the pursuits of one feature may be based on some expense of another feature.

The conventional black oil simulator has already found some kind of a meeting ground; however, the advance of enhanced oil and gas recovery methods have been gradually but intensively requiring more generalized mathematical models. This is because they must be able to describe more universal, hence more complex, physical phenomena such as non-isothermal flow, chemical reactions, and more realistic phase behavior.

To satisfy these demands, considering the second aspect at the same time, more sophisticated formulations are needed, and a significant amount of innovation has been done especially on compositional simulation.

Thele [T1] summarized these histories and made a comparison of the latest three formulations at that time. The formulations were by Coats (C) [C9], Nghiem, Fong, and Aziz (NFA) [N2], and Young and Stephenson (YS) [Y5]. The Peng-Robinson equation of state [P1] was used for all three formulations ; however the YS formulation was designed to easily accomodate much simpler fluid property correlations than a cubic equation of state. Thele's comparison was mainly focused on the second aspect, namely computer memory requirements, accuracy of solution, and computation times. And he concluded that the YS formulation was overall the best.

In this study, the YS formulation was modified to be able to model physical dispersion as one of the first aspect. And this was the main objective of this study. The physical dispersion term was treated explicitly and modeled in as general a form as possible.

To achieve this purpose, the largest obstacle was numerical dispsersion which is an essential nature of numerical simulation. Various attempts [C4, C5, E1, F1, J1, L5, L6, L7, L8] have been made to reduce numerical dispersion ; however, it is still considered an active research topic. Thele tested two-point upstream weighting on composition, and reported good results. Here, this method was extended and accomplished to all transmissibility terms and densities. And Chaudhari's technique was also implemented. These schemes were selected because of their simplicity to be

easily accomodated to an existing simulator.

Summarizing the scope of this work:

1. Implement physical dispersion term.
2. Test numerical dispersion reduction schemes.
3. Investigate the effect of dispersion on various types of displacement process (immiscible, multiple-contact miscible, first-contact miscible), for several kind of solvent injection schemes (continuous, simultaneous injection of water, slug), and for different geometries (1-D, 2-D areal, and 2-D cross-sectional).

Chapter II presents a brief review of the YS formulation. A detailed description of the modifications is given in Chapter III. Three classes of test run results are described in Chapter IV. Cahpter V gives the results of three more classes of runs. These six classes of runs are :

Class-1	1-D tracer runs.
Class-2	1-D two-phase runs.
Class-3	2-D areal first-contact miscible runs.
Class-4	1-D slim tube runs (mainly focused on minimum miscibility pressure, MMP).
Class-5	2-D areal multiple-contact miscible runs.
Class-6	2-D cross-sectional multiple-contact

miscible runs.

Finally, conclusions and recommendations for further work are presented in Chapter VI.

CHAPTER II

BRIEF REVIEW OF THE YS FORMULATION

This chapter presents a mathematical model, the assumptions, and a solution outline of the YS formulation in a compact form followed by miscellaneous correlations used in this study. During the description, the excellent features of the YS formulation will be mentioned ; they explain the reason for the selection of this formulation to be improved. The original paper [Y5] or Thele's thesis [T1] should be consulted for more details.

2.1 Mathematical Model and Assumptions

A fairly general expression for the mass conservation of component i in porous media was given by Lake et al. [L2] as follows :

$$\partial W_i/\partial t + \vec{\nabla}\vec{N}_i = R_i \qquad (2.1\text{-}1)$$

,where

Accumulation Term ;

$$\partial W_i/\partial t = \partial/\partial t\,[\phi\Sigma_j \rho_j S_j \omega_{ij} + (1-\phi)\rho_s \omega_{is}] \qquad (j = 1...N_p) \qquad (2.1\text{-}2)$$

Flux Term ;

$$\vec{\nabla}\vec{N}_i = \vec{\nabla}\Sigma_j(\rho_j\omega_{ij}\vec{u}_j - \phi\rho_j S_j\bar{\bar{K}}_{ij}\vec{\nabla}\omega_{ij}) \qquad (j = 1...N_p) \qquad (2.1\text{-}3)$$

Source Term ;

$$R_i = \phi\Sigma_j S_j r_{ij} + (1-\phi)r_{is} + q_i/V_b \quad (j = 1...N_p) \qquad (2.1\text{-}4)$$

Here,

1. Isothermal process.

was assumed. In addition to this, the original YS formulation assumes,

2. No adsorption .
3. No reaction .
4. No physical dispersion .

Then, Eqs. 2.1-1 --- 2.1-4 may be reduced to :

$$\partial/\partial t\,\{\phi\Sigma_j(\rho_j S_j\omega_{ij})\} + \vec{\nabla}\{\Sigma_j(\rho_j\omega_{ij}\vec{u}_j)\} - q_i/V_b = 0 \qquad (j = 1...N_p) \qquad (2.1\text{-}5)$$

Further assuming,

5. Only two hydrocarbon phases (oil and gas) exist .
6. No hydrocarbon solubility in the water phase .

7. No water solubility in the hydrocarbon phase .

8. Local thermodynamic equilibrium is obtained instantaneously .

and using molar balance instead of mass balance, the basic equations to be solved in the YS formulation are listed below :

Hydrocarbon component balance (number of equations = N_c)

$$\partial/\partial t \{\phi(x_i\xi_o S_o + y_i\xi_g S_g)\} + \vec{\nabla}(x_i\xi_o\vec{u}_o + y_i\xi_g\vec{u}_g) - q_i/V_b = 0$$

(units of q_i was changed to moles/time) (2.1-6)

Water balance (number of equations = 1)

$$\partial/\partial t (\phi\xi_w S_w) + \vec{\nabla}(\xi_w\vec{u}_w) - q_w/V_b = 0$$

(units of q_w was changed to moles/time) (2.1-7)

Thermodynamic phase equilibrium (number of equations = N_c)

$$f_{oi} - f_{gi} = 0 \qquad (2.1\text{-}8)$$

Saturation constraint (number of equations = 1)

$$1 - S_o - S_g - S_w = 0 \qquad (2.1\text{-}9)$$

Composition constraints (number of equations = 2)

$$1 - \Sigma_i x_i = 0 \qquad (i = 1...N_c) \qquad (2.1\text{-}10)$$

$$1 - \Sigma_i y_i = 0 \qquad (i = 1...N_C) \qquad (2.1\text{-}11)$$

There are $(2N_C + 4)$ equations for a grid block which contains $(2N_C + 4)$ unknowns, P, S_o, S_g, S_w, $x_i\,(N_C)$, and $y_i\,(N_C)$. To solve these, the following relationships and assumptions are also required.

$$z_i = L\,x_i + V\,y_i \qquad (2.1\text{-}12)$$

$$L = 1\text{-}V \qquad (2.1\text{-}13)$$

$$V = V(S_o, S_g, \xi_o, \xi_g) \qquad (2.1\text{-}14)$$

$$f_{ji} = f_{ji}(P, Z_j, x_{ji}, j = o \text{ or } g, i = 1...N_C) \qquad (2.1\text{-}15)$$

$$Z_j = Z_j(P, x_{ji}, j = o \text{ or } , i = 1...N_C) \qquad (2.1\text{-}16)$$

,where $x_{ji} = x_i\,(j=o)$ or $y_i\,(j=g)$, and Z_j is a compressibility factor of phase j.

$$\xi_j = \xi_j(P, Z_j, x_{ji}, j = o \text{ or } g, i = 1...N_C) \qquad (2.1\text{-}17)$$

$$\xi_w = \xi_w(P) \qquad (2.1\text{-}18)$$

We also assume that

9. Darcy's law applies, and the permeability tensor is orthogonal and aligned with the coordinate system.

$$\vec{u}_j = -(k_{rj}/\mu_j) \cdot \overline{k} \cdot \vec{\nabla}\Phi_j \qquad (j = o, g, w) \qquad (2.1\text{-}19)$$

$$\mu_j = \mu_j(P,\ \xi_j,\ x_{ji},\ j = o \text{ or } g,\ i = 1...N_c) \qquad (2.1\text{-}20)$$

$$\mu_w = \text{constant (input)} \qquad (2.1\text{-}21)$$

$$k_{rj} = k_{rj}(S_j,\ \sigma,\ x_{ji},\ j = o \text{ or } g,\ i = 1...N_c) \qquad (2.1\text{-}22)$$

$$k_{rw} = k_{rw}(S_w) \qquad (2.1\text{-}23)$$

$$\vec{\nabla}\Phi_j = \vec{\nabla}P_j - \gamma_j\vec{\nabla}D \qquad (2.1\text{-}24)$$

$$P_o = P_g - P_{cog} \qquad (2.1\text{-}25)$$

$$P_w = P_o - P_{cwo} \qquad (2.1\text{-}26)$$

$$P_{cog} = P_{cog}(S_g,\ \sigma,\ x_i,\ y_i,\ i = 1...N_c) \qquad (2.1\text{-}27)$$

$$P_{cwo} = P_{cwo}(S_w) \qquad (2.1\text{-}28)$$

$$\sigma = \sigma(\xi_o,\ \xi_g,\ x_i,\ y_i,\ i = 1...N_c) \qquad (2.1\text{-}29)$$

$$\phi = \phi(P) \qquad (2.1\text{-}30)$$

2.2 Solution Outline

Eqs. 2.1-6 --- 2.1-11 in conjunction with Eqs. 2.1-12 --- 2.1-30 must be solved for every grid block at each time step. Interblock relationships were described by Darcy's law in molar balance equations (2.1-6, 2.1-7),and they must be discretized, using a numerical method (for instance, five-point or nine-point finite difference, or finite elements). An ordinary five-point finite difference was used in this study.

Young and Stephenson used the Newton-Raphson scheme to solve these strongly non-linear equations. They treated the saturation- and concentration-dependent terms explicitly, while pressure was evaluated implicitly, as in the so-called IMPES formulation. The primary variables were carefully chosen and equations were ordered in such a way that the Jacobian matrix has as few elements in the lower triangle as possible. The matrix equation for a three hydrocarbon components system is shown in Fig. 2.2-1 for illustration. Here, new variables are introduced ; they are defined as :

$$F = \xi_o S_o + \xi_g S_g \qquad (2.2\text{-}1)$$

$$W = \xi_w S_w \qquad (2.2\text{-}2)$$

Instead of N_c hydrocarbon component balances, (N_c-1)

hydrocarbon component balances (the heaviest component was omitted) and an overall hydrocarbon balance were used. The overall hydrocarbon balance equation may be obtained by summing up N_c component balance equations :

$$\partial/\partial t\,(\phi F) + \vec{\nabla}(\xi_o \vec{u}_o + \xi_g \vec{u}_g) - q_h/V_b = 0 \qquad (2.2\text{-}3)$$

The fugacity constraints Eq. 2.1-8 are scaled by L to prevent forming a ill-conditioned matrix.

$$L\cdot(f_{oi} - f_{gi}) = 0 \qquad (i = 1...N_c) \quad (2.2\text{-}4)$$

In Fig. 2.2-1, all submatrices are square of order N_b, and all subvectors have N_b elements. Moreover all submatrices except for $\bar{T}_1$ ...$\bar{T}_{Nc-1}$, $\bar{T}_f$, $\bar{T}_w$ have only diagonal entries. $\bar{T}_1$ ... $\bar{T}_{Nc-1}$, $\bar{T}_f$, and $\bar{T}_w$ treat transmissibilities ; hence, they are tridiagonal or pentadiagonal for 1-D or 2-D system, respectively. A detailed description of individual element will not be given here. Refer to Thele's thesis [T1].

Several important notes should be made at this point.

1. Comparing to NFA formulation, little convergence difficulty is expected, since all $2N_c+2$ unknowns are

computed from Newton-Raphson scheme and no approximation are made in the linearization process. (The composition constraints were implicitly used to reduce two unknowns.)

2. The lower triangle of the Jacobian is quite sparse (Fig. 2.2-1).
3. The unknowns are not grouped by grid blocks.

The general solution procedure is as follows :

(a) Generate right side residual vector.

(b) Generate the Jacobian matrix.

(c) Perform forward elimination to obtain upper block triangular matrix. This is easily done, since the lower triangle is sparse and all but the T-submatrices are diagonal. During this process, $\bar{\bar{C}}_p$ is changed to $\bar{\bar{C}}_p'$ (from a diagonal to a banded submatrix). Fig. 2.2-2 illustrates this procedure for the 1-D case.

(d) Solve :

$$\bar{\bar{C}}_p' \, \delta \vec{P} = - \vec{R}_s'$$

for $\delta \vec{P}$ using a bandsolver (this is just a $N_b x N_b$ matrix).

(e) Back substitute to obtain other iterate values.

(f) Update all unknowns.

(g) Compute new right side vector.

(h) Check fugacity, saturation, and material balance for convergence. Unless all of these are satisfied, go to (b).

(i) Go to (a), and start the process anew.

Here, again several comments should be given:

4. The size of the Jacobian matrix may be impractically large, if it is stored as a whole matrix. However, note that, to perform forward elimination, it is enough that each submatrix is individually stored. And as previously mentioned, most are diagonal, hence they may be stored as one-dimensional arrays.
5. At step (d), LU-decomposition is used to solve the pressure submatrix in this study. Several iterative techniques were compared and reported by Ply [P3] and Rood [R3].
6. Once the pressure submatrix is solved, the remaining equations do not depend on the equations from adjacent grid blocks. In other words, there is no need to compute unknowns in an order such as W_{Nb} ... W_1, F_{Nb} ... F_1, ... y_{1Nb} ... y_{11}. Actually, in our code, the unknowns are solved successively from W to V, and

after that, the computation is performed on a grid block basis. Namely, $y_{Nc-1} \ldots y_1$ are computed consecutively for a certain block, only if the V value of that block suggests the existence of two hydrocarbon phases (the flash routine will be called for the grid blocks in which one hydrocarbon phase is suggested). This feature may be used more efficiently, as a partial solution strategy.

The implicit treatment of transmissibility terms may introduce several extra banded submatrices in the lower triangle of the Jacobian. These fill-ins may destroy the effectiveness of the YS formulation ; however, no attempt to do this has been reported. Chien [C6] developed a fully implicit compositional simulator, which has a basic idea similar to the YS formulation, but is different in the selection of primary variables. He compared his new method with NFA, YS, and C formulations, but the efficiency of the new method is not evident from his paper.

2.3 Correlations and Miscellaneous Remarks

The Peng-Robinson equation of state [P1] is used to calculate fugacities and hydrocarbon phase densities. The flash routines are performed by an accelerated successive substitution based on the algorithms by Nghiem and Aziz [N3], and Mehra et al. [M1]. These details are lengthy and the reader should refer to Thele [T1].

Other properties listed in the previous section are computed as :

Water density (lb-moles/ft^3)

$$\xi_w = \xi_w^0 \{1 + c_w(P - P_w^0)\} \qquad (2.3\text{-}1)$$

Porosity

$$\phi = \phi^0 \{1 + c_f(P - P_f^0)\} \qquad (2.3\text{-}2)$$

Vapor-liquid interfacial tension (Macleod-Sugden correlation [R1])

$$\sigma = 0.016018 \, \Sigma_i [P_i](\xi_o x_i - \xi_g y_i) \quad \text{(dynes/cm)}$$

$$(i = 1 \ldots N_c) \qquad (2.3\text{-}3)$$

Hydrocarbon phase viscosity (Lohrentz et al. [L10])

This method was well explained by Thele [T1]; however, several mistyped expressions have been found. The correct forms are given below :

The low-pressure, pure component viscosity ; μ_i(cp).

$$\mu_i\zeta_i = 34 \times 10^{-5} T_{ri}^{0.94} \qquad \text{for } T_{ri} \le 1.5$$

$$\mu_i\zeta_i = 17.78 \times 10^{-5}(4.58\, T_{ri} - 1.67)^{5/8} \qquad \text{for } T_{ri} > 1.5$$

(2.3-4)

(17.76 was used instead of 17.78 in Thele's Eq. 3.5.1 .)

,where

$$\zeta_i = \{5.440\, [T_{ci}(R)]^{1/6}\} / \{M_i^{1/2} [P_{ci}(psia)]^{2/3}\} \quad (2.3\text{-}5)$$

(1/2 was used instead of 2/3 in Thele's Eq. 3.5.2 .)

mixture viscosity of phase j (j = o or g), μ_j^* (cp)

$$\mu_j^* = [\Sigma_i(x_{ji}\mu_i\sqrt{M_i})] / [\Sigma_i(x_{ji}\sqrt{M_i})] \quad (j = o \text{ or } g,\ i = 1 \ldots N_c)$$

(2.3-6)

The high-pressure mixture viscosity of phase j, μ_j (cp)

$$\mu_j = \mu_j^* + 2.05\, \xi_{rj}/(10^4\, \zeta) \qquad \text{for } \xi_{rj} \le 0.18$$

(2.3-7)

,where

$$\zeta = \{5.440\, [\Sigma_i(x_{ji}T_{ci})]^{1/6}\} / \{[\Sigma_i(x_{ji}M_i)]^{1/2}\, [\Sigma_i(x_{ji}P_{ci})]^{2/3}\}$$

(2.3-8)

$$\xi_{rj} = \xi_j\, \Sigma_i(x_{ji}V_{ci}) \qquad (i = 1 \ldots N_c) \quad (2.3\text{-}9)$$

or

$$\mu_j = \mu_j^* + [\eta(\xi_{rj})^4 - 1] / (10^4\,\zeta) \quad \text{for } \xi_{rj} > 0.18 \tag{2.3-10}$$

(4 of $\eta(\xi_{rj})^4$ was missed in Thele's Eq. 3.5.7 .)

,where

$$\eta(\xi_{rj}) = 1.023 + 0.23364\,\xi_{rj} + 0.58533\,\xi_{rj}^2 - 0.40758\,\xi_{rj}^3 + 0.093324\,\xi_{rj}^4 \tag{2.3-11}$$

Finally, well constraints are given as :

(a) Constant molar rate injection (Specify q_T, q_w, z_i).

$$q_i = (q_T - q_w)\,z_i \tag{2.3-12}$$

$$q_w = q_w \tag{2.3-13}$$

(b) Constant reservoir volumetric rate injection

(Specify Q_T, Q_w, z_i).

$$q_i = [(Q_T - Q_w)\xi_o\xi_g z_i] / [\xi_g + V(\xi_o - \xi_g)] \tag{2.3-14}$$

$$q_w = Q_w\xi_w \tag{2.3-15}$$

(c) Constant molar rate production (Specify q_T).

$$q_i = [(\lambda_{ro}\xi_o x_i + \lambda_{rg}\xi_g y_i) / \Sigma_j(\lambda_{rj}\xi_j)]\, q_T \quad (j = o,\ g,\ w) \tag{2.3-16}$$

$$q_w = [\lambda_{rw} / \Sigma_j(\lambda_{rj}\xi_j)]\, q_T \quad (j = o,\ g,\ w) \tag{2.3-17}$$

(d) Constant volumetric rate production (Specify Q_T).

$$q_i = [(\lambda_{ro}\xi_o x_i + \lambda_{rg}\xi_g y_i) / \Sigma_j\lambda_{rj}]\, Q_T \quad (j = o,\ g,\ w) \tag{2.3-18}$$

$$q_w = (\lambda_{rw}\xi_w / \Sigma_j\lambda_{rj})\, Q_T \quad (j = o,\ g,\ w) \tag{2.3-19}$$

(e) Constant bottomhole pressure production

(Specify P_{bh}, PI).

$$q_i = PI\,(\lambda_{ro}\xi_o x_i + \lambda_{rg}\xi_g y_i)\,(P_{bh} - P) \tag{2.3-20}$$

$$q_w = PI\,(\lambda_{rw}\xi_w)\,(P_{bh} - P) \tag{2.3-21}$$

,where the productivity index PI (or II) is defined as :

$$PI \text{ (or II)} = (k_X \Delta Y h) / (\Delta X/2) \quad \text{for 1-D} \tag{2.3-22}$$

$$PI \text{ (or II)} = (2\pi\sqrt{k_X k_Y}\, h) / \{\ln[C(r_{eq}/r_w)] + S\} \quad \text{for 2-D} \tag{2.3-23}$$

r_{eq} is the equvalent radius and C is used to take into account the geometry of the grid block and the location of the well within it [K2].

These variables, except for the grid block pressures in (e), are treated explicitly in the well term. Negligible capillary and gravity forces are assumed in the well blocks.

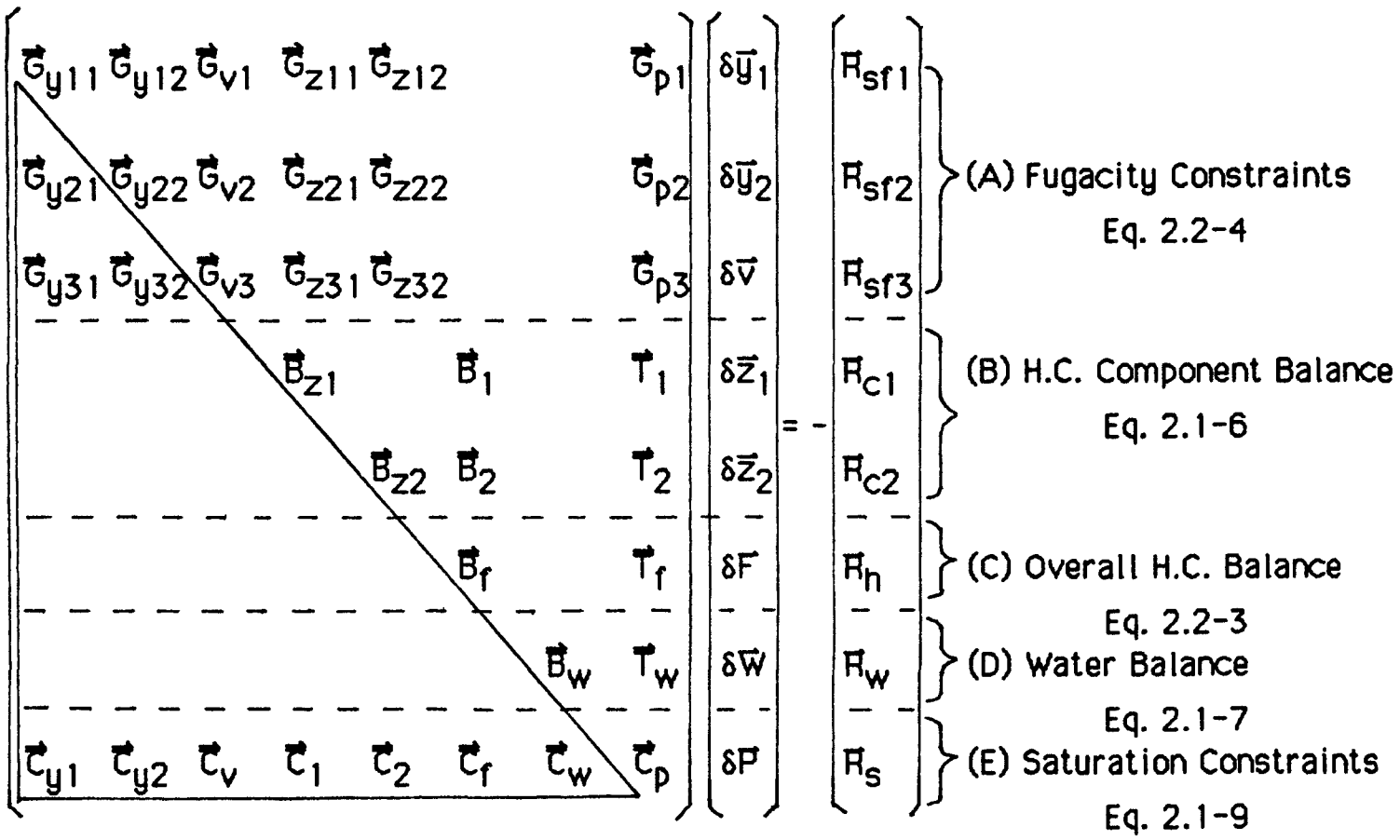

Fig. 2.2-1 Block matrix system in the YS formulation for 3 components.

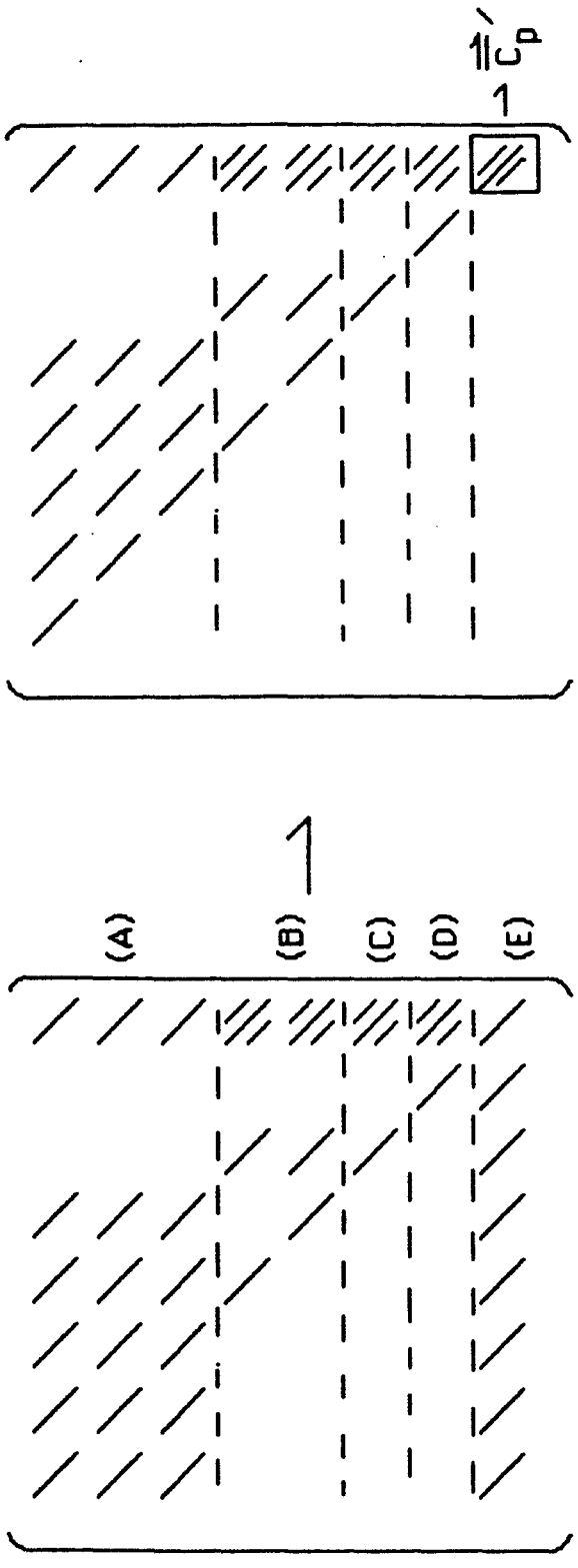

Fig. 2.2-2 Schematic diagram of forward elimination procedure.

CHAPTER III

MODIFICATIONS OF THE MODEL

As shown in the previous chapter, the original Young and Stephenson (YS) formulation neglected the dispersive flux term. In this chapter, the important role which dispersion plays in a miscible displacement processes is briefly reviewed. Then, a detailed treatment of the physical dispersion term will be presented followed by a discussion of numerical dispersion reduction schemes. Finally, the well representation in a cross-sectional version will be mentioned.

3.1 Physical Dispersion

3.1.1 Review of Mechanisms and Roles of Physical Dispersion

One of the main transport mechanisms taking place in porous media is dispersion. This is initiated by concentration gradients, while convection is caused by potential gradients. As shown in the previous chapter, the flux term of the species conservation equation for component i may be written as :

$$\vec{\nabla}\vec{N}_i = \vec{\nabla}\Sigma_j(\rho_j\omega_{ij}\vec{u}_j - \phi\rho_j S_j\bar{\bar{K}}_{ij}\vec{\nabla}\omega_{ij}) \qquad (j = 1...N_p) \qquad (2.1\text{-}3)$$

The second term on the right side expresses the dispersive flux where $\bar{K}_{ij}$ is a dispersion coefficient tensor. In the original YS formulation, this term was neglected.

The dispersion coefficient is quite a complicated function. According to Perkins and Johnston [P2], and Salter and Mohanty [S1, M4, M5], it is a function of :

(1) Molecular diffusion.

(2) Tortuosity.

(3) Phase velocity.

(4) Phase saturation.

(5) Scale of the system and degree of heterogeneity.

The exact mathematical expression will be given in the next section.

The role of dispersion in miscible displacements has been well explained in the literature [K1, L1, F3, S3], and may be summarized as follows :

(A) Favorable Features

(1) Transverse dispersion may mitigate viscous fingering to a certain extent [G3].

(2) Transverse dispersion may suppress a gravity tongue of solvent [P4].

(3) Additional hydrocarbon may be recovered from dead-end pore volume or water blocked hydrocarbon phase by molecular diffusion [B1, C7, O1].

(B) Adverse Features

Miscibility may be lost due to solvent dilution caused by dispersion. As a result, an immiscible displacement will take place instead of a miscible one, and a residual hydrocarbon left behind. This is particularly significant when solvent is injected as a slug [S3].

In spite of the favorable features listed above, the character which gives the largest impact on an EOR process might be this adverse feature --- dilution of solvent slug.

Some examples of these features will be shown in the following chapters.

3.1.2 Mathematical Formulation of Physical Dispersion Term

As reviewed in Chapter II, the YS formulation is solved by mole balance basis. Hence, cancelling molecular weight, physical dispersion term in Eq. 2.1-3 may be expressed in units of moles/vol./time as follows :

$$\omega_{ij} = (M_i \xi_j x_{ji}) / \rho_j \quad \text{hence, cancelling } M_i,$$

$$\vec{\nabla} \Sigma_j \{ \phi \rho_j S_j \bar{K}_{ij} [\vec{\nabla} (\xi_j x_{ji}) / \rho_j] \}$$

$$= \vec{\nabla} \Sigma_j \{ \phi \rho_j S_j \bar{K}_{ij} [(1/\rho_j) \vec{\nabla} (\xi_j x_{ji}) - (\xi_j x_{ji} / \rho_j^2) \vec{\nabla} \rho_j] \}$$

$$\approx \vec{\nabla} \Sigma_j [\phi S_j \bar{K}_{ij} (\vec{\nabla} \xi_j x_{ji})] \qquad (j = o, g) \qquad (3.1.2\text{-}1)$$

,where x_{ji} is a mole fraction of the i th component in phase j. Here, in the final expression, $-(\xi_j x_{ji}/\rho_j)\vec{\nabla}\rho_j$ was neglected in order to easily apply Chaudhari's technique to be described in Sec. 3.2.3. This assumption can be valid if one of the following conditions is satisfied :

(1) $|\vec{\nabla}(\xi_j x_{ji})| >> |-(\xi_j x_{ji}/\rho_j)\vec{\nabla}\rho_j|$

(2) |Convective Flux| >> |Dispersive Flux|

(3) |Net Flux| ≈ 0

The effect of this neglected term will be investigated in Sec. 4.3.3.

The physical dispersion coefficient in a two-dimensional tensor form is :

$$\bar{K}_{ij} = \begin{vmatrix} K_{XXij} & K_{XYij} \\ K_{YXij} & K_{YYij} \end{vmatrix}$$

,where the expansion of individual component was given by Bear [B2] as :

$$K_{XXij} = D_{ij}/\tau + [\alpha_{lj}/(\phi S_j)] \cdot (u_{Xj}^2/|\vec{u}_j|) + [\alpha_{tj}/(\phi S_j)] \cdot (u_{Yj}^2/|\vec{u}_j|) \quad (3.1.2\text{-}2a)$$

$$K_{XYij} = K_{YXij} = [(\alpha_{lj} - \alpha_{tj}) / (\phi S_j)] \cdot |u_{Xj} u_{Yj}| / |\vec{u}_j| \qquad (3.1.2\text{-}2b)$$

$$K_{YYij} = D_{ij}/\tau + [\alpha_{lj}/(\phi S_j)] \cdot (u_{Yj}^2/|\vec{u}_j|) + [\alpha_{tj}/(\phi S_j)] \cdot (u_{Xj}^2/|\vec{u}_j|) \qquad (3.1.2\text{-}2c)$$

$$|\vec{u}_j| = \sqrt{(u_{Xj}^2 + u_{Yj}^2)} \qquad (3.1.2\text{-}3)$$

Superficial velocities, u_{Xj}, u_{Yj}, were already defined in Eq. 2.1-19.

If molecular diffusion coefficients are negligible, the dispersion coefficients are propotional to interstitial phase velocity $(u_j/\phi S_j)$. This implies the concentration profiles depend on the length they traveled but not on velocity.

Salter and Mohanty [S1] suggested that longitudinal and transverse dispersivity of phase j were not only the functions of system scale but also functions of phase saturation S_j ; however, here, these were treated as constants.

Using the above notation, the mole conservation equation for component i (i = 1... N_c-1) in residual form expanded in a two-dimensional cartesian coordinate system is as follows :

$$R_{ci} = \partial/\partial t\,[\phi z_i \Sigma_j(\xi_j S_j)]$$
$$+ \partial/\partial X\,\{\Sigma_j\,[x_{ji}\xi_j u_{Xj} - \phi S_j K_{XXij}(\partial/\partial X\,(\xi_j x_{ji}))$$
$$- \phi S_j K_{XYij}(\partial/\partial Y\,(\xi_j x_{ji}))]\}$$
$$+ \partial/\partial Y\,\{\Sigma_j\,[x_{ji}\xi_j u_{Yj} - \phi S_j K_{YYij}(\partial/\partial Y\,(\xi_j x_{ji}))$$
$$- \phi S_j K_{YXij}(\partial/\partial X\,(\xi_j x_{ji}))]\}$$
$$- q_{ci}/V_b = 0 \qquad (j = o,\ g) \quad (3.1.2\text{-}4)$$

And overall hydrocarbon mole balance equation will be :

$$R_h = \partial/\partial t\,[\phi\ \Sigma_j(\xi_j S_j)]$$
$$+ \partial/\partial X\,\{\Sigma_j[\xi_j u_{Xj} - \phi S_j \Sigma_i(K_{XXij}(\partial/\partial X(\xi_j x_{ji}))$$
$$- K_{XYij}(\partial/\partial Y(\xi_j x_{ji}))\ )\ ]\}$$
$$+ \partial/\partial Y\,\{\Sigma_j[\xi_j u_{Yj} - \phi S_j \Sigma_i(K_{YYij}(\partial/\partial Y(\xi_j x_{ji}))$$
$$- K_{YXij}(\partial/\partial X(\xi_j x_{ji}))\ )\ ]\}$$
$$(j = o,\ g) \qquad (i = 1 \ldots N_c) \quad (3.1.2\text{-}5)$$

In this study, these dispersion terms are treated explicitly, which means evaluated at the previous time step and added to the residual vector. The complete finite difference

formulation with numerical reduction schemes will be given in Sec. 3.2.2 and 3.2.3 .

3.2 Numerical Dispersion Reduction Schemes

3.2.1 Nature of Numerical Dispersion

Consider a convection-diffusion equation in a dimensionless form for an illustrative purpose :

$$\partial C_D/\partial t_D = - \partial C_D/\partial X_D + K^P \cdot \partial^2 C_D/\partial X_D{}^2 \qquad (3.2.1\text{-}1)$$

,where K^P is an inverse of a Peclet number (= $1/N_{pe}{}^P$).

Solving this equation numerically (not restricted to finite difference methods) will introduce so-called numerical dispersion through truncation error. A numerical solution of Eq. 3.2.1-1 will correspond to the analytic solution of following equation :

$$\partial C_D/\partial t_D = - \partial C_D/\partial X_D + (K^P + K^N)\, \partial^2 C_D/\partial X_D{}^2 \qquad (3.2.1\text{-}2)$$

Here, K^N is a numerical dispersion coefficient (= $1/N_{pe}{}^N$). From Lantz [L4], the magnitude of K^N for a finite difference appoximation using a backward difference for the first-order space derivative is :

$$K^N = (\Delta X_D - \Delta t_D) / 2 \qquad \text{(explicit)} \qquad (3.2.1\text{-}3)$$

$$K^N = (\Delta X_D + \Delta t_D) / 2 \qquad \text{(implicit)} \qquad (3.2.1\text{-}4)$$

Unfortunately, these quantities are tens to hundreds times larger than K^P for the combination of practical grid and time step size. For example, an explicit K^N will be 0.0225 ($N_{pe}{}^N = 44.4$) by setting $\Delta X_D = 0.05$ (20 G.B.), and $\Delta t_D = 0.1\ \Delta X_D$. The range of K^P depends on the variables listed in Sec. 3.1.1, and has been considered approximately to be 0.02 --- 0.0001 ($N_{pe}{}^P = 50$ --- 10000) [L1]. Thus, K^N is substantially larger than K^P in usual cases. This means that the calculated concentration front will be smeared out excessively, and the true effect of physical dispersion, which must be important in a miscible process as mentioned in Sec. 3.1.1, will be masked.

On the other hand, the large numerical dispersion stabilizes a numerical solution. Note that Eq. 3.2.1-3 can be seen as a stability criterion for an explicit solution keeping K^N positive. Also note that K^N for implicit solution (Eq. 3.2.1-4), which is always positive and larger than the explicit one, guarantees unconditional stability of the implicit solution. So, a demand for a capability to evaluate physical dispersion precisely by reducing numerical dispersion and a quest for stable solution have a competitive nature.

Numerous attempts have been made to reduce numerical dispersion and to accurately model physical dispersion.

Lantz[L4] utilized K^N as K^P without implementing the second-order space derivative. Chaudhari's techniques were essentially the same as Lantz's but he put a negative numerical

dispersion coefficient on the second-order space derivative to cancel numerical dispersion [C4, C5].

Todd et al. [T4] proposed a two-point upstream weighting scheme to make the first-order space derivative second-order correct. Generalization of this method was investigated by Yokoyama [Y3].

The truncation cancellation procedure was introduced by Laumbach [L7]. This method cancels a part of the error in the first-order space derivative with that in the first-order time derivative. He claimed this method approached fourth-order correct in time and space as K^P became small.

Larson [L5, L6] developed a variably timed flux updating scheme in one and two dimensions to control numerical dispersion.

Li [L8] applied the method of random choice, which has been used in gas dynamics, with the operator splitting and reported that the method was unconditionally stable.

Jensen and Finlayson [J1] examined a front tracking scheme with a finite element simulator and compared the results with a conventional finite element formulation.

From these literature survey, the variational formulation solved by finite element methods and front tracking techniques seem to have great potential, and generality. However, in this study, Chaudhari's technique and Todd et al. 's two-point upstream weighting were chosen and tested because of their capability to be easily implemented in an existing simulator. As shown in the later

chapters these methods may be effective with careful use, but they are far from perfect.

Another important aspect of numerical dispersion is an alteration of principal axes. This causes the well known grid orientation effects with preferential flow along grid paths. This multidimensional numerical dispersion was investigated by Fanchi [F1]. And an excellent discussion was given in [E1].

Two-point upstream weighting failed to reduce this effect for highly adverse mobility ratio miscible displacements. This will be shown in Sec. 4.4.

Yanosik and McCracken [Y1] developed a nine-point finite difference scheme, and Young [Y4] applied a finite element method. Both methods showed successful results.

Russell and Wheeler [E1] suggested a possibility to reduce this effect by adjusting physical longitudinal and transverse dispersivity, and they proposed very sophisticated methods, interior penalties with finite elements, a modified method of characteristics with finite differences and finite elements, and a cell-balance finite element scheme.

3.2.2 Two-Point Upstream Weighting

Thele [T1] showed that the artificial smearing of concentration fronts could be improved by two-point upstream weighted mole fractions (x_i, y_i) as originally proposed by Nghiem et al. [N2]. (Hereafter, this method will be refered as "Composition 2-Point".)

In this study, other factors, relative permeabilities, viscosities, and densities, which have to be evaluated at grid block faces (i+1/2, or i-1/2) are also two-point upstream weighted ("All 2-Point"). The water conservation equation was treated in the same manner. Comparison of three methods ("Composition 2-Point", "All 2-Point", and "Chaudhari") will be given in the following chapter.

These two-point upstream weighted factors are treated as :

$$A_{k-1/2} = A_{k-1} + (A_{k-1} - A_{k-2}) \cdot \Delta X_{k-1} / (\Delta X_{k-1} + \Delta X_{k-2}) \qquad (\Phi_{k-1} > \Phi_k) \qquad (3.2.2\text{-}1a)$$

$$A_{k-1/2} = A_k + (A_k - A_{k+1}) \cdot \Delta X_k / (\Delta X_k + \Delta X_{k+1}) \qquad (\Phi_{k-1} < \Phi_k) \qquad (3.2.2\text{-}1b)$$

,where A is one of the two-point upstream weighted variables. $A_{k\pm1/2}$ must be constrained to prevent over- or under-shoot :

$$A_{k\pm1/2} \leq \text{Max}\,(A_{k\pm1}, A_k) \qquad (3.2.2\text{-}2)$$

$$A_{k\pm1/2} \geq \text{Min}\,(A_{k\pm1}, A_k) \qquad (3.2.2\text{-}3)$$

In addition to these, mole fractions (x_i, y_i) are normalized at the grid face to assure that these sum to unity.

With this scheme (or with an ordinary single-point upstream weighting), the physical dispersion term may be discretized as below [M3] :

From Eq. 3.1.2-4, for a grid (k,m),

$$\partial/\partial X \{\phi S_j K_{XXij} [\partial/\partial X(\xi_j x_{ji})] + \phi S_j K_{XYij} [\partial/\partial Y(\xi_j x_{ji})] \}$$

$$\approx (1/\Delta X_k)$$

$$\cdot \{2\cdot[(\xi_j x_{ji})_{k+1,m} - (\xi_j x_{ji})_{k,m}] (\phi S_j K_{XXij})_{k+1/2,m} / (\Delta X_{k+1} + \Delta X_k)$$

.....(A)

$$- 2\cdot[(\xi_j x_{ji})_{k,m} - (\xi_j x_{ji})_{k-1,m}] (\phi S_j K_{XXij})_{k-1/2,m} / (\Delta X_k + \Delta X_{k-1})$$

.....(B)

$$+ [(\xi_j x_{ji})_{k+1/2,m+1/2} - (\xi_j x_{ji})_{k+1/2,m-1/2}] (\phi S_j K_{XYij})_{k+1/2,m} / \Delta Y_m$$

.....(C)

$$- [(\xi_j x_{ji})_{k-1/2,m+1/2} - (\xi_j x_{ji})_{k-1/2,m-1/2}] (\phi S_j K_{XYij})_{k-1/2,m} / \Delta Y_m \}$$

.....(D)

(3.2.2-4)

The terms (A) and (C) are calculated only if phase j exists in both grids (k, m) and (k+1, m). Similarly only when the grids (k-1, m) and (k, m) have phase j are the terms (B) and (D) evaluated.

Individual factors in Eq. 3.2.2-4 are treated as :

$$\phi_{k\pm1/2} = (\phi_k + \phi_{k\pm1}) / 2 \qquad (3.2.2\text{-}5)$$

$$S_{jk\pm1/2} = (S_{jk} + S_{jk\pm1}) / 2 \qquad (3.2.2\text{-}6)$$

$$(\xi_j \times_{ji})_{k+1/2,\, m+1/2}$$

$$= [(\xi_j \times_{ji})_{k,m} + (\xi_j \times_{ji})_{k+1,m} + (\xi_j \times_{ji})_{k,m+1} + (\xi_j \times_{ji})_{k+1,m+1}] / 4 \qquad (3.2.2\text{-}7)$$

The superficial velocities along the grid face to evaluate physical dispersion coefficients are :

$$(u_{Yj})_{k+1/2,\, m}$$

$$= [(u_{Yj})_{k,m-1/2} + (u_{Yj})_{k,m+1/2} + (u_{Yj})_{k+1,m-1/2} + (u_{Yj})_{k+1,m+1/2}] / 4 \qquad (3.2.2\text{-}8)$$

These velocities are upstream weighted (either single- or two-point) to be consistent with the convection term ; however, this treatment is not rigorous.

Finally, at the boundary, the following conditions were assumed to guarantee no dispersive flux across the boundary (only the X-direction is shown) :

$$\partial/\partial X\,(\xi_j x_{ji}) = 0 \qquad (3.2.2\text{-}9)$$

$$u_{Xj} = 0 \qquad (3.2.2\text{-}10)$$

3.2.3 Chaudhari's Technique

Hong [H5] extended Chaudhari's technique to multiphase flow and implemented it in a two-dimensional incompressible micellar/polymer simulator. She assumed negligible time truncation error. This assumption may be reasonable since fairly small time step size is usually required to solve strongly non-linear systems. And the validity of the time truncation error expression derived analogous to Chaudhari's is doutful because our system is far more general and complicated (multiphase) than his application. However, here, Chaudhari's analog was derived including off-diagonal numerical dispersion coefficients. The detailed derivation will be given in Appendix-A.

As a result, the numerical dispersion coefficients are expressed in a tensor form as :

$$\bar{K}_j^N = \begin{vmatrix} K_{XXj}^N & K_{XYj}^N \\ K_{YXj}^N & K_{YYj}^N \end{vmatrix} \qquad (3.2.3\text{-}1)$$

,where in a discretized form

$$(K_{XXj}{}^{N})_{k+1/2} = -\{\Delta t\,[|u_{Xj}|/(\phi S_j)]_{k+1/2} - \Delta X_{up}\} \cdot |u_{Xj}|_{k+1/2} / (2\phi S_j)_{k+1/2}$$

$$\Delta X_{up} = \Delta X_k \quad \text{if } \Phi_{jk} > \Phi_{jk+1}$$

$$\Delta X_{up} = \Delta X_{k+1} \quad \text{if } \Phi_{jk} < \Phi_{jk+1} \qquad (3.2.3\text{-}2)$$

$$(K_{XYj}{}^{N})_{k+1/2} = -\{\Delta t\,[u_{Yj}/(\phi S_j)]_{k+1/2} \cdot u_{Xjk+1/2}\} / (2\phi S_j)_{k+1/2} \qquad (3.2.3\text{-}3)$$

$$(K_{YXj}{}^{N})_{m+1/2} = -\{\Delta t[u_{Xj}/(\phi S_j)]_{m+1/2} \cdot u_{Yjm+1/2}\} / (2\phi S_j)_{m+1/2} \qquad (3.2.3\text{-}4)$$

$$(K_{YYj}{}^{N})_{m+1/2} = -\{\Delta t[|u_{Yj}|/(\phi S_j)]_{m+1/2} - \Delta Y_{up}\} \cdot |u_{Yj}|_{m+1/2} / (2\phi S_j)_{m+1/2}$$

$$\Delta Y_{up} = \Delta Y_m \quad \text{if } \Phi_{jm} > \Phi_{jm+1}$$

$$\Delta Y_{up} = \Delta Y_{m+1} \quad \text{if } \Phi_{jm} < \Phi_{jm+1} \qquad (3.2.3\text{-}5)$$

These numerical dispersion coefficient component are subtracted from physical dispersion coefficient component in Eq. 3.2.2-4, when Chaudhari's technique is applied.

3.3 Treatment of Well Constraints in a Cross-Sectional Model

Basically two methods have been proposed to allocate total production or injection rate to each layer ; the potential allocation and the mobility allocation. The former method is theoretically correct but may introduce prohibitive stability problems if the saturation dependent terms are treated explicitly. The later method will not cause significant error unless the well is completed through a very low permeability zone [A2, N4, T2].

Here, the mobility allocation was used, and only the molar rate constraint was coded for injection wells in a cross-sectional model, while three production schemes, molar rate, volumetric rate, and bottomhole pressure constraint, were implemented. After an addition of a three-phase flash routine, the last two injection specifications may be modeled. And semi-implicit or fully implicit treatment of the well term [W1, C3, C9] may be required for more complicated runs.

3.3.1 Molar Rate Specification for Injection and Production Wells

For injection wells, we can specify molar rate of water (q_w) and each hydrocarbon component (q_i, $i=1...N_c$), then the injection rate into the l-th layer as :

$$q_{wl} = q_w \cdot (II\ \Sigma_j \lambda_{rj} \xi_j)_l \,/\, [\ \Sigma_k (II\ \Sigma_j \lambda_{rj} \xi_j)_k]$$

$$(j = o,\ g,\ w)\ (k = 1...N_l) \qquad (3.3.1\text{-}1)$$

$$q_{il} = q_i \cdot (II\ \Sigma_j \lambda_{rj} \xi_j)_l \,/\, [\ \Sigma_k (II\ \Sigma_j \lambda_{rj} \xi_j)_k]$$

$$(i = 1...N_c)\ \ (j = o,\ g,\ w)\ \ (k = 1...N_l) \qquad (3.3.1\text{-}2)$$

For production wells, specify total molar production rate (q_T) :

$$q_{Tl} = q_T \cdot (PI\ \Sigma_j \lambda_{rj} \xi_j)_l \,/\, [\ \Sigma_k (PI\ \Sigma_j \lambda_{rj} \xi_j)_k]$$

$$(j = o,\ g,\ w)\ \ (k = 1...N_l) \qquad (3.3.1\text{-}3)$$

$$q_{wl} = q_{Tl} \cdot (\lambda_{rw} \xi_w)_l \,/\, (\Sigma_j \lambda_{rj} \xi_j)_l \qquad (j = o,\ g,\ w)\ (3.3.1\text{-}4)$$

$$q_{il} = q_{Tl} \cdot (\lambda_{ro} \xi_o x_i + \lambda_{rg} \xi_g y_i)_l \,/\, (\Sigma_j \lambda_{rj} \xi_j)$$

$$(i = 1...N_c)\ \ (j = o,\ g,\ w) \qquad (3.3.1\text{-}5)$$

,where injectivity index (II) and productivity index (PI) were given in

Eqs. 2.3-22 and 2.3-23 , and the relative mobility λ_{rj} is defined as :

$$\lambda_{rj} = (k_{rj}/\mu_j) \,/\, [\,\Sigma_j(k_{rj}/\mu_j)] \qquad (j = o, g, w) \quad (3.3.1\text{-}6)$$

3.3.2 Volumetric Rate Specification for Production Wells

Specify total volumetric production rate Q_T :

$$q_{wl} = Q_T \cdot (PI\ \lambda_{rw}\xi_w)_l \,/\, [\,\Sigma_k(PI\ \Sigma_j\lambda_{rj})_k]$$

$$(j = o,\ g,\ w)\ \ (k = 1...N_l) \qquad (3.3.2\text{-}1)$$

$$q_{il} = Q_T \cdot [PI(\lambda_{ro}\xi_o x_i + \lambda_{rg}\xi_g y_i)] \,/\, [\,\Sigma_k(PI\ \Sigma_j\lambda_{rj})_k]$$

$$(i = 1...\ N_c)\ \ (j = o,\ g,\ w)\ \ (k = 1...N_l) \qquad (3.3.2\text{-}2)$$

3.3.3 Bottomhole Pressure Specification for Production Wells

Specify the bottomhole pressure at the upper most layer (P_{bhU}) :

$$P_{bhl} = P_{bhU} + \Sigma_k[\gamma_{k+1/2}(D_{k+1} - D_k)] \qquad (k = 1...l-1)$$

(3.3.3-1)

$$\gamma_{k+1/2} = (\gamma_k + \gamma_{k+1}) \,/\, 2 \qquad (3.3.3\text{-}2)$$

$$\gamma_k = \Sigma_j(\rho_j Q_{vj})_k \,/\, [\Sigma_j(Q_{vj})_k] \approx \Sigma_j(\rho_j \lambda_j)_k \,/ \Sigma_j(\lambda_j)_k$$

$$= \Sigma_j(\rho_j \lambda_{rj})_k \qquad (j = o, g, w) \quad (3.3.3\text{-}3)$$

$$q_{wl} = (PI\ \lambda_w \xi_w)_l (P_{bhl} - P_l^{n+1}) \qquad (3.3.3\text{-}4)$$

$$q_{il} = [PI(\lambda_o \xi_o x_i + \lambda_g \xi_g y_i)]_l (P_{bhl} - P_l^{n+1}) \qquad (3.3.3\text{-}5)$$

CHAPTER IV

TEST RUN RESULTS AND DISCUSSIONS

A modified version of the YS simulator descrived in the previous chapter will be tested here. The simple test cases consisted of three classes, (1) tracer runs (Sec. 4.2), (2) two-phase runs (Sec. 4.3), and (3) 2-D areal runs to check grid orientation effects (Sec. 4.4). Early on, Chaudhari's technique was discarded because of its instability to model small physical dispersion. Run-statistics, such as computation times and material balance errors, and the complete specifications for each run are summarized in Appendix-C.

4.1 General Remarks

The following notes are valid throughout the chapters IV and V (application runs), unless otherwise mentioned:

(1) Zero capillary pressures are assumed.

(2) Molecular diffusion coefficients are set to zero.

(3) Constant grid block sizes are always used.

(4) Injection conditions are specified by molar rate, and the bottom hole pressure constraints are used for production wells.

(5) Dimensionless times are calculated as a ratio of the injected fluid volume and the displaceable pore volume,

both evaluated at the initial pressure and temperature. Hence, a large pressure drop or a large volume change due to mixing may cause these numbers to be meaningless.

(6) The same dispersivities are used in both the oil and gas phases.

These specifications are not from the limitation of the simulator but arbitrarily selected.

(7) Hydrocarbon components and water properties are listed in Table 4.1-1 [R1, O1].

(8) Run-numbering is slightly different from class to class, but the first digit always shows the class number which that particular run belongs to.

4.2 Tracer Runs (Class-1)

4.2-1 Description of Runs

The purpose of Class-1 tracer runs are to investigate the nature of the numerical dispersion reduction schemes ("two-point upstream weighting" and "Chaudhari"). The accuracy of modeling physical dispersion is deduced by comparing numerical and analytical solutions. To do this, the system was approximately reduced to a convection-diffusion equation (Eq. 3.2.1-1), (1) by setting very large permeability (negligible pressure drop), and (2) by making the

displacing and displaced fluids have the same properties. Note that in this class, the "Composition 2-Point" and "All 2-Point" schemes reduce to the same one.

The reservoir data are given in Table 4.2-1. The dimensions and properties of this reservoir (slim tube) are basically based on Holm and Josendal [H4]. Initially this reservoir was saturated with butane-2, and displaced by butane-1 (tracer) continuously or as a slug followed by butane-2.

The exact analitic solution of Eq. 3.2.1-1 may be given as follows [N1]:

$$C_D = (1/2)\,\mathrm{erfc}\,[(X_D - t_D) / 2\sqrt{t_D/N_{pe}}] + \exp(-X_D N_{pe}) \cdot \mathrm{erfc}\,[(X_D + t_D) / 2\sqrt{t_D/N_{pe}}] \quad (4.2.1\text{-}1)$$

,where erfc is the complementary error function and N_{pe} is the Peclet number ($=1/K^p$). The dimensionless displacing fluid concentration C_D is defined as $(C-C_I)/(C_J-C_I)$.

Finally, run-numbering of Class-1 runs consists of the first digit (1) followed by the sequential number of one or two digits.

4.2.2 Results and Discussions

This subsection presents the magnitude of the numerical dispersion without any reduction schemes, and then the test results of these schemes for various Peclet numbers.

Remember that Eq. 3.2.1-3 showed the possibility of

cancelling numerical dispersion by adjusting ΔX_D and Δt_D for an explicit method. A sequence of runs was made with single-point upstream weighting, keeping ΔX_D constant (= 0.025, 40 G.B.), and changing Δt_D. These runs were with zero physical dispersivity (infinite N_{pe}). So, the exact solution must be a shock front. Fig. 4.2-1 shows that the concentration front becoming sharper as Δt_D approaching ΔX_D ($K^N \rightarrow 0$), and the solution seems to converge as Δt_D reduce to zero ($K^N \rightarrow \Delta X_D/2$).

Another sequence of runs was made using constant Δt_D ($= 0.1\Delta X_D$). From Fig. 4.2-1, the effect of time step size is fairly small at this level. Increasing the number of grid blocks (decreasing ΔX_D) the solution became sharper (Fig. 4.2-2). But the incremented computation time due to using a large number of grid blocks can be prohibitive (see Appendix-C). Hereafter 40 grid blocks were used for all 1-D runs consistently.

Figs. 4.2-3 --- 4.2-8 show the comparison of four solutions, exact, single and two-point upstream weighting, and Chaudhari's tecnique, with a Peclet number of 500. The concentration profiles at 0.4 DPV injected are shown in Fig. 4.2-3. The labels, A, B, C, A', B', and C', indicate the same point in Figs. 4.2-3, 4.2-7, and 4.2-8. It is obvious from this figure that the ordinary single-point upstream weighting (Run #1.7) may not be used

for this kind of simulation since the smearing due to numerical dispersion is so large. From a probability paper plot (the second term in Eq. 4.2.1-1 was neglected) [P2] in Fig. 4.2-4, the actual Peclet number (N_{pe}^{act}) may be calculated as follows : (The straight lines were drawn by the least squares method, using the points between C_D = 10 % and C_D = 90 %.)

$$1/N_{pe}^{act} = (1/t_D) [(X_D|_{90} - X_D|_{10}) / 3.625]^2 \quad (4.2.2\text{-}1)$$

We get N_{pe}^{act} = 75.1 for Run #1.7. This corresponds to the sum of physical and numerical dispersivity:

$$1/N_{pe}^{T} = 1/N_{pe}^{P} + 1/N_{pe}^{N} = 1/500 + (0.025\text{-}0.1\times0.025)/2 = 1/75.47$$

Thus, there is a big difference between the input Peclet number (500) and output Peclet number (75.1). Both two-point upstream weighting (Run #1.8) and Chaudhari's technique (Run #1.9) presented better profiles than the single-point scheme (Run #1.7) in Fig. 4.2-3. However the actual Peclet numbers calculated from Figs. 4.2-5 and 4.2-6 are 282.5 and 249.8 respectively. Probably at least 80 grid blocks are required for this level of physical dispersion with Chaudhari's technique or two-point upstream weighting to get reasonable accuracy. However, 225 grid blocks with $\Delta t_D = 0.1\Delta X_D$ or 40 grid blocks with $\Delta t_D = 0.84\Delta X_D$ may be required if Lantz's method

is used to express this Peclet number. The former combination is expensive, and for the latter one a large time step size may be prohibitive for more complicated non-linear systems. There may be the optimal combination, but it is not practical to search for such a combination for run by run.

Two other types of plots were made. The first type is a plot of net flux per time step (in other words, this is the accumulation). This quantity is defined as :

Net Flux/time step = {(number of moles of component i in k th block)$^{n+1}$
- (number of moles of component i in k th block)^{n} } / Δt

The second plot may be called the dispersive accumulation ratio :

Dispersive Accumulation Ratio = (Dispersive Accumulation)
/ (Convective Accumulation) = $\vec{\nabla}\Sigma_j(\xi_j x_{ji}\vec{u}_j)/\vec{\nabla}\Sigma_j[\phi S_j \overline{K}_{ij}(\vec{\nabla}\xi_j x_{ji})]$

These plots were made for two reasons. First, the movement of the displacing front and the location of the dispersive mixing-dominated zone can be emphasized. This is especially useful for 2-D slug runs (Sec. 5.3, 5.4). The second reason is to check the validity of the assumption mentioned in Sec. 3.1.2, where a term was neglected from the physical dispersion term. This will be investigated in Sec. 4.3.3 .

Fig. 4.2-7 shows the net flux of displacing fluid for Run #1.8 (two-point) and #1.9 (Chaudhari). For the exact solution (not plotted here), the peak position corresponds to the position of mean concentration (should be at $\Delta X_D = 0.4$, in this case), and the shape of the curve is symmetric. It is clear that Chaudhari's technique has a very sharp trailing edge and a little bit slower front. On the other hand, two-point upstream weighting run moves faster and has an acute leading edge.

From Fig. 4.2-8, it can be seen that dispersive flux dominates at both edges (but net fluxes are very small at those points), and becomes zero at the mean concentration. The negative values of dispersive accumulation ratio indicates where the directions of dispersive accumulation and convective accumulation are opposite. The trends of Chaudhari's technique and two-point upstream weighting are reverse, since Chaudhari's technique has a negative dispersion coefficient in this case.

Larger physical dispersion cases are shown in Figs. 4.2-9 --- 4.2-14. For these cases, both methods presented excellent results. As previously mentioned in Sec. 3.2.1, it is easier to model large dispersion than a small one. These results are summarized in Fig. 4.2-15. All runs included in this figure used 40 grid blocks and $\Delta t_D = 0.1\Delta X_D$. Hence, without numerical dispersion reduction scheme and physical dispersion term, the actual (outputted) dispersivity should be 1/88.9 = 0.0112 ((0.025 - 0.1x0.025)/2). Around this

value, both two-point upstream weighting and Chaudhari's technique present Excellent results. And each side of this point shows the opposite error trend ; namely, the numerical solution shows the sharper front than the analytic solution when the inputted dispersivity is larger than the numerical dispersion level, and the reverse is true for the smaller dispersivity. The reason of this observation is not explicit, however, probably the remaining higher order terms (remember both methods only treat the second-order term) may affect this.

One more series of runs was made to study the profiles and the effluent histories of tracer slugs (0.1 DPV). N_{pe} = 200 was used. Fig. 4.2-16 shows the profiles at 0.4 DPV and 0.8 DPV injected, and the effluent histories are shown in Fig. 4.2-17. The exact solution was obtained by the superposition of Eq. 4.2.1-1 [L1]. Here again, the slug is diluted with the single-point scheme, and two-point upstream weighting drives the slug slightly too fast. Fig. 4.2-18 shows the net flux, and from this figure, the net flux is positive at the front of the bank and becomes zero at the peak concentration, then has negative value behind the bank.

At this point, through continuous tracer and slug runs, no significant drawbacks have been found for either method. Chaudhari's technique may be prefered since two-point upstream weighting showed a faster movement of slug in Run #1.13. However, Chaudhari's technique has a serious defect because it may be unstable unless the inputted physical dispersivity is equal or larger

than the numerical dispersivity which will appear when an ordinary first-order correct finite difference is used. In other words, the total dispersivity ($K^P - K^N$) which is the coefficient of the discretized second-order space derivative in Chaudhari's technique must be positive to get a stable solution. The stability analysis by the matrix method using Gerschgorin's theorem (Appendix-B) shows that a necessary and sufficient condition for a solution without the growth of the initial error is that physical dispersion be equal or larger than numerical dispersion and that the proper small time step size be selected (region A in Fig. B-2). Although this analysis gives no information about the stability in the area where physical dispersion is smaller than numerical dispersion (region B in Fig. B-1), namely the total dispersivity is negative, a possibility of the initial error growth in this region is clearly indicated by this analysis and it well agrees the numerical results which has been reported by several investigators [L9, H5].

Lin [L9] used a first-order correct finite difference scheme, two-point backward for the first-order space derivative and three-point central for the second-order space derivative, without any numerical dispersion reduction scheme. And he attempted to represent a small total dispersivity by inputting a negative physical dispersivity. This idea is essentially the same as Chaudhari's technique. He concluded that a positive total dispersivity was required to prevent oscillations. This completely agrees with our discussion mentioned above. (In this case, the total dispersivity is

($K^N - K^P$), where K^N is not explicitly used in his codes but appears from the first-order correct finite difference. Comparing with Chaudhari's technique:

Lin's method --- output dispersivity = $(K^N - K^P) > 0$

Chaudhari's technique --- output dispersivity = $K^P > K^N > 0$

Hence, Lin's method can model smaller dispersivity than Chaudhari's technique, although the grid block size and the time step size must be constant.)

Hong [H5] tested Chaudhari's technique and presented similar results. She showed oscillatory behaviors of concentration profiles, and concluded that the Peclet number used for a given simulation could be up to about four times the number of grid blocks (assuming small time truncation error, $(\Delta X_D - \Delta t_D)/2 \approx \Delta X_D/2 = 1/(2N_X) = 1/N_{pe}^N$). This means that Chaudhari's technique can stably model physical dispersivity which is larger than about a half of numerical dispersivity. Qualitatively this argument is correct, but quantitatively the condition may be harder as previously mentioned. Physical dispersivity should be larger than numerical dispersivity. In our simulator, mole fractions are always constrained between zero and one, and, moreover, the sum of mole fractions of each phase is normalized to unity. These manipulations are necessary to guarantee the function of flash routine; however, it makes the global material balance worse. Because of these handling, no concentration oscillation can be seen in our profiles, but Chaudhari's technique

shows hundreds to thousands times worse material balance error than the two-point upstream weighting. See Table 4.2-2 abstracted from Appendix-C. The magnitude of these errors may be tolerable in simple Class-1 runs, but in the next section, it will become very difficult to complete runs with Chaudhari's technique since saturations, which were not constrained as were the mole fractions, start fluctuating. This fluctuation makes the iteration scheme useless, and, hence, the simulation can not be completed.

Probably one good feature of Chaudhari's technique is the ability to cancel the time truncation error. Two-point upstream weighting only treats the first-order space derivative. One attempt was made to combine these two schemes. That is, the time truncation error was treated by Chaudhari's technique and two-point upstream weighting took care of the space truncation error. The results are shown in Figs. 4.2-19 --- 4.2-21. Larger Δt_D (= 0.4 ΔX_D) was used to magnify the time truncation effect. As shown in Fig. 4.2-19, the concentration profile from the pure two-point upstream scheme is too steep and the reverse is true for the combined method. To derive the expression for the time truncation error in terms of space derivative, several assumptions were made (neglect physical dispersion term, ignore higher order terms). The nature of the time truncation error may not be so simple.

4.3 Two-Phase Runs (Class-2)

4.3.1 Description of Runs

The purpose of the Class-2 runs is to extend the investigation in the previous section to a more complicated fluid system. The reservoir (slim tube) is exactly the same as the Class-1 runs. The fluid system is represented the ternary diagram shown in Fig. 4.3-1. Two subclasses of runs, small and large interphase mass-transfer cases, were made. The only difference between these subclasses is the displacing fluid composition which is listed in Table 4.3-1.

The relative permeabilities were modeled based on Nghiem et al. [N2] as functions of interfacial tension and saturation. These are shown in Fig. 4.3-2 and Table 4.3-2.

The run-numbering convention is the same as Class-1 runs, the first digid (2) indicates the class and is followed by sequential number.

No physical dispersivity was used for any of the runs except for one (*2.8) which was used to check the significance of the neglected term in physical dispersion term. Hence, these runs should be the great ordeals for Chaudhari's technique.

4.3.2 Results and Discussions for the Small Interphase Mass-Transfer Case

Four runs including single-point upstream weighting, "Composition 2-Point", "All 2-Point", and "Chaudhari" were made, but

there is little thing to be mentioned since all solutions showed no significant difference. This is because the composition of oil and gas phases remain almost constant throughout the run in a nearly perfect immiscible displacement. Hence, the concentration gradient in a phase is so small that the effect of dispersion (numerical and physical) is not emphasized.

Composition routes, saturation and composition profiles are shown in Figs. 4.3-3 --- 4.3-10.

Digressing slightly from dispersion, Figs. 4.3-11 --- 4.3-14 show production rate histories. The decane production rate starts oscillating shortly after the beginning of production and continues until methane breaks through. This phenomenon can be explained by noting that there are exactly the same number of oscillations peaks as the number of grid blocks (in this case 40).

Consider the composition route and the grid system simultaneously. Methane is injected into the first block (the composition is moving from the initial condition toward the injection condition), and, after a short while, the first block composition goes into the two phase region. This causes the evolution of gas phase accompanied with sudden volume increase, since we assumed the instantaneous local thermodynamic equilibrium (assumption 8). The first peak of the decane production rate was made by this volume change which was actually a pressure change. Remember, the production rate was the bottom hole pressure specified. Then the same process will take place in the second

block and so on.

4.3.3 Results and Discussions for the Large Interphase Mass-Transfer Case

For these runs, the displacing fluid was enriched by increasing the fraction of the intermediate component (butane).

Chaudhari's technique failed here because of a saturation error due to the instability caused by the negative dispersion coefficient (as mentioned in the previous section, this run could be completed by adding large amount of physical dispersivity, $N_{pe}^{P} = 80$, although it is not presented here).

Fig. 4.3-15 shows the composition routes for single-point, "Composition 2-Point", and "All 2-Point" schemes. Both two-point schemes are indistinguishable on this diagram, while the single-point upstream weighting is obviously different.

The saturation profiles are shown in Fig. 4.3-16. The gas phase front moved fastest in the "All 2-Point" and slowest in the single-point scheme. The oscillations in this figure are caused by the artificial naming of phases (near the critical composition, infinitesimal changes of composition affect the name of the phase). In this case, the composition route goes through the vicinity of the plait point (which actually doesn't exist in this system), where the compositions of gas and oil coincide, hence, the flash calculation becomes very difficult.

Figs. 4.3-17 --- 4.3-18 present the composition profiles

of each component. The single-point upstream weighting shows the most smeared front since the concentration gradient in a phase is larger than in the previous case where the phase composition was almost constant. This large concentration gradient magnifies the effect of numerical dispersion. On the other hand, both two-point schemes have identically sharp fronts, but they can be discriminated behind the front.

Insight from the method of characteristics [H1, G2, G4, L1, C1] enables us to imagine the features of the exact solution. From the initial condition (see Fig. 4.3-15), the composition route jumps into the two phase region along a tie line extension as a shock (Point A). Then it follows one of the non tie line paths where the velocity should be almost constant [C1], finally, from Point B, one tie line path will be chosen, which leads to the injection condition, and along which the velocity may be varying. The difference between the two-point upstream weighting schemes should be because of the evaluation of velocity, since the composition routes are basically the same.

The solutions may be compared to the method of characteristics solution to decide which scheme should be chosen. However, remember that the ideal mixing has not been assumed owing to the usage of the equation of state. Hence, a quite generalized method of characteristics which doesn't assume zero volume change upon mixing has to be prepared. This is beyond the scope of this study. Fig. 4.3-20 shows the recovery history of

decane. There is a small discrepancy between the two-point schemes.

The production rate histories are shown in Figs. 4.3-21 and 4.3-22. Notice that the amplitude of the oscillation is smaller than the previous case (Figs. 4.3-11 --- 4.3-14). This is because the composition difference between the oil and gas phases becomes smaller and smaller as the composition route moves toward the injection condition (recall the injection composition is very close to the critical composition). Therefore, the volume change noted above decreases. Further, note that the composition route of the two-point schemes locates outside of that of single-point scheme, consequently the amplitude of the fluctuation is smaller.

Finally, as mentioned in Sec. 3.1.2, the effect of the neglected term in physical dispersion expression was investigated. Run #2.8 is exactly the same as #2.7 except for a small inputted physical dispersivity (0.01 ft/day). The ratio of $\vec{\nabla}(\xi_j x_{ji})$ and $-(\xi_j x_{ji})/\rho_j \cdot \vec{\nabla}\rho_j$ was calculated and plotted in Fig. 4.3-23. The error is very large at several point, but fortunately the positions of these error peaks do not coincide with the peaks of the net flux (Fig. 4.3-24) and the dispersive accumulation ratio (Fig. 4.3-25). Therefore, the effect was fairly small in this case, and this assumption may be valid generally. However, Chaudhari's technique was discarded and there is no reason to neglect this term. In this study, it remains neglected, but it may be desirable to be

implemented for completeness.

4.4 2-D Areal Runs (Class-3) for the Study of Grid Orientation Effects

4.4.1 Description of Runs

Todd et al. mentioned in their paper [T4] that two-point upstream weighting successfully reduced grid orientation effects for various mobility ratios in the range from 0.5 (favorable) to 10 (adverse) by increasing the number of grid blocks. (If it is true, it means that grid orientation effects are mainly the products of numerical dispersion.) However, Coats et al. [C8] pointed out that a finite difference solution could converge to two different results, which depend on the grid system, and it could not be remedied by adding grid blocks. Aziz and Settari [A2] summarized that grid orientation effects would not be a result of truncation error alone, but would be the combined effect of truncation error and preferential flow along grid lines. Yanosik and McCracken [Y1] demonstrated the efficiency of a nine-point finite difference scheme, simulating mobility ratios up to 50. Their simulator was not compositional ; hence, a miscible diplacement was expressed by adjusting a fractional flow curve. They concluded that the two-point upstream weighting with a five point finite difference scheme might be sufficient for an unfavorable mobility ratio immiscible displacement, but it would fail to simulate an unfavorable miscible

displacement. Also, a certain amount of numerical dispersion would be required near the displacement fronts to stabilize the solution. Young [Y4] studied the same kind of problem by a finite element simulator with physical dispersion. He also showed an attractive result.

This subsection presents the degree of grid orientation effects with two-point upstream weighting for a favorable and an unfavorable first-contact miscible (FCM) displacement, in which the mobility ratio is simply the viscosity ratio. Decane was injected into a methane reservoir to get a favorable initial mobility ratio of 0.088. The reverse process was done to realize an adverse initial mobility ratio of 11.4. Physical dispersion was set to zero, unless otherwise noted.

The grid systems are given in Table 4.4-1, where 7x7 and 10x10 system was used for diagonal runs and parallel runs, respectively.

In this class, one letter (A or B) will appear between the class number (3) and the sequential run number. "A" indicates adverse mobility ratio runs, and "B" shows favorable mobility ratio runs. And an odd sequential number corresponds to a diagonal run (7x7), while a parallel run (10x10) has an even sequential number.

4.4.2 Results and Discussions

Only two runs were made for a favorable mobility ratio, FCM displacement. Single-point upstream weighting was used in both

runs, and yet it was sufficient.

Fig. 4.4-1 shows the decane mole fraction contours at 0.4 DPV injected. The production rate histories are shown in Fig. 4.4-2. From the view point of grid orientation effects, the discrepancy shown in these figures is tolerable. However, the mixing zone is spread out by numerical dispersion. This is shown in Fig. 4.4-2 as a gradual break through of decane. As a result, the recoveries show little difference, and there is no obvious break off point on both curves (Fig. 4.4-3).

As a good contrast with these runs, the adverse mobility ratio simulation with single-point scheme shows terrible results. Methane mole fraction contours are shown in Fig. 4.4-4. Methane breakthrough has already occured in the parallel grid system, while it is still on the way in the diagonal system. Fig. 4.4-5 shows completely different production histories. The mobility ratio may be considered as a velocity ratio. The mechanism of how the mobility ratio affects grid orientation is not explicit ; however, the velocity dependent dispersion coefficients (both physical and numerical) should play an important role.

Two-point upstream weighting shows essentially the same failure. In Fig. 4.4-6, methane fronts have not reached the production well yet, and the mixing zones are smaller than the single-point runs, but the disagreement of solutions is still striking. Sharper breakthrough curves are shown in Fig. 4.4-7.

Here again, as was done in Sec. 4.2.2, Chaudhari's time

truncation cancellation including the off-diagonal elements of the numerical dispersion tensor and two-point upstream weighting were combined. The results are shown in Figs. 4.4-8 and 4.4-9. There is little improvement observed. The 10 % line of the methane contour for the diagonal system went forward slightly. Conversly, to make matters worse, small fluctuations of the production rate occured especially in the parallel system. Probably, a smaller time step size is required to eliminate these fluctuations.

To reduce the time truncation error, another alternative approach was taken, by simply using a smaller time step size, one fifth of the previous runs, with pure two-point upstream weighting. The results (Figs. 4.4-10 and 4.4-11) are very similar to the combined method mentioned above. A comparison of recovery histories shows that, by the reduction of time step size, in other words by the diminution of time truncation error, the two recovery curves became closer, but the improvement is very small.

From these results and the discussion of Aziz and Settari [A2], grid orientation effects may exist even if an impractically large number of grid blocks and small time step sizes are used for five-point finite difference method.

Finally, one more attempt was made to further investigate the nature of grid orientation effects. The following argument was given by Russell and Wheeler [E1].

Neglecting time truncation error, the numerical dispersion tensor, Eq. 3.2.3-1, may be written as:

$$\bar{K}_j^N = \begin{vmatrix} (h/2)[u_{Xj}/(\phi S_j)] & 0 \\ 0 & (h/2)[u_{Yj}/(\phi S_j)] \end{vmatrix} \quad (4.4.2\text{-}1)$$

,where $h = \Delta X = \Delta Y$.

From Eqs. 3.1.2-2a --- 3.1.2-2c, the physical dispersion tensor may be given as :

$$\bar{K}_j^P = |\vec{u}_j|/(\phi S_j) \begin{vmatrix} (\alpha_{lj}\cos^2\theta+\alpha_{tj}\sin^2\theta) & (\alpha_{lj}-\alpha_{tj})\cos\theta\sin\theta \\ (\alpha_{lj}-\alpha_{tj})\cos\theta\sin\theta & (\alpha_{lj}\sin^2\theta+\alpha_{tj}\cos^2\theta) \end{vmatrix} \quad (4.4.2\text{-}2)$$

,where θ is the angle between $\vec{u}_j$ and the X-axis, and molecular diffusion was neglected. This θ is changing along the stream lines; however, considering the shortest stream line (straight line) between the injector and the producer, θ becomes constant and equal to zero or $\pi/2$ for the parallel grid system, and equal to $\pi/4$ for the diagonal grid system. Therefore, along these shortest stream lines, numerical dispersivity may be expressed in terms of the physical

dispersivity as :

$$\alpha_{lj} = h / 2 \qquad \alpha_{tj} = 0 \qquad \text{(parallel)} \qquad (4.4.2\text{-}3)$$

$$\alpha_{lj} = \alpha_{tj} = h / 2\sqrt{2} \qquad \text{(diagonal)} \qquad (4.4.2\text{-}4)$$

Thus, if these dispersivities are inputted as negative numbers, the numerical dispersion effect, including the change of principal flow axes, should be cancelled along the shortest stream lines.

To check this, Run *3A.13 and 14 were made assuming a longitudinal physical dispersivity of 5.0 ft, and a transverse physical dispersivity of 1.0 ft. (Note that the actual inputted values are $\alpha_l = 0$, $\alpha_t = 1.0$ for the parallel system and $\alpha_l = 1.46$, $\alpha_t = -2.54$ for the diagonal system, since "h" equals 10 ft in these cases. Further note that the single-point scheme had to be used.) Methane mole fraction contours are shown in Fig. 4.4-13. The leading edges (10 % line) became closer around the diagonal (the shortest stream line) compared to the previous runs. But the regions far from the diagonal do not show any improvement since no adjustment was made for these parts. Fig. 4.4-14 shows the production rate histories. The agreement of the breakthrough time of methane is not so bad, but after the breakthrough, the discrepancy is still obvious.

It should be noted that, in a parallel grid system, the numerical dispersion along the shortest stream line expressed as Eq. 4.4.2-3 can be cancelled by two-point upstream weighting. Also, the

effect of preferential flow is small since the principal flow axes coincide with the coordinate axes. Therefore, the results from a parallel grid system with two-point upstream weighting are more practical and realistic than those from a diagonal system, although they still contain some error from the region far from the shortest stream line. The motivation of the use of curvilinear grid system [H2, R2] may be understood from these facts. For an ordinary five-point finite difference simulator, the use of a parallel grid system with two-point upstream weighting may be recommended, but it requires about twice as many grid blocks compared to a diagonal system.

TABLE 4.1-1

Hydrocarbon Component Data and Water Properties

Water density (lb-moles/ft^3)	3.467
Water compressibility (psi^{-1})	3.0×10^{-6}
Water molar weight	18.0
Water viscosity (cp)	0.5

Critical Properties

Component	Press. (psia)	Temp. (R)	Vol. (ft^3/lb.mol)	Mol. Weight	Acentric Factor	Parachor ($dyne^{1/4} cm^{11/4}$/g.mol)
CO_2	1071	548	1.50	44.0	0.223	49
C_1	673	343	1.59	16.0	0.014	71
C_4	551	765	4.08	58.1	0.193	191
C_{10}	306	1115	9.66	142.3	0.489	431

TABLE 4.1-1 (Continued)

Binary Interaction Coefficients

	CO_2	C_1	C_4	C_{10}
CO_2	0.0			
C_1	0.10	0.0		
C_4	0.13	0.0	0.0	
C_{10}	0.11	0.0	0.0	0.0

TABLE 4.2-1

Reservoir (Slim Tube) Description for
Class-1, Class-2, and Class-4 Runs

Dimensions (ft)	
Length	52
Width	0.035
Thickness	0.035
Permeability (md)	20000
Porosity (fraction)	0.39
Rock compressibility (psi^{-1})	0.2×10^{-5}
Temperature (F)	200
Initial water saturation (fraction)	
Class-1 and Class-2	0.0
Class-4 (secondary)	0.2
(tertiary)	0.7
Initial pressure (psia)	
Class-1	5000
Class-2	1500
Class-4	1400 --- 2400

TABLE 4.2-2

Material Balance Errors (%) for Class-1 Runs

(abstracted from Appendix-C)

The global material balance errors were calculated as :

$$E_i = (W_{Ii} + N_{Ji} - N_{Pi} - W_i) / W_{Ii} \quad (i=1...N_c) \qquad .(C.4)$$

,where

W_{Ii} : initial-in-place of component i

N_{Ji} : cumulative injection of component i

N_{Pi} : cumulative production of component i

W_i : currently-in-place of component i

	N_{pe} P			
	20	80	200	500
Two-point Scheme	0.234×10^{-5} (butane-1)	0.234×10^{-5} (butane-1)	0.309×10^{-5} (butane-1)	0.234×10^{-5} (butane-1)
Chaudhari	0.604×10^{-1} (butane-1)	0.632×10^{-1} (butane-1)	-0.205 (butane-1)	-0.853 (butane-1)

TABLE 4.3-1

Displaced and Displacing Fluid Composition
for Class-2 Runs

Displaced Fluid Composition (mole fractions)

C_1	0.0001
C_4	0.2999
C_{10}	0.7000

Displacing Fluid Composition (mole fractions)

Small Interphase Mass-Transfer Case

C_1	0.9
C_4	0.1

Large Interphase Mass-Transfer Case

C_1	0.6
C_4	0.4

TABLE 4.3-2

Relative Permeability Functions for Class-2 Runs

$$\overline{K}_{rg} = K_{roiw}\left(\frac{S_g - S_{gr}}{1 - S_{gr} - S_{wr}}\right)^{EG}$$

$$\overline{K}_{ro} = K_{roiw}\left(\frac{1 - S_g - S_{org} - S_{wr}}{1 - S_{org} - S_{wr}}\right)^{EOG}$$

$$K_{rg} = (1 - e^{-AG\cdot R})\cdot\overline{K}_{rg} + e^{-AG\cdot R}\cdot K_{roiw}\left(\frac{S_g}{1 - S_w}\right)^{1+BG\cdot R}$$

$$K_{ro} = (1 - e^{-AO\cdot R})\cdot\overline{K}_{ro} + e^{-AO\cdot R}\cdot K_{roiw}\left(\frac{S_o}{1 - S_{wr}}\right)^{1+BO\cdot R}$$

$$R = \sigma / \sigma^*$$

σ^* =	2.0	S_{wr} =	0.0	S_{gr} =	0.0
S_{org} =	0.2	K_{roiw} =	1.0	AG =	1.0
BG =	2.0	AO =	1.0	BO =	2.0
EG =	2.0	EOG =	2.5		

TABLE 4.4-1

Reservoir Description for Class-3 Runs

Parallel Grid (10x10)	
Dimensions (ft)	
Length	100
Width	100
Thickness	10
Permeability (md)	20000
Porosity (fraction)	0.3
Rock compressibility (psi^{-1})	0.45×10^{-5}
Temperature (F)	200
Initial water saturation (fraction)	0.0
Initial pressure (psia)	6000

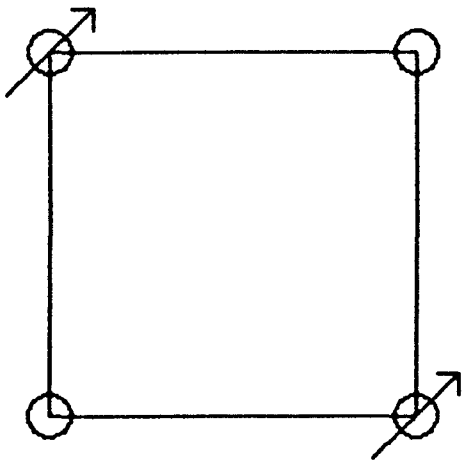

TABLE 4.4-1 (Continued)

Diagonal Grid (7x7)	
Dimensions (ft)	
Length	70
Width	70
Thickness	10
Permeability (md)	the same as Parallel Grid
Porosity (fraction)	
Rock compressibility (psi^{-1})	
Temperature (F)	
Initial water saturation (fraction)	
Initial pressure (psia)	

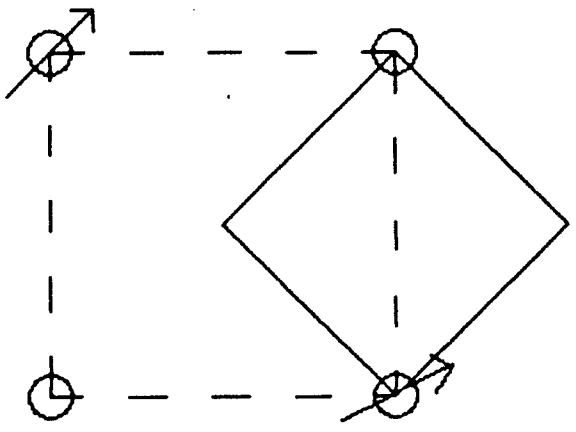

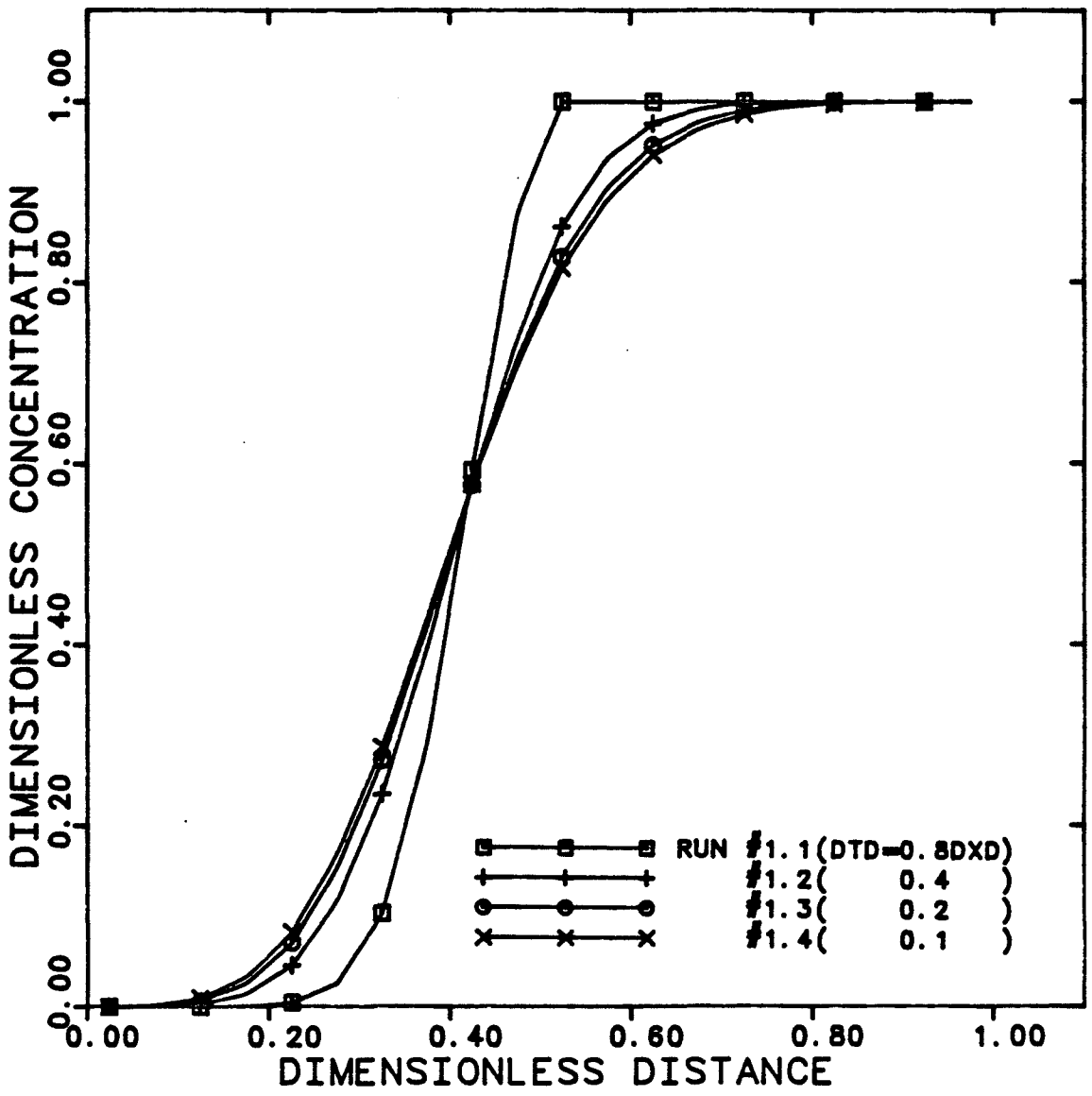

Fig. 4.2-1 Concentration profiles for Runs * 1.1 ---1.4 (all 40 G.B.) at 0.4 DPV.

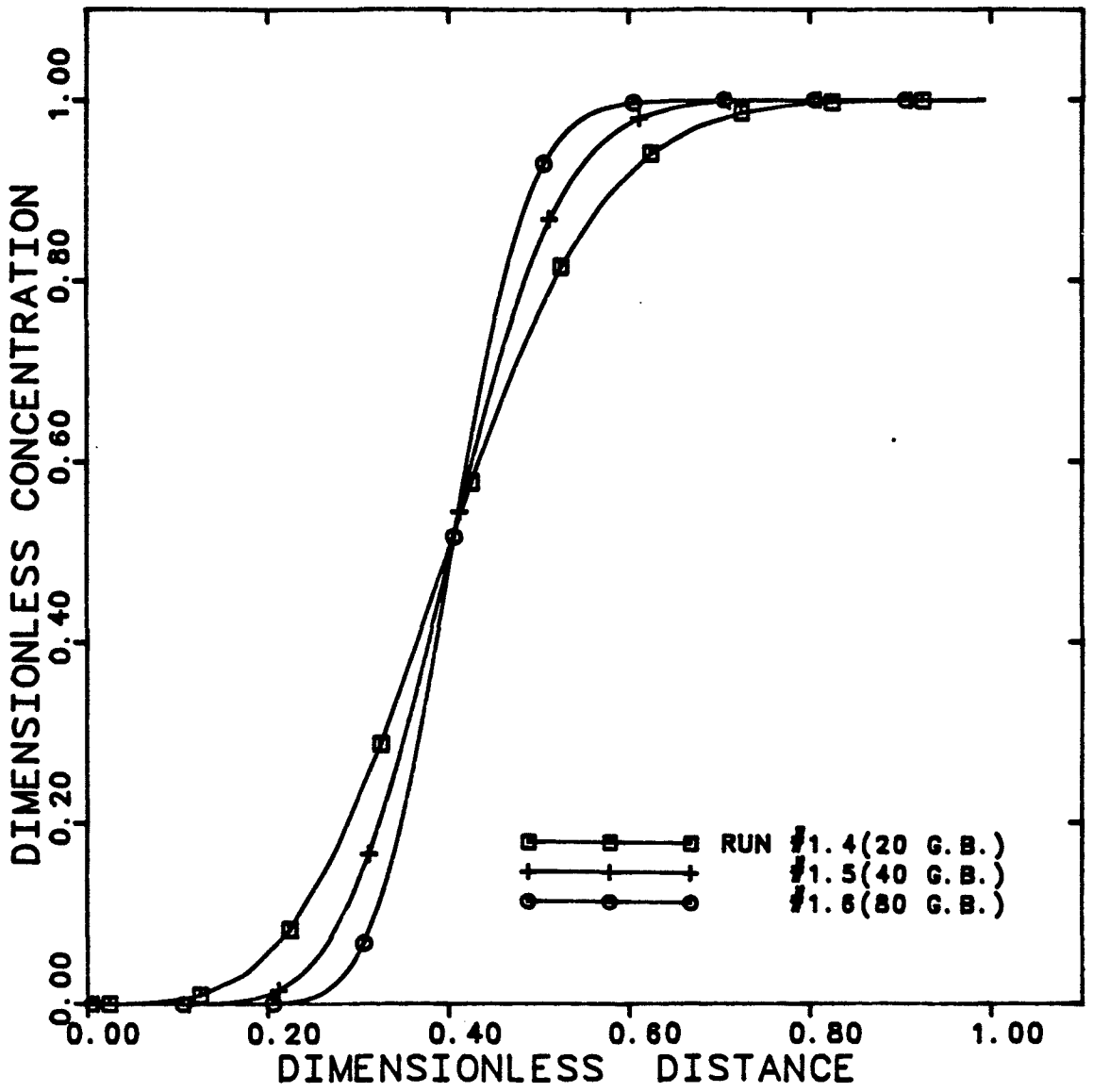

Fig. 4.2-2 Concentration profiles for Runs # 1.4 --- 1.6 (all $\Delta t_D = 0.1 \Delta X_D$) at 0.4 DPV.

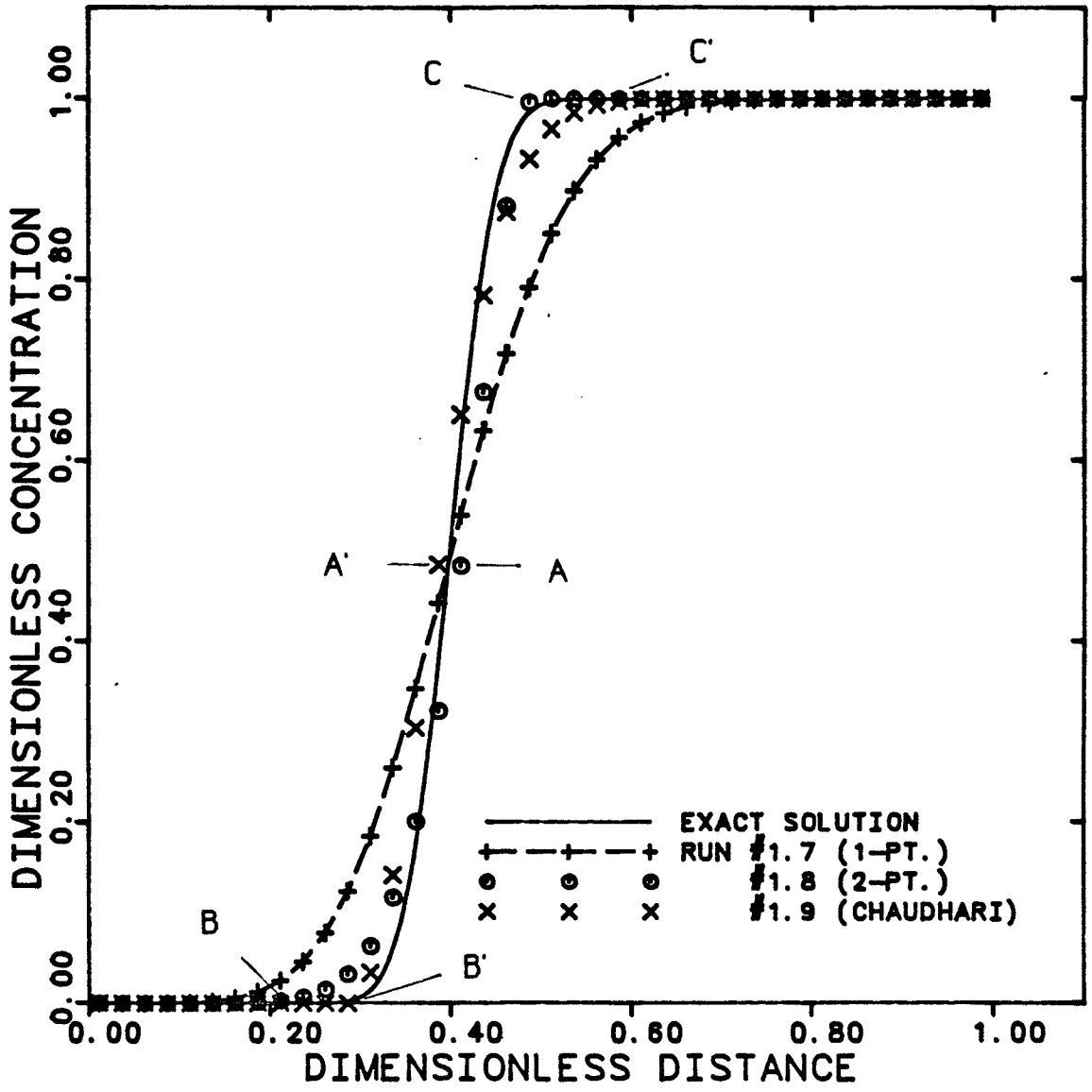

Fig. 4.2-3 Concentration profiles for Runs # 1.7 --- 1.9 ($N_{pe}{}^{P}$ = 500) at 0.4 DPV.

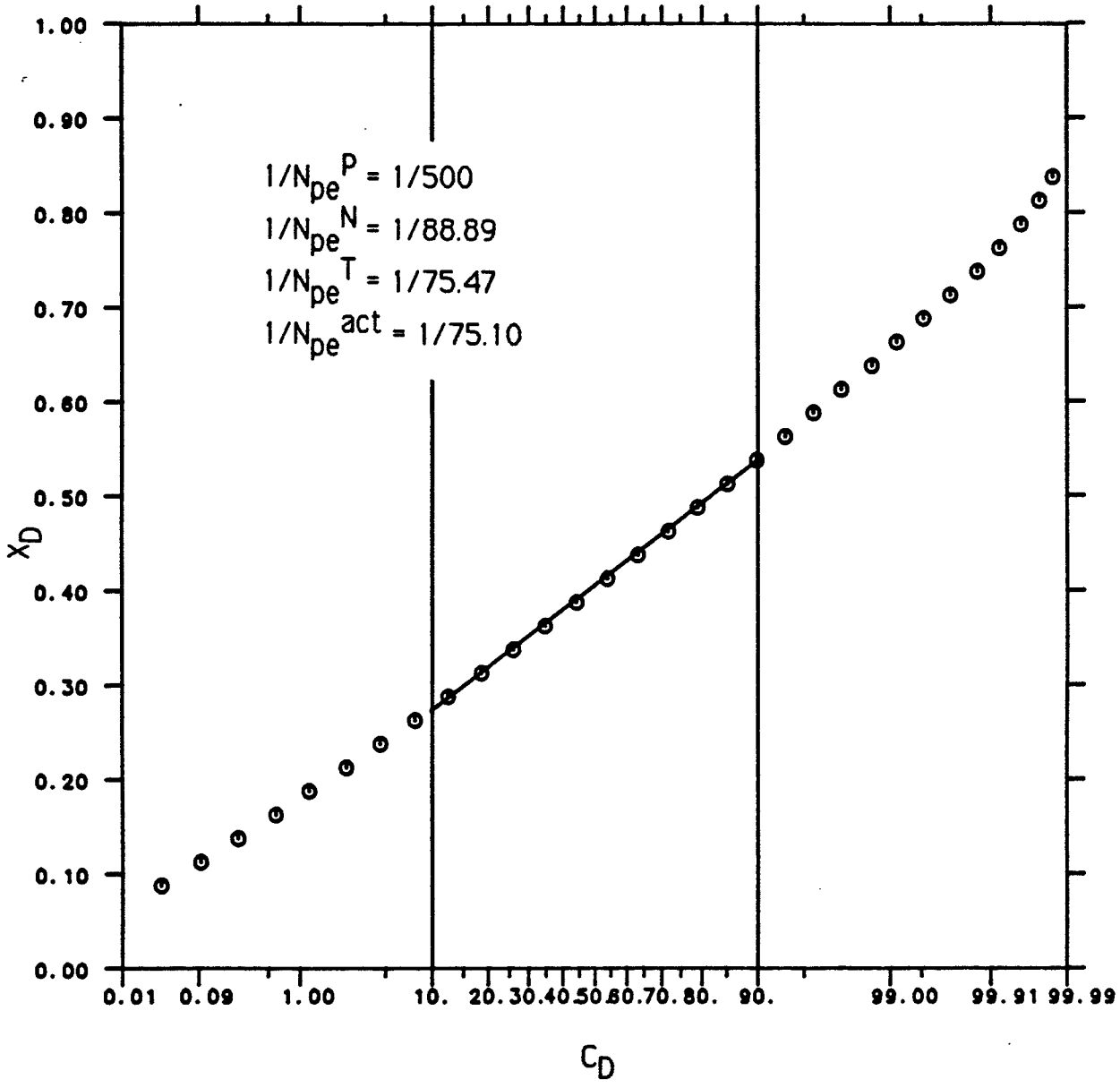

Fig. 4.2-4 Profile probability paper plot for Run # 1.7 (single-point) at 0.4 DPV.

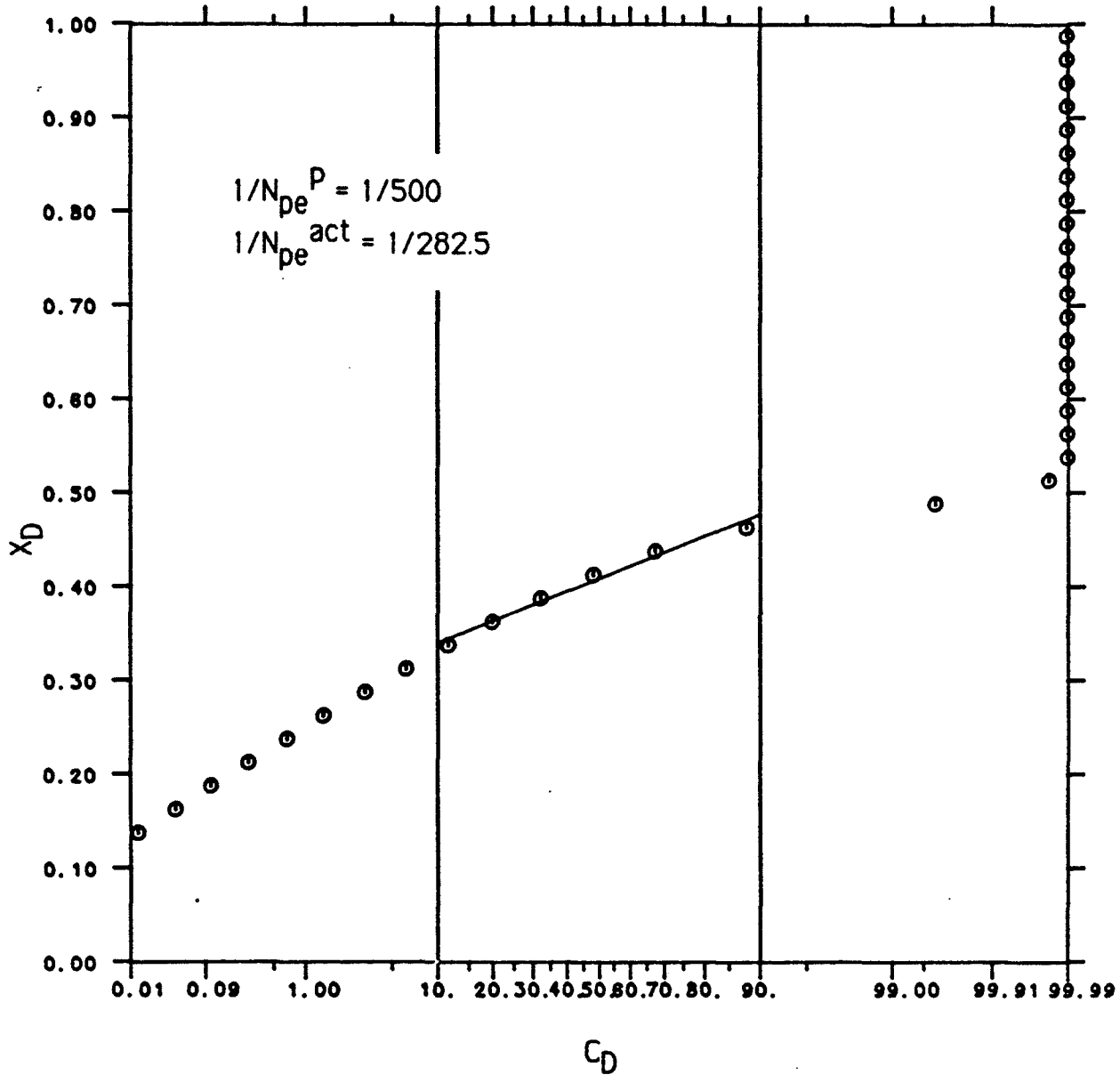

Fig. 4.2-5 Profile probability paper plot for Run # 1.8 (two-point) at 0.4 DPV.

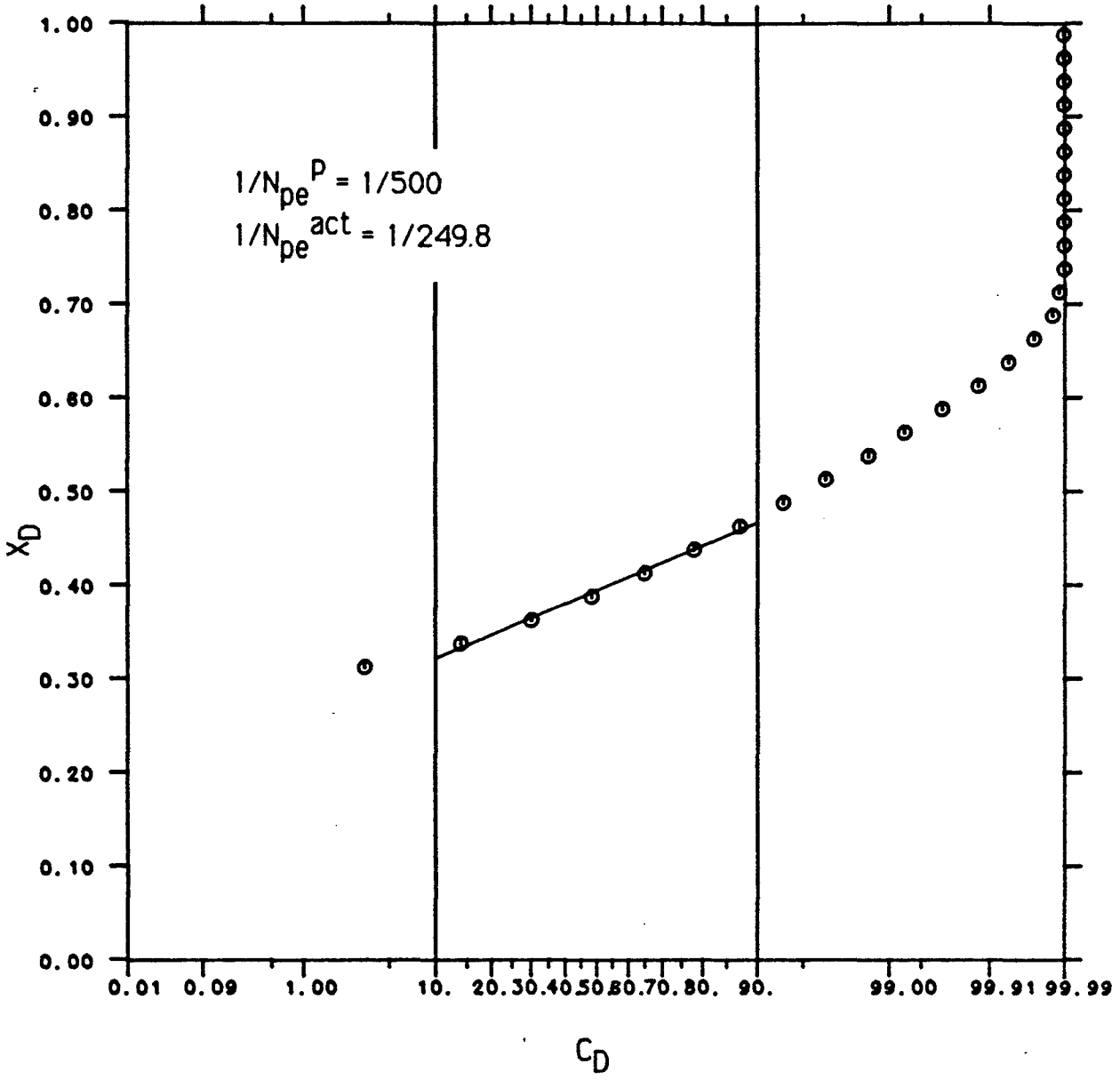

Fig. 4.2-6 Profile probability paper plot for Run # 1.9 (Chaudhari) at 0.4 DPV.

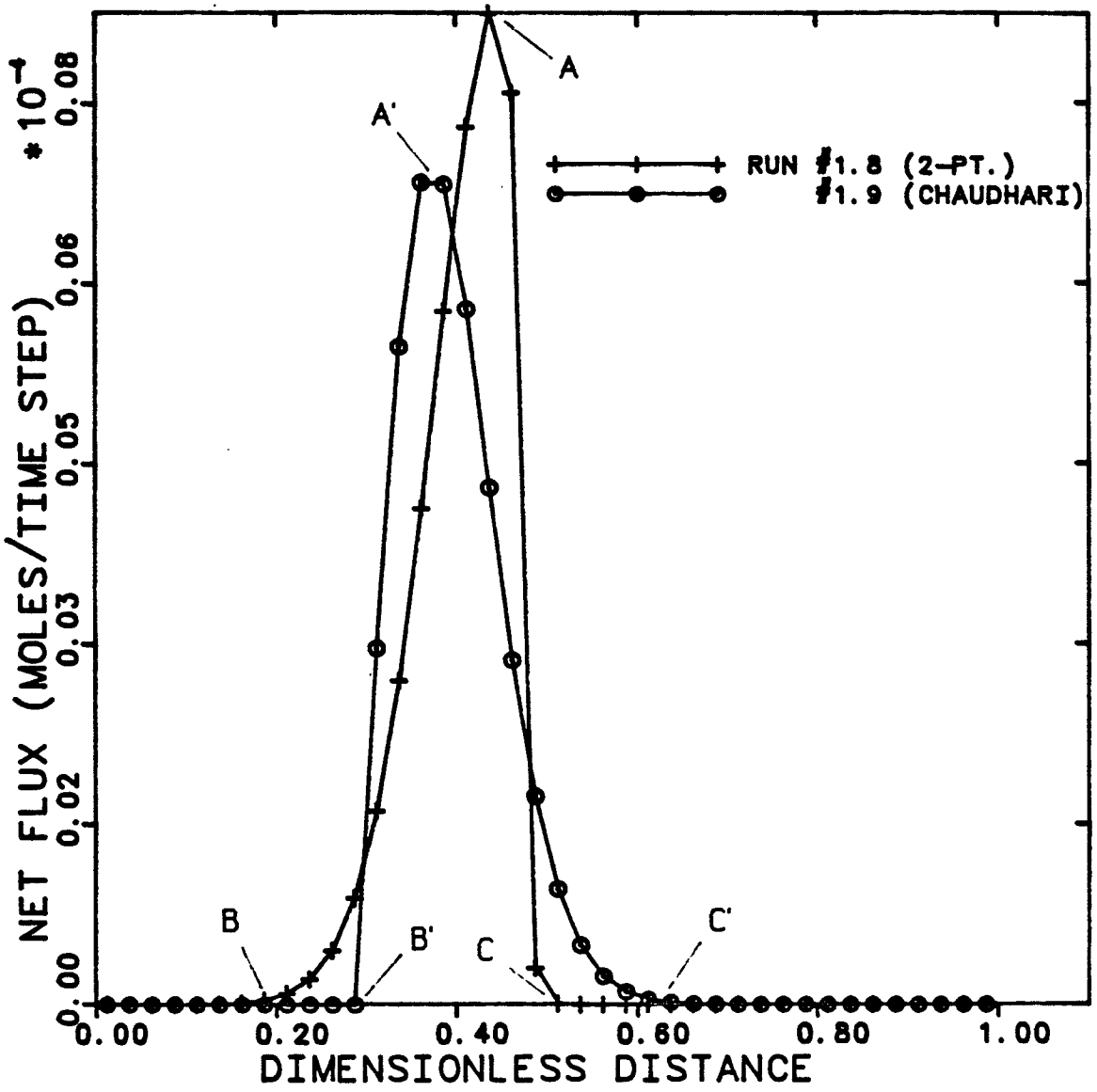

Fig. 4.2-7 Net flux profiles for Runs # 1.8 and 1.9 at 0.4 DPV.

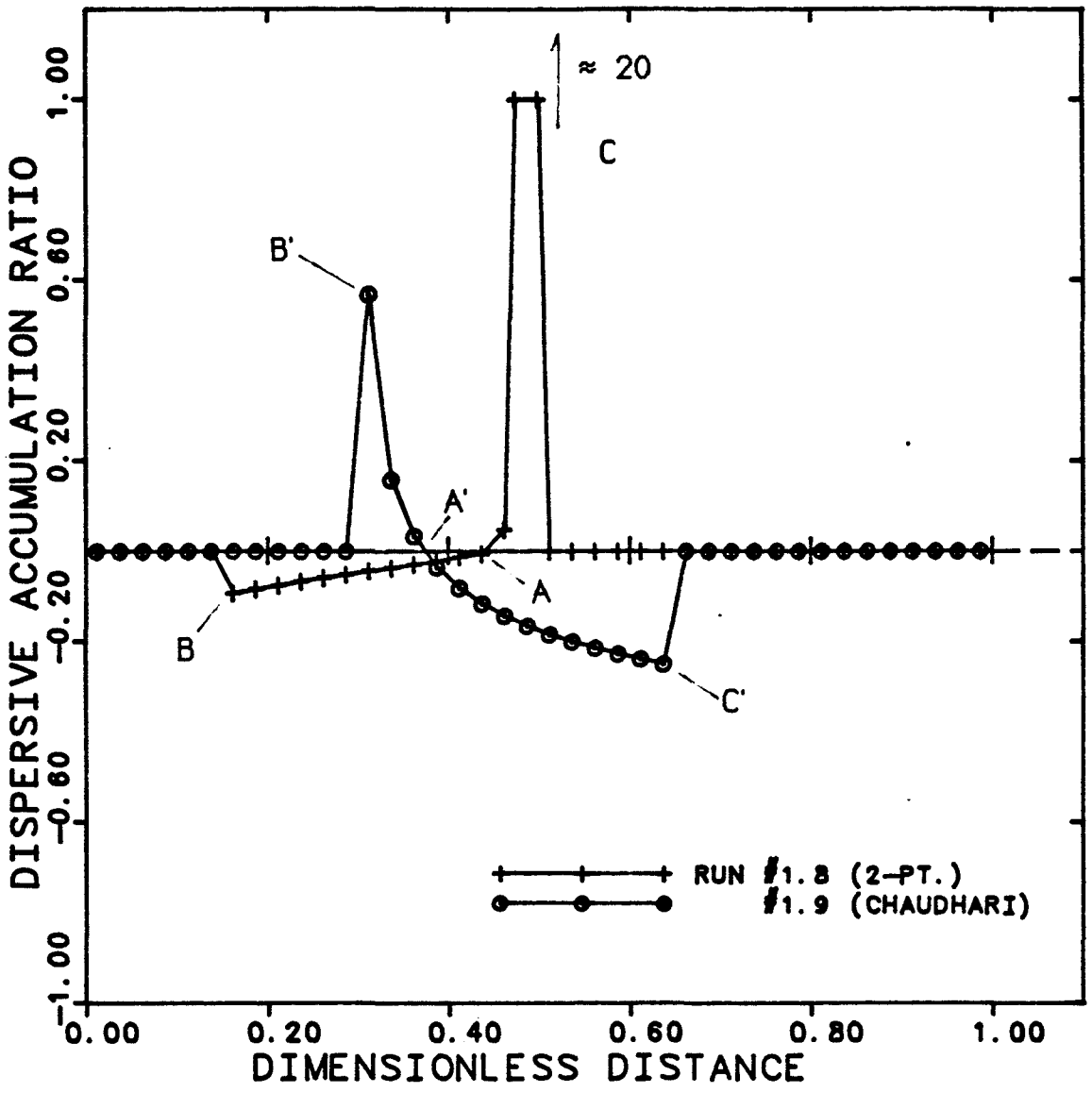

Fig. 4.2-8 Dispersive accumulation ratio profiles for Runs # 1.8 and 1.9 at 0.4 DPV.

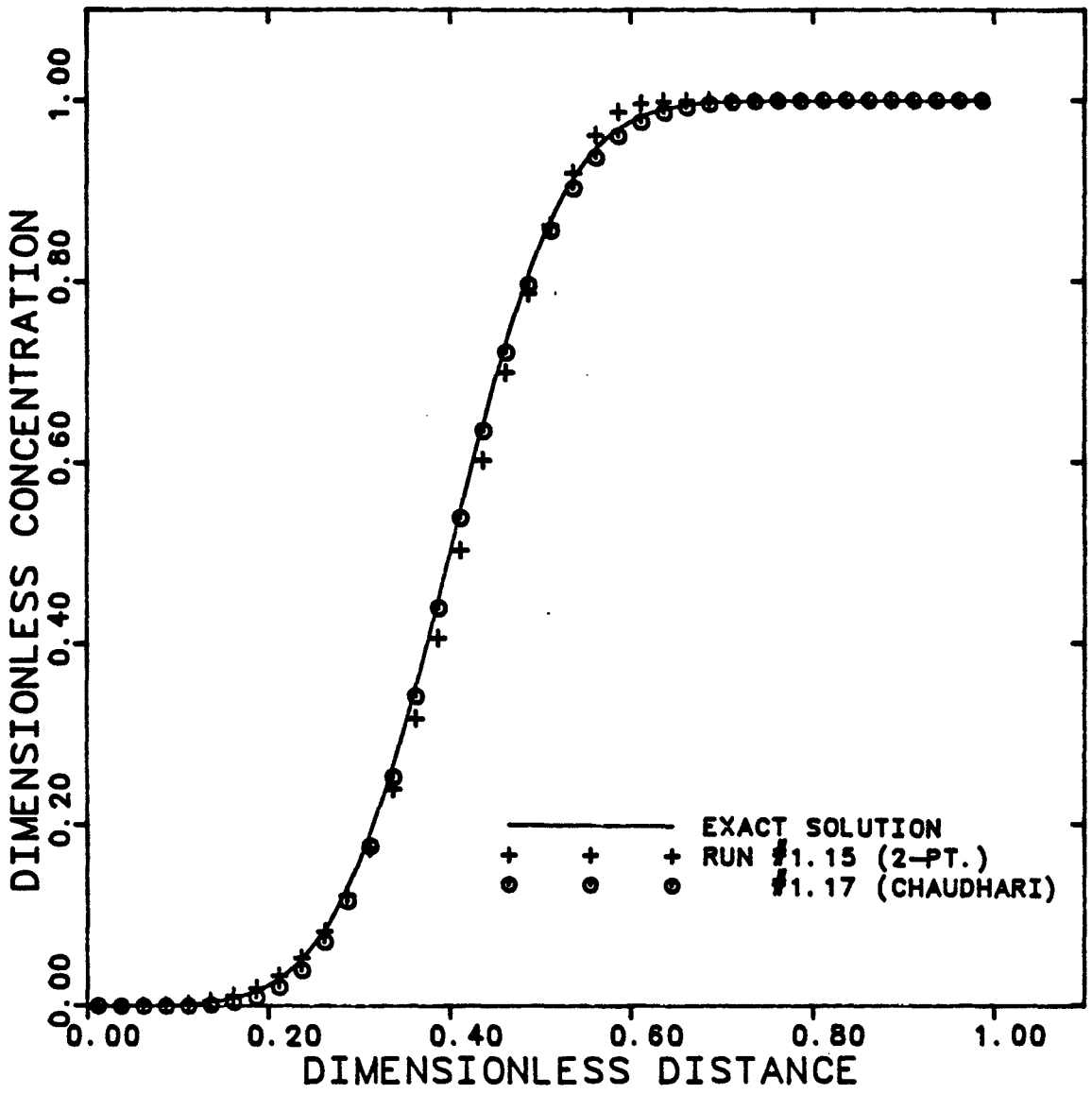

Fig. 4.2-9 Concentration profiles for Runs # 1.15 and 1.17 ($N_{pe}^{P} = 80$) at 0.4 DPV.

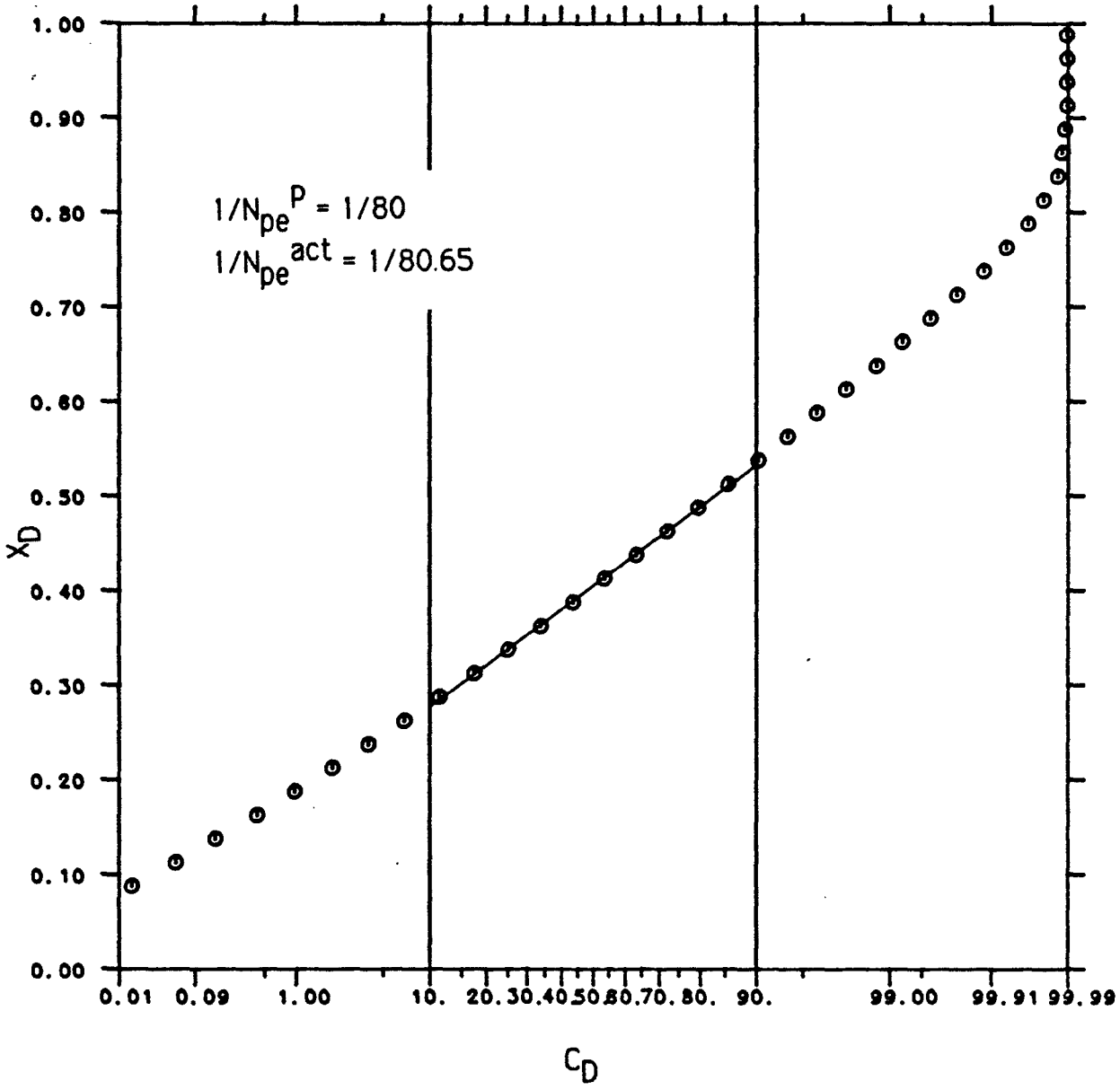

Fig. 4.2-10 Profile probability paper plot for Run * 1.17 (Chaudhari) at 0.4 DPV.

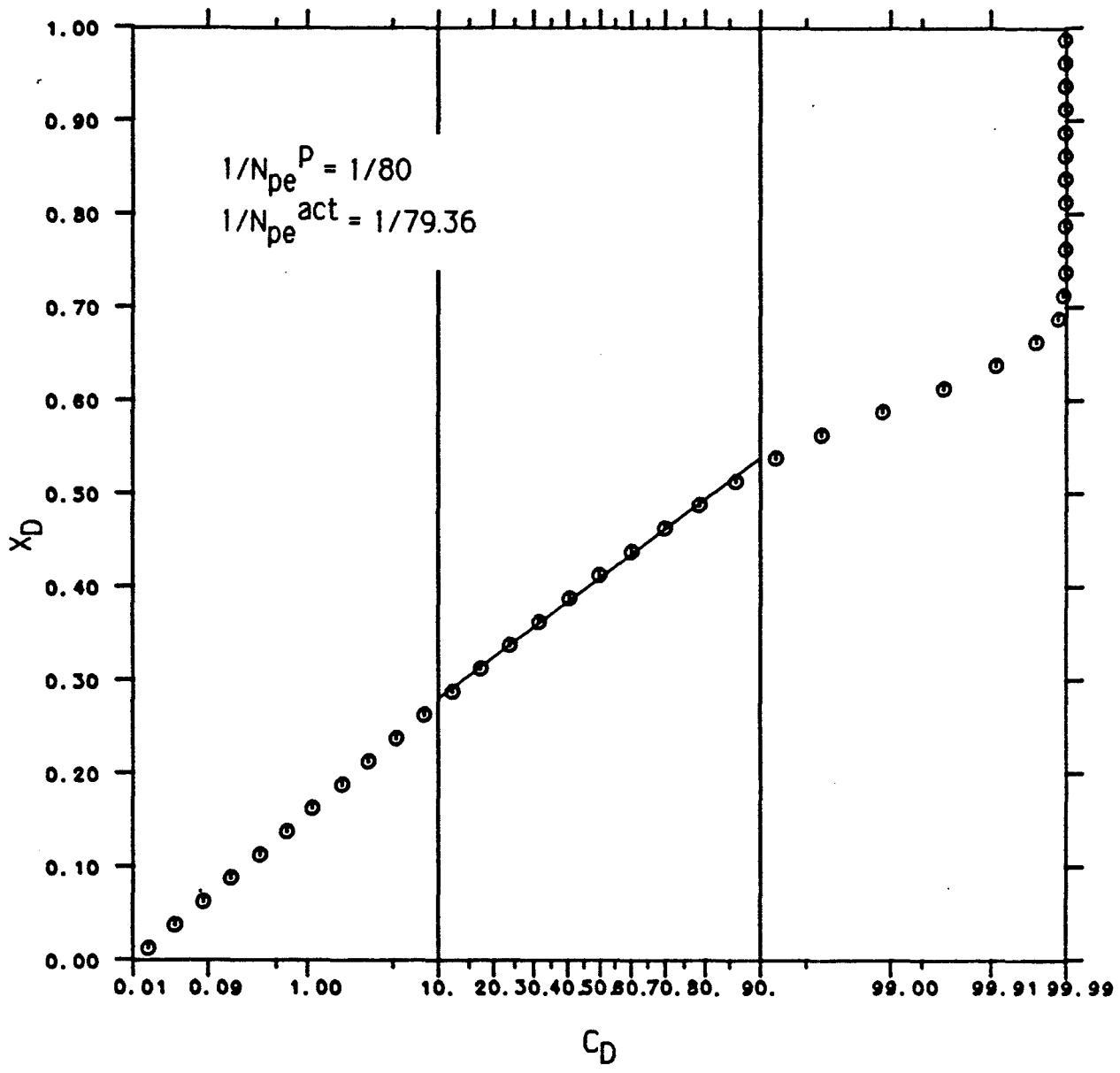

Fig. 4.2-11 Profile probability paper plot for Run # 1.15 (two-point) at 0.4 DPV.

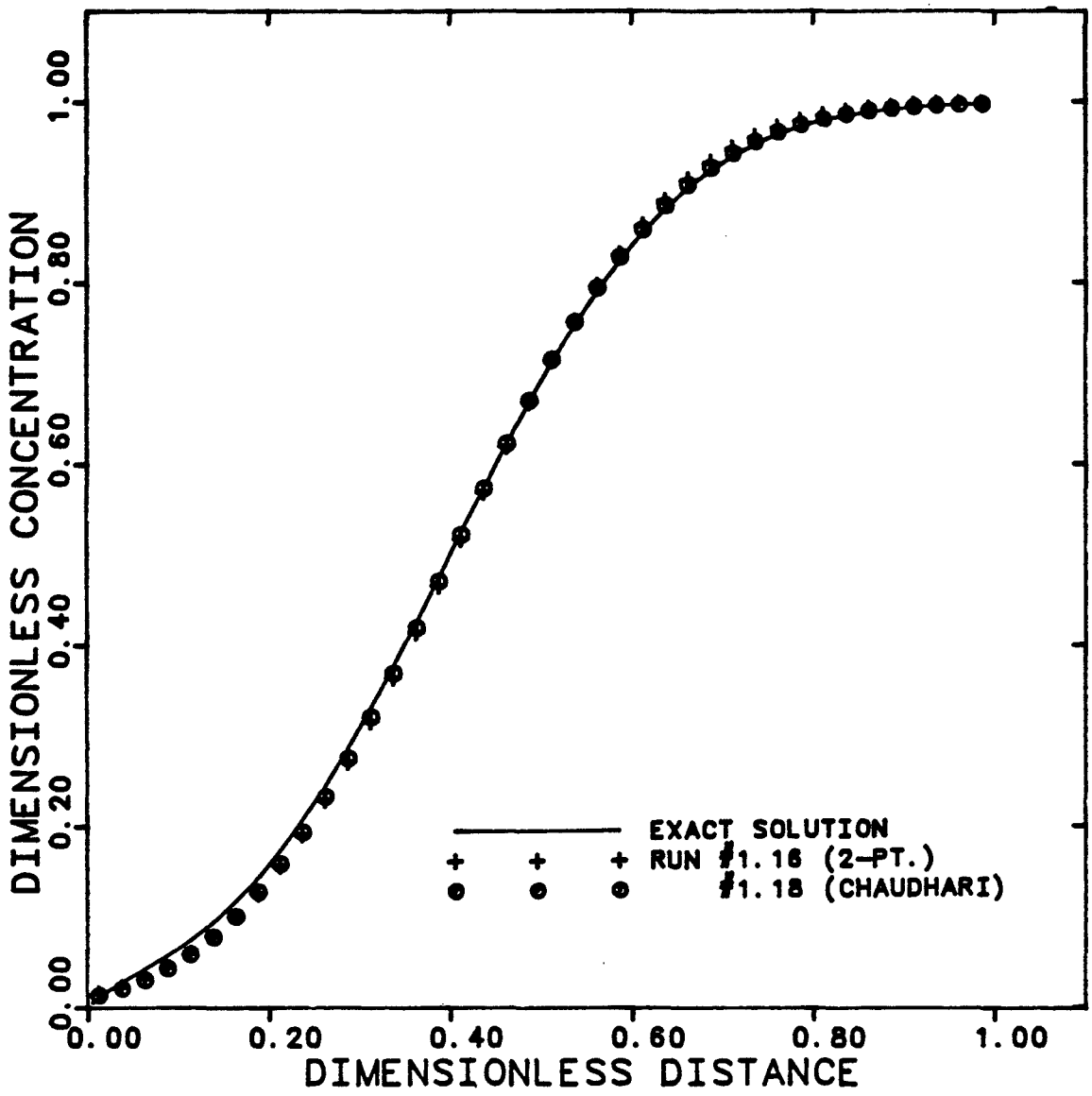

Fig. 4.2-12 Concentration profiles for Runs # 1.16 and 1.18 ($N_{pe}{}^{P} = 20$) at 0.4 DPV.

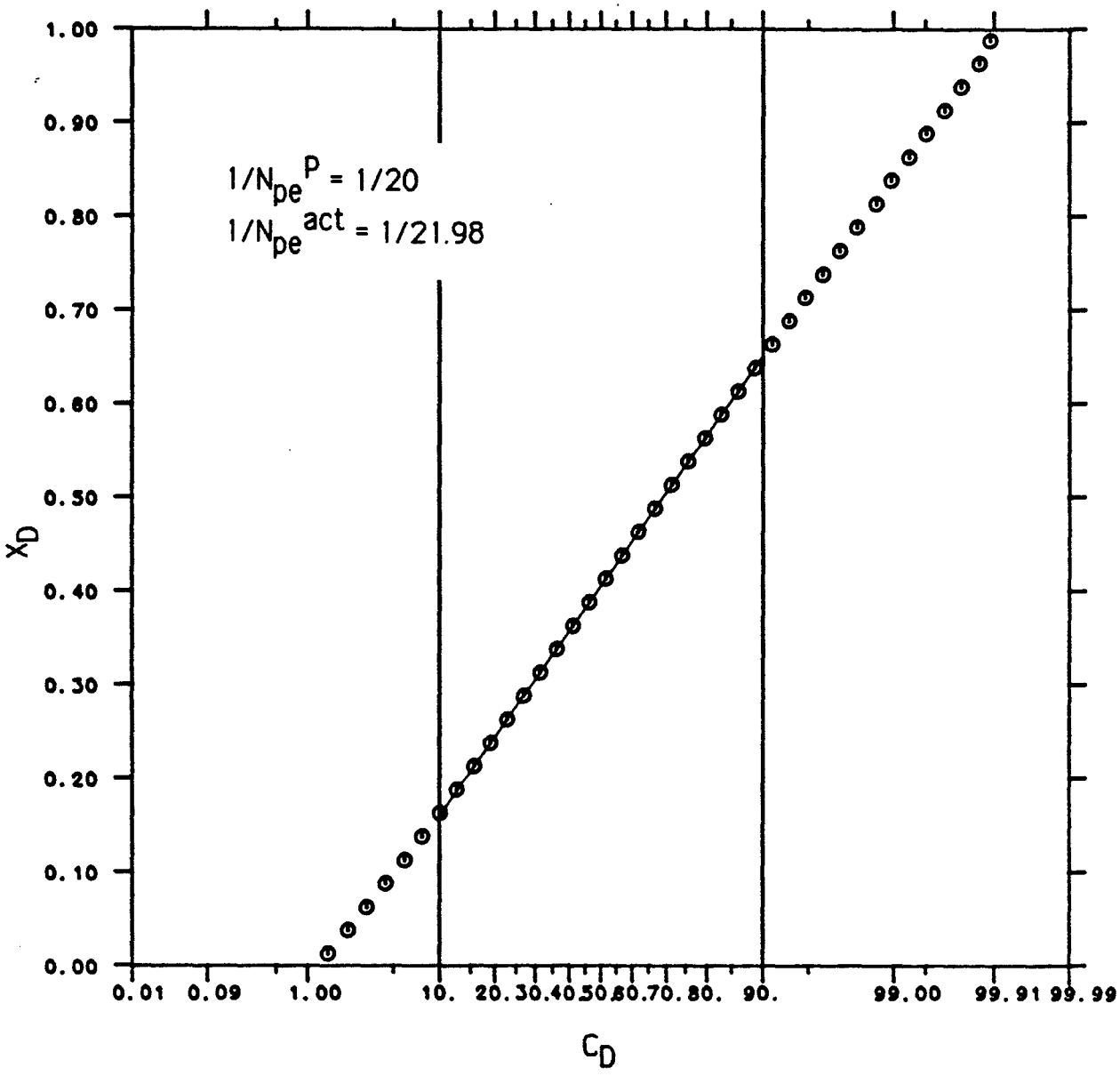

Fig. 4.2-13 Profile probability paper plot for Run * 1.16 (two-point) at 0.4 DPV.

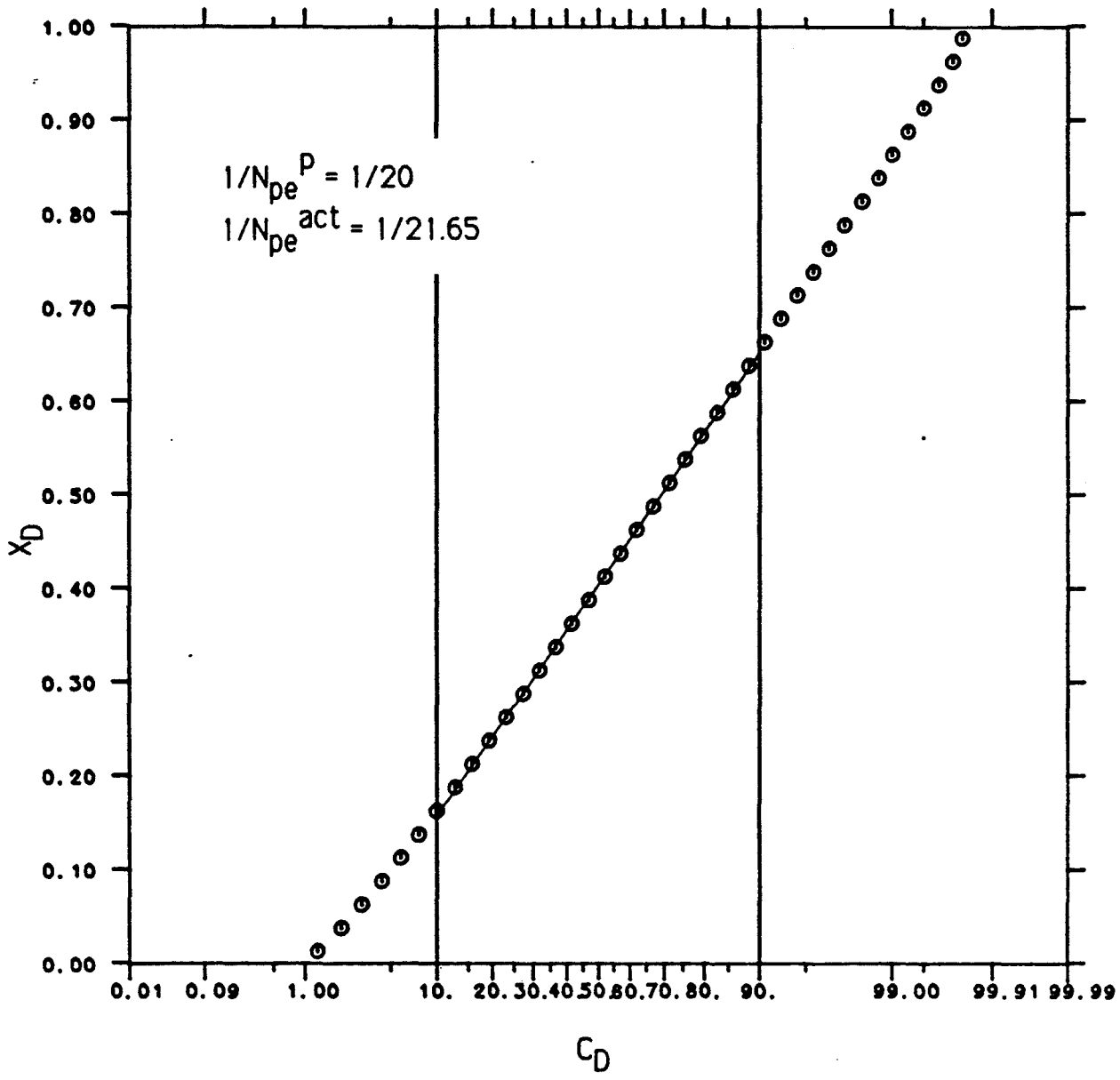

Fig. 4.2-14 Profile probability paper plot for Run # 1.18 (Chaudhari) at 0.4 DPV.

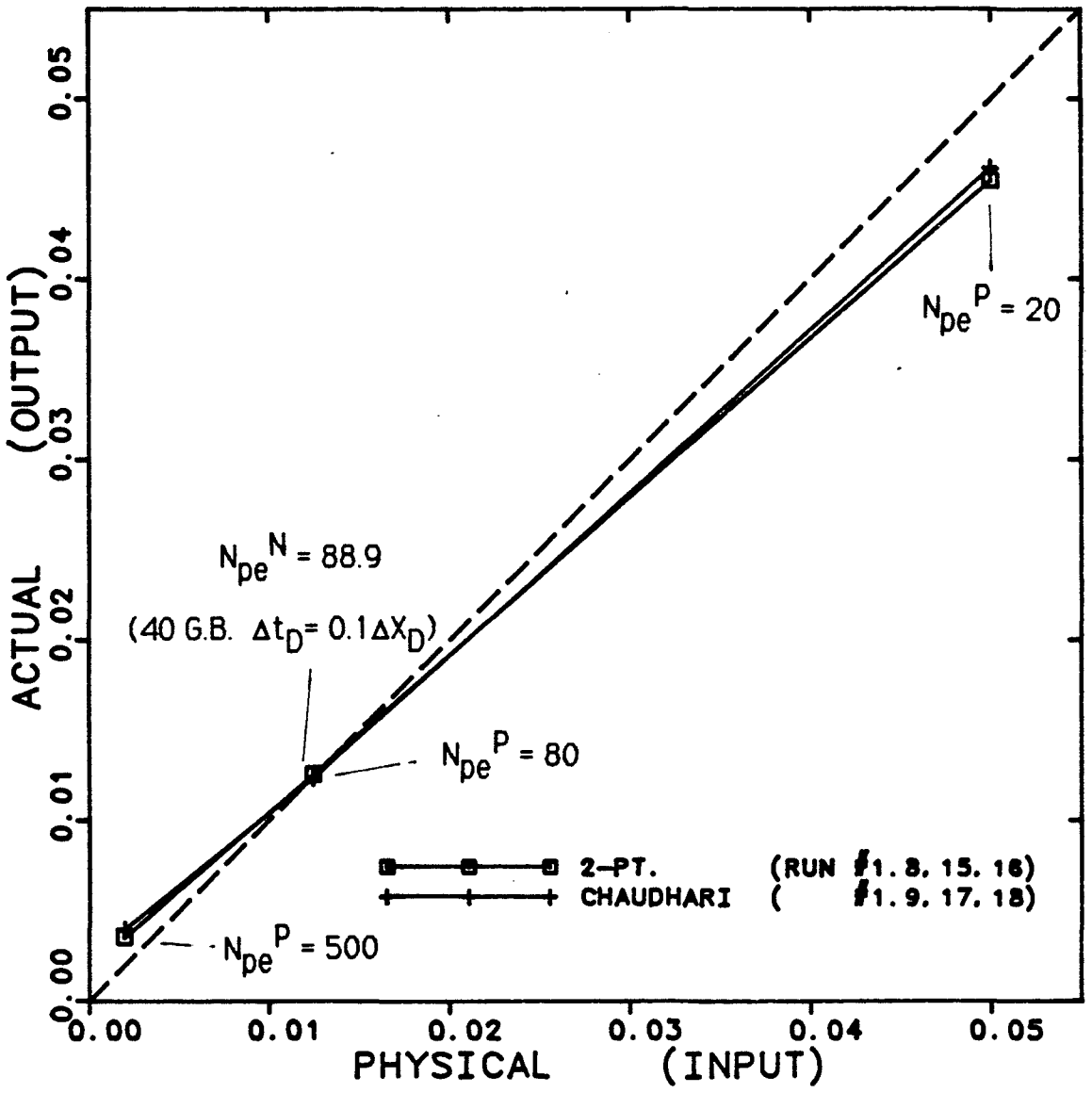

Fig. 4.2-15 Comparison of physical(input) and actual(output) dimensionless dispersivity ($1/N_{pe}$) for Runs # 1.8, 1.9, 1.15, 1.16, 1.17, 1.18.

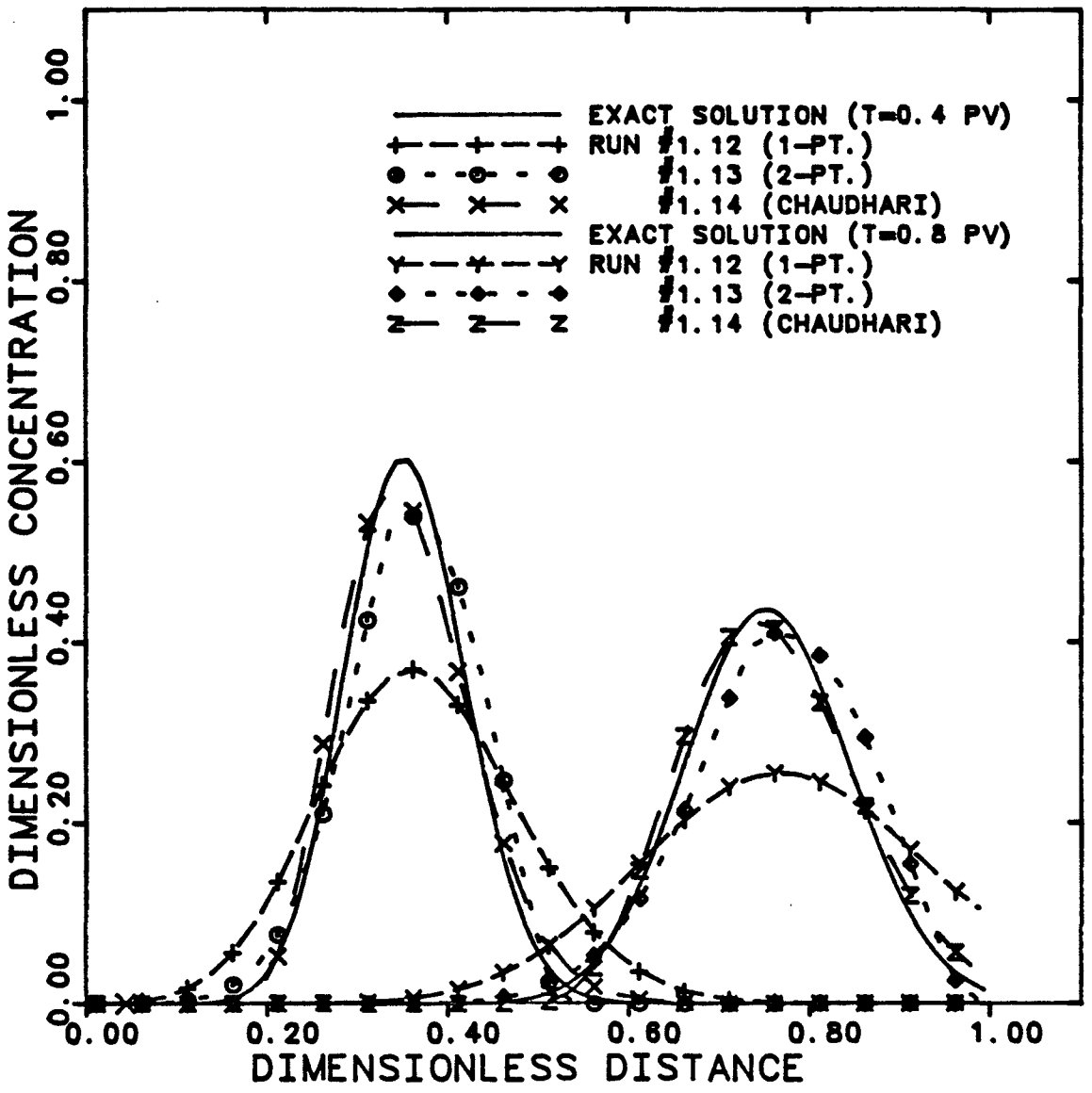

Fig. 4.2-16 Concentration profiles (slug) for Runs # 1.12 --- 1.14 at 0.4 and 0.8 DPV ($N_{pe}^{P} = 200$).

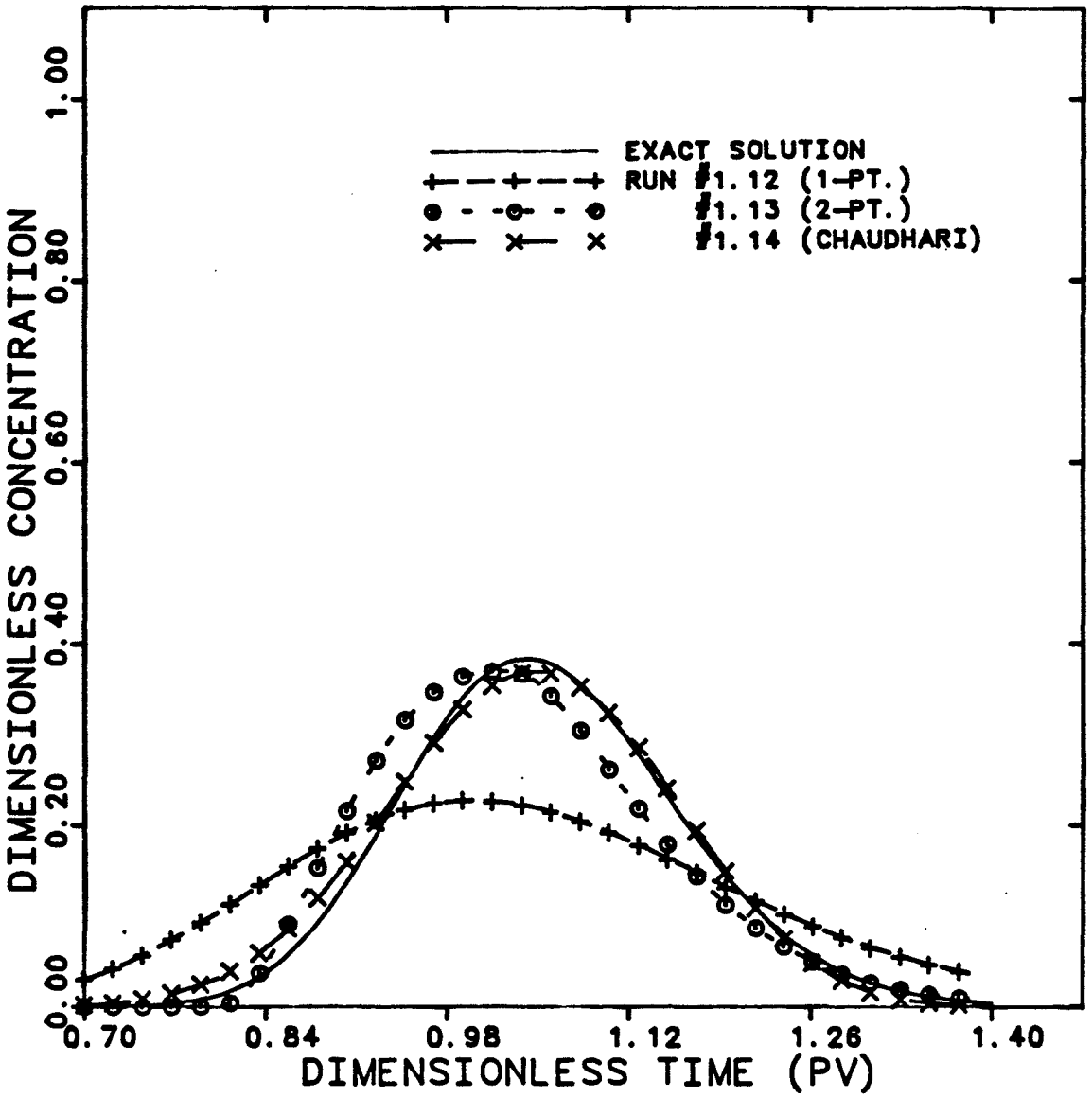

Fig. 4.2-17 Effluent histories for Runs # 1.12 --- 1.14 (N_{pe}^{P} = 200).

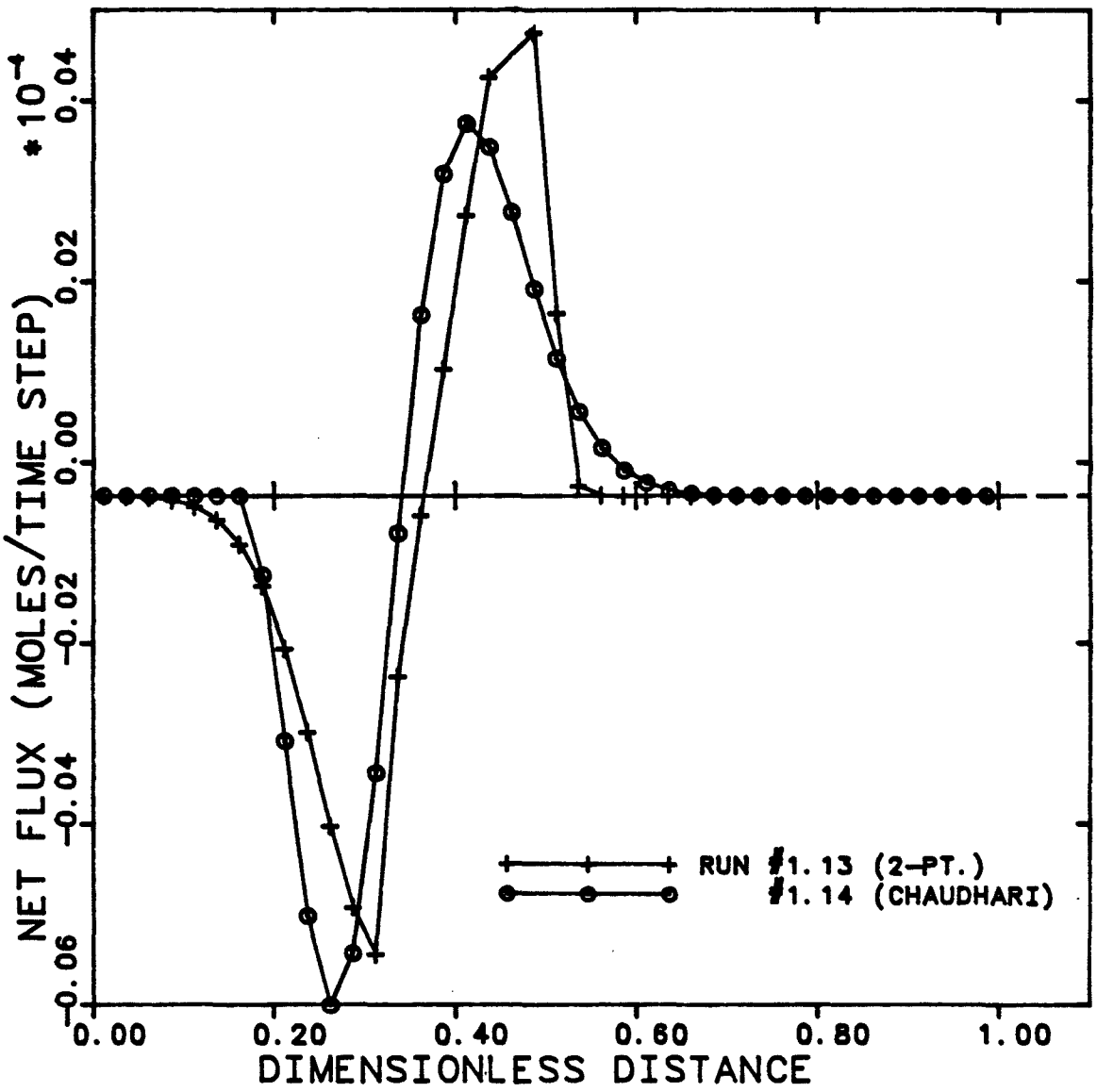

Fig. 4.2-18 Net flux profiles for Runs # 1.13 and 1.14 at 0.4 DPV.

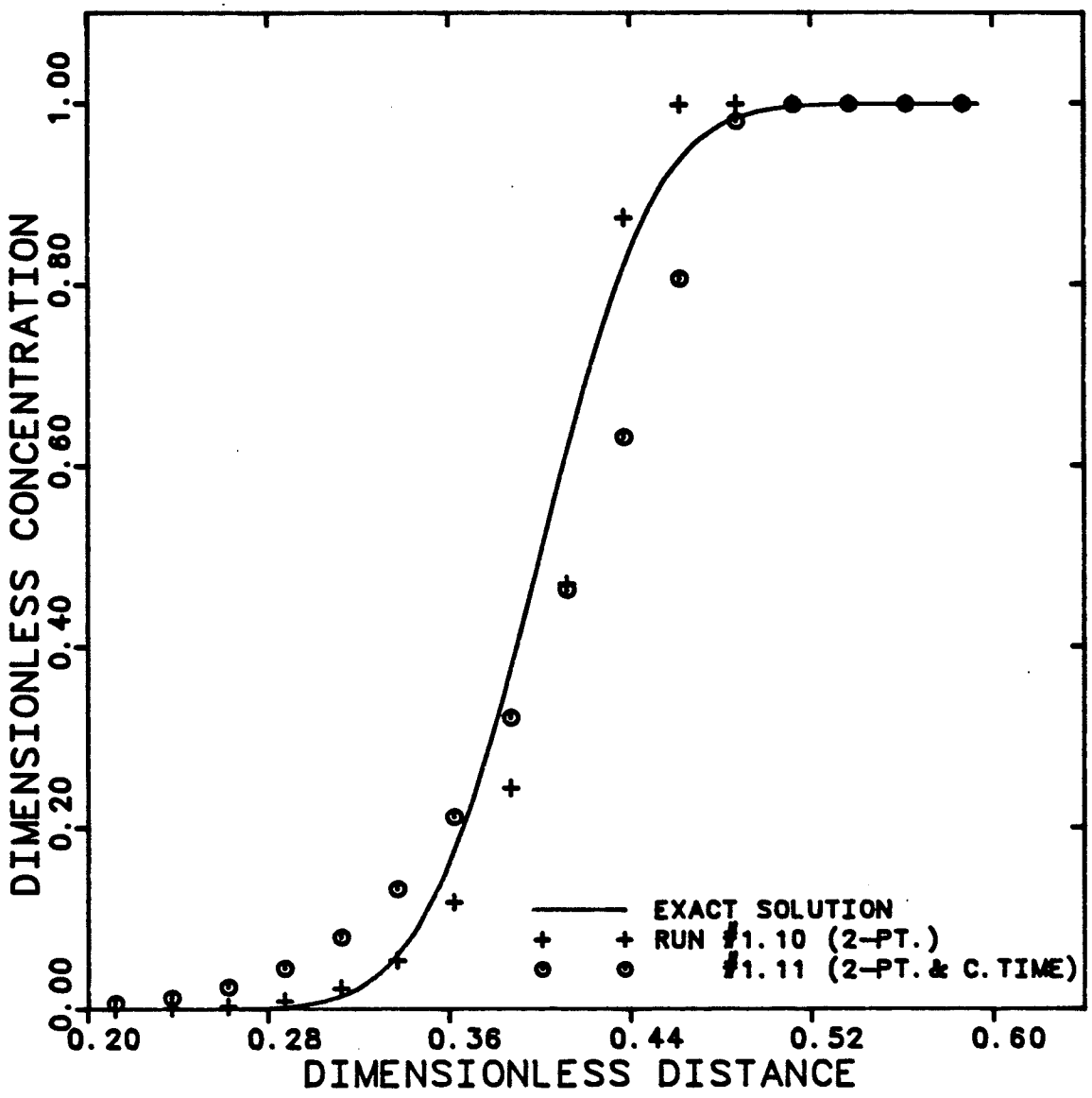

Fig. 4.2-19 Concentration profiles for Runs # 1.10 and 1.11 ($N_{pe}{}^{P} = 500$) at 0.4 DPV.

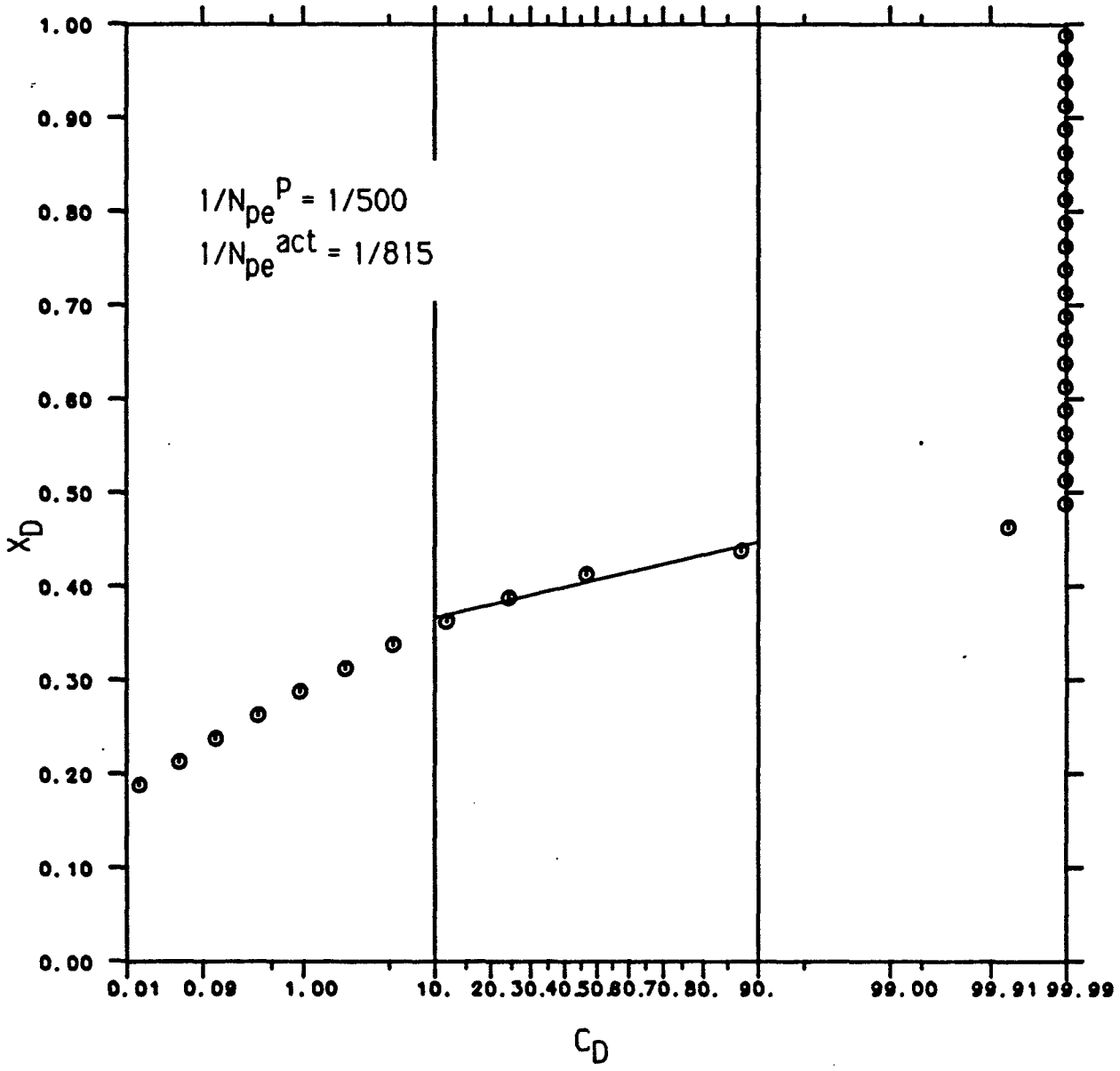

Fig. 4.2-20 Profile probability paper plot for Run # 1.10 (two-point) at 0.4 DPV.

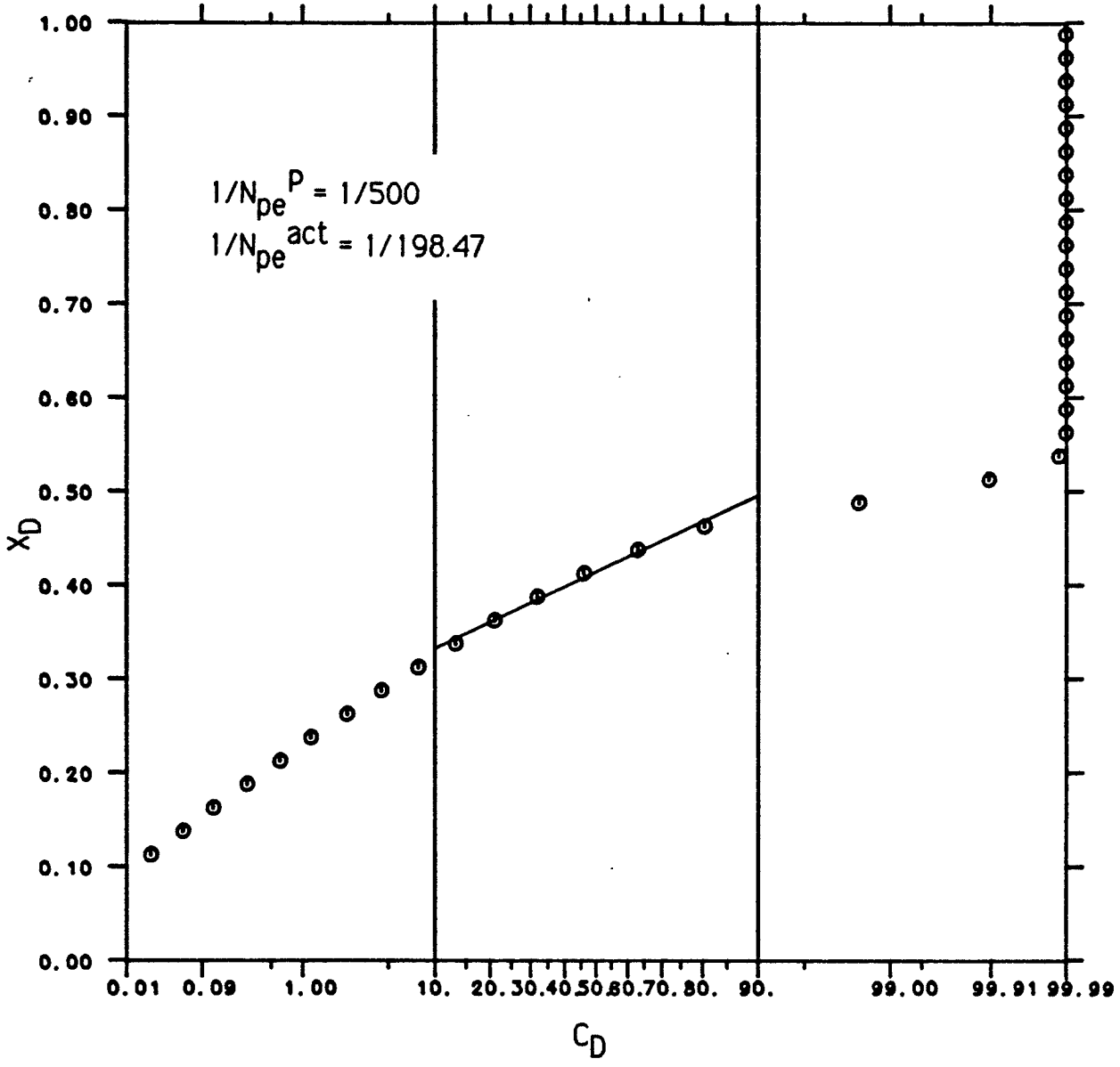

Fig. 4.2-21 Profile probability paper plot for Run # 1.11 (two-point plus Chaudhari's time treatment) at 0.4 DPV.

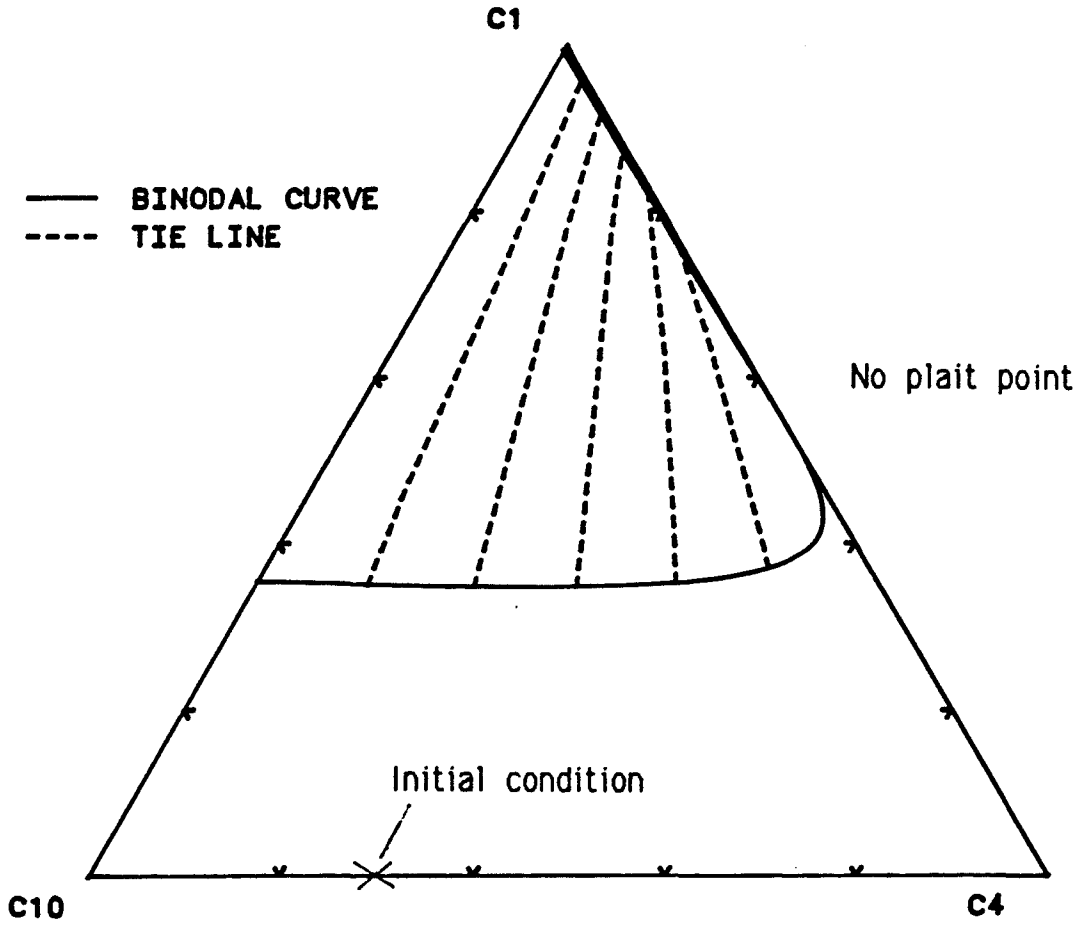

Fig. 4.3-1 Ternary diagram for methane-butane-decane system at 1500 psia and 200 F.

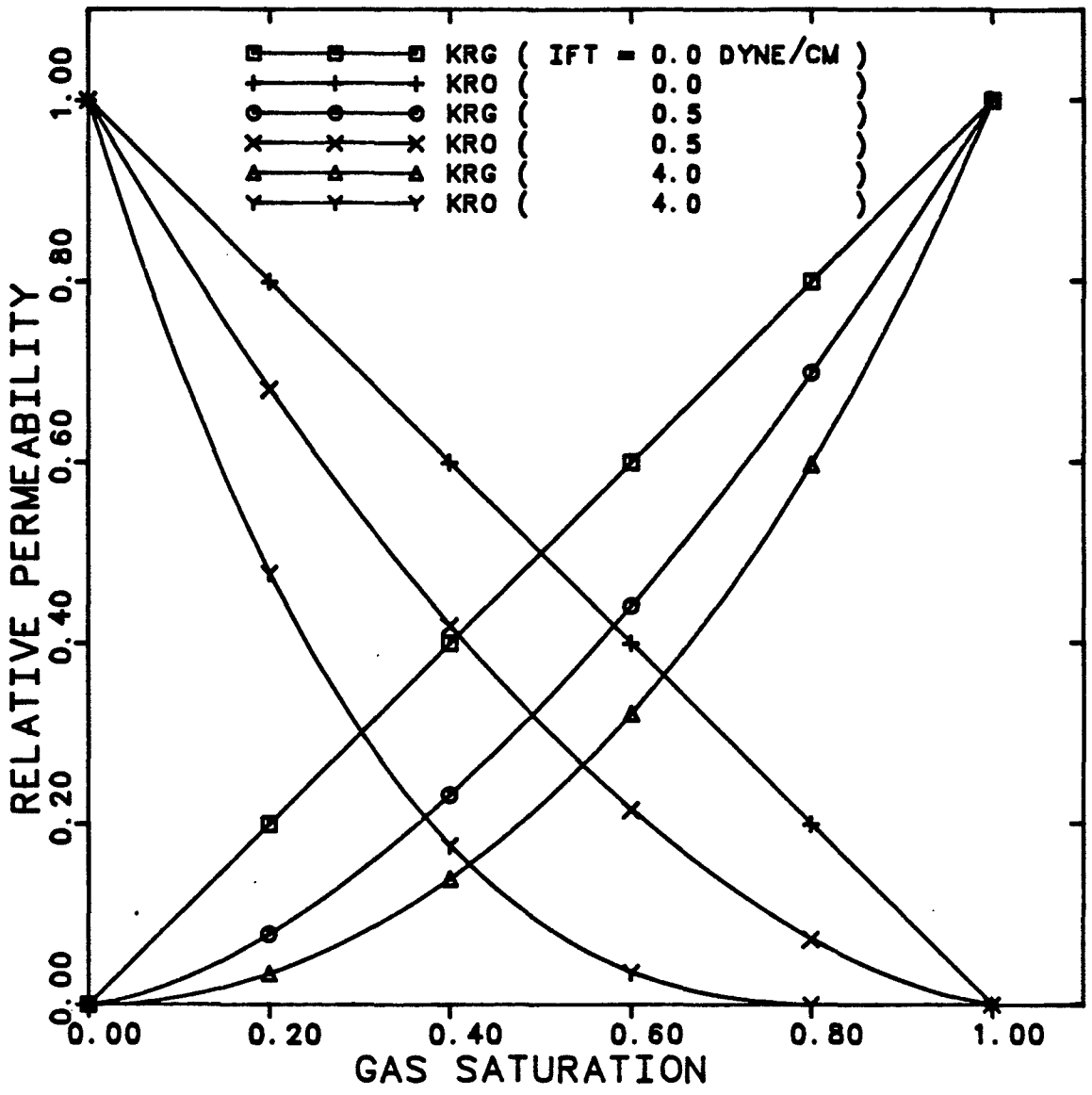

Fig. 4.3-2 Gas-oil relative permeability functions for Class-2 runs.

RUN #2.1(1-PT.)

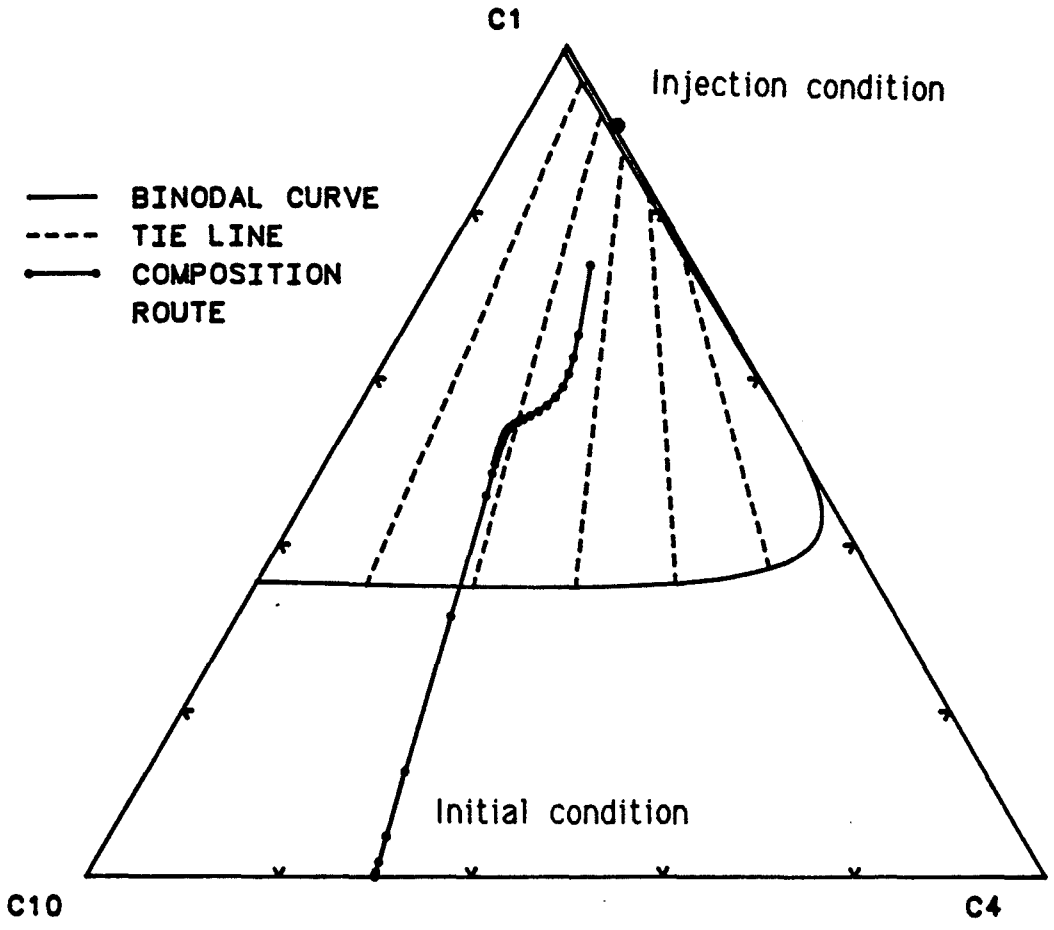

TEMP. 200 (F)
PRESS. 1500 (PSIA)

Fig. 4.3-3 Composition route for Run # 2.1 (single-point) at 0.6 DPV.

RUN #2.2(COMP. 2-PT.)

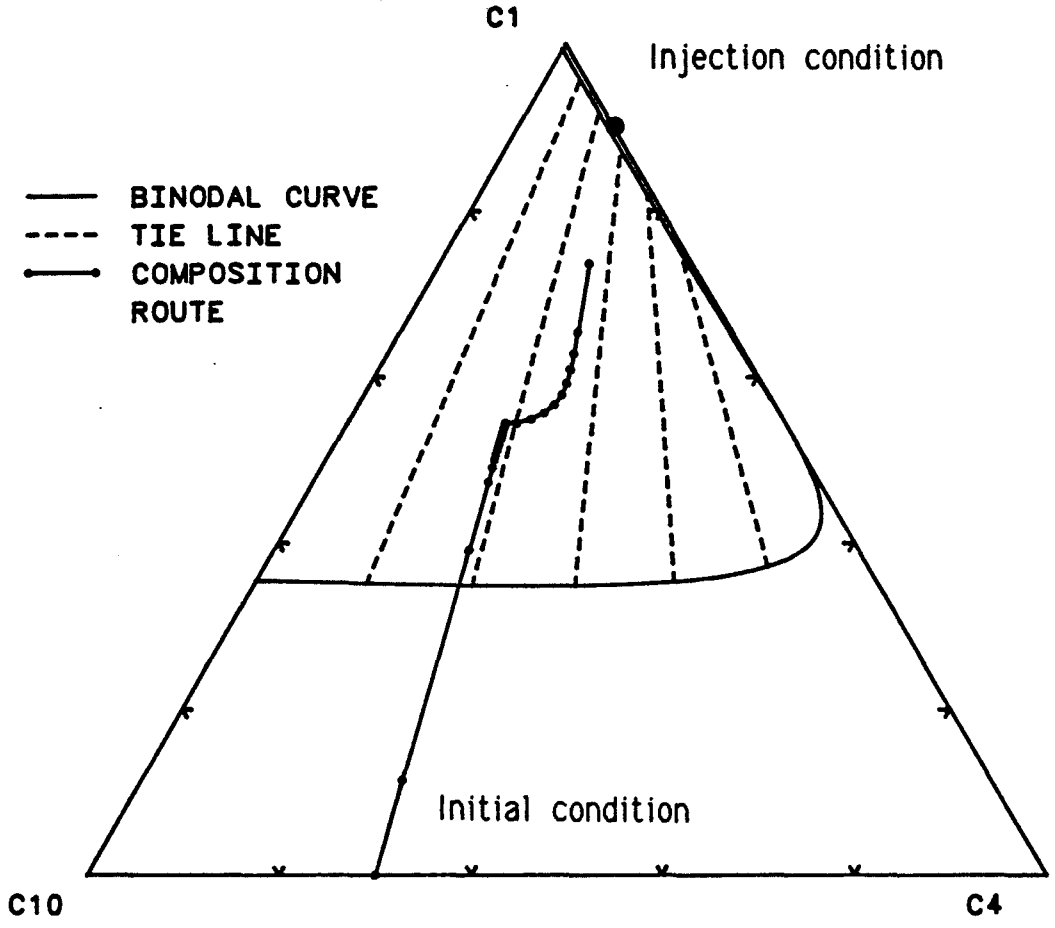

TEMP. 200 (F)
PRESS. 1500 (PSIA)

Fig. 4.3-4 Composition route for Run # 2.2 ("Comp. 2-Point") at 0.6 DPV.

RUN #2.3(ALL 2-PT.)

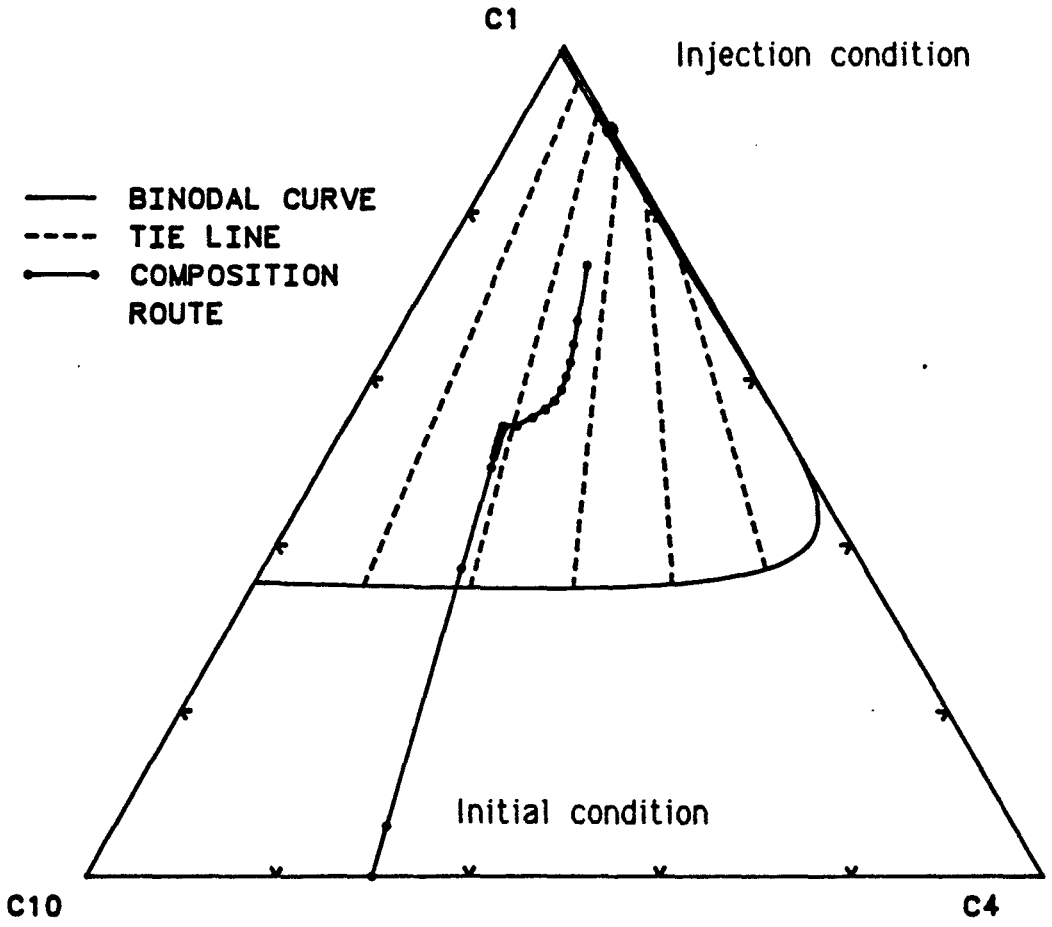

TEMP. 200 (F)
PRESS. 1500 (PSIA)

Fig. 4.3-5 Composition route for Run # 2.3 ("All 2-POint") at 0.6 DPV.

RUN #2.4(CHAUDHARI)

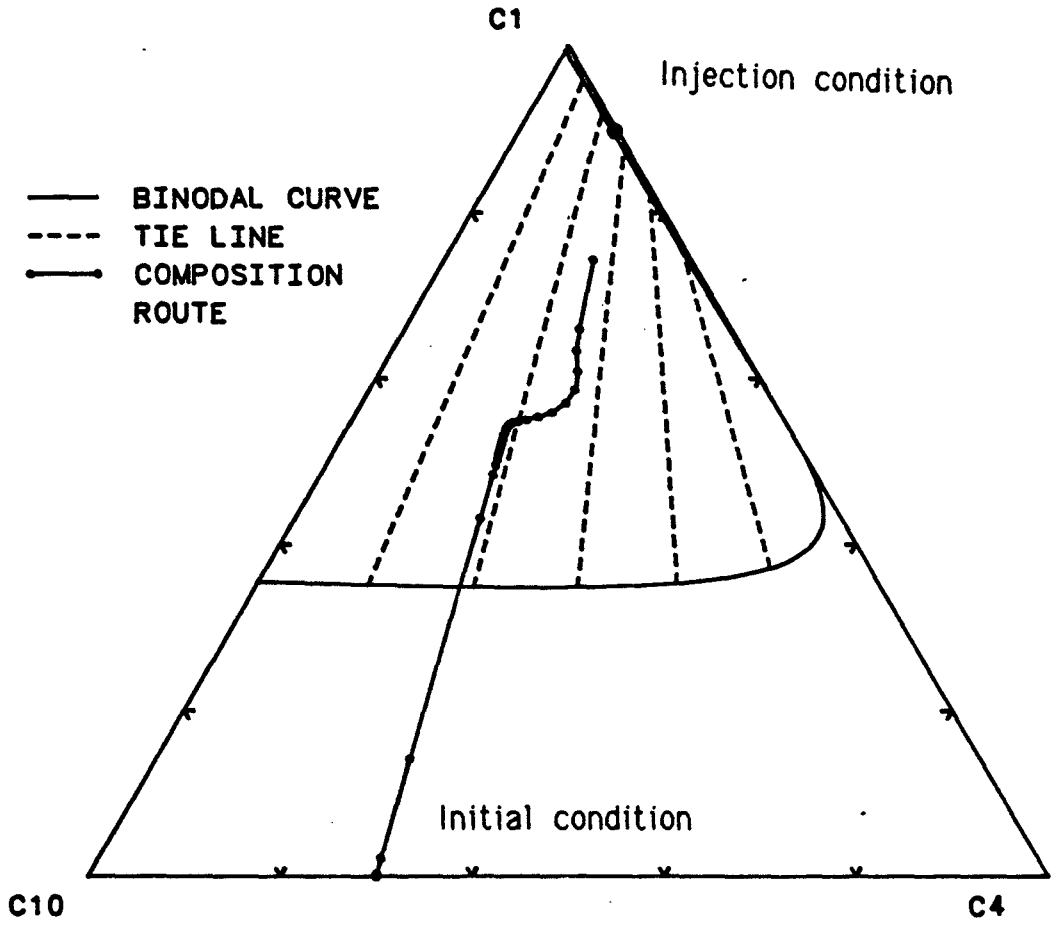

TEMP. 200 (F)
PRESS. 1500 (PSIA)

Fig. 4.3-6 Composition route for Run # 2.4 ("Chaudhari") at 0.6 DPV.

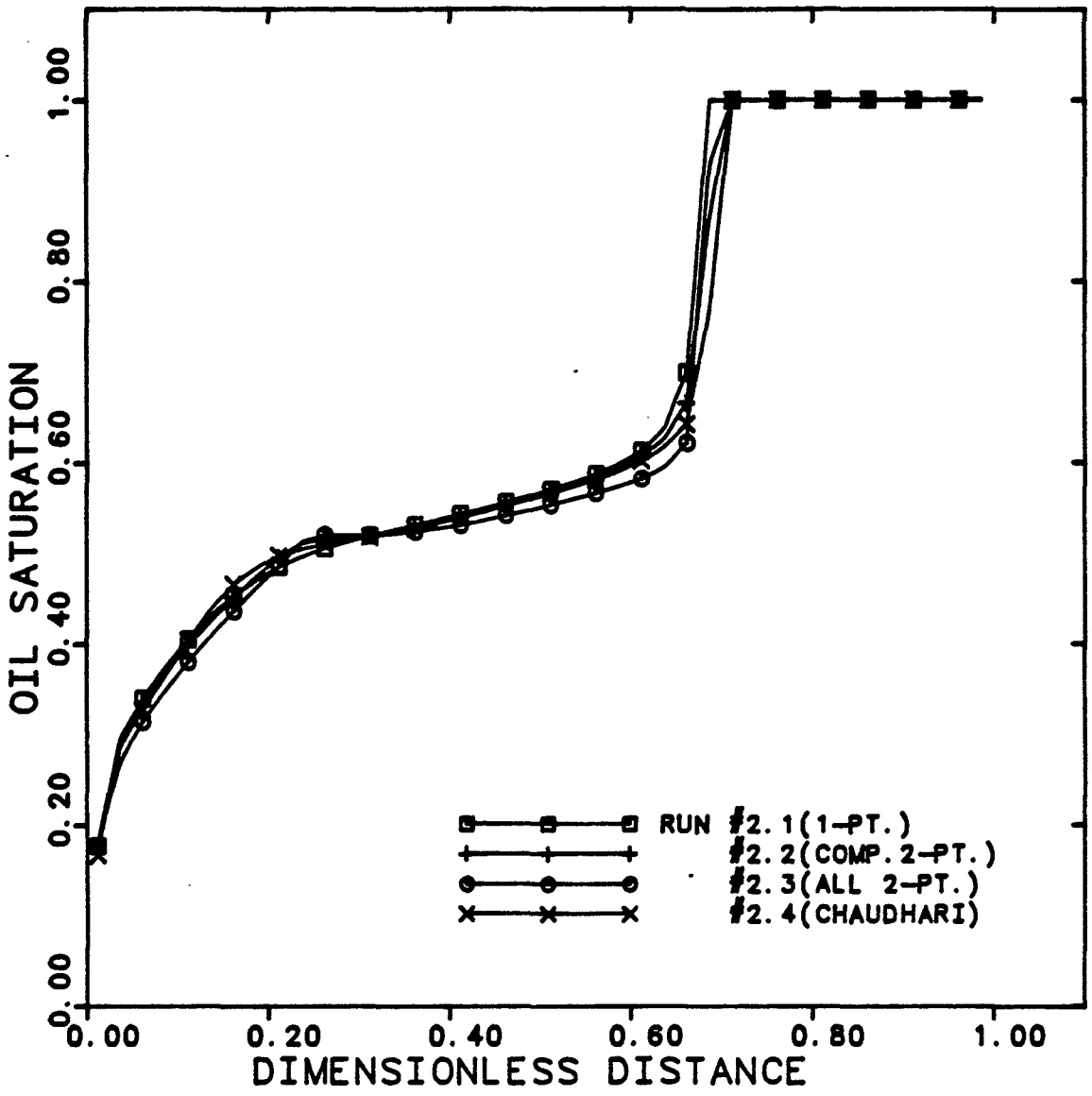

Fig. 4.3-7 Oil saturation profiles for Runs # 2.1 --- 2.4 at 0.6 DPV.

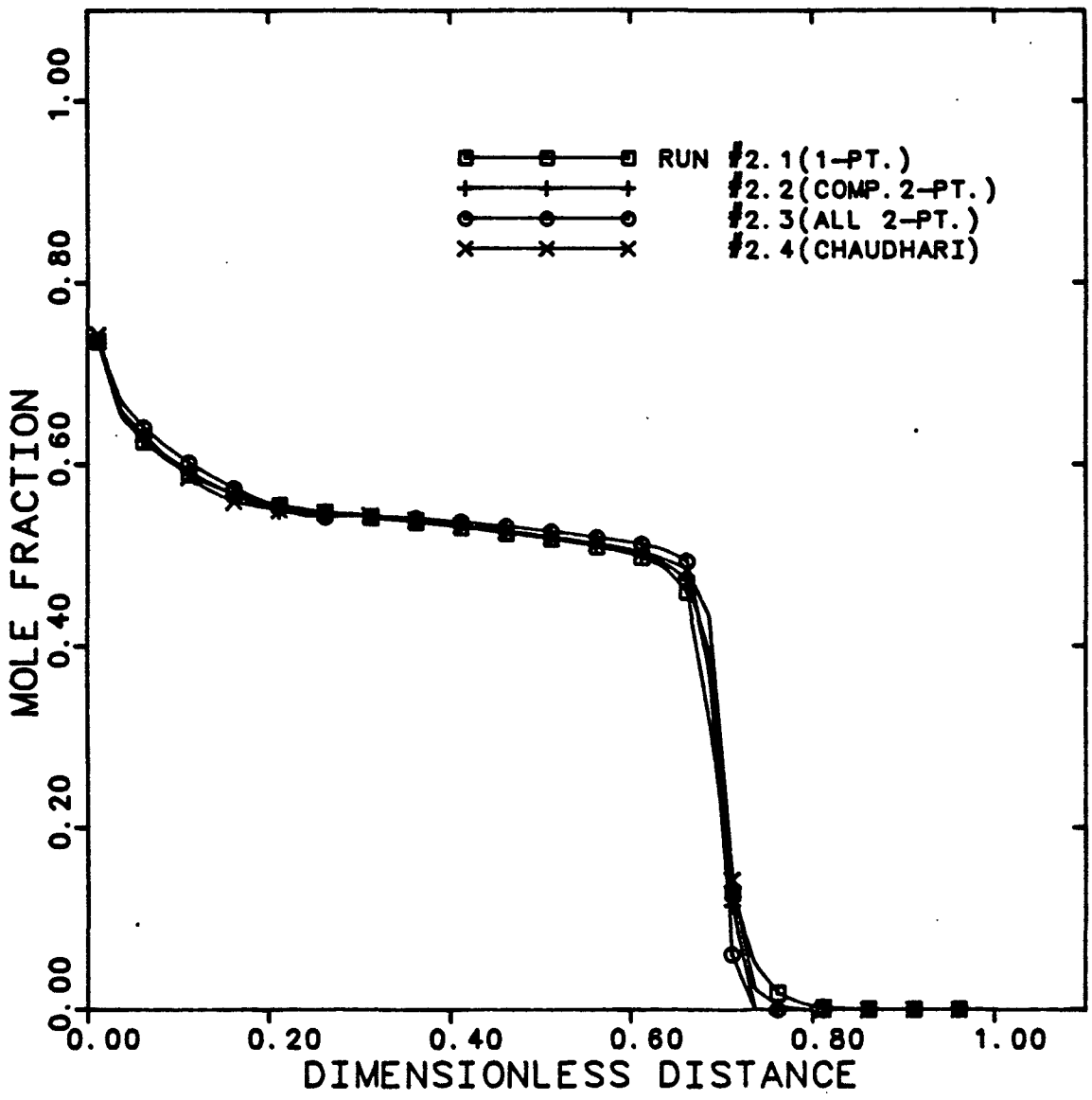

Fig. 4.3-8 Overall methane mole fraction profiles for Runs * 2.1 --- 2.4 at 0.6 DPV.

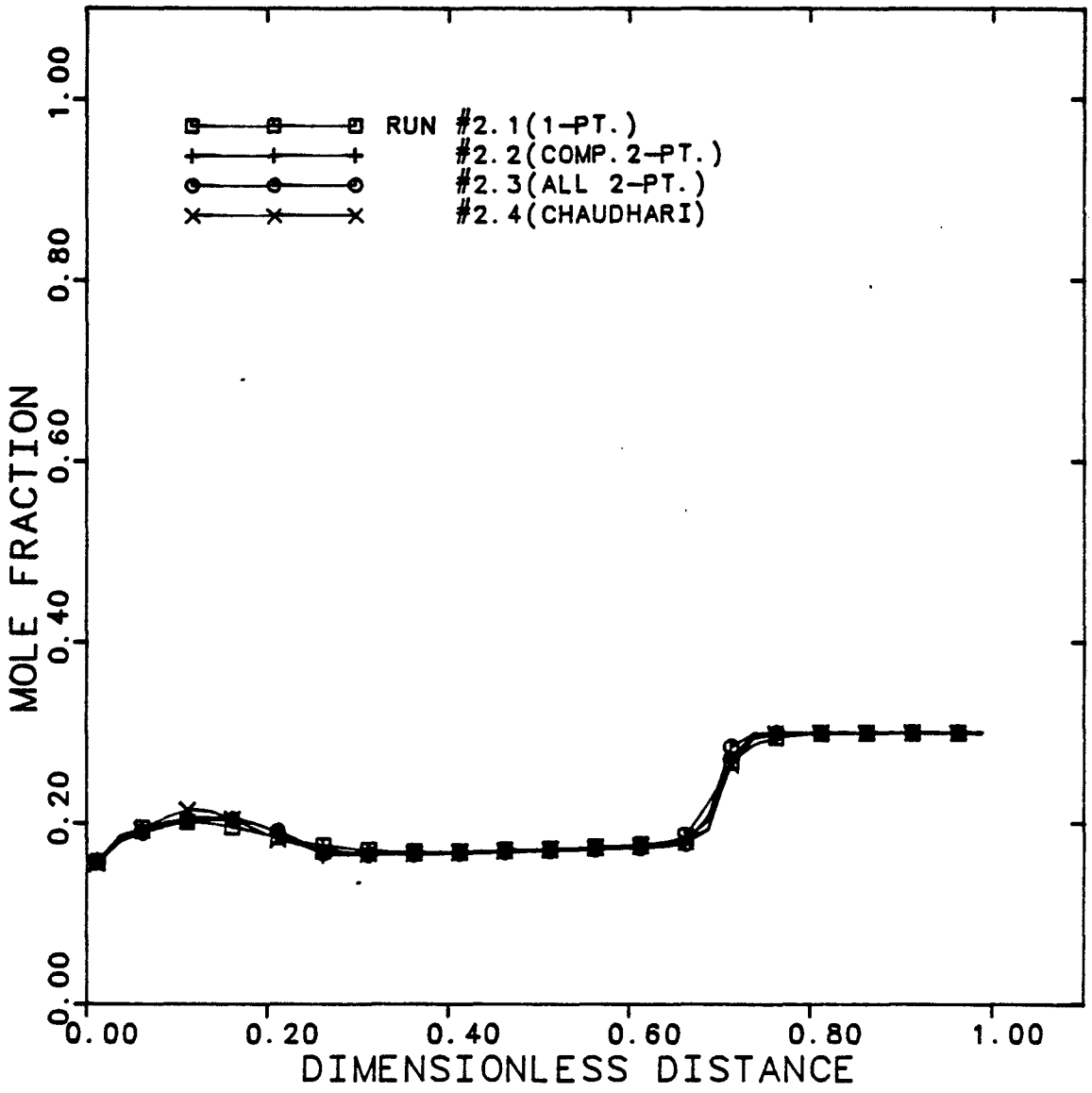

Fig. 4.3-9 Overall butane mole fraction profiles for Runs # 2.1 --- 2.4 at 0.6 DPV.

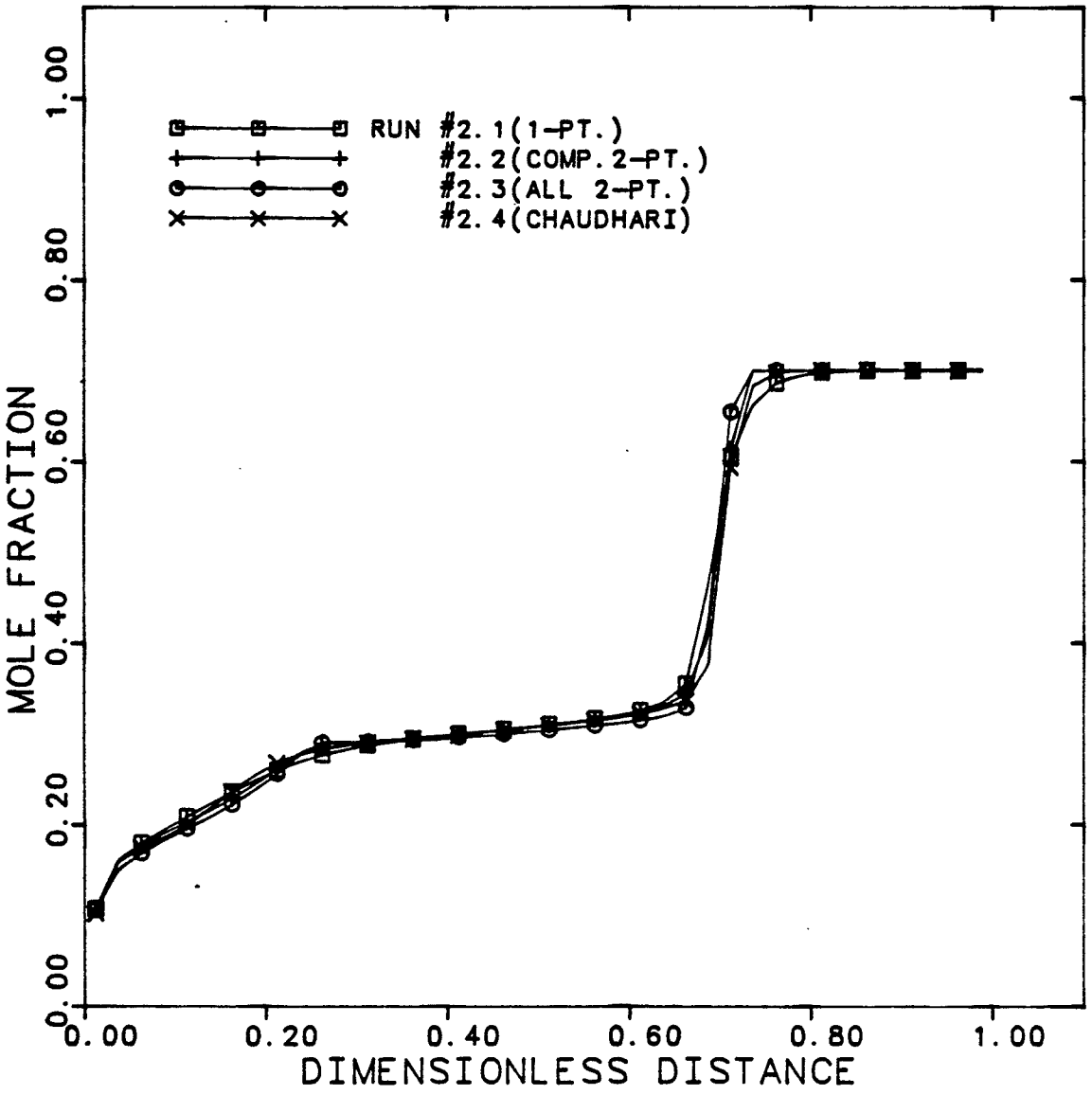

Fig. 4.3-10 Overall decane mole fraction profiles for Runs # 2.1 --- 2.4 at 0.6 DPV.

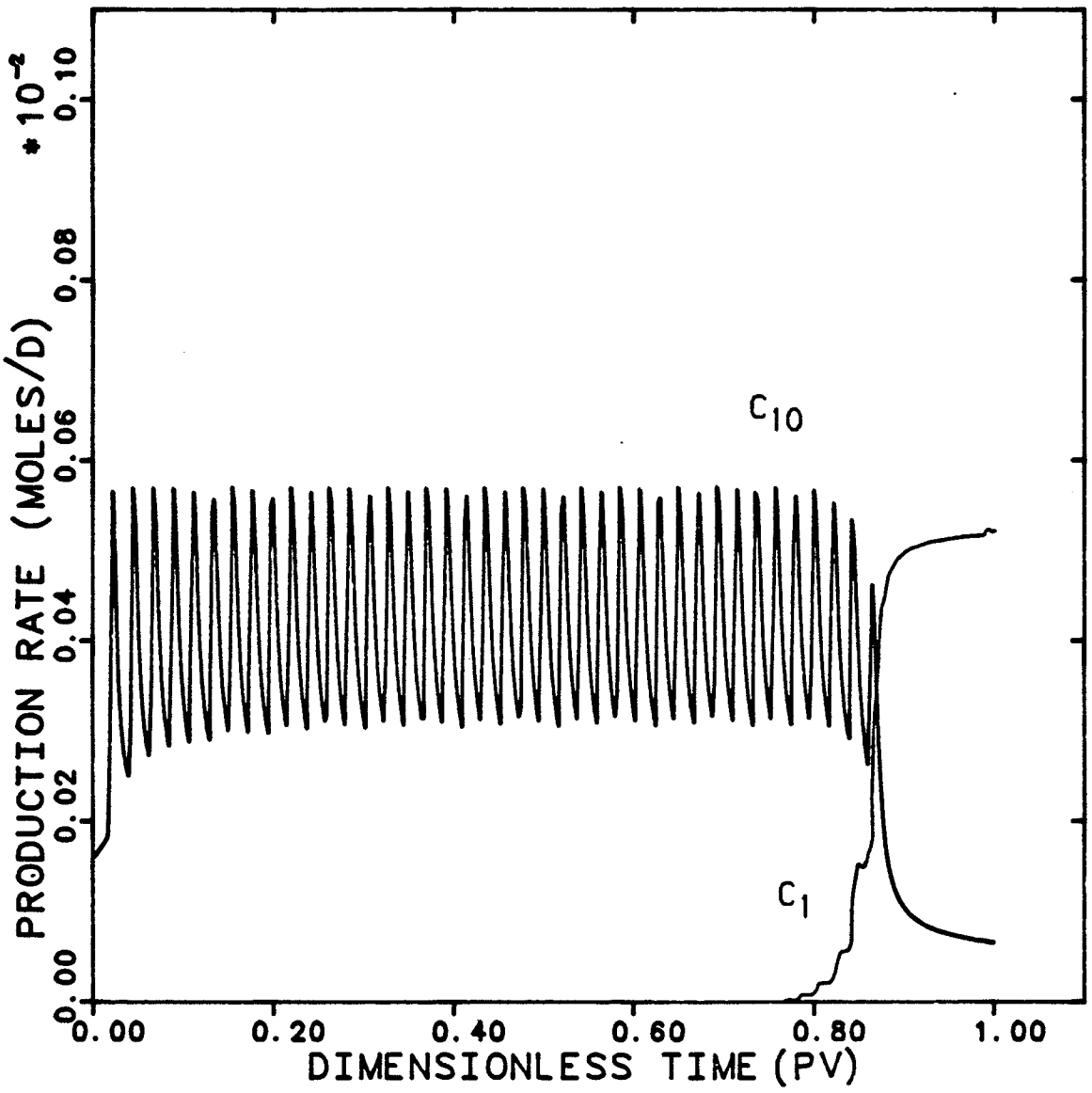

Fig. 4.3-11 Methane and decane production rate history for Run # 2.1 (single-point).

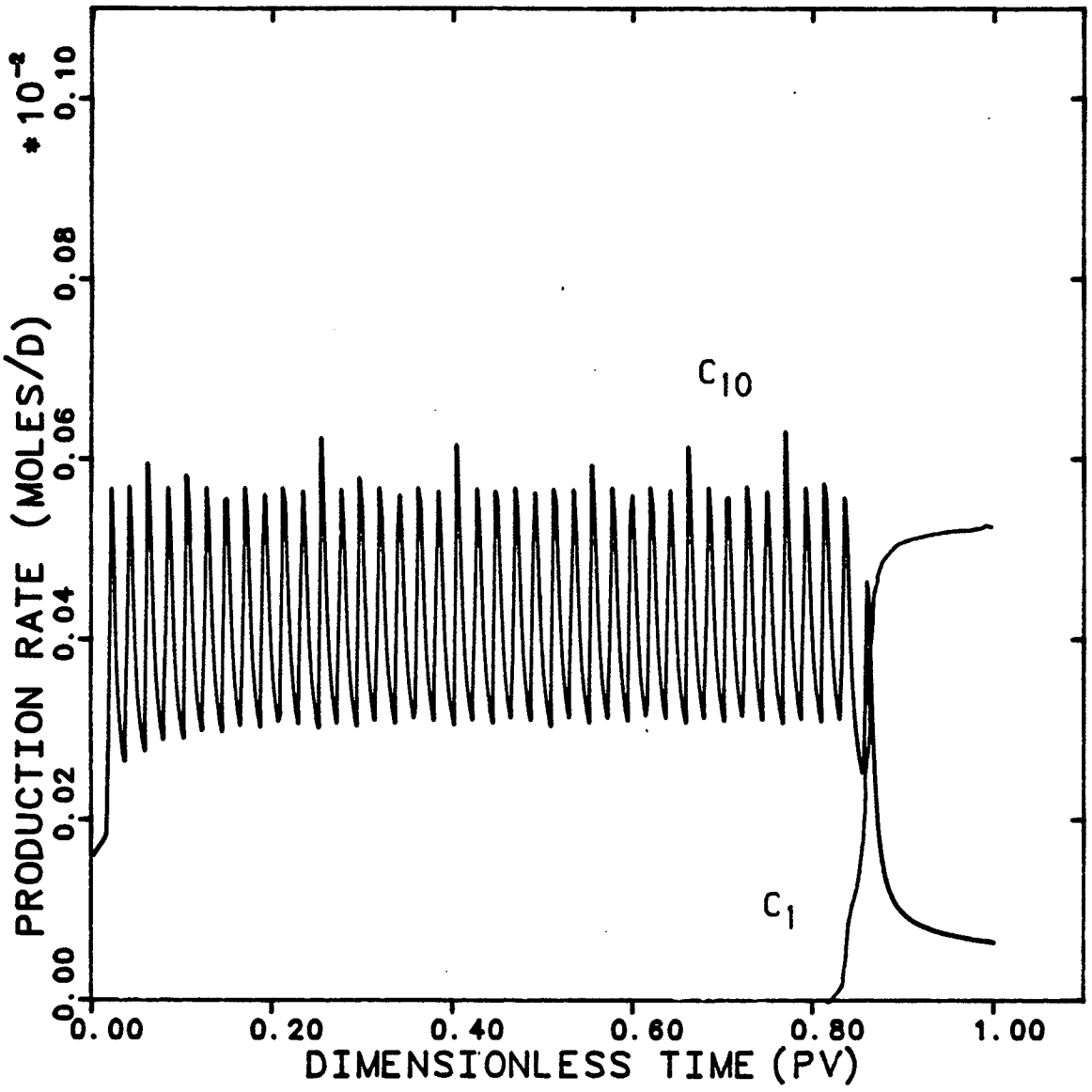

Fig. 4.3-12 Methane and decane production rate history for Run # 2.2 ("Comp. 2-Point").

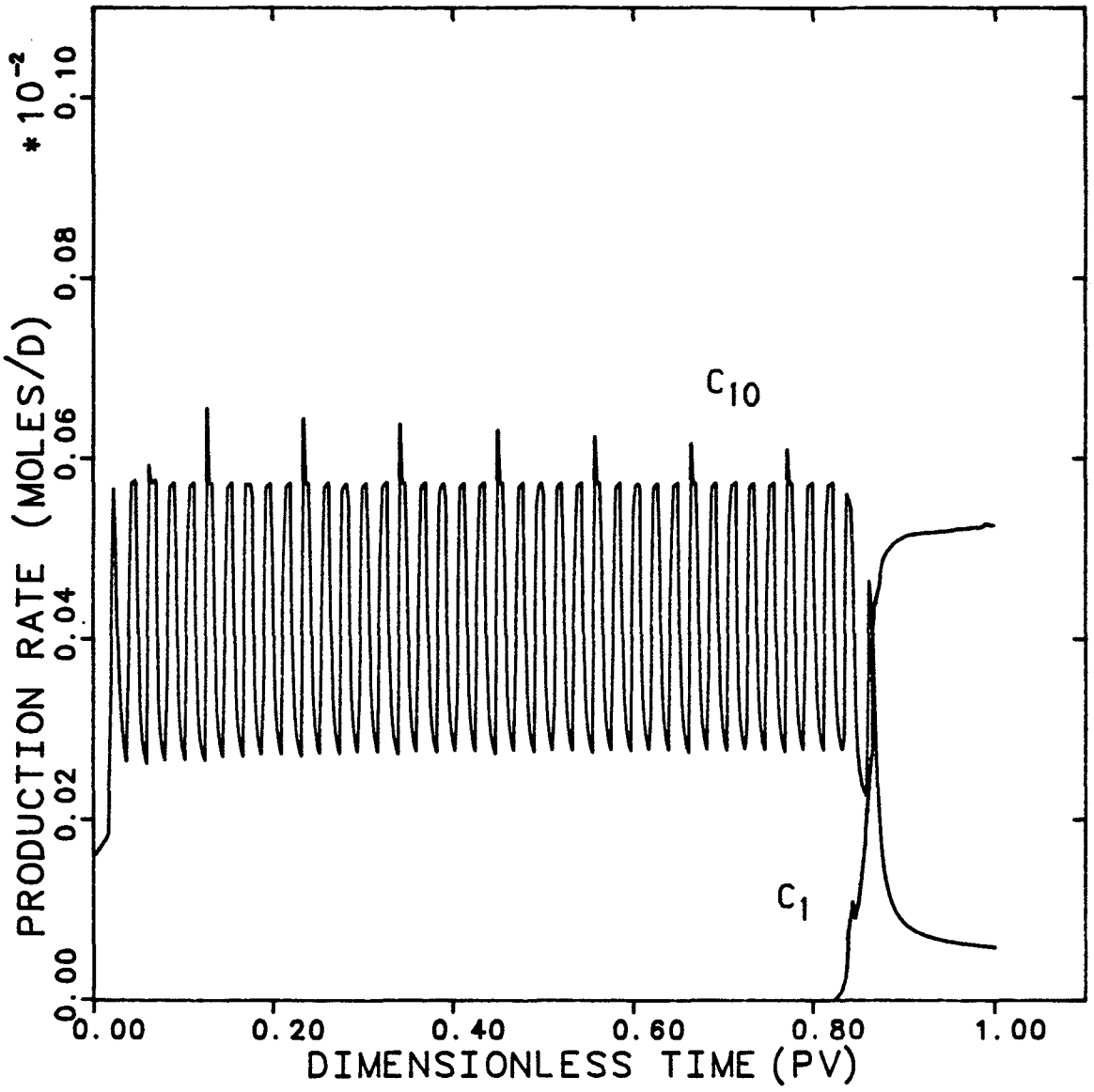

Fig. 4.3-13 Methane and decane production rate history for Run # 2.3 ("All 2-Point").

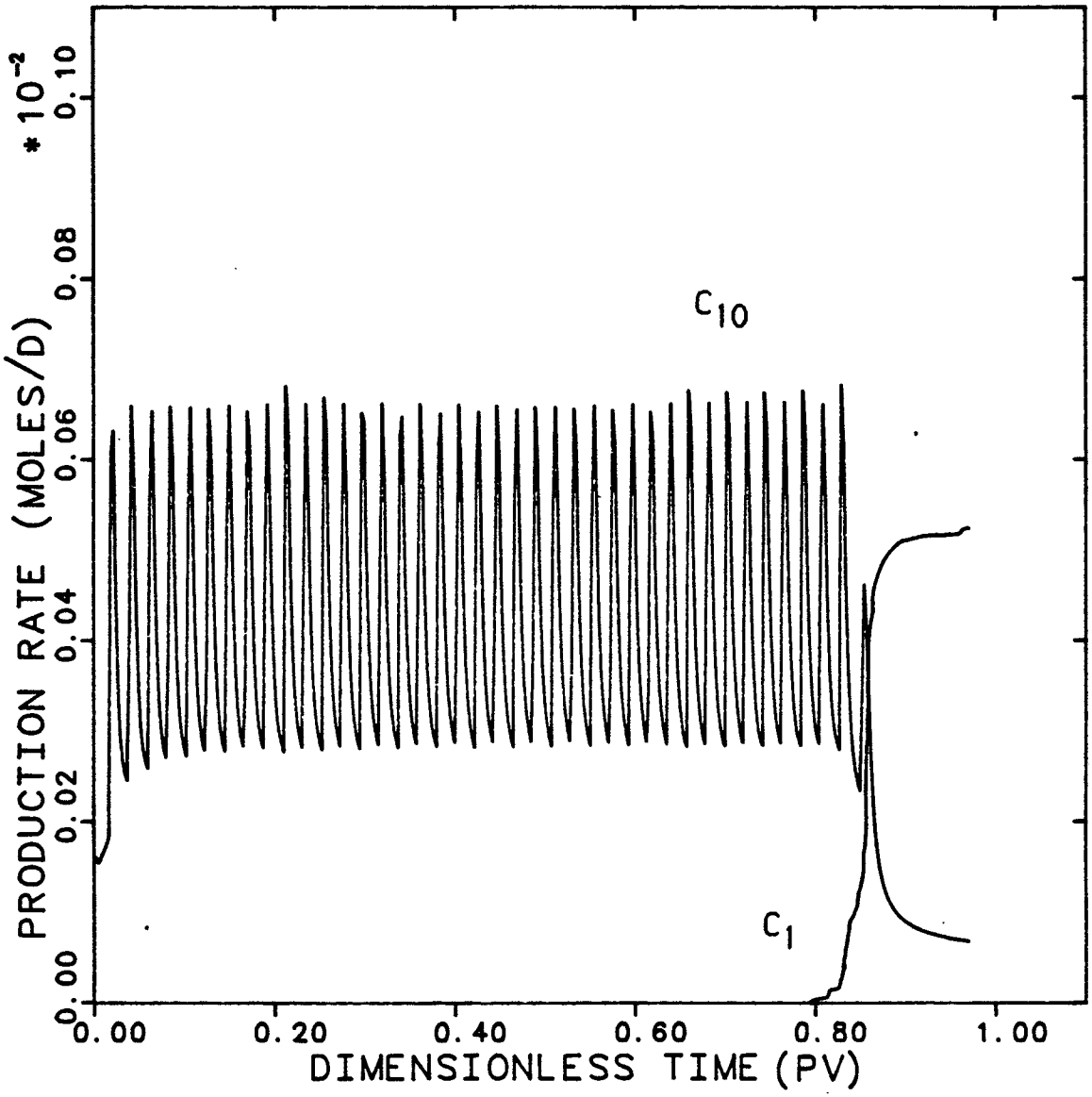

Fig. 4.3-14 Methane and decane production rate history for Run # 2.4 ("Chaudhari").

RUN #2.5 #2.6 #2.7

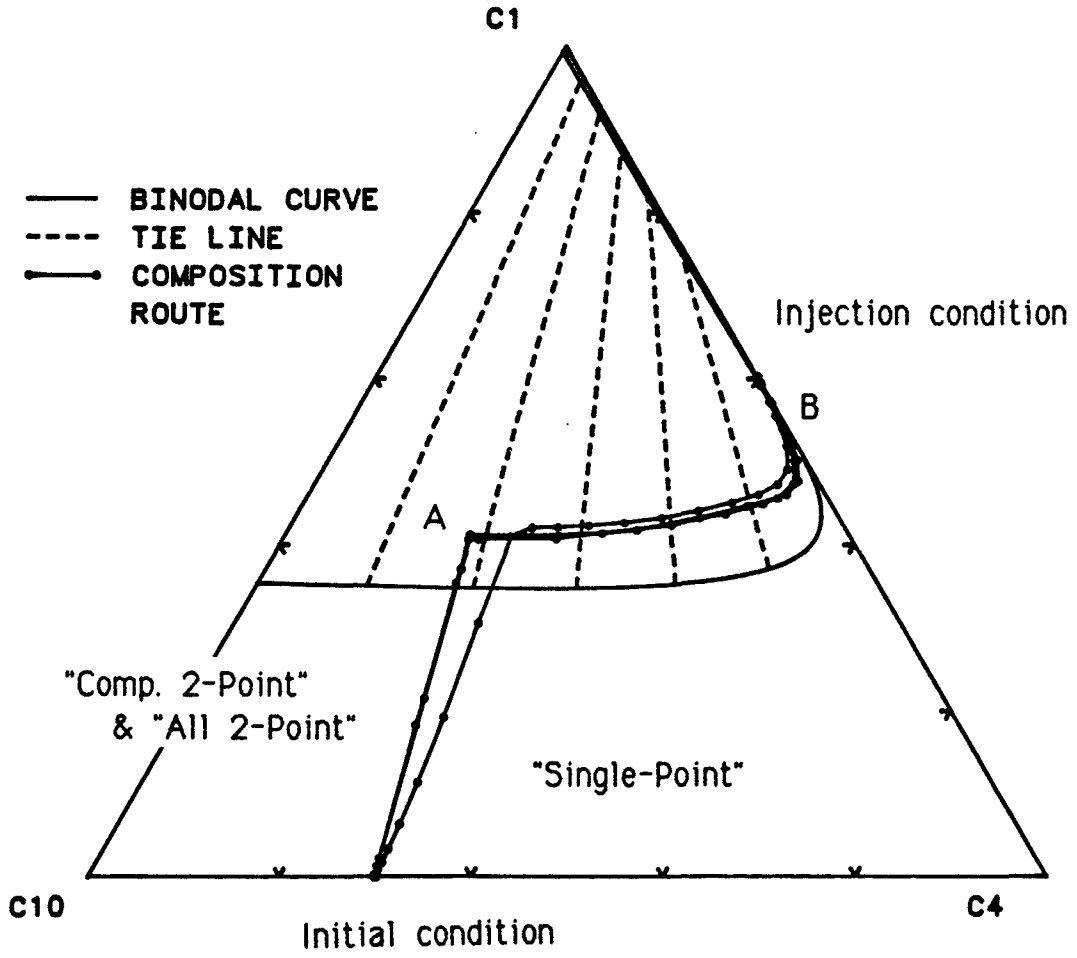

TEMP. 200 (F)
PRESS. 1500 (PSIA)

Fig. 4.3-15 Composition routes for Runs # 2.5 --- 2.7 at 0.4 DPV.

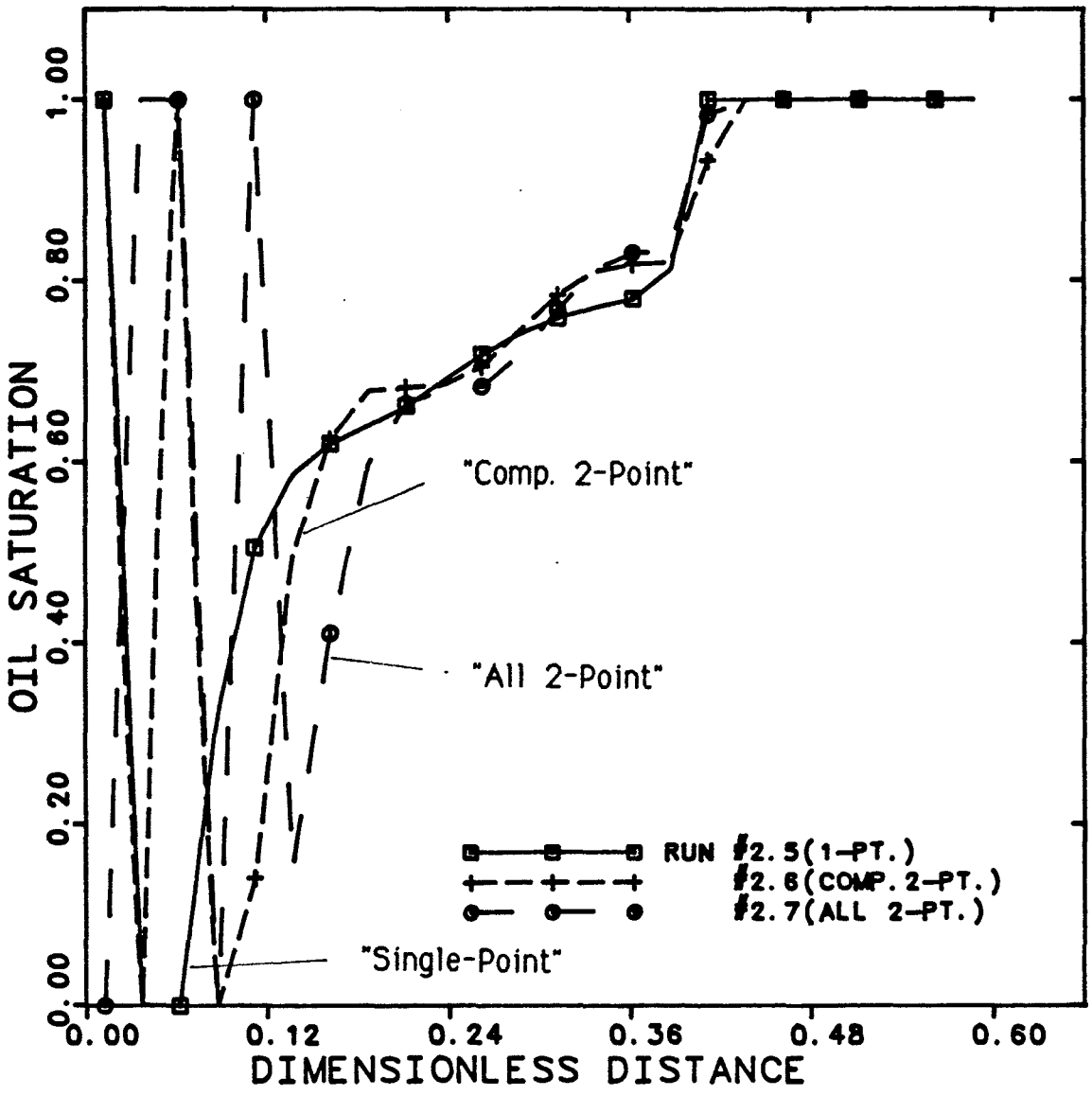

Fig. 4.3-16 Oil saturation profiles for Runs # 2.5 --- 2.7 at 0.4 DPV.

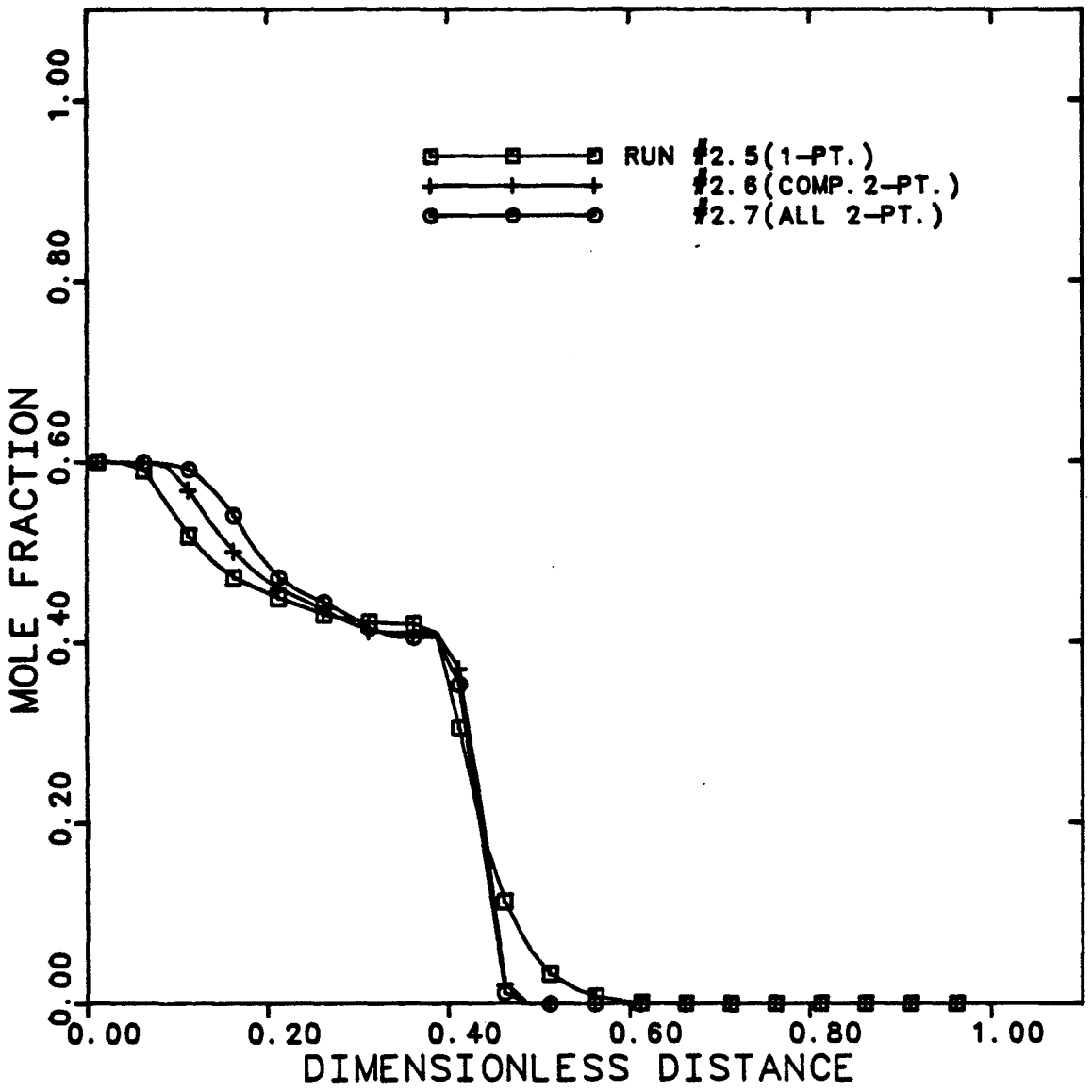

Fig. 4.3-17 Overall methane mole fraction profiles for Runs # 2.5 --- 2.7 at 0.4 DPV.

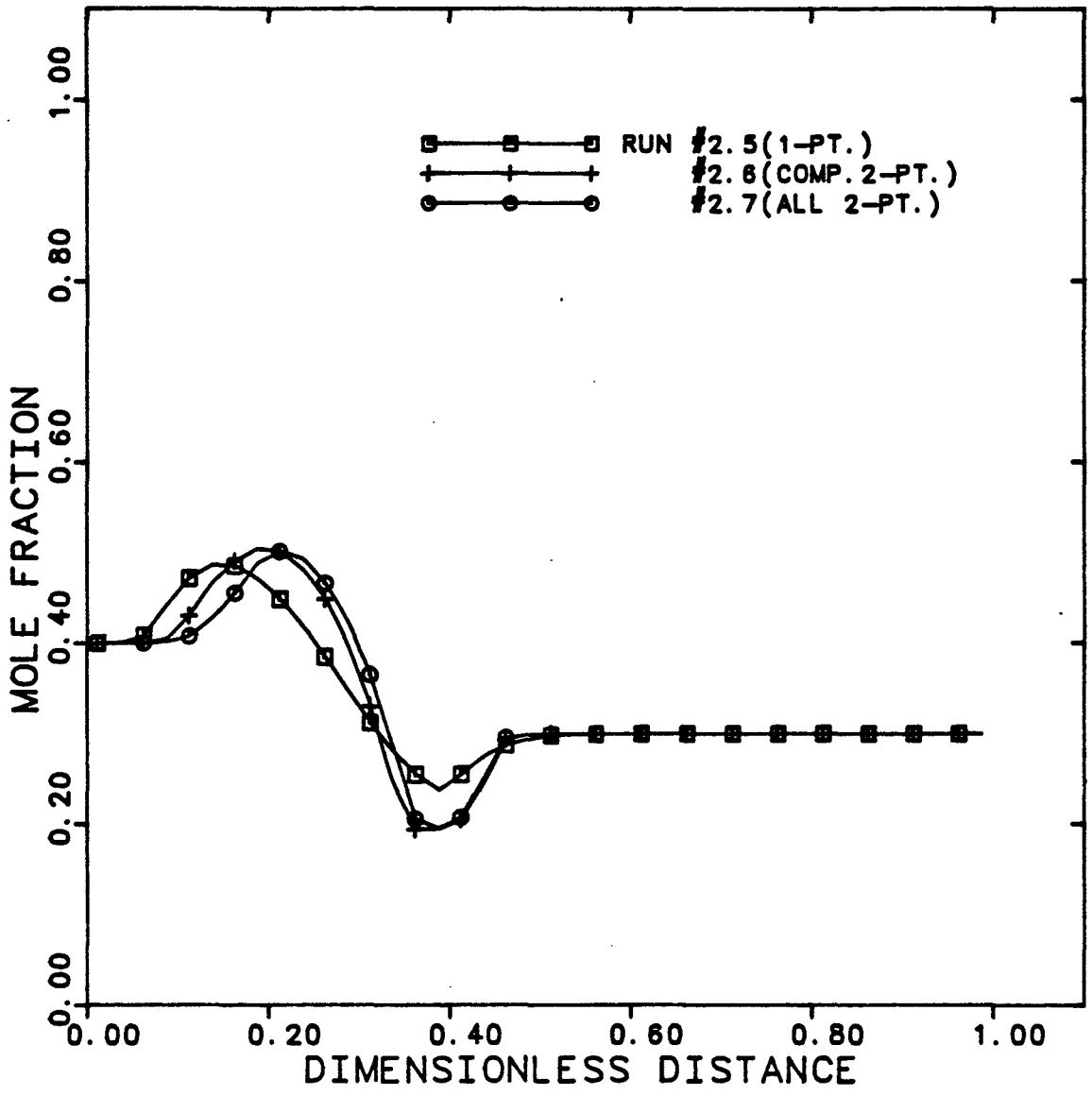

Fig. 4.3-18 Overall butane mole fraction profiles for Runs #2.5 --- 2.7 at 0.4 DPV.

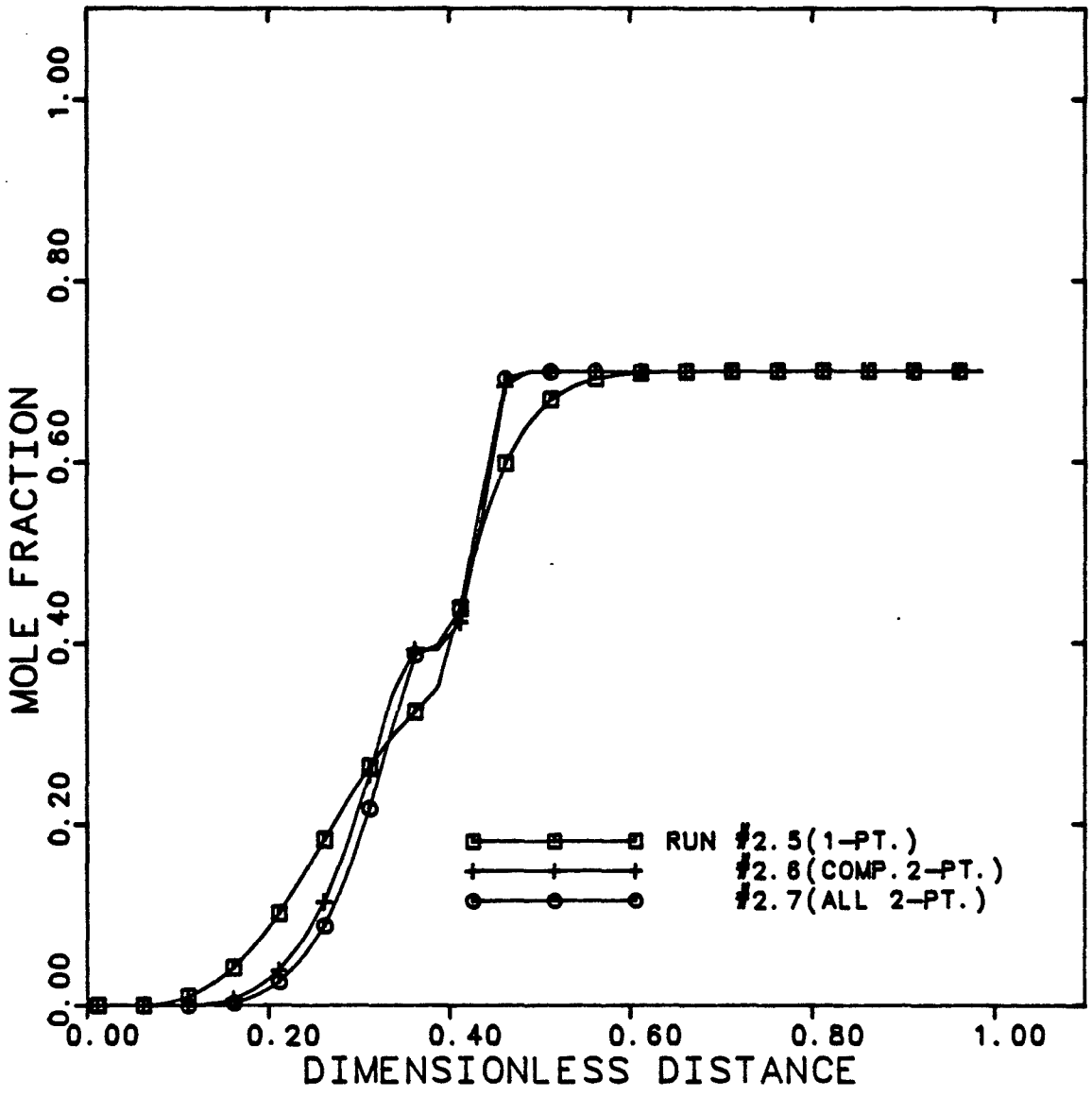

Fig. 4.3-19 Overall decane mole fraction profiles for Runs #2.5 --- 2.7 at 0.4 DPV.

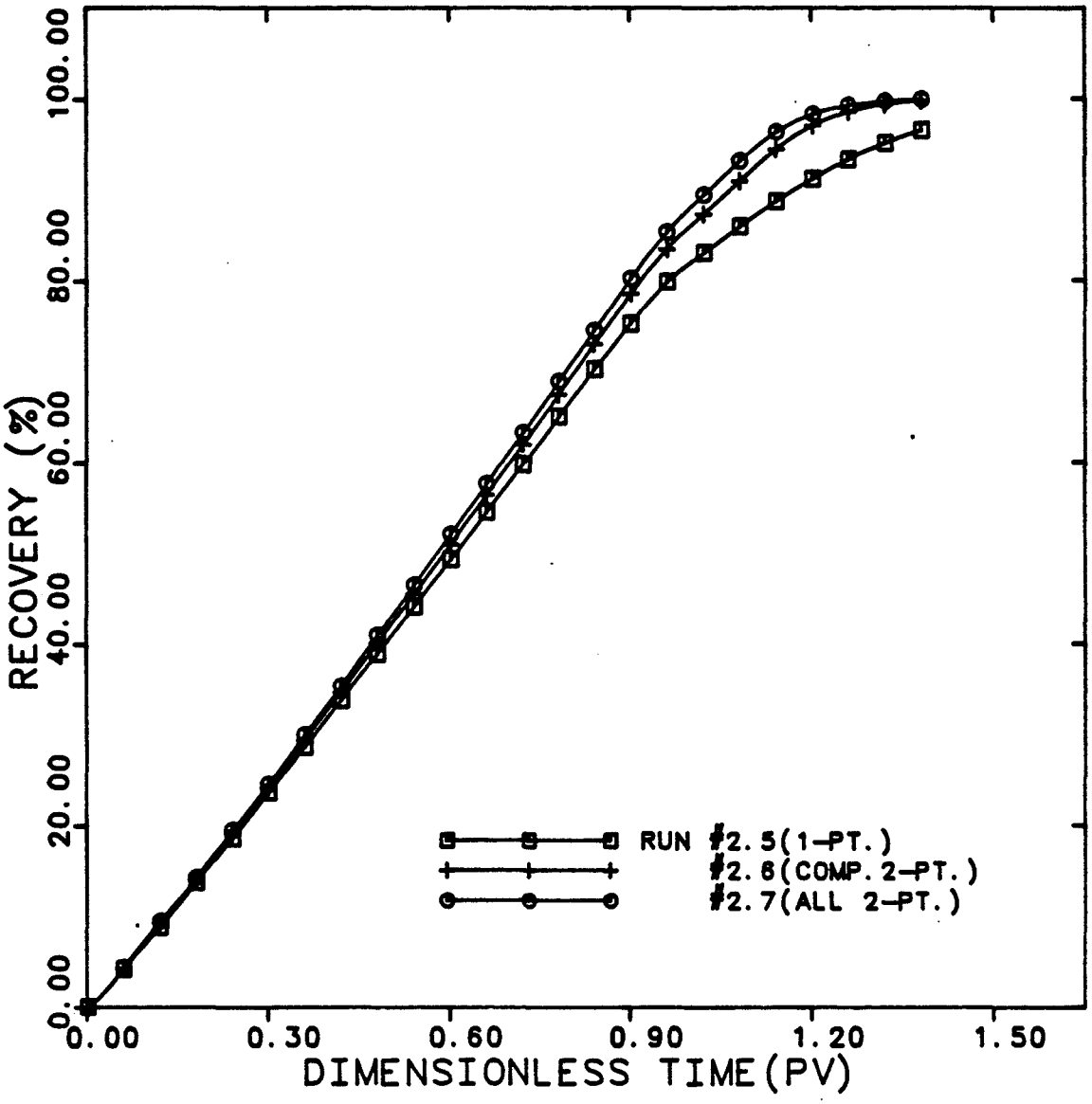

Fig. 4.3-20 Decane recovery history for Runs # 2.5 --- 2.7.

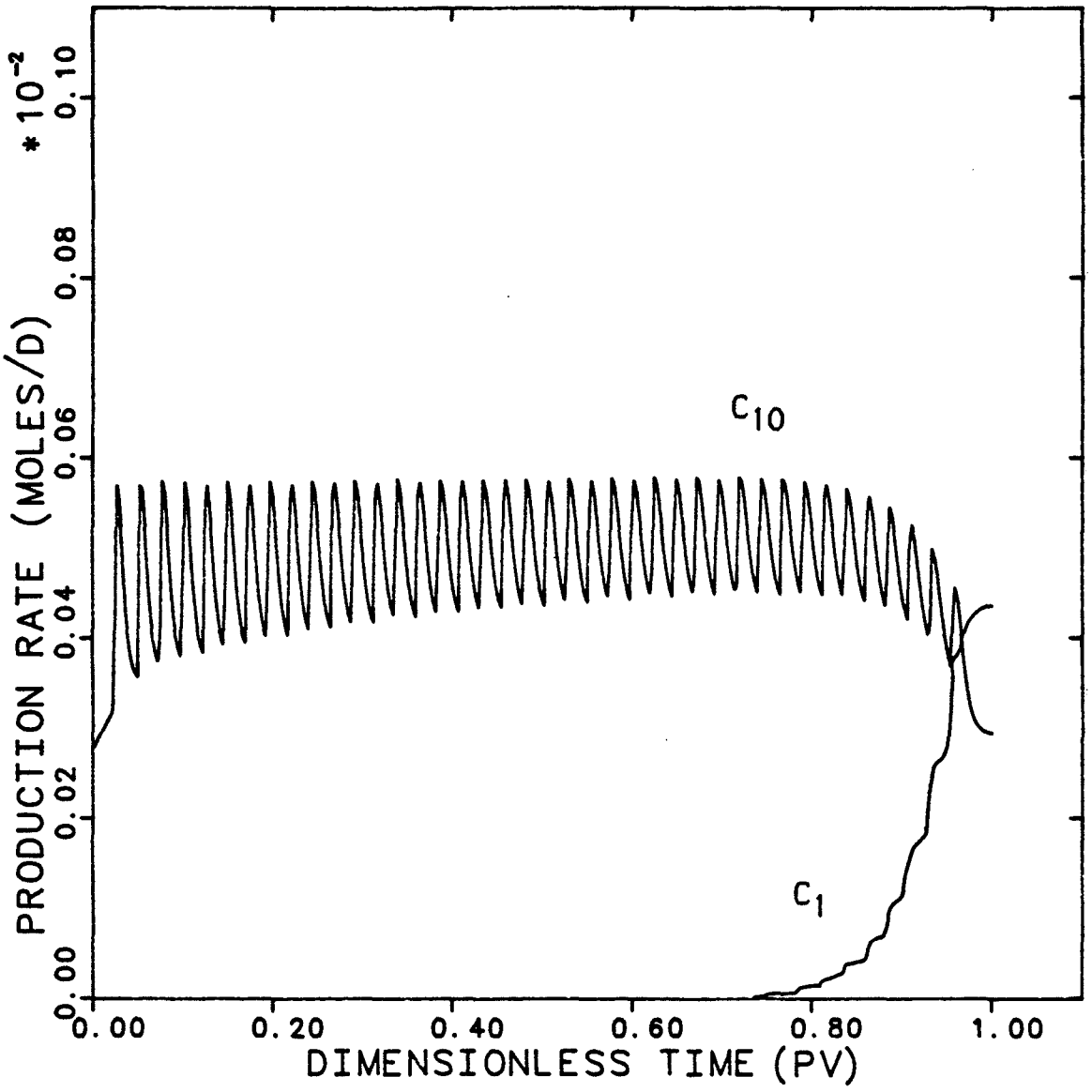

Fig. 4.3-21 Methane and decane production rate history for Run # 2.5 (single-point).

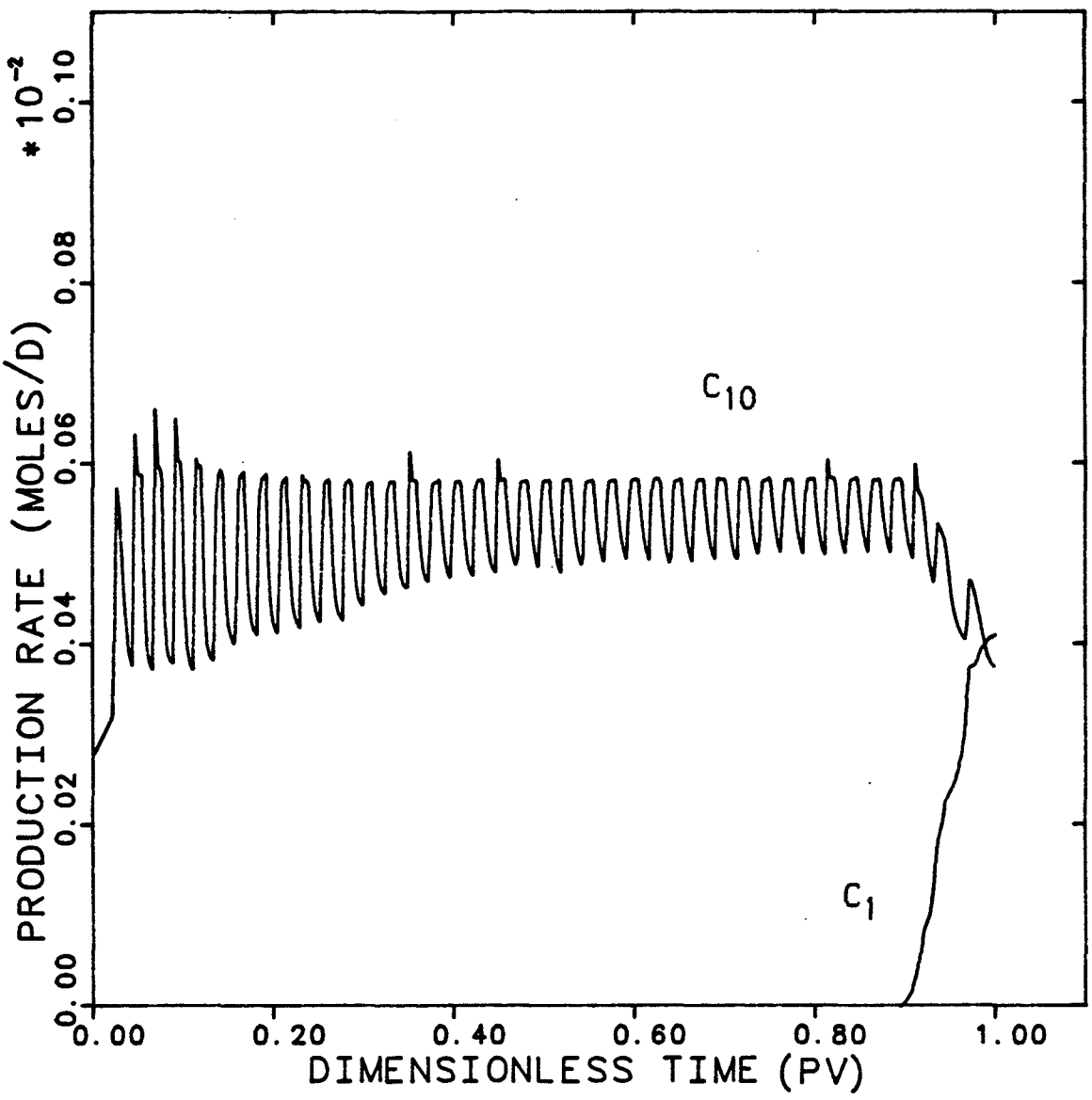

Fig. 4.3-22 Methane and decane production rate history for Run # 2.7 ("All 2-Point").

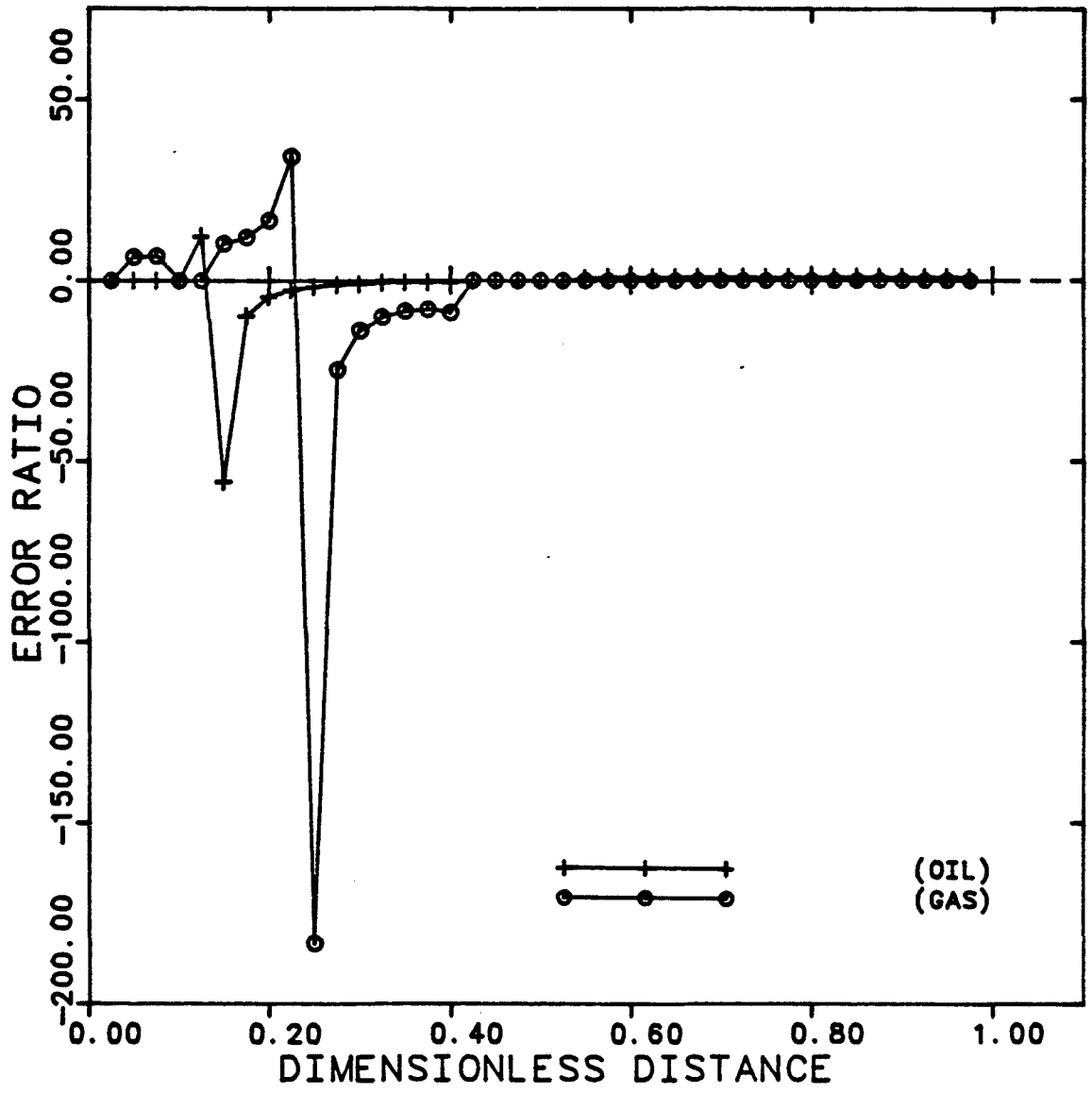

Fig. 4.3-23 Ratio of $\nabla(\xi_j x_{ji})$ and $-(\xi_j x_{ji})/\rho_j \nabla\rho_j$ for Run * 2.8 at 0.4 DPV.

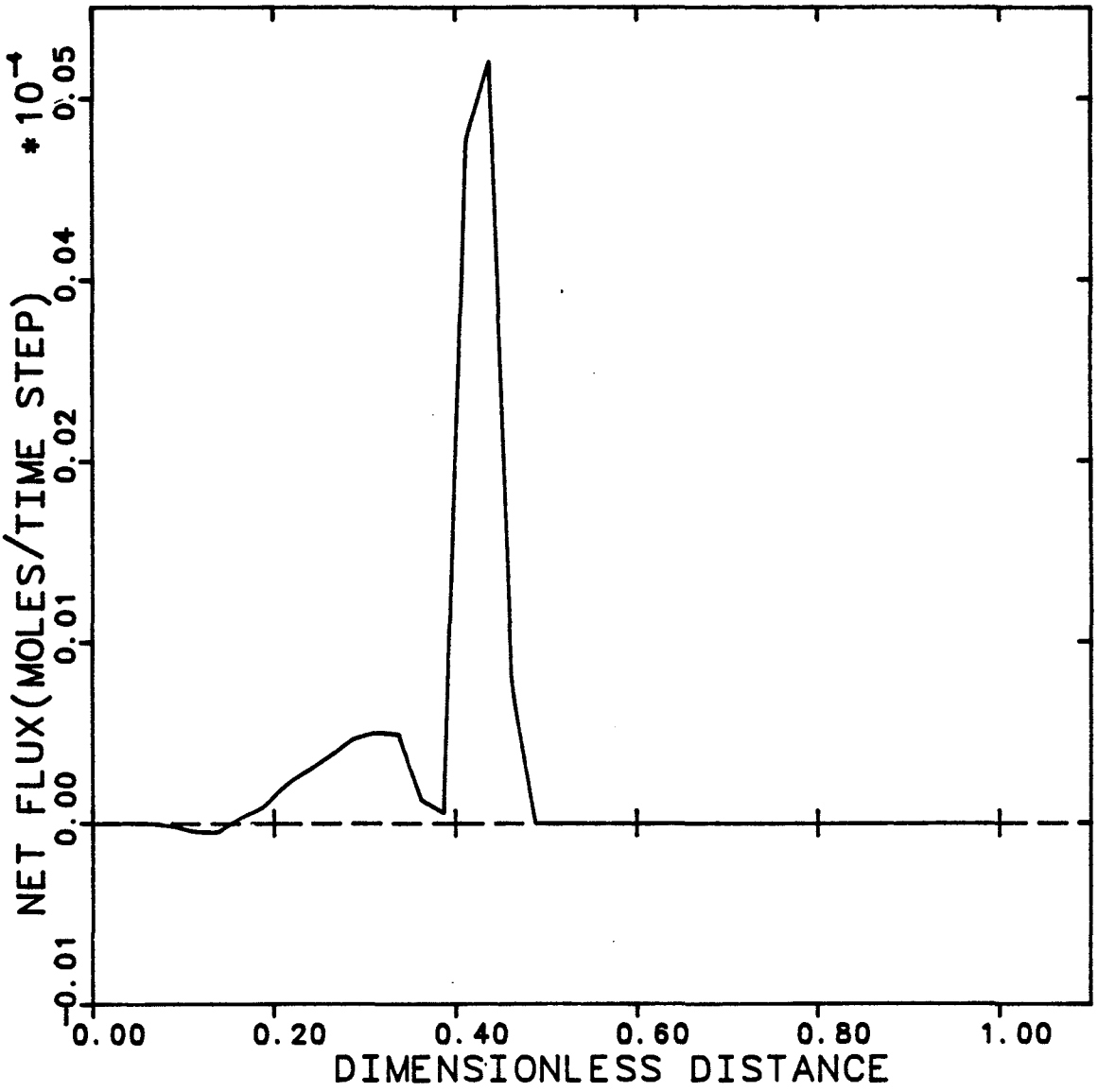

Fig. 4.3-24 Methane net flux profile for Run * 2.8 at 0.4 DPV.

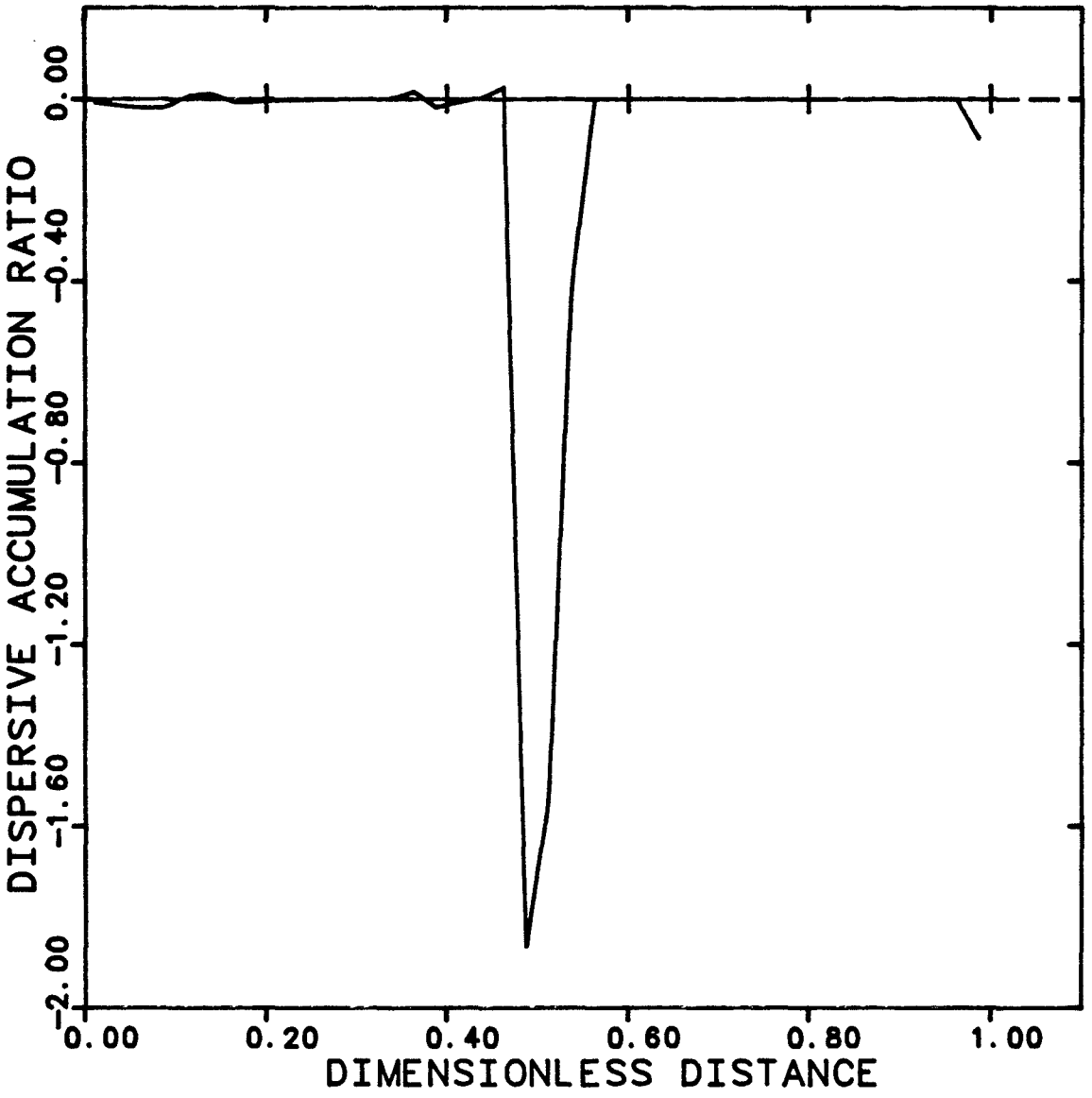

Fig. 4.3-25 Methane dispersive accumulation ratio for Run * 2.8 at 0.4 DPV.

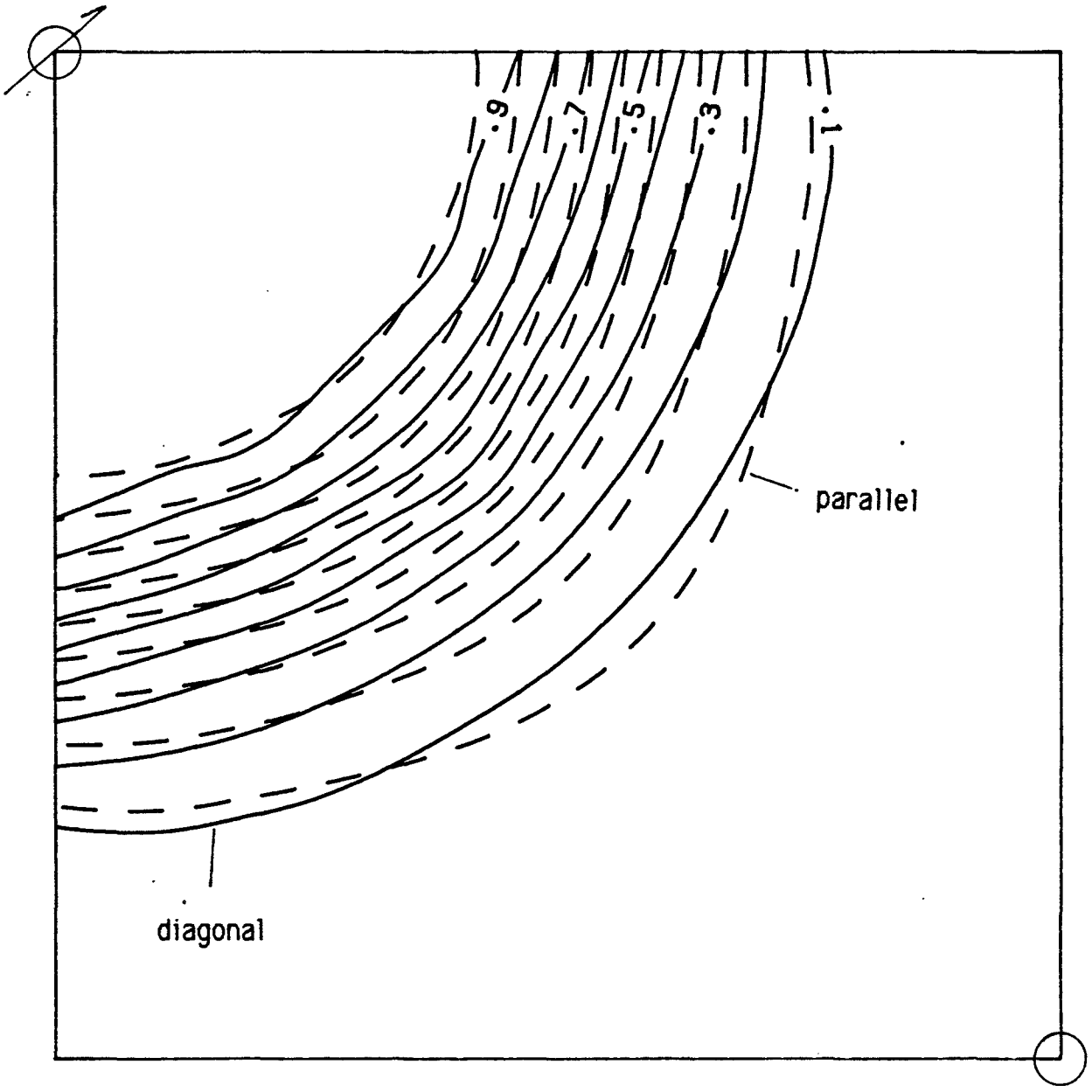

Fig. 4.4-1 Decane mole fraction contours for Runs # 3B.1 and 3B.2 (single-point) at 0.4 DPV (M = 0.088).

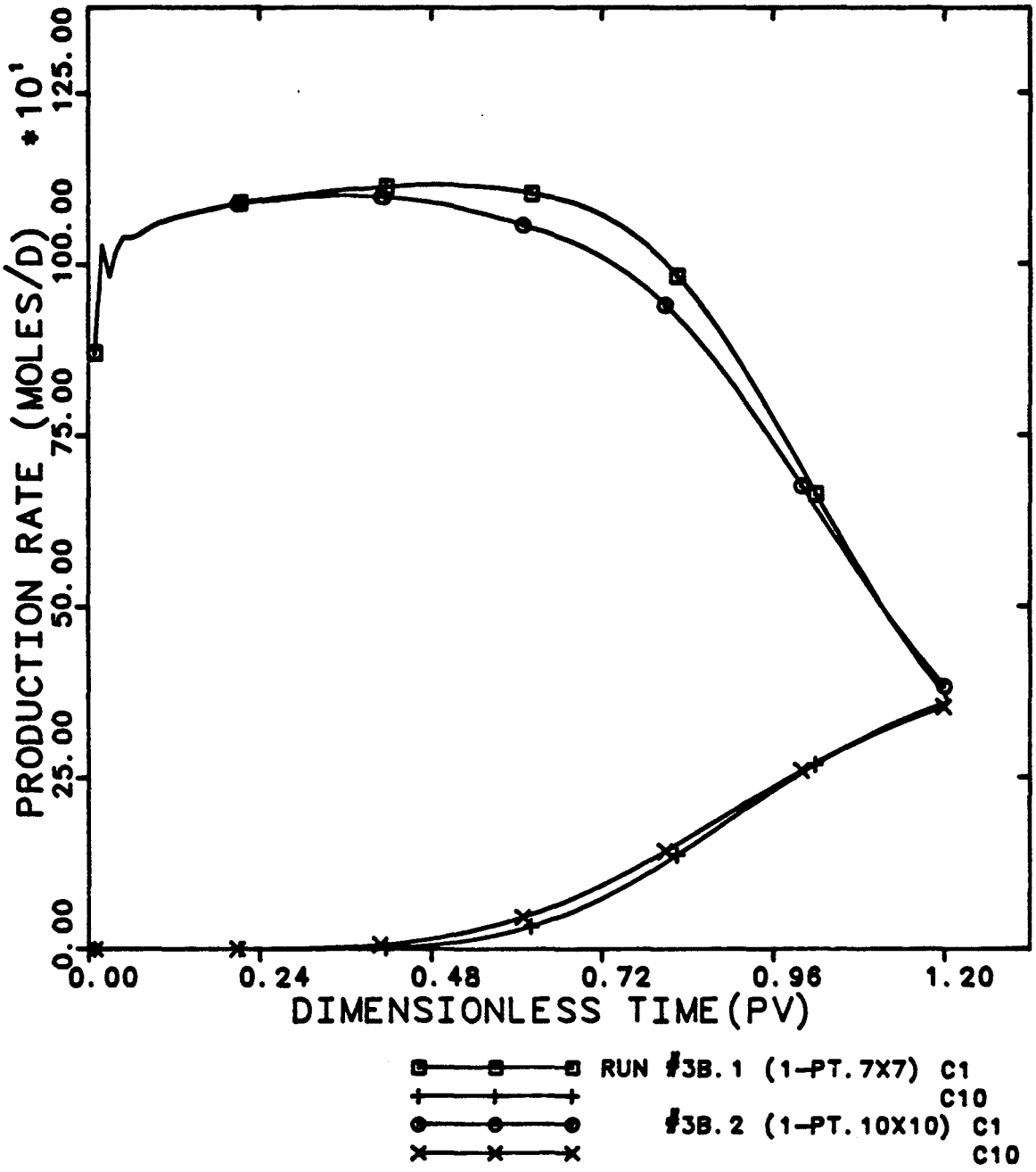

Fig. 4.4-2 Methane and decane production rate histories for Runs # 3B.1 and 3B.2.

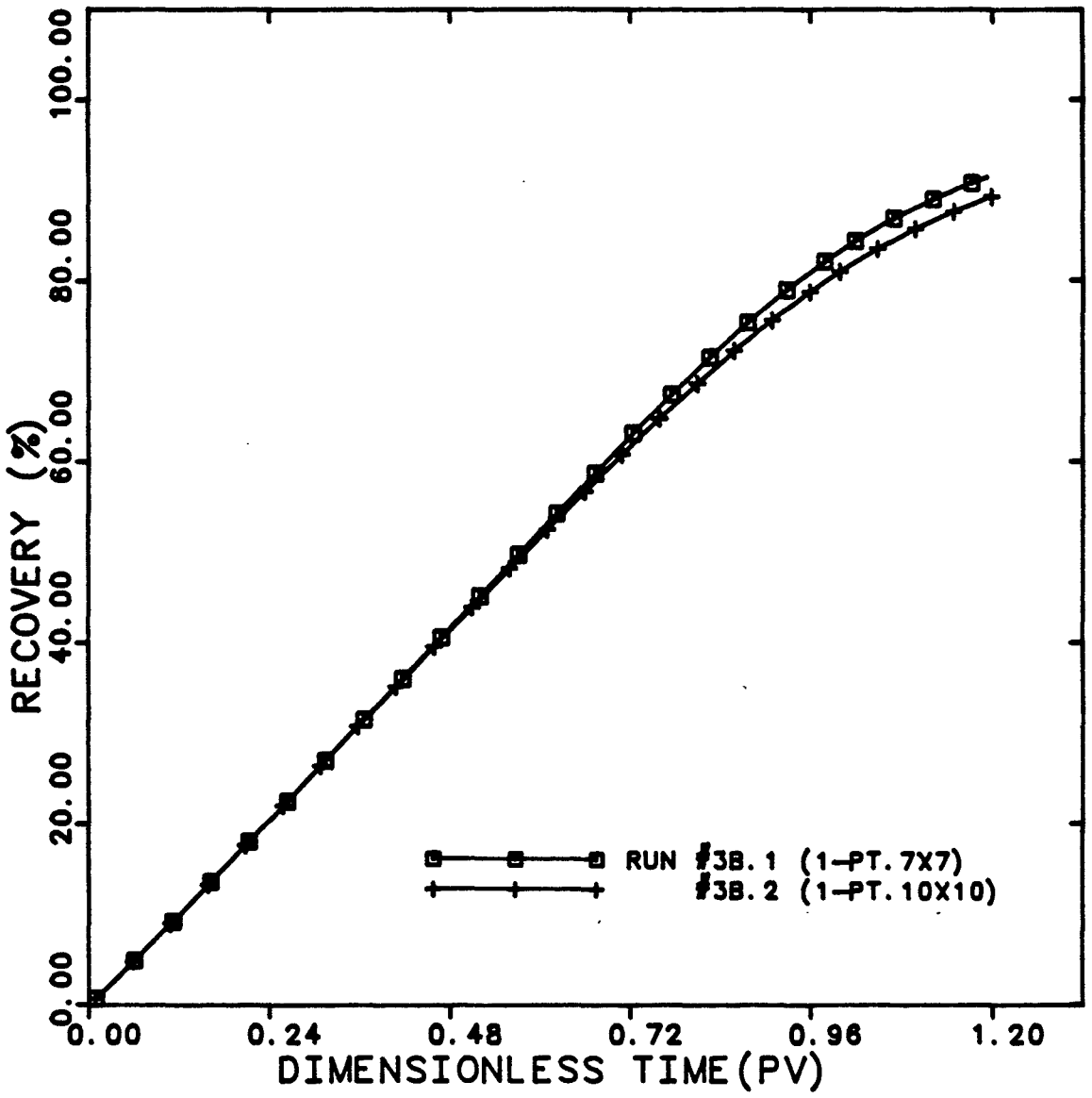

Fig. 4.4-3 Methane recovery histories for Runs # 3B.1 and 3B.2.

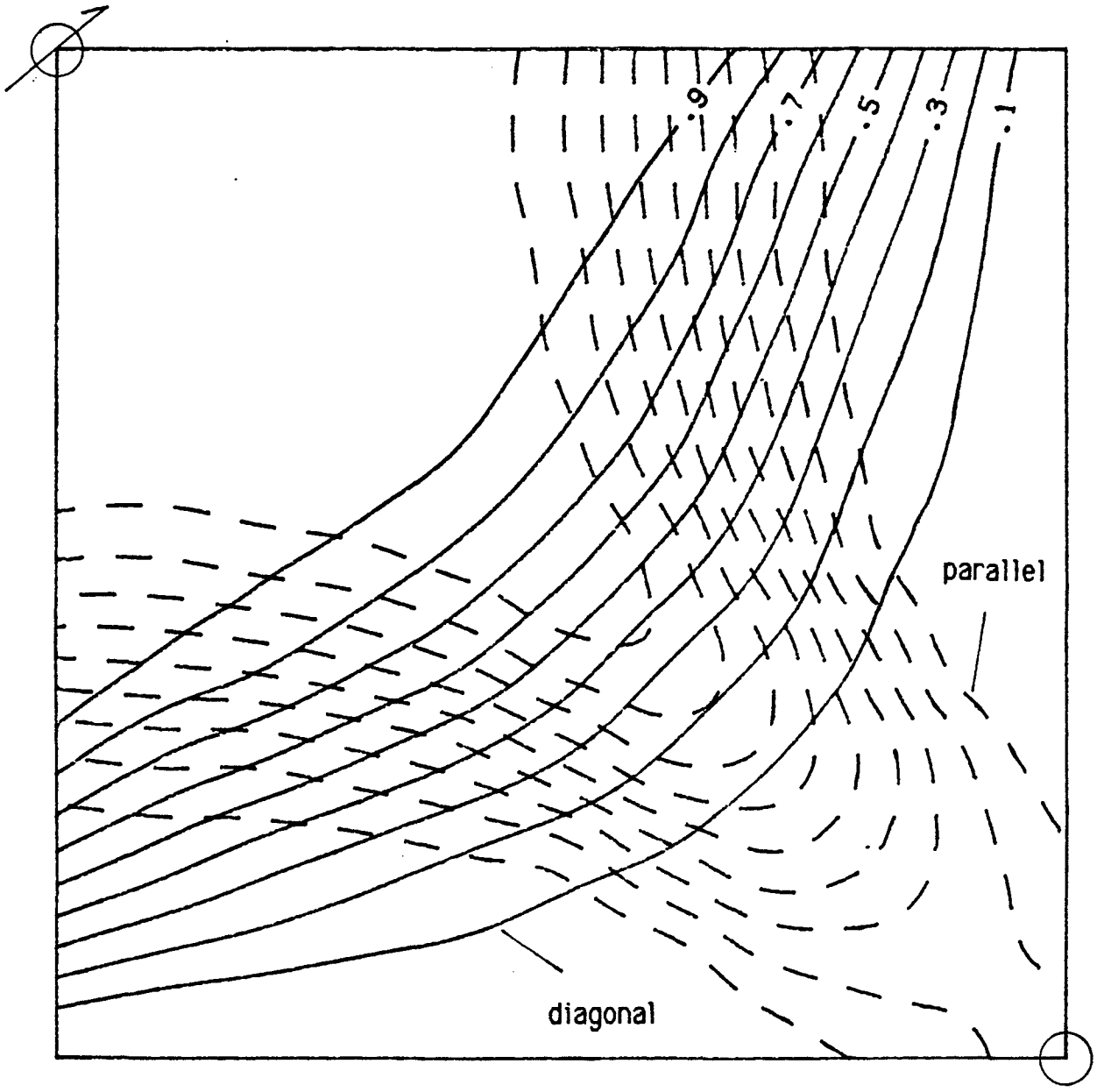

Fig. 4.4-4 Methane mole fraction contours for Runs * 3A.1 and 3A.2 (single-point) at 0.4 DPV (M = 11.4).

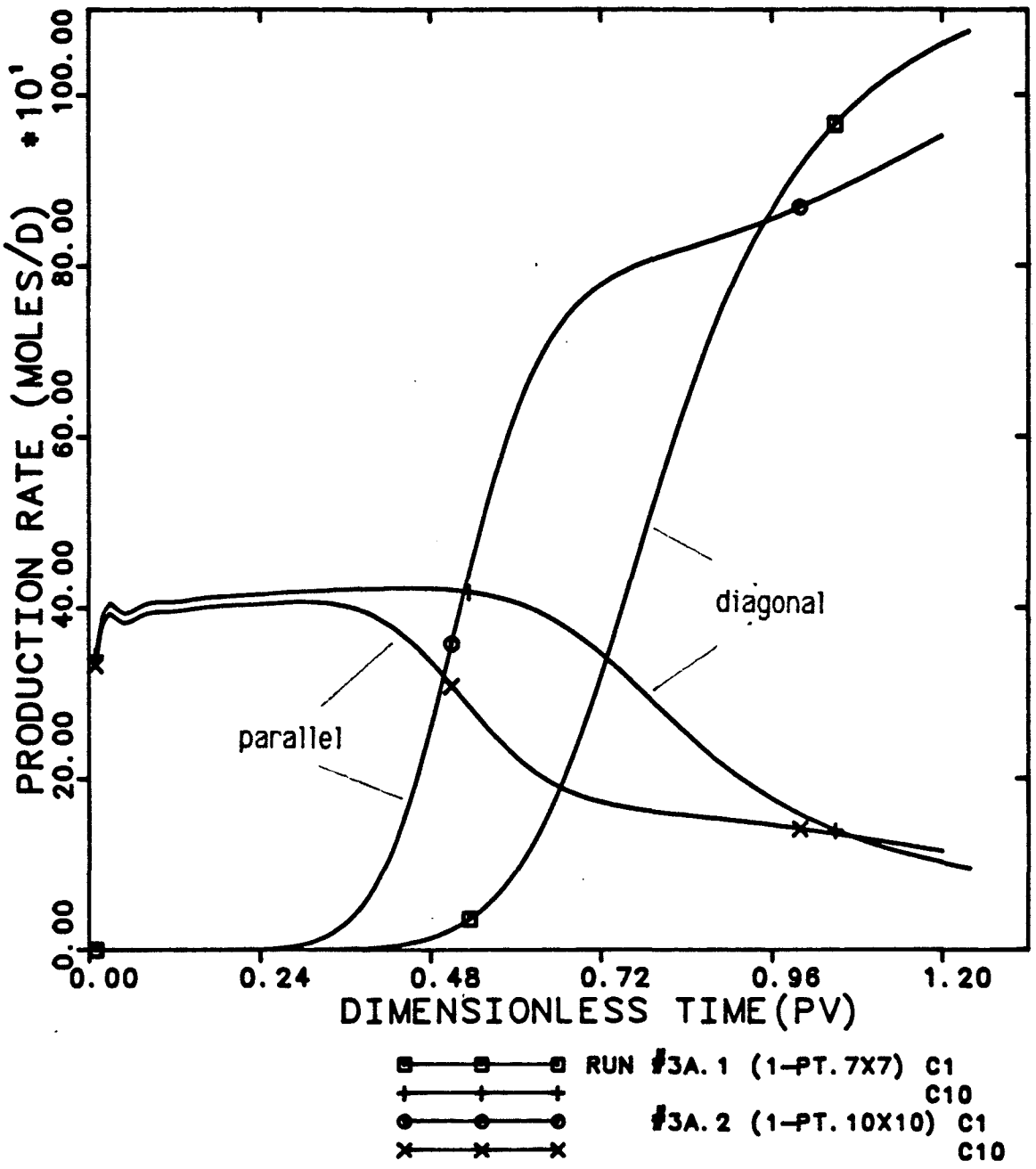

Fig. 4.4-5 Methane and decane production rate histories for Runs # 3A.1 and 3A.2.

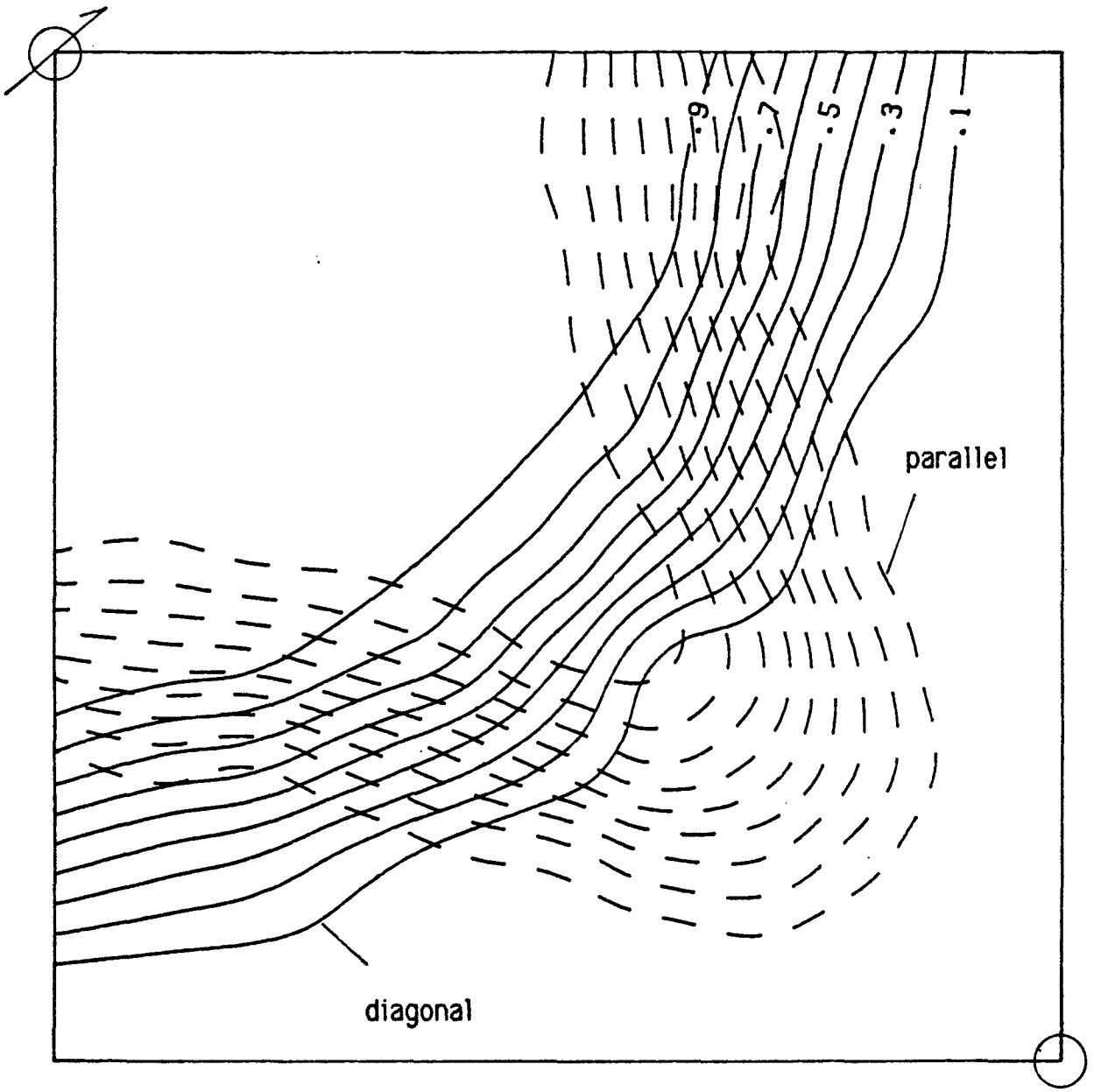

Fig. 4.4-6 Mehtane mole fraction contours for Runs * 3A.3 and 3A.4 (two-point) at 0.4 DPV (M = 11.4).

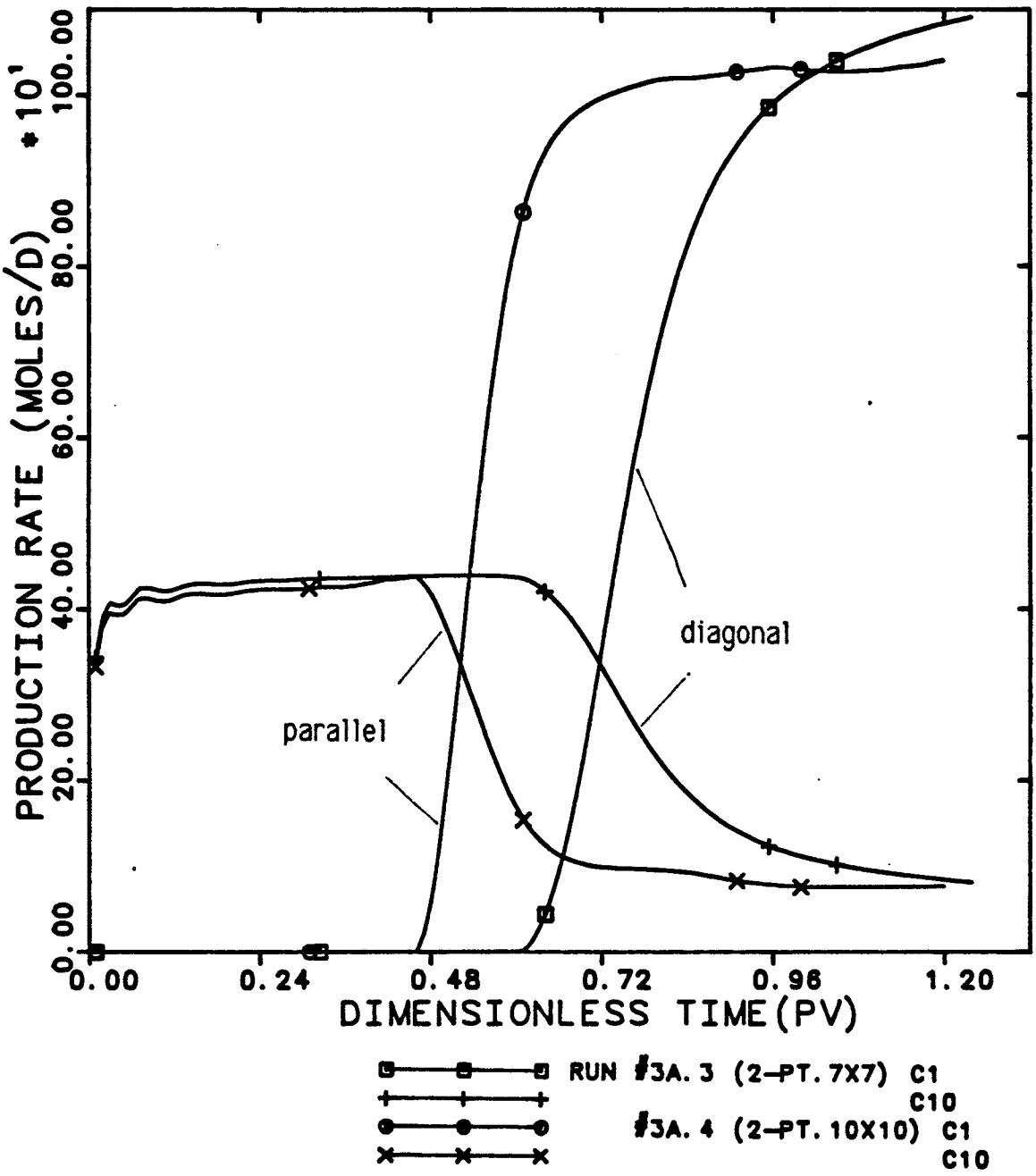

Fig. 4.4-7 Methane and decane production rate histories for Runs # 3A.3 and 3A.4.

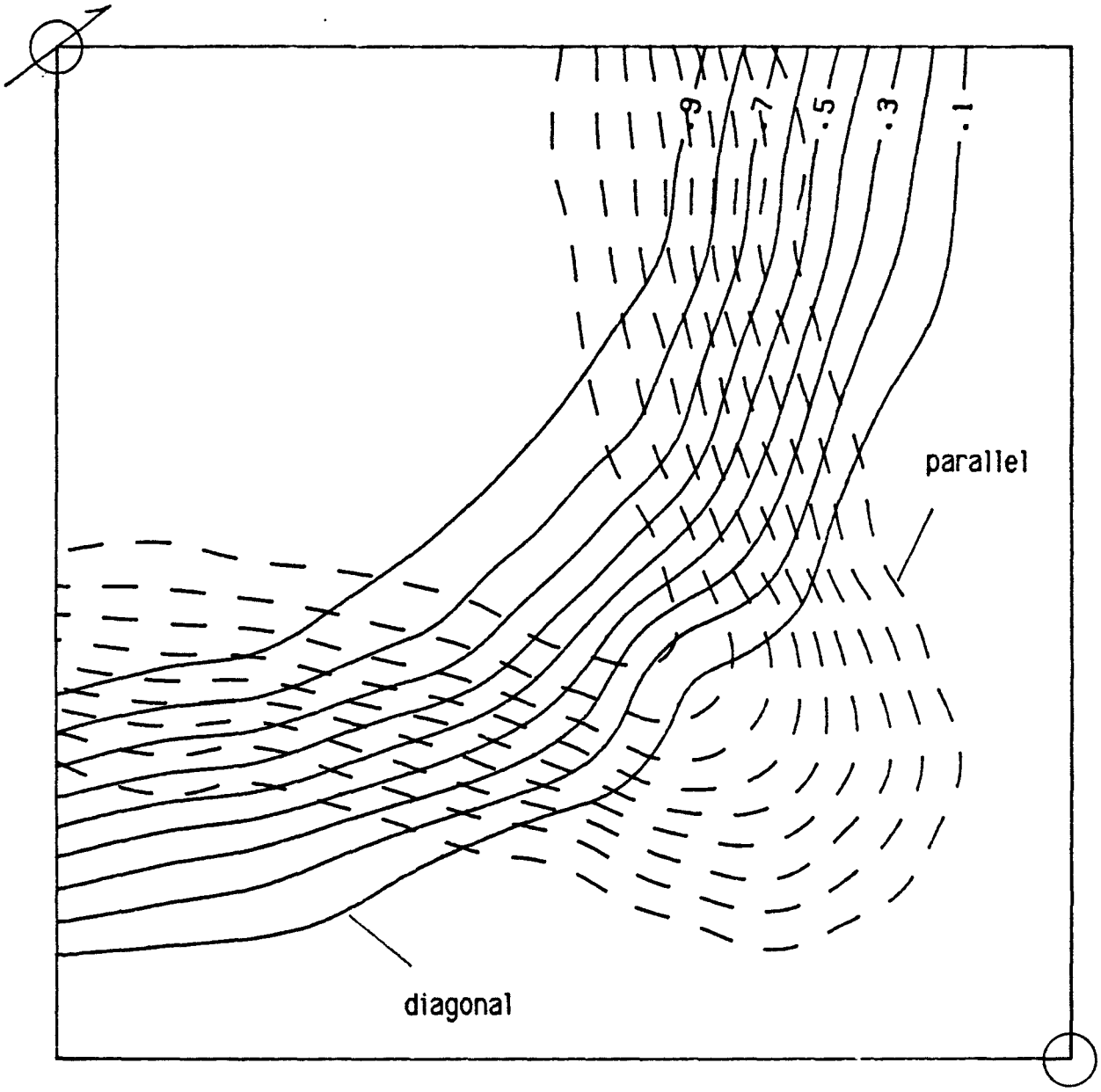

Fig. 4.4-8 Methane mole fraction contours for Runs # 3A.9 and 3A.10 (two-point plus Chaudhari time treatment) at 0.4 DPV (M = 11.4).

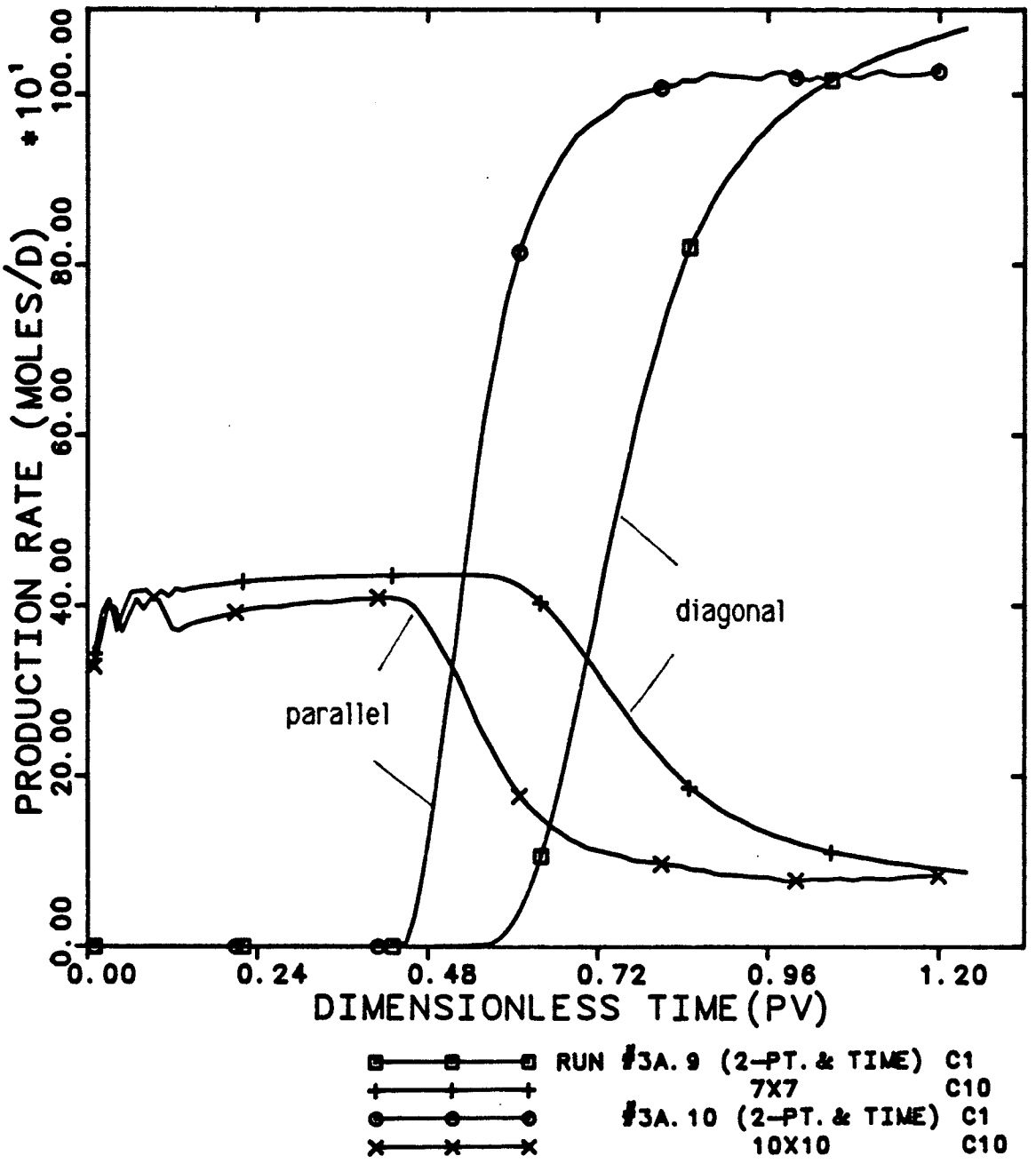

Fig. 4.4-9 Methane and decane production rate histories for Runs * 3A.9 and 3A.10.

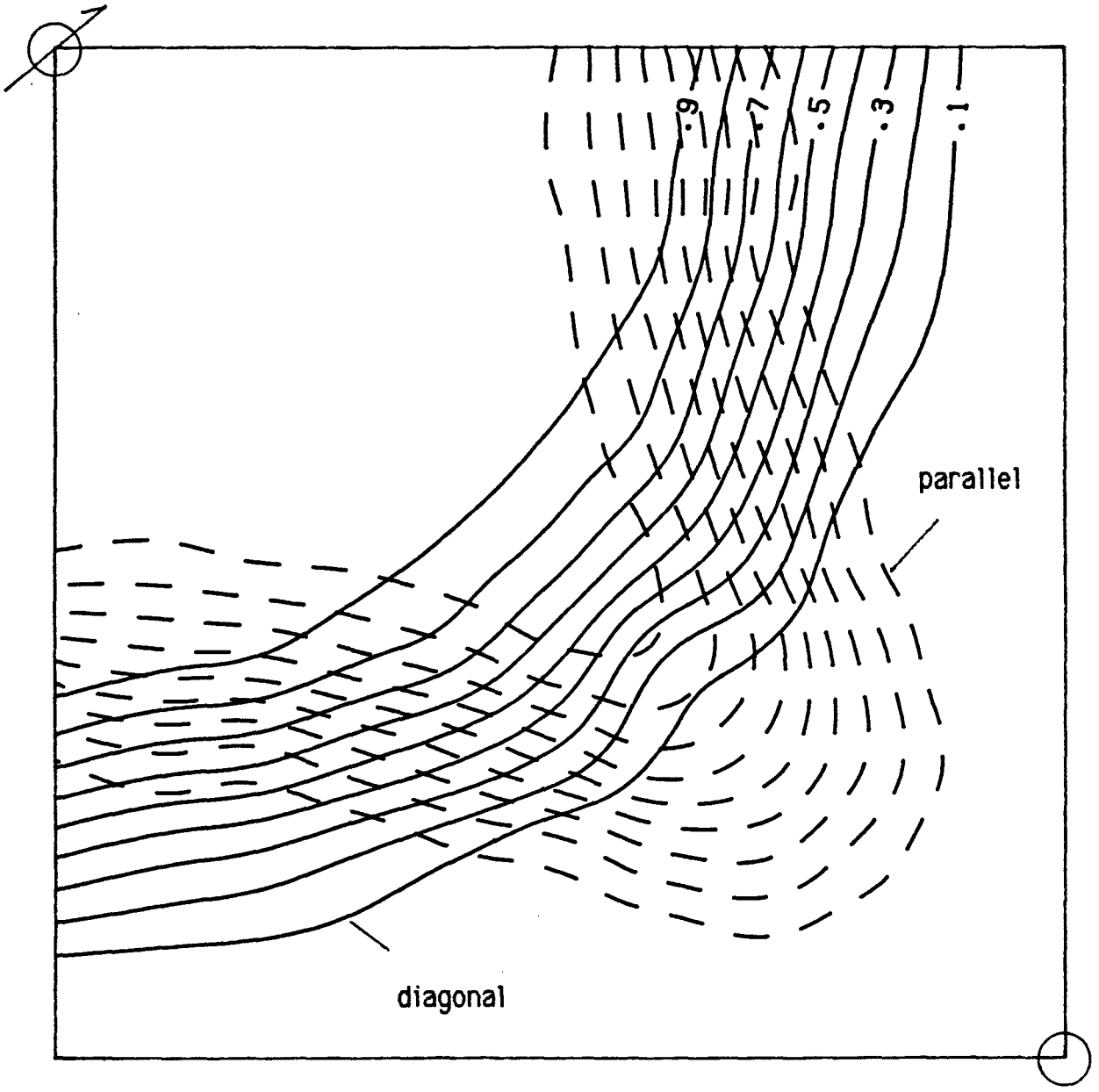

Fig. 4.4-10 Methane mole fraction contours for Runs * 3A.11 and 3A.12 (small Δt) at 0.4 DPV (M = 11.4).

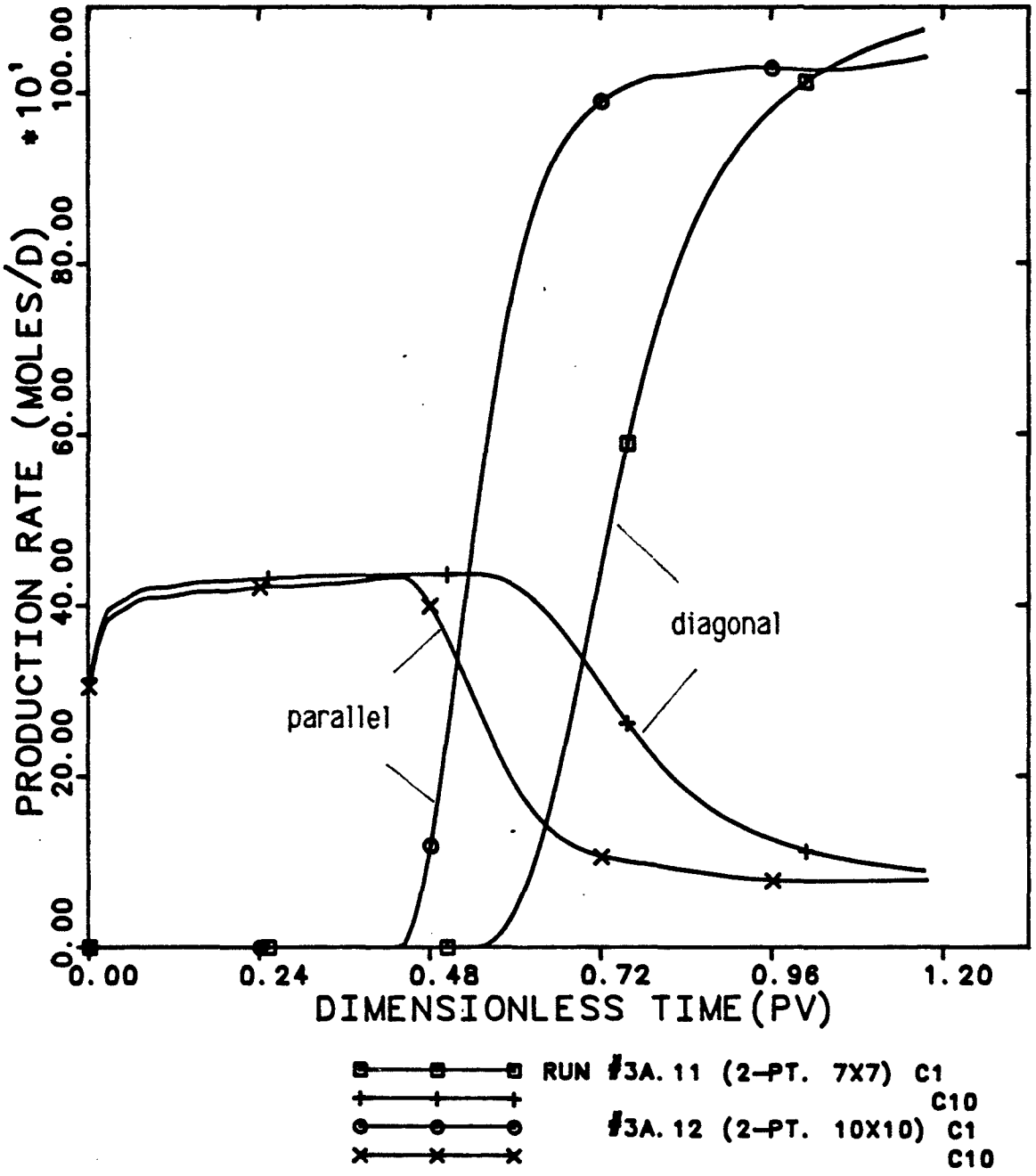

Fig. 4.4-11 Methane and decane production rate histories for Runs # 3A.11 and 3A.12.

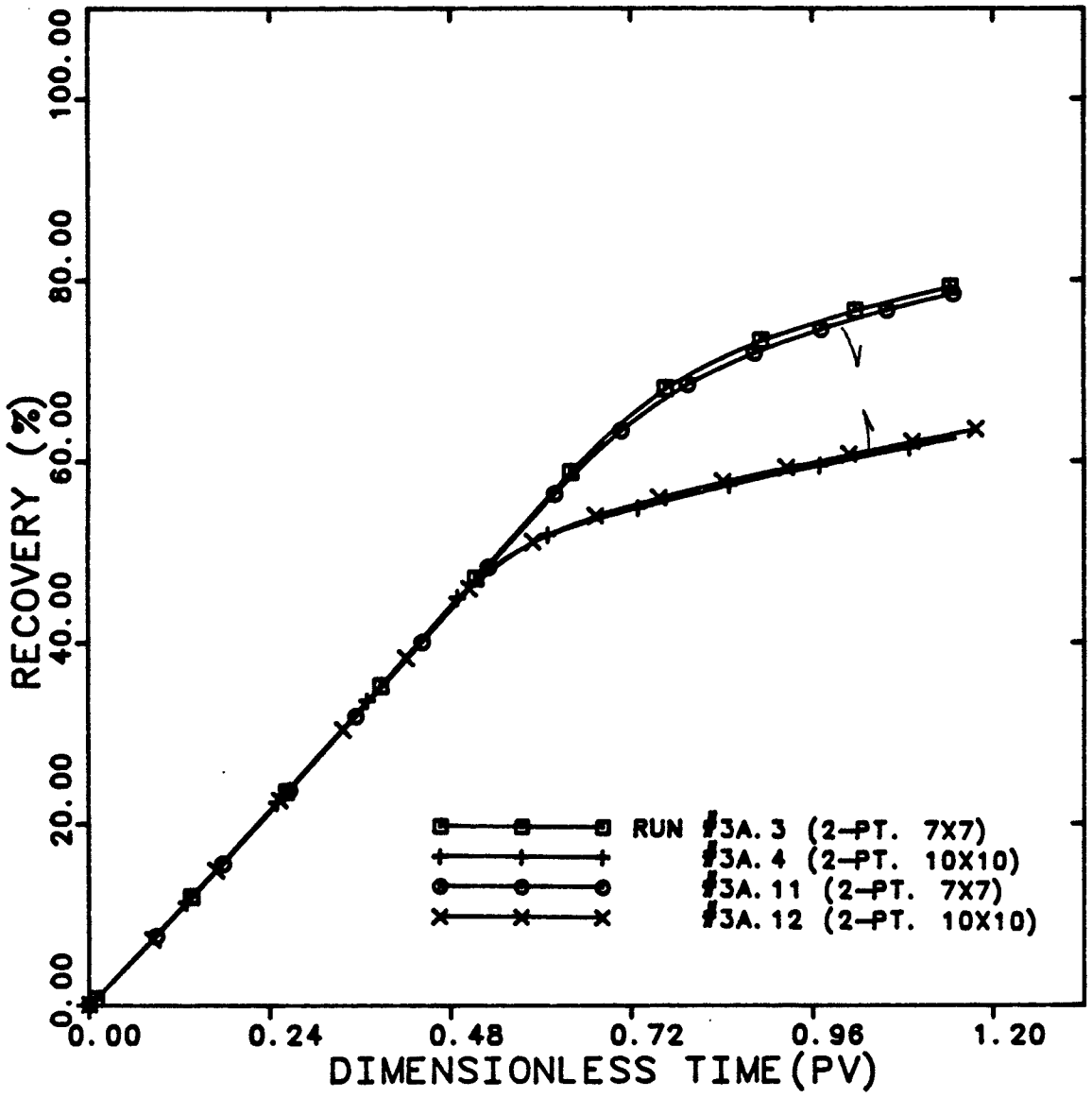

Fig. 4.4-12 Decane recovery histories for Runs # 3A.3, 3A.4, 3A.11, and 3A.12.

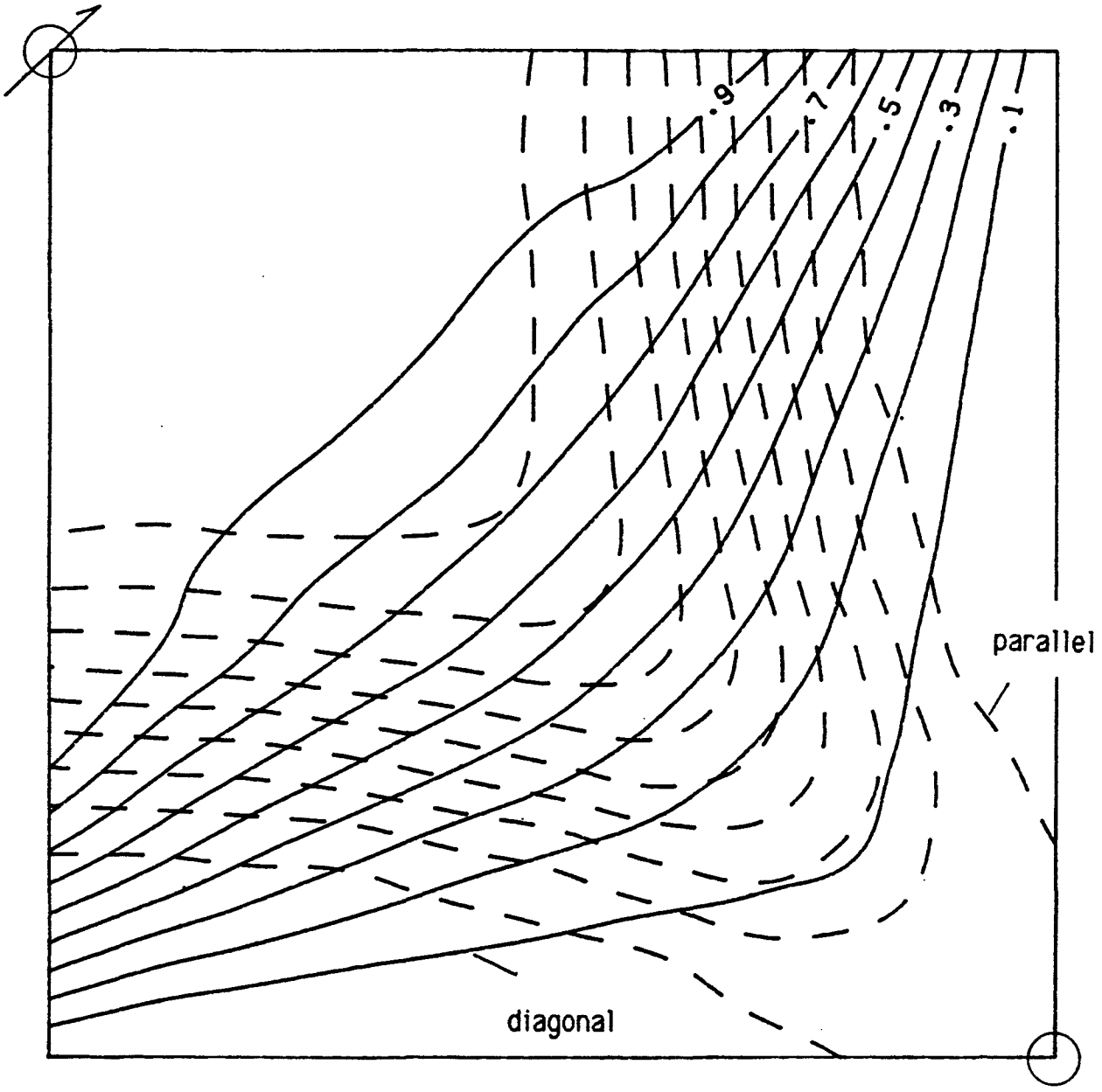

Fig. 4.4-13 Methane mole fraction contours for Runs * 3A.13 and 3A.14 (α_l^P = 5.0 ft, α_t^P = 1.0 ft)
(parallel --- α_l^{input} = 0, α_t^{input} = 1.0 ft)
(diagonal -- α_l^{input} = 1.46 , α_t^{input} = -2.54)

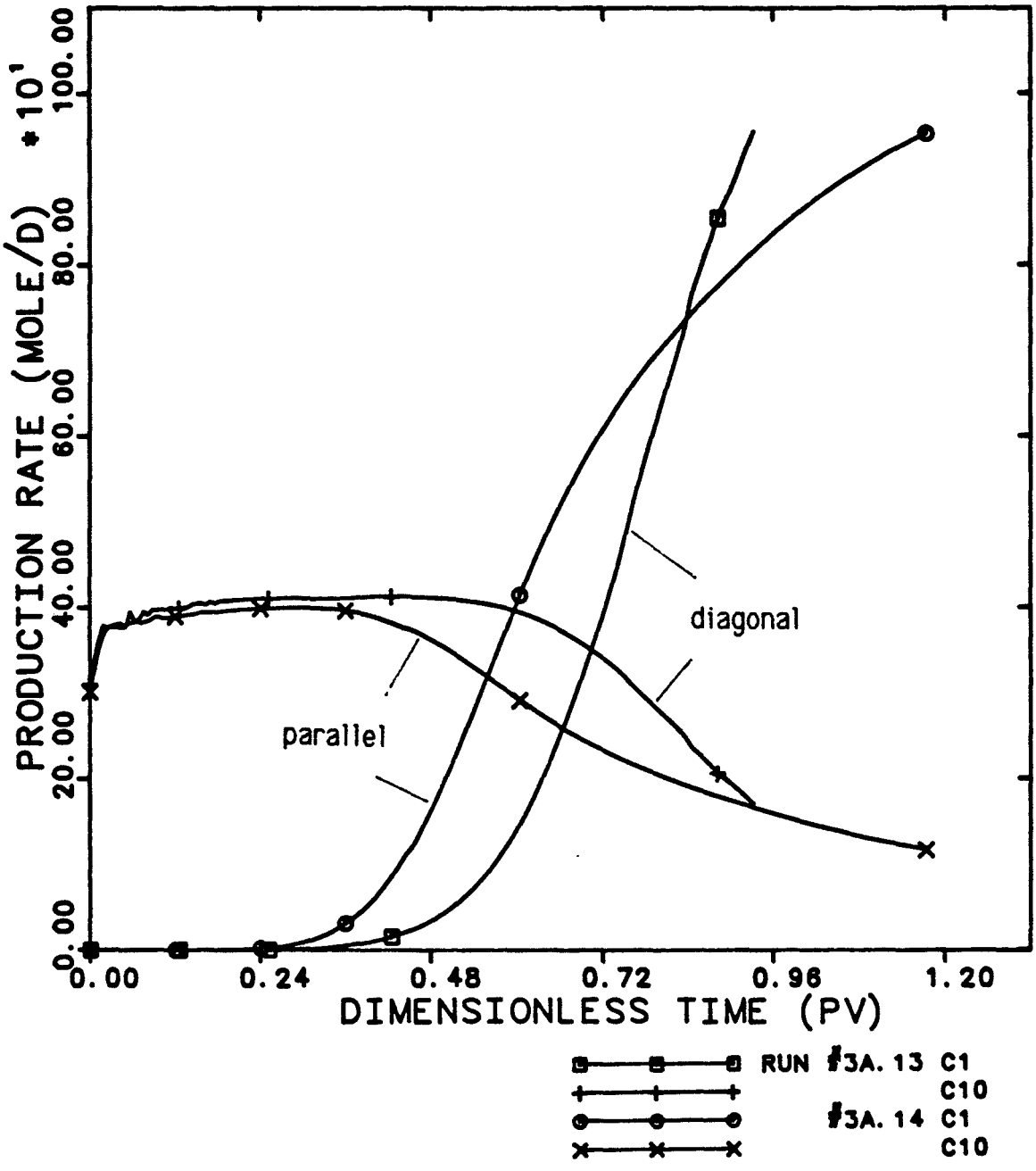

Fig. 4.4-14 Methane and decane production rate histories for Runs # 3A.13 and 3A.14.

CHAPTER V

APPLICATION RUN RESULTS AND DISCUSSIONS

The importance of numerical dispersion reduction in the miscible displacements was well recognized through the simple test runs described in the previous chapter. This chapter presents the results of runs which are a little bit more realistic than the test runs.

The application runs also consist of three classes of runs. Class-4 runs are a series of slim tube displacements to investigate the minimum miscibility pressure (MMP), simultaneous injection of solvent and water, and slug process followed by water. Class-5 runs and Class-6 runs are 2-D areal, and 2-D cross-sectional displacements, respectively. Run-statictics and specifications are listed in Appendix-D.

5.1 General Remarks

In addition to the remarks listed in Sec. 4.1, the following are valid through this chapter.

(1) The "All 2-Point" scheme is used consistently, unless otherwise mentioned. Theoretically, "All 2-Point" scheme should be better than the "Composition 2-Point" which treats only mole fractions as second-order correct. However, the two-point upstream weighted relative

permeabilities have some hazardous aspects as described in the original paper [T4]. For example, suppose we are simulating a first-contact miscible displacement followed by water. There are three grid blocks (i-1, i, i+1), and the (i-1) th grid contains 100 % water (all hydrocarbons are displaced, K_{rw} = 1.0) while the (i) th grid still has a finite hydrocarbon saturation ($0 < K_{rw} < 1.0$). The (i+1) th grid has residual water saturation (K_{rw} = 0.0). Then, the extrapolated value of water relative permeability at the (i+1/2) face may become negative, and must be reset to the smallest adjacent value (the downstream value in this case) by the constraint Eq.(3.2.2-3). If this situation occurs, water can never flow into the (i+1) th grid from the (i) th grid. This is, of course, incorrect, but its also an extreme case. If this kind of phenomena were to be met frequently in practical simulation runs, the use of the "All 2-Point" scheme becomes questionable. To check this, "All 2-Point" was used extensively (the water conservation equation is also treated by two-point upstream weighting).

(2) Forty (40) grid blocks are always used for 1-D runs.

(3) Solvent is always CO_2, and the displaced fluid, oil, has the following composition (mole fractions):

CO_2	0.0001
C_4	0.5999
C_{10}	0.4000

(4) Recovery of component i is calculated as:

Recovery = (moles produced) /
(moles inplace when flood started)

Hence, recovery in a tertiary flood is a fraction of waterflood residual.

5.2 MMP, WAG, and SLUG Runs (Class-4)

5.2.1 Description of Runs

The run-numbering convention is slightly more complicated in this class; therefore, it will be given first. The first digit, which indicates the class number as usual, will be followed by two letters. The first letter will be "S" or "T". "S" refers to a secondary displacement, and "T" means a tertiary displacement. The second letter will be "A", "B", "C", "D", "E", "F", and "K". The letters from "A" to "F" indicate the volume fraction of water in the displacing fluid at reservoir condition. "A" refers to pure solvent injection and "F" is pure water injection, that is, waterflooding. "B", "C", "D", and "E" indicates 0.2, 0.4, 0.6, and 0.8

water volume, respectively. "K" is something special, it means pure solvent injection with single-point upstream weighting. Finally, the run-number ends with a digit, varying from "1" to "6", which represents the run pressure, 1400, 1600, 1700, 1800, 2000, and 2400 psia, respectively. For example, "4TD5" describes a run which is tertiary, simultaneous injection of solvent and water (0.6 volume fraction), and is conducted at 2000 psia. Besides these, there are several slug runs which have run-number of "4SLG2" type, and Table 5.2-1 shows the summary of run-numbering for Class-4 runs.

The reservoir system (slim tube) is exactly the same as Class-1 and Class-2 runs (Table 4.2.-1).

There are three reasons for Class-4 runs. The first one is to investigate the effect of dispersion on MMP. ALL Class-4 runs were made without physical dispersion, but the effect of nemerical dispersion will be presented. Second, the effect of mobile water phase on MMP will be described. The simulator has neither the capability of modeling the water solubility of solvent nor the water blocking phenomenon. Therefore, only the effect of the hydrodynamics of the flowing water phase can be studied. The final purpose is to compare the efficiency of various slug sizes under the developed miscibility. The MMP and the effective slug size will be used for Class-5 and Class-6 runs.

5.2.2 Three Phase Relative Permeability Functions

Coats [C9] and Nghiem et al. [N2] proposed three-phase

relative permeability functions which were basically based on Stone's model. They treated gas-oil relative permeabilities as functions of saturations and interfacial tension (see Table 4.3-2), and combined them with fixed water-oil relative permeability curves to produce three-phase relative permeability functions.

However, this treatment is not consistent. Suppose that a grid glock contains water and a fluid, named oil under this particular condition, whose composition is very close to the plait point composition, and its saturation is at the residual to water, S_{orw}^{*}. This fluid, oil, could never flow out from this block as long as fixed oil-water relative permeability curves are used. However, this fluid might be renamed as gas by an infinitesimal pressure change. At this moment, The fluid, gas, could start moving, since the residual saturation of gas to water is usually less than that of oil. In other words, the relative permeability value for this fluid would shift discontinuously from zero (on the oil relative permeability curve of oil-water system) to a certain finite value (on the gas relative permeability curve of gas-oil system). This discontinuous change is due to the fixed residual oil saturation to water.

To prevent this, the hydrocarbon residual saturation to water should continuously change from oil to gas, probably as a function of fluid composition. In this study, a simple cubic which is only a function of the lightest component mole fraction was used to

connect S_{orw}^* and S_{grw}^*. Actually, this connecting function should be a function of total composition and capillary number. Perhaps phase density is a good candidate for the dependent variable.

Fayers and Matthews [F2] mentioned that Stone's Method I, with an improved definition of S_{om}, would be more accurate than the normalized Method II. However, here Method II was used to combine K_{rog} and K_{row}. A detailed description is given in Table 5.2-2. These functions were used consistently through this chapter.

5.2.3 Results and Discussions

Our solvent (CO_2) and oil (C_4-C_{10}) system is so simple that it is suitable for a ternary representation. Fig. 5.2-1 shows the two phase envelops for various pressures. The two phase region shrinks very rapidly as pressure increases because of the simplisity of the system.

The definition of minimum miscibility pressure (MMP) and the correlations to estimate MMP have been appeared in many papers [B3, H3, M2, Y2, H4, A1], and summarized by Stalkup [S3] and Klins [K1]. For practical purposes, MMP may be roughly estimated by the break point in the recovery versus pressure curve as a result of a series of slim tube experiment or simulation runs. On the other hand, theoretically MMP for a certain composition of oil may be obtained from the critical tie line extension. Fig. 5.2-2 shows the tie line extensions at 1700 psia. MMP for all compositions on this

critical tie line extension (including our oil composition) should be 1700 psia for CO_2 injection.

Recovery versus pressure plots were made from the results of 4SA and 4SK runs (Fig. 5.2-3). Remember that these runs were pure CO_2 injection without water, and single-point upstream weighting was used in 4SK runs while 4SA runs adopted two-point upstream weighting. 4SA runs show a clear break point around 1600 psia for both the butane and decane curves. This agrees fairly well with the estimation from the tie line extension. However, 4SK runs give gradually increasing curves and the break point is not obvious. Fig. 5.2-4 shows the composition routes for Run * 4SK3 and *4SA3 (1700 psia). The route for single-point upstream weighting goes deeply into the two-phase region because of large amount of numerical dispersion. The same tendency should be observed, when a physical dispersivity is used [G1]. The reason for the curvature of the composition route of the two-point upstream weighting in one phase region is unknown. The decane recovery curve of the 4SA runs (Fig. 5.2-3) shows a sudden increase of recovery from 1800 psia to 2000 psia. This is due to the simplicity of the system. As shown in Fig. 5.2-1, the two-phase region shrinks very first with pressure increases, and at 2000 psia, this system is first-contact miscible (FCM). For a vaporizing-gas drive displacement, a small amount of liquid phase will be left behind the displacing front, which causes a slightly lower recovery of the heavy component than

the FCM [S3]. Thus, the change from MCM (multiple-contact miscible, 1800 psia) to FCM (2000 psia) produced a jump in the decane recovery. Figs. 5.2-5 and 5.2-6 show overall composition profiles of Run * 4SA4 (1800 psia) and * 4SA5 (2000 psia). In Fig. 5.2-5, decane tail can be seen behind the front, but not in Fig. 5.2-6.

The results from the 4S (except for 4SK) and 4T runs are summarized in the recovery contour plots in Figs. 5.2-7 --- 5.2-10. In these figures, the horizontal axis shows the water volume fraction in the injection fluid, and the vertical axis indicates pressure. Therefore, the displacement mechanism is changing from IM (immiscible) to FCM, moving from the bottom to the top. The right most side corresponds to waterflooding while the left most side is continuous CO_2 injection without water (Fig. 5.2-3 was made along this line). Thirty four (34) and thirty (30) data points were used for the 4S and 4T plots, respectively (Table 5.2-1). The recoveries were picked 1.2 displaceable pore volume was injected.

Several observations may be made from these figures. First, in general, recovery is very high since the system is so simple. Second, the optimal water volume fraction is probably 0.8. This corresponds to a WAG ratio, W_R, defined as Q_W/Q_S, of 4. From the view point of conserving solvent, a combination of this value and MMP (1700 psia) should be the best (marked as "A" in the figures). Remember that S_{orw}^* (the initial residual oil saturation to

water) was set to 0.3. Above this optimal water volume fraction of 0.8, water moves faster than solvent (CO_2), and displace oil immiscibly leaving water residual oil behind the front. Less than 0.2 volume fraction of CO_2 would not be enough to recover this residual oil. Third, the characteristic shape of the contours is the same for the 4S and 4T runs except for the starting value of waterflood recovery. (Of course, zero for tertiary runs.) Fourth, and finally, the presence of the mobile water phase doesn't affect significantly the MMP.

Tiffin and Yellig [T3] concluded from their experiments that the overall recovery and the mechanism of developing miscibility was basically the same for secondary and tertiary CO_2 flood, however, the simultaneous injection of water with CO_2 in water-wet tertiary displacements trapped a significant amount of oil. Dai and Orr [D1] showed the effect of dendritic and trapped fraction for secondary and tertiary floods from the results of their 1-D simulator. These properties were also modeled by Chase and Todd [C2]. At this time, these phenomena are neglected in our simulator, however, the basic observations agrees well with these authors.

Several typical profile plots will be demonstrated and explained briefly. Figs. 5.2-11 and 5.2-12 are the overall composition profiles of 4SK3 (single-point upstream weighting) and 4SA3 (two-point upstream weighting). The front smeared by

numerical dispersion is obvious in Fig. 5.2-11.

Figs. 5.2-13 --- 5.2-24 are sets of profiles, saturations, overall compositions, and molar fluxes, of 4TB3, 4TD1, 4TD3, and 4TD6 runs. The following can be observed from these plots.

(1) 4TB3 (water vol. frac. 0.2) and 4TD3 (water vol. frac. 0.6) Figs. 5.2-13 --- 5.2-15, 5.2-19 --- 5.2-21

The size of the oil bank and its composition are almost the same. In 4TD3, water and CO_2 (gas) fronts are moving together, while the water is slower than CO_2 in 4TB3. 4TD3 is more economical.

(2) 4TD1 (IM) and 4TD3 (MCM) Figs. 5.2-16 --- 5.2- 21.

The oil bank saturation is higher in 4TD3, since a larger amount of oil is left behind the displacing front in 4TD1. Also, the composition profiles shows the amount of decane in the residual oil is higher in 4TD1.

(3) 4TD3 (MCM) and 4TD6 (FCM) Figs. 5.2-19 --- 5.2-24

All butane and decane were displaced ; hence, the oil bank is larger in 4TD6. Moreover, the shape of oil bank looks stable, since the numerical solution itself is much easier in FCM. Fugacity constraints are not required because only one hydrocarbon phase exists. Fractional flow curves for this FCM system are shown in Fig. 5.2-25. The oil bank saturation at the leading edge

from this figure may be obtained as about 48 %. This value well agrees the simulation result (Fig. 5.2-22). On the other hand, the trailing edge saturation from the fractional flow construction (60 %) is slightly lower than the value from Fig. 5.2-22 (65 %). This is because the fractional flow construction assumes no mixing of oil and solvent, but our simulator doesn't. Hence, the composition of the trailing edge of the oil bank from the simulation result is almost pure CO_2. The location of oil bank can not be estimated from the fractional flow curve construction, because, as previously mentioned (Sec. 4.1), the definition of dimentionless time is not rigorous.

Finally, this section presents the results of slug runs. A series of slug runs was made for each secondary and tertiary case. A finite volume of solvent was chased by water at MMP (1700 psia). The results are summarized in Fig. 5.2-26, which is the plots of displacement efficiency, since the system is one dimensional and areal (E_A) and vertical sweep efficiency (E_V) are unity. This figure shows the minimum slug size requirement is approximately 0.2 DPV for both the secondary and tertiary displacements. Figs. 5.2-27 and 5.2-28 show the molar flux profiles for 4SLG1 and 4SLG3 (both secondary). In Fig. 5.2-27, CO_2 was almost completely lost in the

residual oil phase and leaving the water to push the oil immiscibly, while Fig. 5.2-28 shows a still moving CO_2 bank. The minimum requirement of solvent slug volume is related to the residual oil saturation.

5.3 2-D Areal MCM Runs (Class-5)

5.3.1 Description of Runs

The purpose of Class-5 runs is to investigate the effect of longitudinal and transverse dispersion on 2-D areal slug displacements. Oil and solvent compositions are exactly the same as in the previous section (oil - C_4 0.5999, C_{10} 0.4, CO_2 0.0001, solvent - pure CO_2). The minimum miscibility pressure (1700 psia) from the slim tube simulation in Sec. 5.2 was chosen for the bottom hole production pressure. This was to ensure a MCM displacement, and it was required since, as shown in Sec. 4.3.2, the dispersion effect is more important when interphase mass transfer is large. A homogeneous and isotropic reservoir was assumed; this is detailed in Table 5.3-1. A diagonal grid system was selected simply because it saves storage and computation time. Two sets of physical dispersivities (longitudinal and transverse) were used to model a relatively small dispersion case ($N_{pe,l}$ =1000), and a fairly large dispersion case ($N_{pe,l}$ = 20). The ratio of longitudinal and transverse dispersivity was always kept constant at 10.

Run-numbering is simple ; the class number (5) is followed by the sequential number.

5.3.2 Results and Discussions

This subsection presents a comparison of small and large dispersion runs through several types of contour plots. And

after this, the effect of slug size will be shown.

A slug size of 0.2 DPV was chosen as a base case from the results of Sec. 5.2. Water was used as a driving fluid. Fig. 5.3-1 shows the CO_2 dimensionless concentration (defined as the concentration divided by the concentration of injected CO_2) contour at 0.5 DPV injected for the small dispersion case. Compare with Fig. 5.3-2, a large dispersion case. The position of the peak concentration is the same ; however, the dilution of CO_2 bank is much more in the large dispersion case. The contours of net flux and dispersive accumulation ratio present the difference even more clearly (Figs. 5.3-3 --- 5.3-6). The definition of these terms were given in Sec. 4.2.2. Fig. 5.3-3 shows that CO_2 is moving mainly along the diagonal (the shortest stream line) in a small dispersion case, while the large dispersion case shows more averaged movement. A comparison of dispersive accumulation ratio gives a more drastic contrast. In Fig. 5.3-5, the region where dispersive flux dominates is very compact, while the large dispersion case shows a wide band of dispersive flux dominated region (Fig. 5.3-6). Note that, behind the bank, dispersive flux is very small since water is displacing CO_2 immiscibly. Fig. 5.3-7 and 5.3-8 shows water saturation contours.

Finally, the recoveries as a function of slug size are shown in Fig. 5.3-9. The recovery from the large dispersion case is

about 5 percent lower than the small dispersion case. This is because the dilution of the solvent bank due to large dispersion reduced the effectiveness of the miscible displacement and caused a faster break through of CO_2. There is a peak in the recovery plots, although the location of the peak (optimum slug size) may be moved by the additional runs. This peak is a product of the displacement efficiency (Fig. 5.2-26) and the areal sweep efficiency which is probably a monotonically decreasing function of solvent slug size.

From run experience , a very small time step size was required for the small dispersion case when the leading or trailing fronts of solvent was near the injection well block. The same was true for cross-sectional runs. (See Appendix-D.) It was very troublesome and expensive to select the time step size manually. An automatic time step selector should be required.

5.4 2-D Cross-sectional MCM Runs (Class-6)

5.4.1 Description of Runs

As for the Class-5 runs, the study of the effect of longitudinal and transverse dispersion is the purpose of the Class-6 runs ; however, the behavior in the vertical direction will be emphasized using a cross-sectional model.

The reservoir is isotropic, and contains two layers, the top of which is five times more permeable than the bottom one. A detailed description of the reservoir and the grid system (20x4) is given in Table 5.4-1 and Fig. 5.4-1. The reservoir fluid (oil) and

solvent (CO_2) are exactly the same as the Class-5 runs.

A large dispersion case (longitudinal dispersivity = 5.0 ft, transverse dispersivity = 0.5 ft) and a small dispersion case (0.1 ft, 0.01 ft respectively) were run using the same slug size (0.2 DPV) followed by water. The bottom hole pressure of the upper most production well block was set to 1700 psia (MMP). These results will be compared with a waterflood case.

The run-numbering convention is the same as for the Class-5 runs ; the class number (6) is followed by a sequential number.

5.4.2 Results and Discussions

Remember, in Sec. 3.1.1, the suppression of viscous fingering was given as one of the favorable features of dispersion. A similar phenomenon will be shown by the results of Class-6 runs. It probably should be called a suppression of macroscopic fingering or channelling.

Figs. 5.4-2 and 5.4-3 show the CO_2 dimensionless concentration (defined in Sec. 5.3-2) at 0.4 DPV injected for the small and large dispersion cases, respectively. The position of CO_2 leading edge in the upper layer is approximately the same, but the area of high concentration region is small in large dispersion case, since a large amount of CO_2 was moved into the lower layer by

transverse dispersion. The movement of the CO_2 bank can be seen more clearly by net flux contours (Figs. 5.4-4 and 5.4-5). In the small dispersion case, CO_2 accumulation is mainly taking place in the upper layer at just before the production end. In the large dispersion case, there is little CO_2 accumulation observed, suggesting an averaged or spread out CO_2 concentration.

Figs. 5.4-6 and 5.4-7 show the contours of C_{10} (displaced component) dimensionless concentration (defined as the concentration divided by the initial concentration). Clearly, the lower layer was swept better in the large dispersion case. The resaturation of decane occured in the small dispersion case (shaded region A in Fig. 5.4-6). Decane in this region was displaced once by the CO_2 bank and was driven forward. After the CO_2 bank passed by, decane was supplied from unswept lower layer. This resaturated decane would be partially displaced immiscibly by chase water. Fig. 5.4-8 indicates the movement of this decane (region B) and the trailing edge of decane which was miscibly displaced by CO_2 bank (region C). Fig. 5.4-9 doesn't show this kind of phenomenon, but it does show a uniform displacement of decane.

Figs. 5.4-10 and 5.4-11 show very similar profiles of water saturation. This is because gravity worked favorably to stabilize the water front. If the order of layers were reversed, namely the lower layer is the more permeable, most of water flows

into the lower layer and this results very rapid water break through.

Finally, the decane residual concentration (dimensionless) at the end of flood (1.2 DPV) is shown in Figs. 5.4-12 and 5.4-13 A large amount of decane was left in the lower layer in the small dispersion case.

The recoveries are listed in Table 5.4-2. Note that the large dispersion case showed a slightly higher recovery than the small dispersion case. In the previous section (Class-5 runs), the large dispersion case recovered smaller amount of oil. In this class (6), the aspect ratio (the reservoir length devided by the reservoir width or thickness depends on the 2-D geometry) is large (100/20 = 5), and therefore transverse dispersion plays a more important part than in the Class-5 runs (the aspect ratio = 1), as shown by Lake and Hirasaki [L3], and Giordano and Salter [G3] through dimensional analysis. Large transverse dispersion prevented early break through of CO_2, and effectively recovered oil from the lower layer.

TABLE 5.2-1

Summary of Run-numbering for Class-4 Runs

Secondary Displacement :

$$Q_w/(Q_w \pm Q_s)$$

Pressure (psia)	0	0.2	0.4	0.6	0.8	0.95	1.0
2400	4SK6 4SA6	4SB6	4SC6	4SD6	4SE6	-----	4SF6
2000	4SK5 4SA5	4SB5	4SC5	4SD5	4SE5	-----	-----
1800	4SK4 4SA4	4SB4	4SC4	4SD4	4SE4	-----	-----
1700	4SK3 4SA3	4SB3	4SC3	4SD3	4SE3	4SEF3	-----
1600	4SK2 4SA2	4SB2	4SC2	4SD2	4SE2	-----	-----
1400	4SK1 4SA1	4SB1	4SC1	4SD1	4SE1	4SEF1	4SF1

TABLE 5.2-1 (Continued)

Tertiary Displacement :

$Q_W/(Q_W+Q_S)$

Pressure (psia)	0	0.2	0.4	0.6	0.8	0.95
2400	4TA6	-----	-----	4TD6	-----	-------
2000	4TA5	4TB5	4TC5	4TD5	4TE5	4TEF5
1800	4TA4	4TB4	4TC4	4TD4	4TE4	-------
1700	4TA3	4TB3	4TC3	4TD3	4TE3	4TEF3
1600	4TA2	4TB2	4TC2	4TD2	4TE2	-------
1400	4TA1	4TB1	4TC1	4TD1	4TE1	4TEF1

TABLE 5.2-1 (Continued)

Slug Displacement : (followed by water)

Pressure (psia) 1700

	Slug Size (displaceable pore volume)				
	0.1	0.18	0.2	0.3	0.4
Secondary	4SLG1	-----	4SLG2	4SLG3	-----
Tertiary	4SLG4	4SLG5	-----	-----	4SLG7

TABLE 5.2-2

Relative Permeability Functions

for Class-4, 5, 6 Runs

$$K_{rw} = K_{rwro}\left(\frac{S_w - S_{wr}}{1 - S_{wr} - S_{orw}}\right)^{EW}$$

$$K_{row} = K_{roiw}\left(\frac{1 - S_w - S_{orw}}{1 - S_{wr} - S_{orw}}\right)^{EOW}$$

$$\overline{K}_{rg} = K_{roiw}\left(\frac{S_g - S_{grw}}{1 - S_{grw}^{*} - S_{wr}}\right)^{EG}$$

$$\overline{K}_{rog} = K_{roiw}\left(\frac{S_o - S_{org}}{1 - S_{org} - S_{wr}}\right)^{EOG}$$

$$K_{rg} = (1-e^{-AG\cdot R})\cdot \overline{K}_{rg} + e^{-AG\cdot R}\cdot K_{roiw}\cdot [S_g/(1-S_{wr})]^{1+BG\cdot R}$$

$$K_{rog} = (1-e^{-AO\cdot R})\cdot \overline{K}_{rog} + e^{-AO\cdot R}\cdot K_{roiw}\cdot [S_o/(1-S_{wr})]^{1+BO\cdot R}$$

$$K_{ro} = K_{roiw}\cdot [(K_{row}/K_{roiw} + K_{rw})\cdot(K_{rog}/K_{roiw} + K_{rg}) - (K_{rw}+K_{rg})]$$

TABLE 5.2-2 (Continued)

,where $S_{org} = S_{org}^{*} \cdot (1-e^{-AG \cdot R})$, $R = \sigma / \sigma^{*}$

$S_{orw} = \text{Min}\,(S_o\,,\ S_{orw}^{**})$

$S_{grw} = \text{Min}\,(S_g\,,\ S_{grw}^{**})$

$S_{orw}^{**} = A \cdot (x_{1,N})^3 + B \cdot (x_{1,N})^2 + S_{orw}^{*}$

$S_{grw}^{**} = A \cdot (y_{1,N})^3 + B \cdot (y_{1,N})^2 + S_{orw}^{*}$

$A = 2 \cdot (S_{orw}^{*} - S_{grw}^{*})$

$B = 3 \cdot (S_{grw}^{*} - S_{orw}^{*})$

$x_{1,N}$ $(y_{1,N})$: mole faraction of the lightest hydrocarbon in oil (gas) phase in N th grid block.

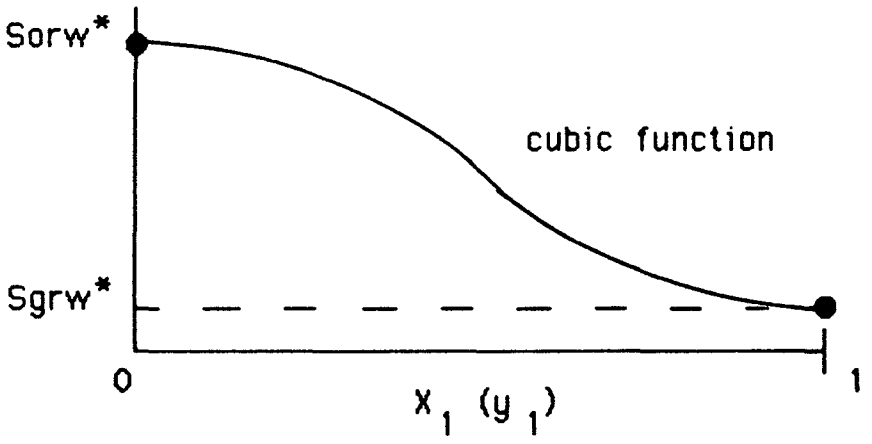

TABLE 5.2-2 (Continued)

σ^* =	2.0	AG =	1.0	EW =	2.0
S_{wr} =	0.2	BG =	2.0	EOW =	2.0
S_{grw}^* =	0.0	AO =	1.0	EOG =	2.5
S_{orw}^* =	0.3	BO =	1.0		
S_{org}^* =	0.2	EG =	2.0		
K_{roiw} =	1.0	K_{rwro} =	0.39		

TABLE 5.3-1

Reservoir Description for Class-5 Runs

Diagonal Grid (7x7)

Dimensions (ft)	
Length	70
Width	70
Thickness	10
Permeability (md)	500
Porosity (fraction)	0.3
Rock compressibility (psi^{-1})	0.45×10^{-5}
Temperature (F)	200
Initial water saturation (fraction)	0.2
Initial pressure (psia)	1700
Dispersivity (ft)	
small case (longitudinal)	0.1
(transverse)	0.01
large case (longitudinal)	5.0
(transverse)	0.5

TABLE 5.4-1

Reservoir Description for Class-6 Runs

Dimensions (ft)	
Length	100
Width	5
Thickness	20
Permeability (md)	
Top layer	2500
Bottom layer	500
Porosity (fraction)	0.3
Rock compressibility (psi^{-1})	0.45×10^{-5}
Temperature (F)	200
Initial average pressure (psia)	1710
Dispersivity (ft)	
small case (longitudinal)	0.1
(transverse)	0.01
large case (longitudinal)	5.0
(transverse)	0.5

TABLE 5.4-2

C_4 and C_{10} Recovery (@ 1.2 DPV)

	Percent Recovery	
	C_4	C_{10}
Small Dispersion Case (*6.1)	68.8	68.1
Large Dispersion Case (*6.3)	69.9	69.6
Waterflood (*6.4)	60.9	60.9

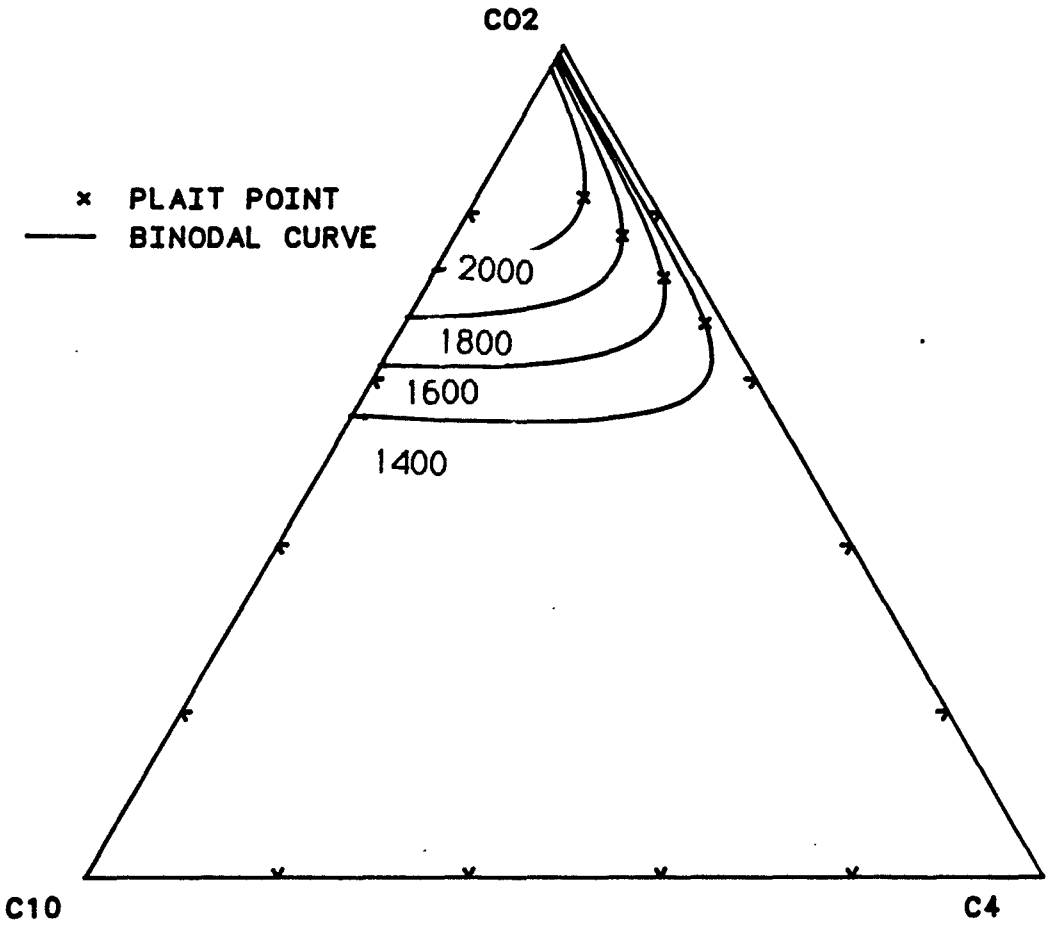

Fig. 5.2-1 Ternary diagram for $CO_2 - C_4 - C_{10}$ system at 1400, 1600, 1800, 2000 psia and 200 F.

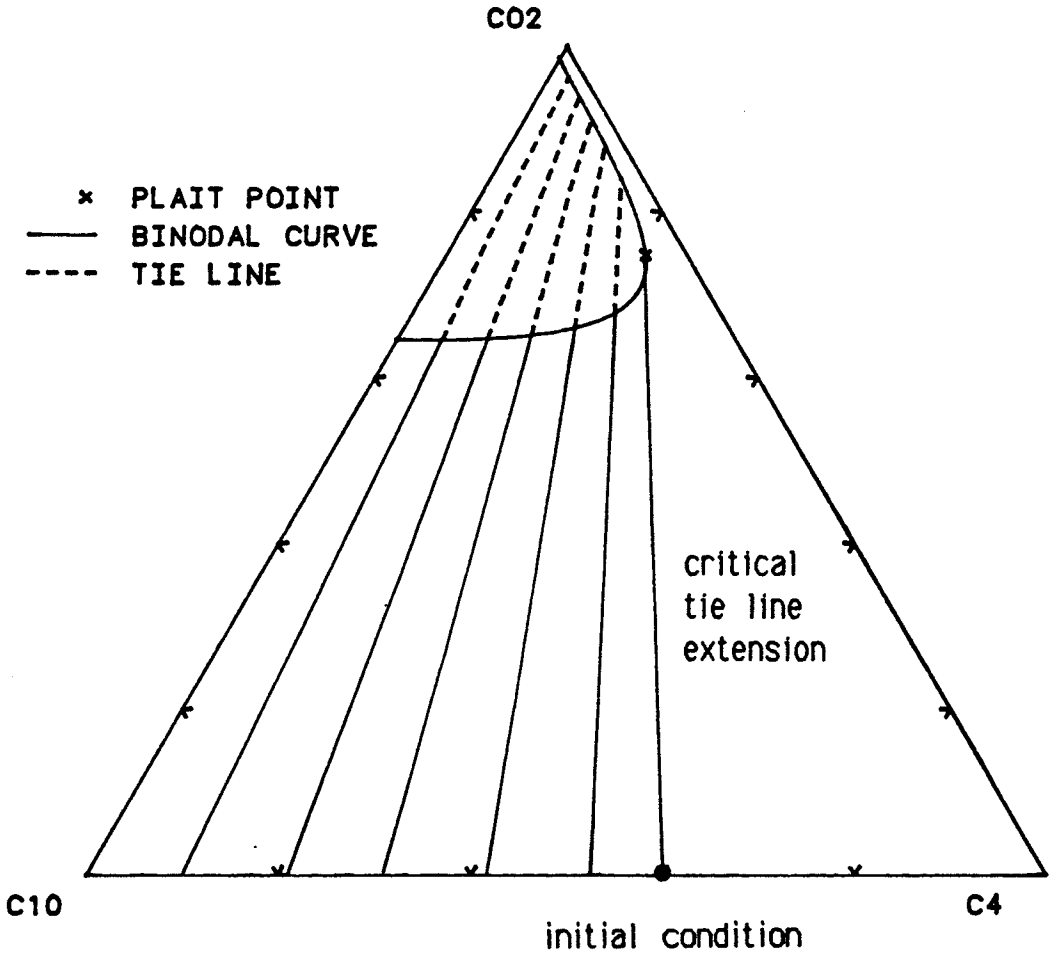

Fig. 5.2-2 Ternary diagram for $CO_2 - C_4 - C_{10}$ system at 1700 psia and 200 F.

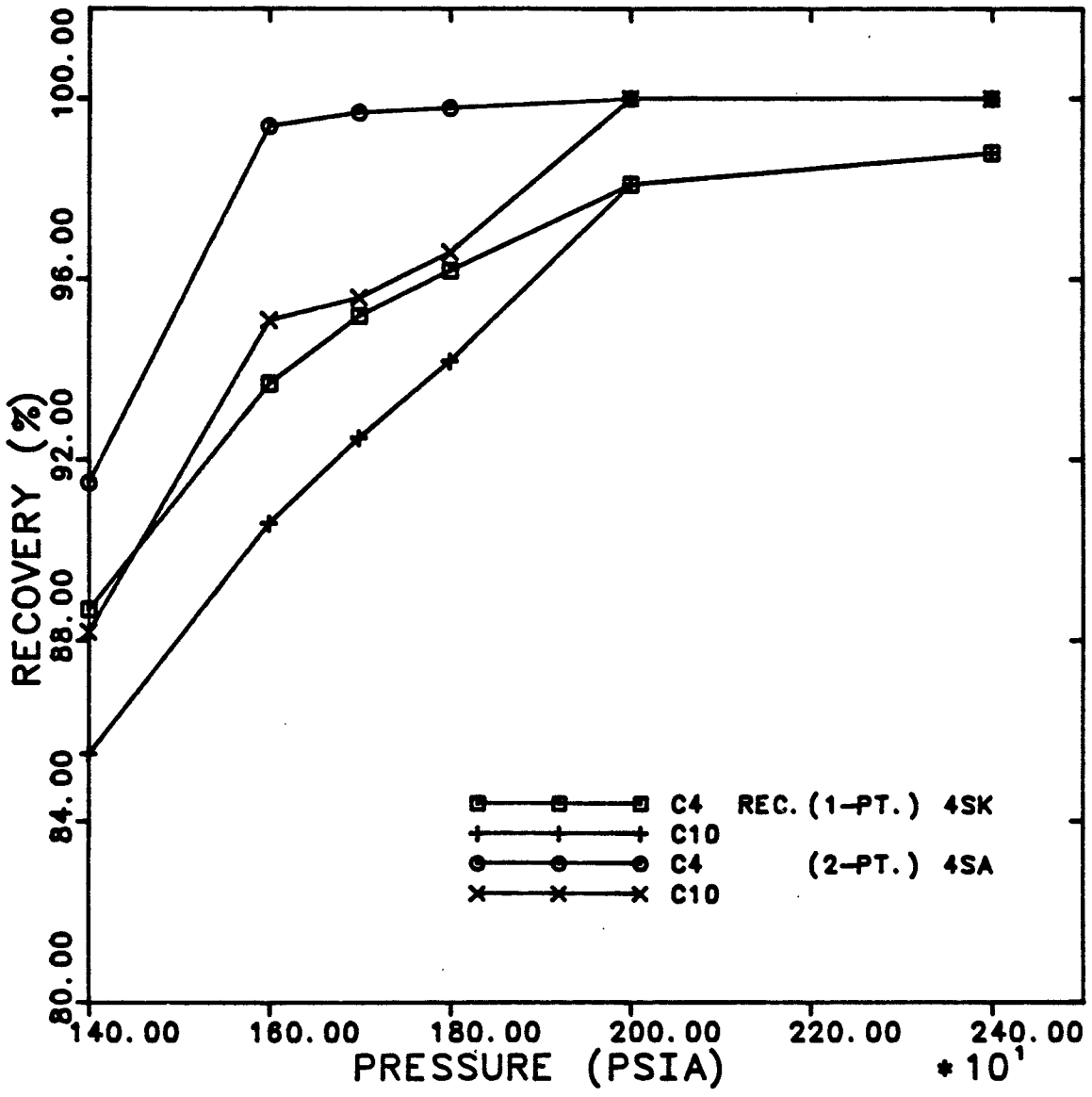

Fig. 5.2-3 Butane and decane recovery for 4SA and 4SK runs versus pressure.

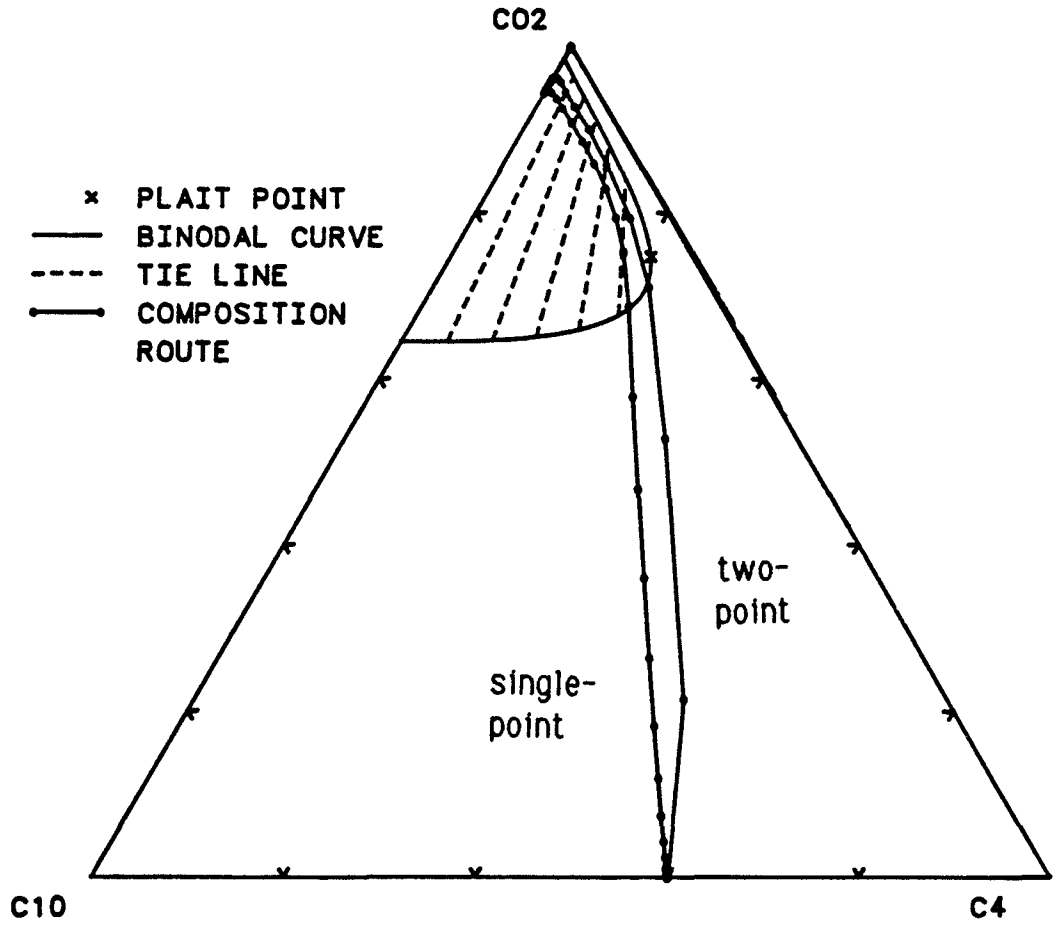

Fig. 5.2-4 Composition routes for Runs # 4SK3 and 4SA3.

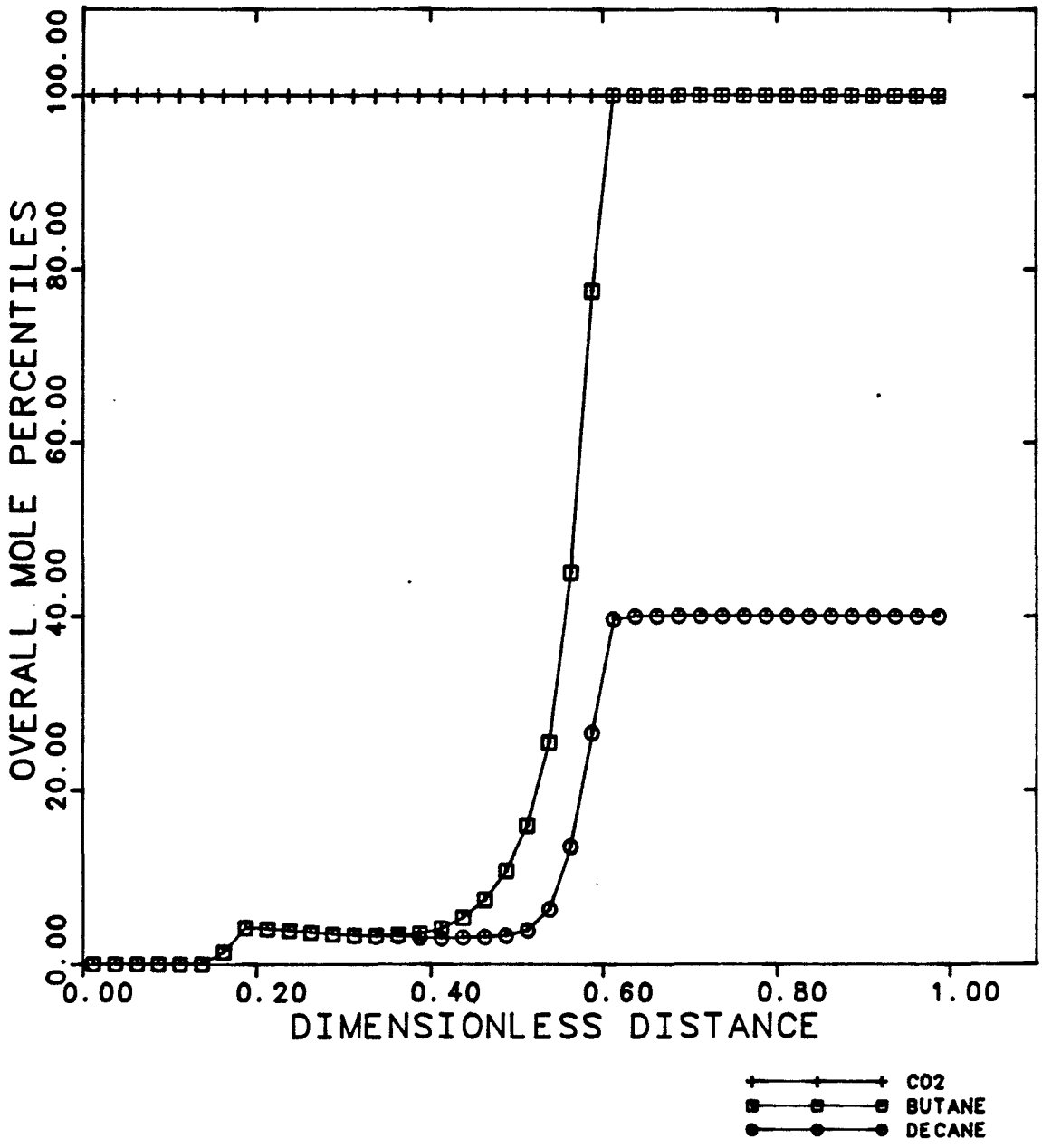

Fig. 5.2-5 Overall composition profiles for Run # 4SA4 at 0.6 DPV.

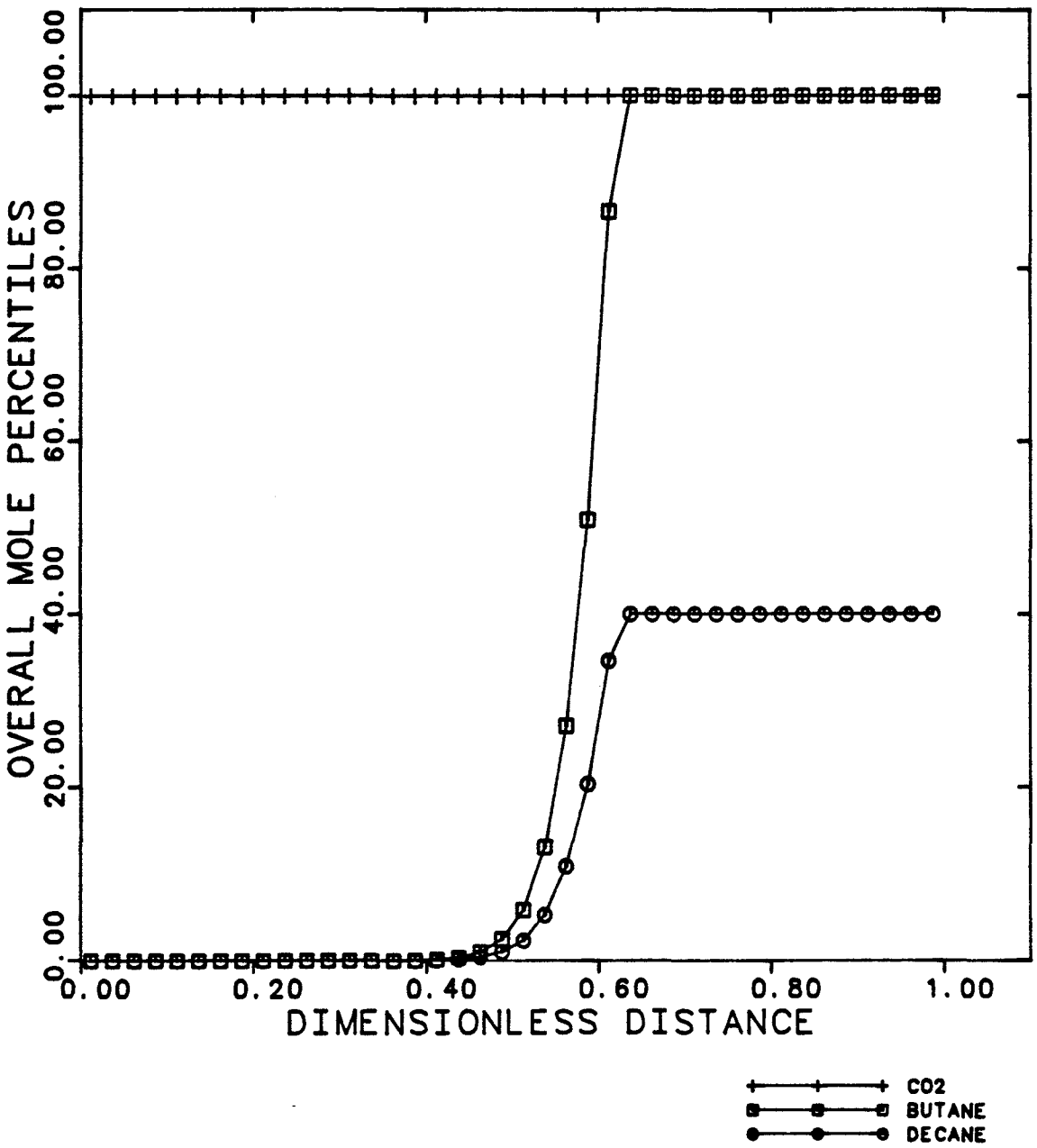

Fig. 5.2-6 Overall composition profiles for Run # 4SA5 at 0.6 DPV.

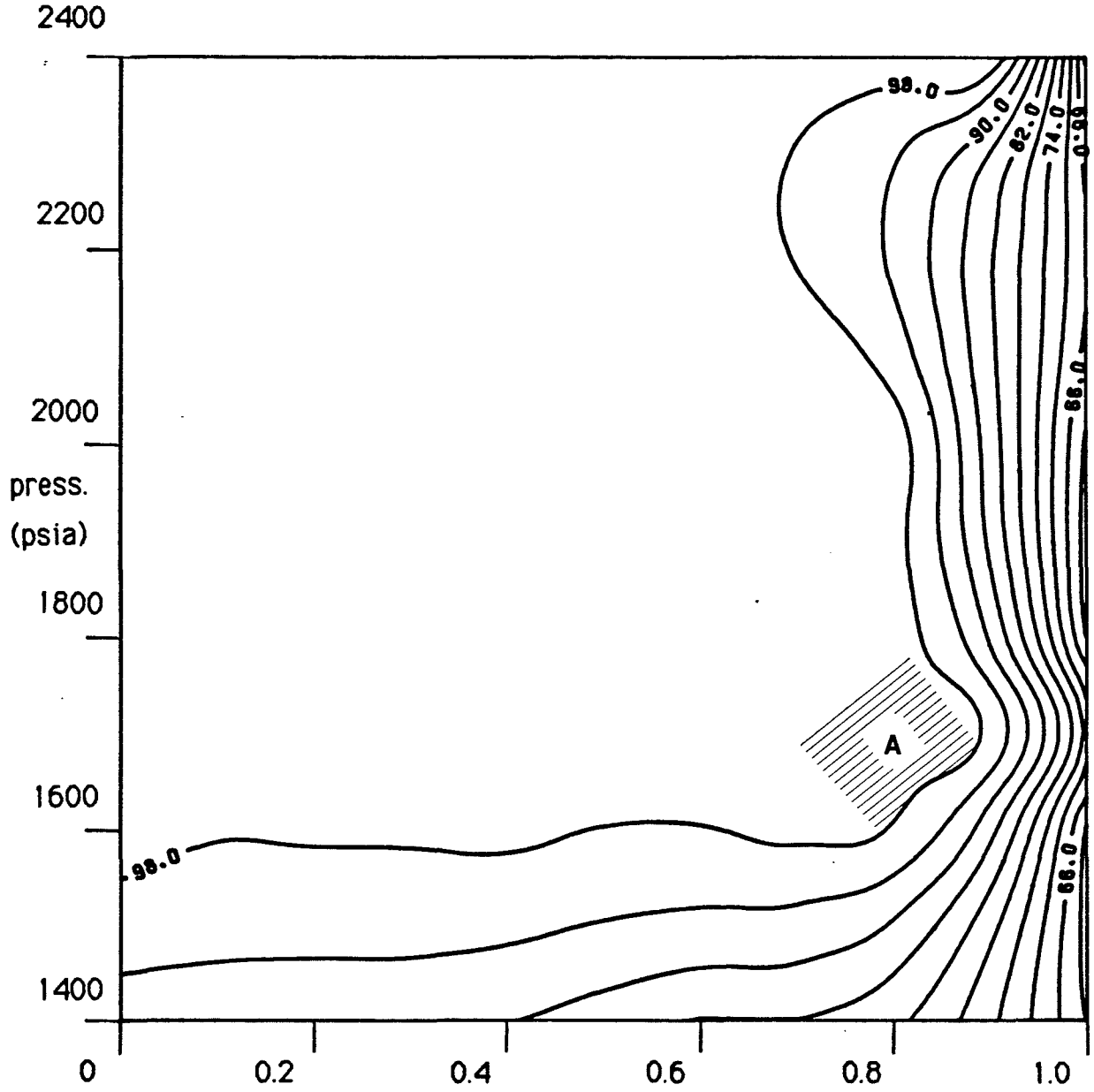

Fig. 5.2-7 Butane recovery contours for 4S runs at 1.2 DPV.

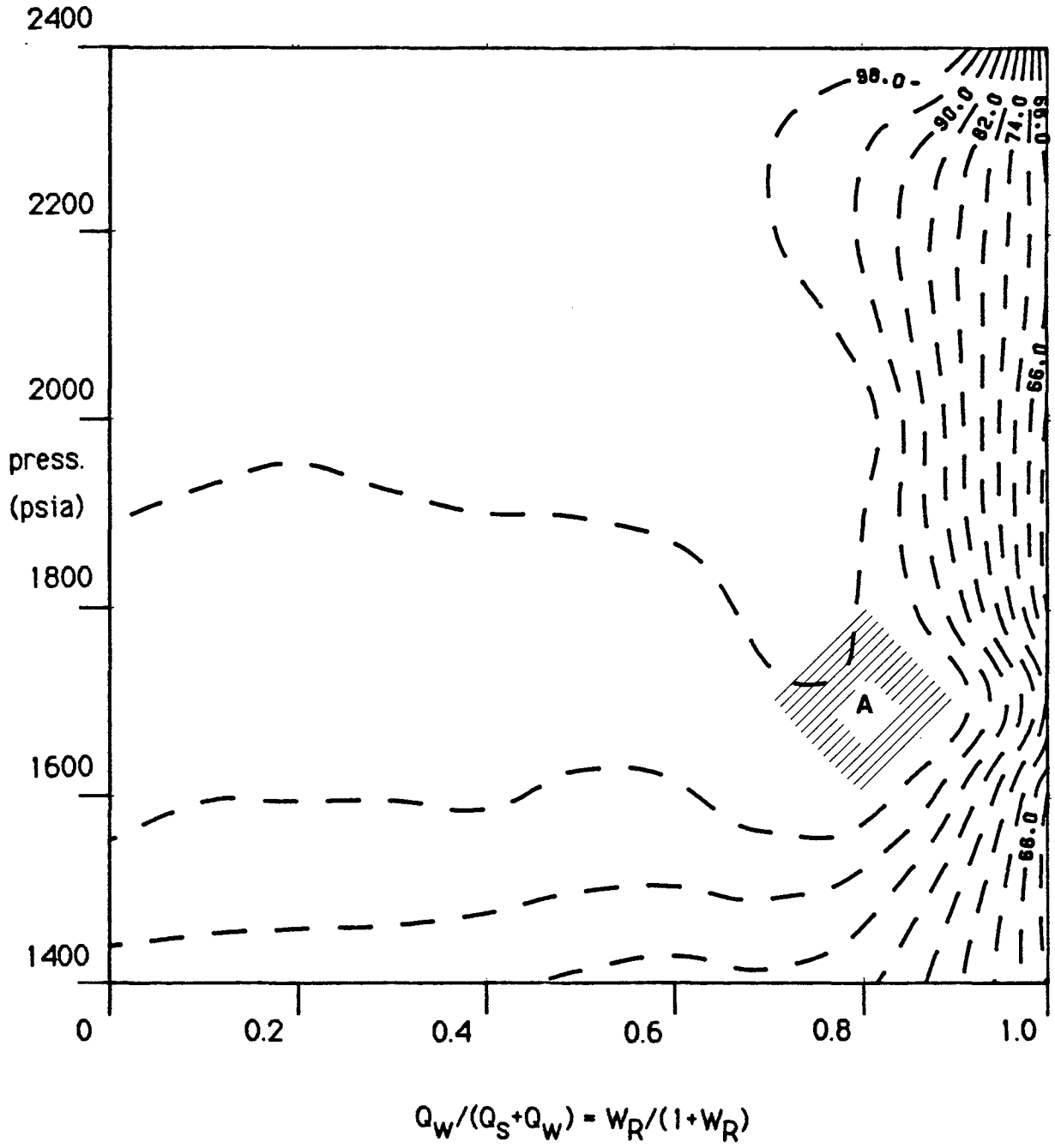

Fig. 5.2-8 Decane recovery contours for 45 runs at 1.2 DPV.

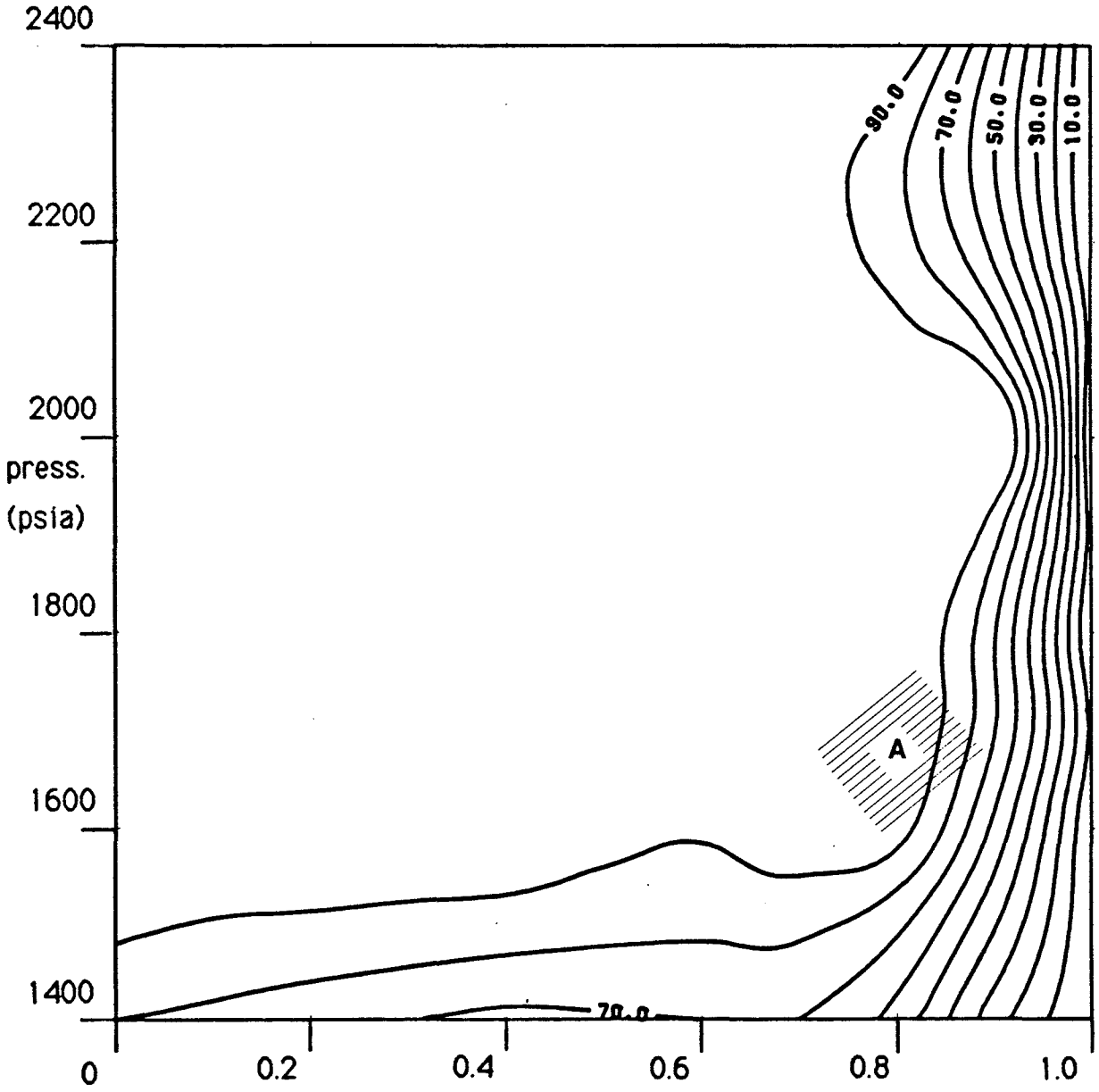

Fig. 5.2-9 Butane recovery contour for 4T runs at 1.2 DPV.

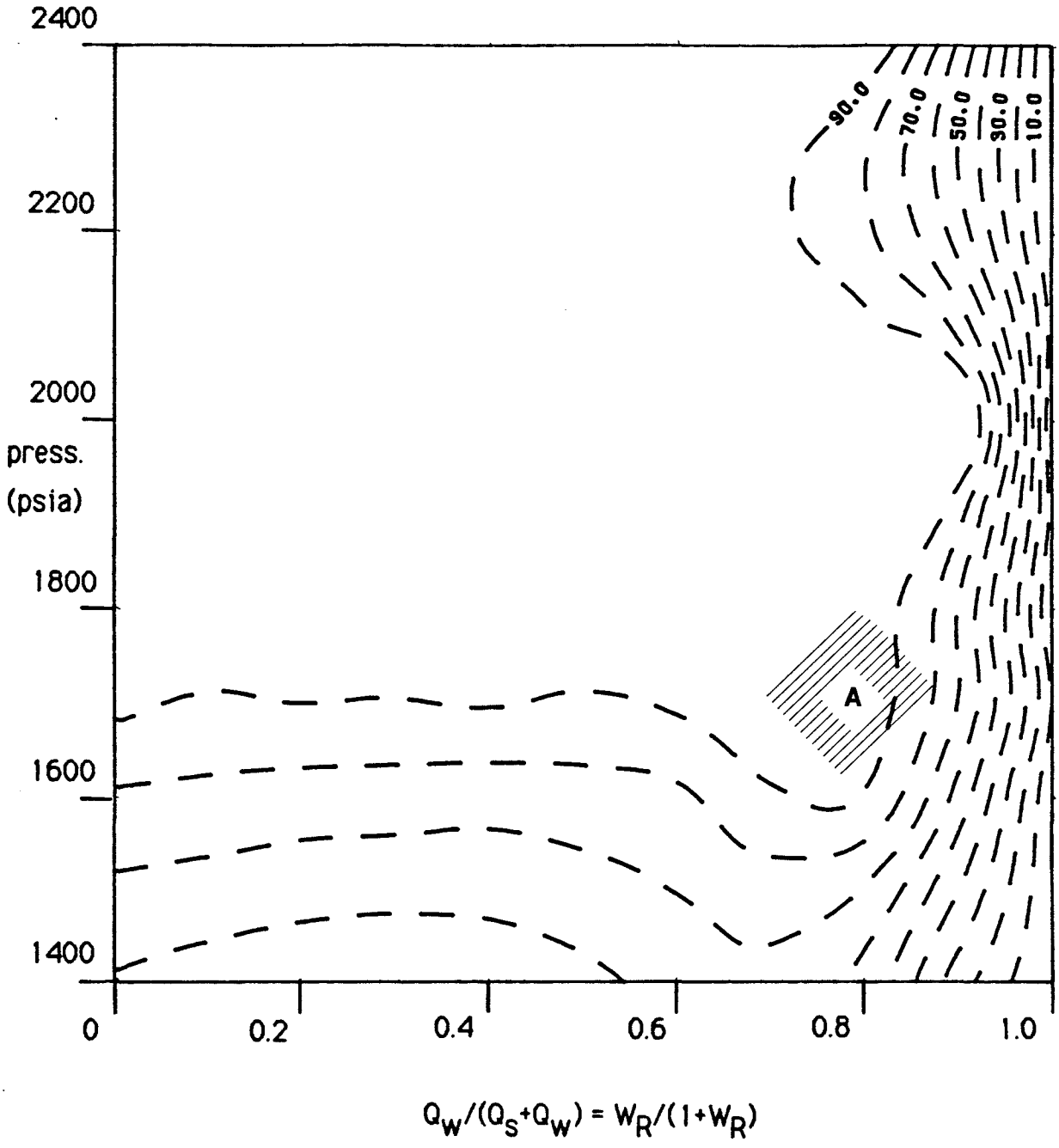

Fig. 5.2-10 Decane recovery contour for 4T runs at 1.2 DPV.

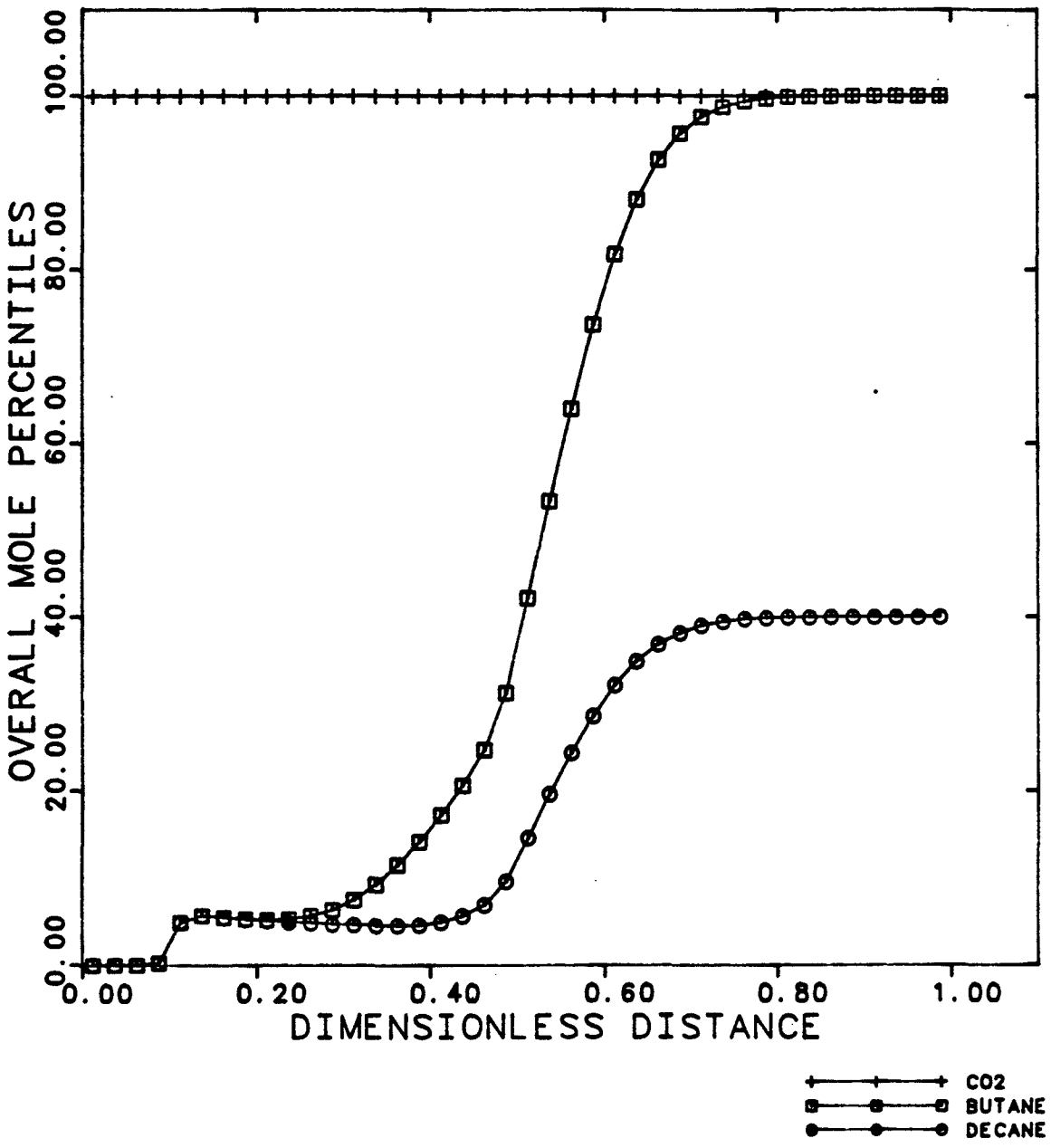

Fig. 5.2-11 Overall composition profiles for Run * 4SK3 at 0.6 DPV.

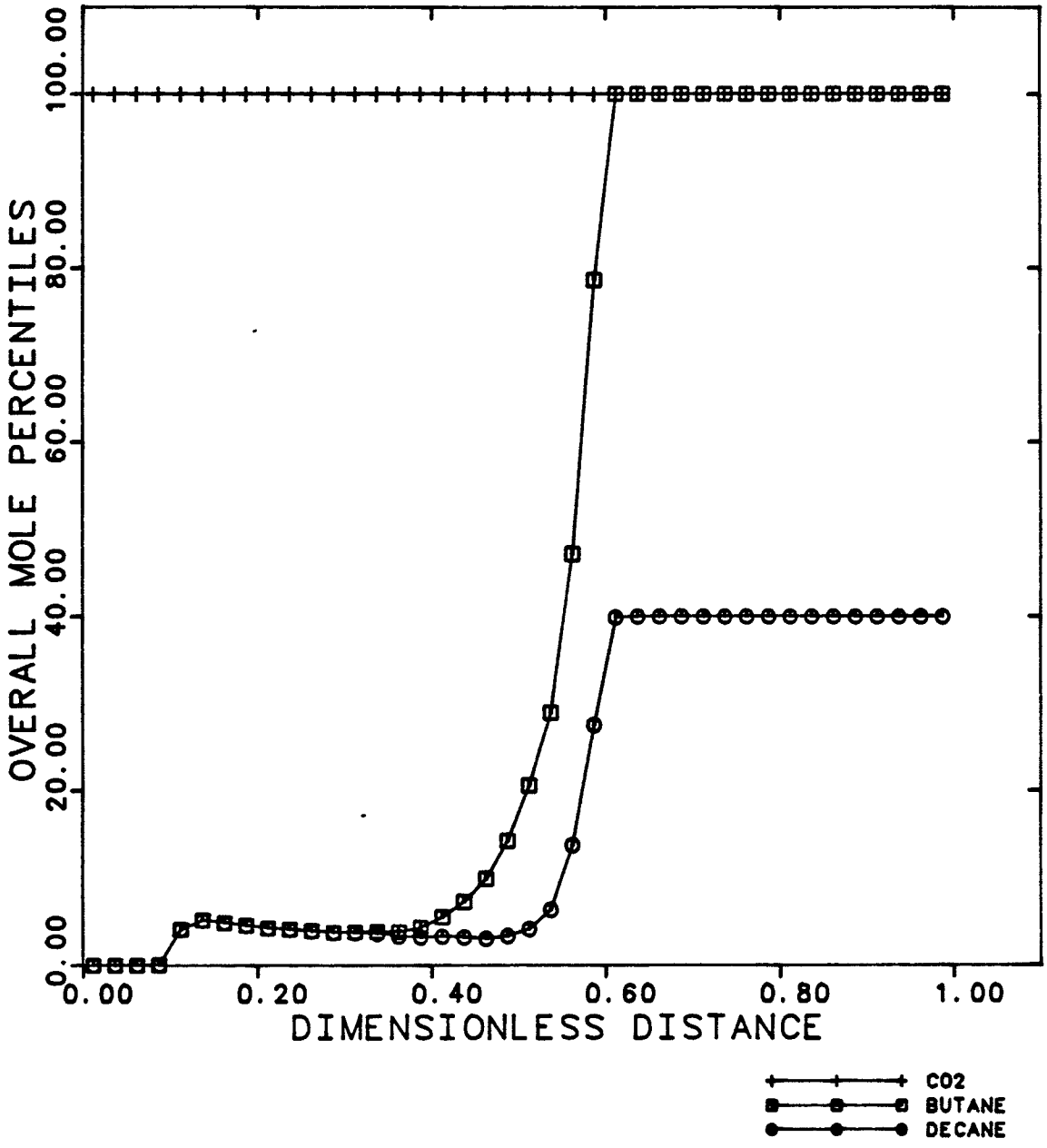

Fig. 5.2-12 Overall composition profiles for Run * 4SA3 at 0.6 DPV.

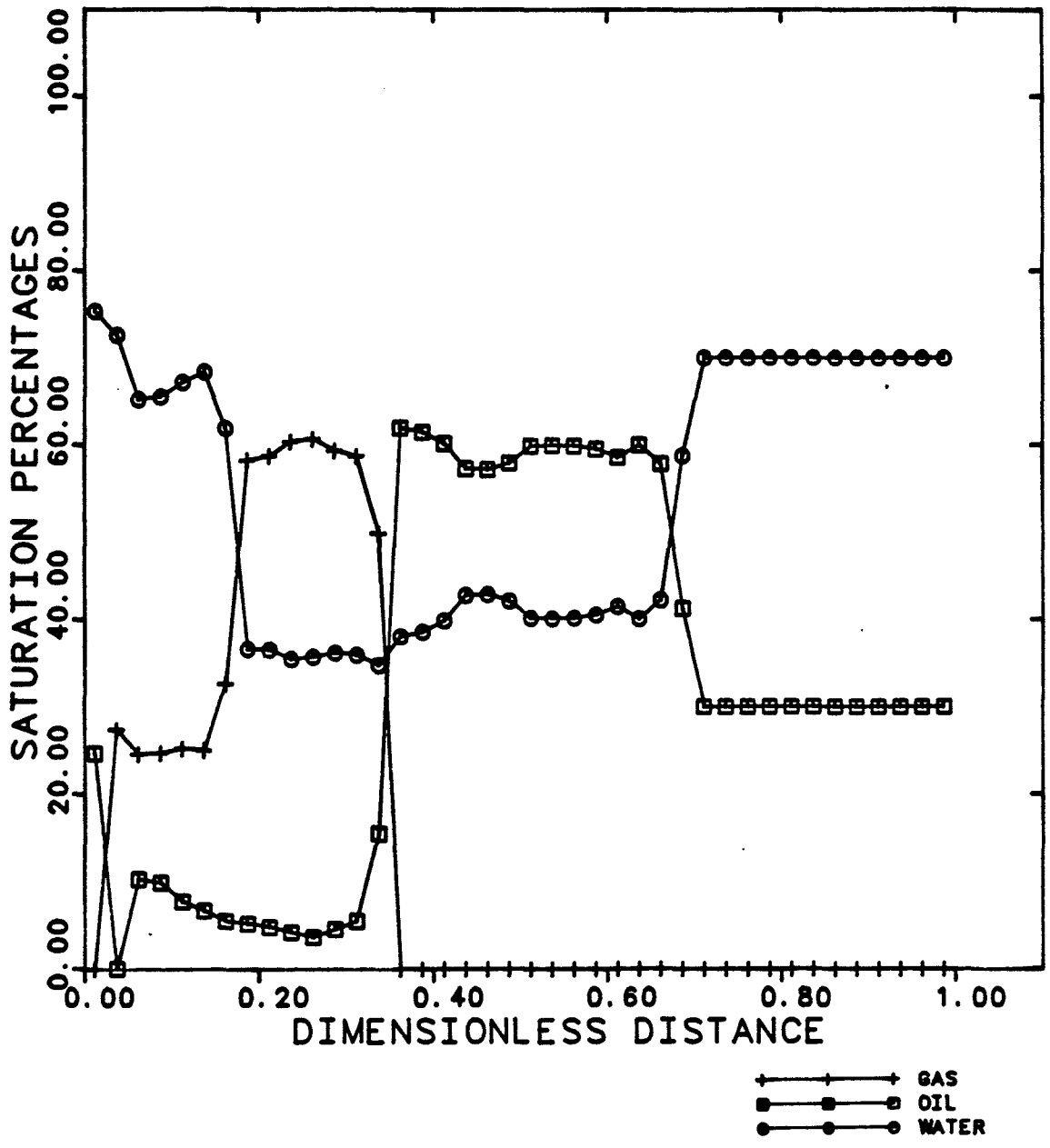

Fig. 5.2-13 Saturation profiles for Run # 4TB3 at 0.4 DPV.

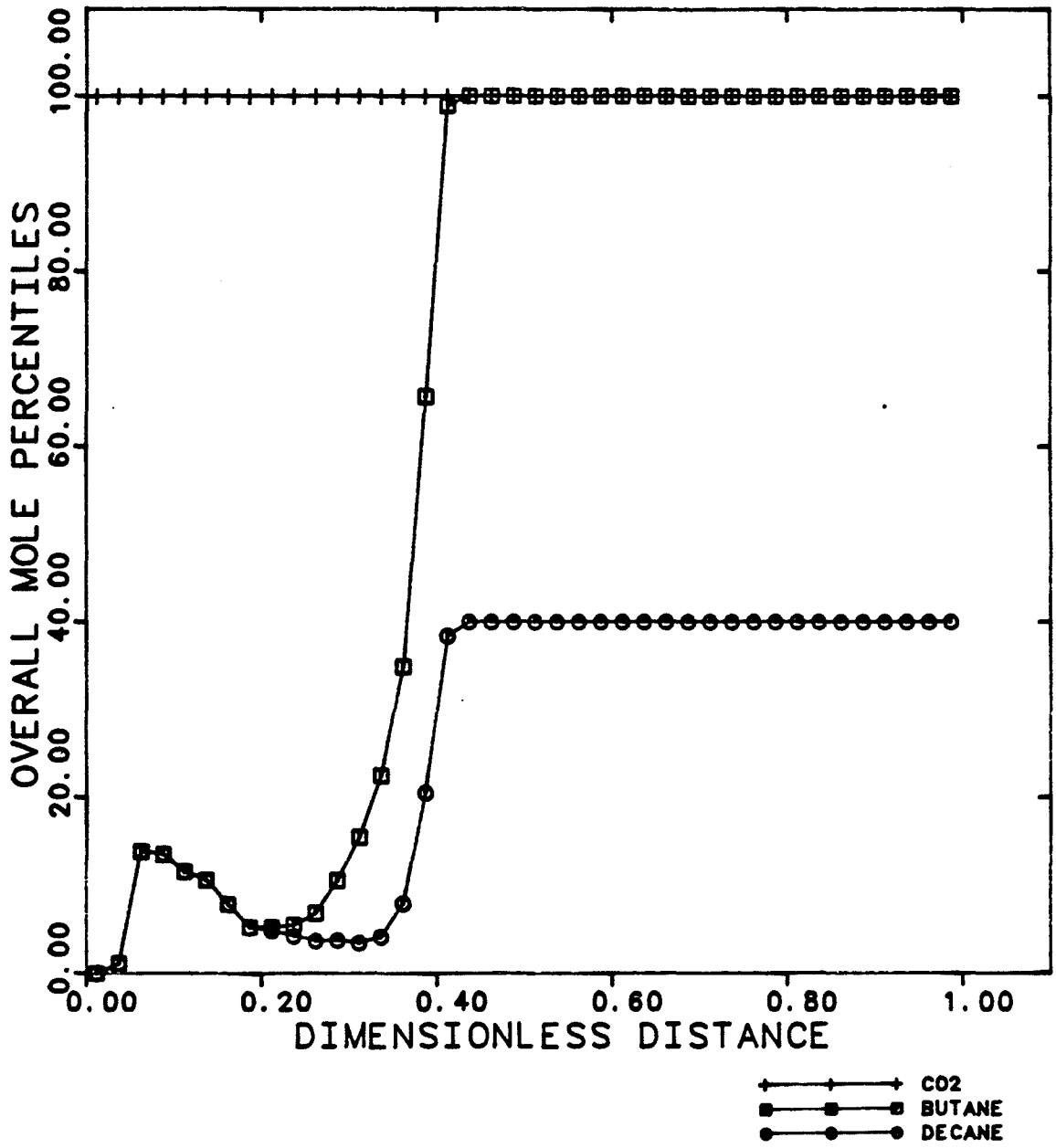

Fig. 5.2-14 Overall composition profiles for Run * 4TB3 at 0.4DPV.

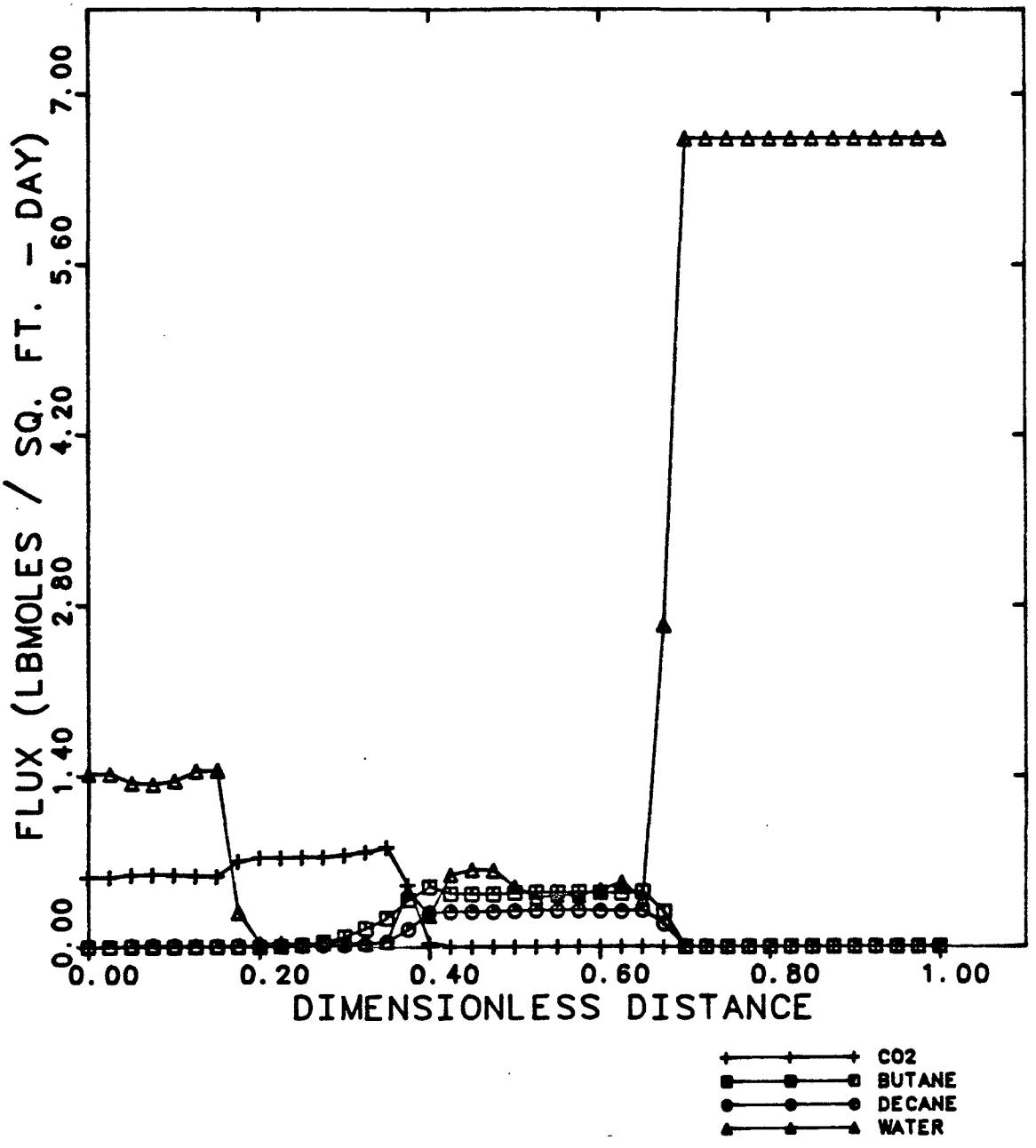

Fig. 5.2-15 Molar flux profiles for Run # 4TB3 at 0.4 DPV.

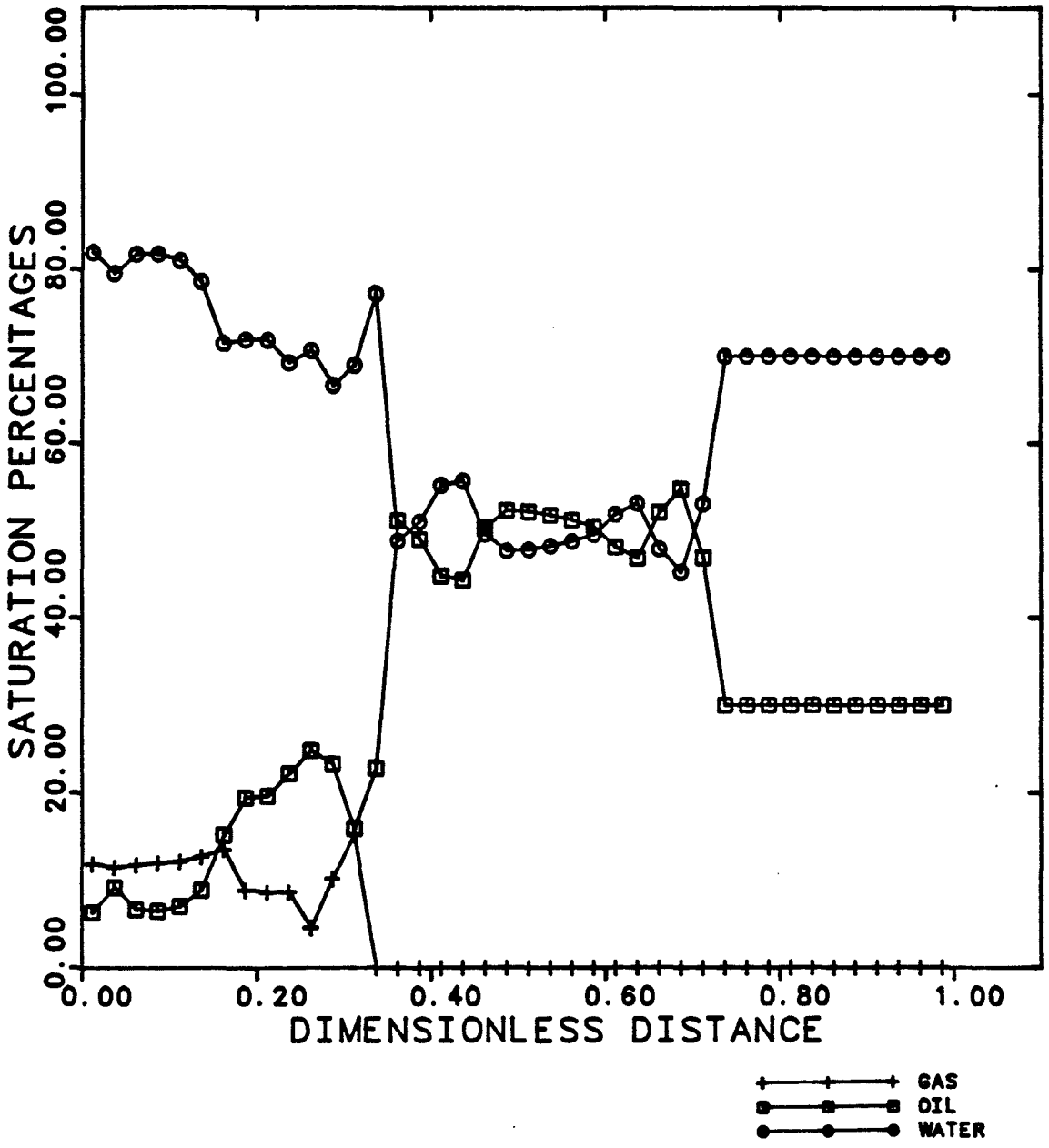

Fig. 5.2-16 Saturation profiles for Run # 4TD1 at 0.4 DPV.

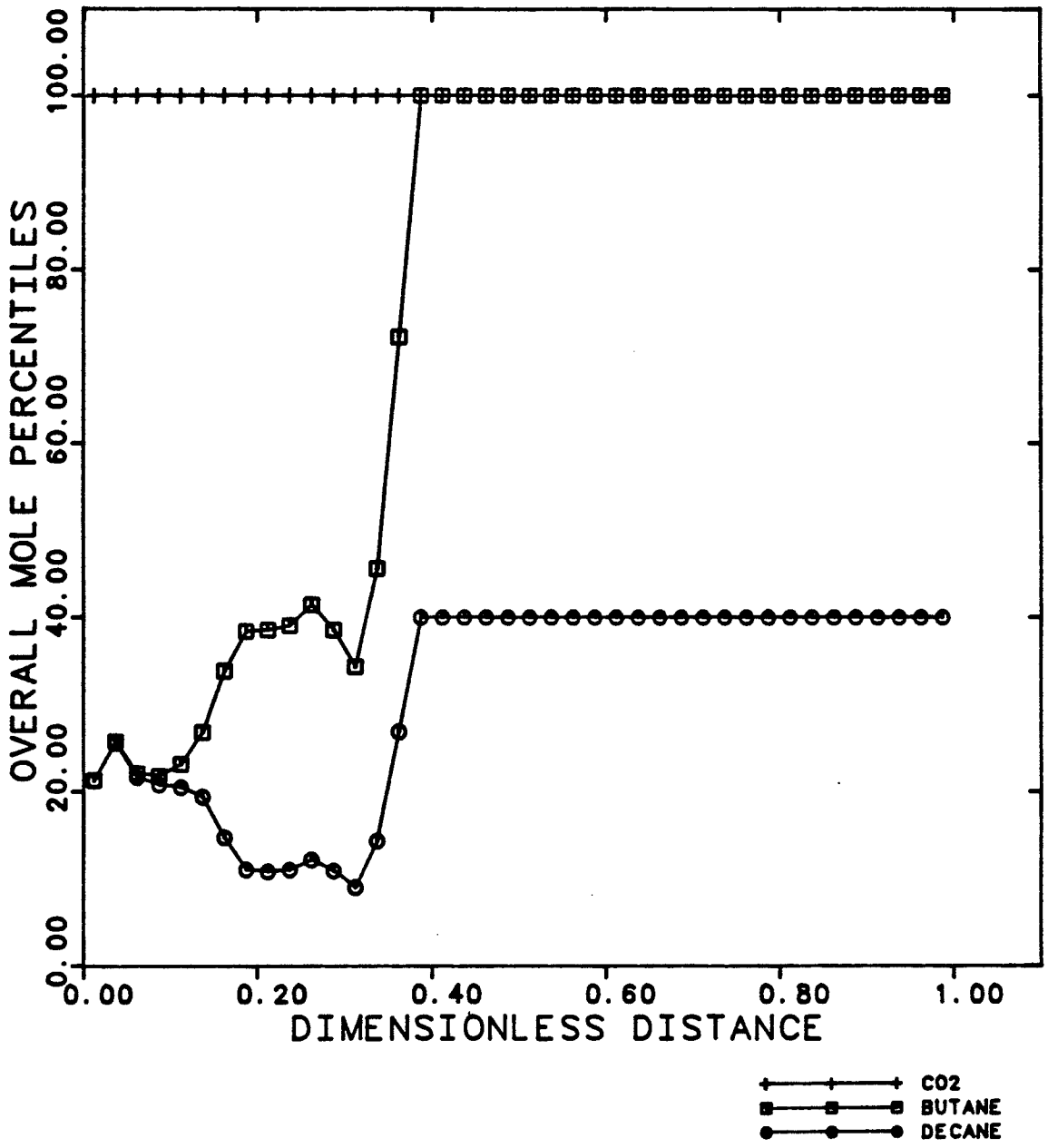

Fig. 5.2-17 Overall composition profiles for Run # 4TD1 at 0.4 DPV.

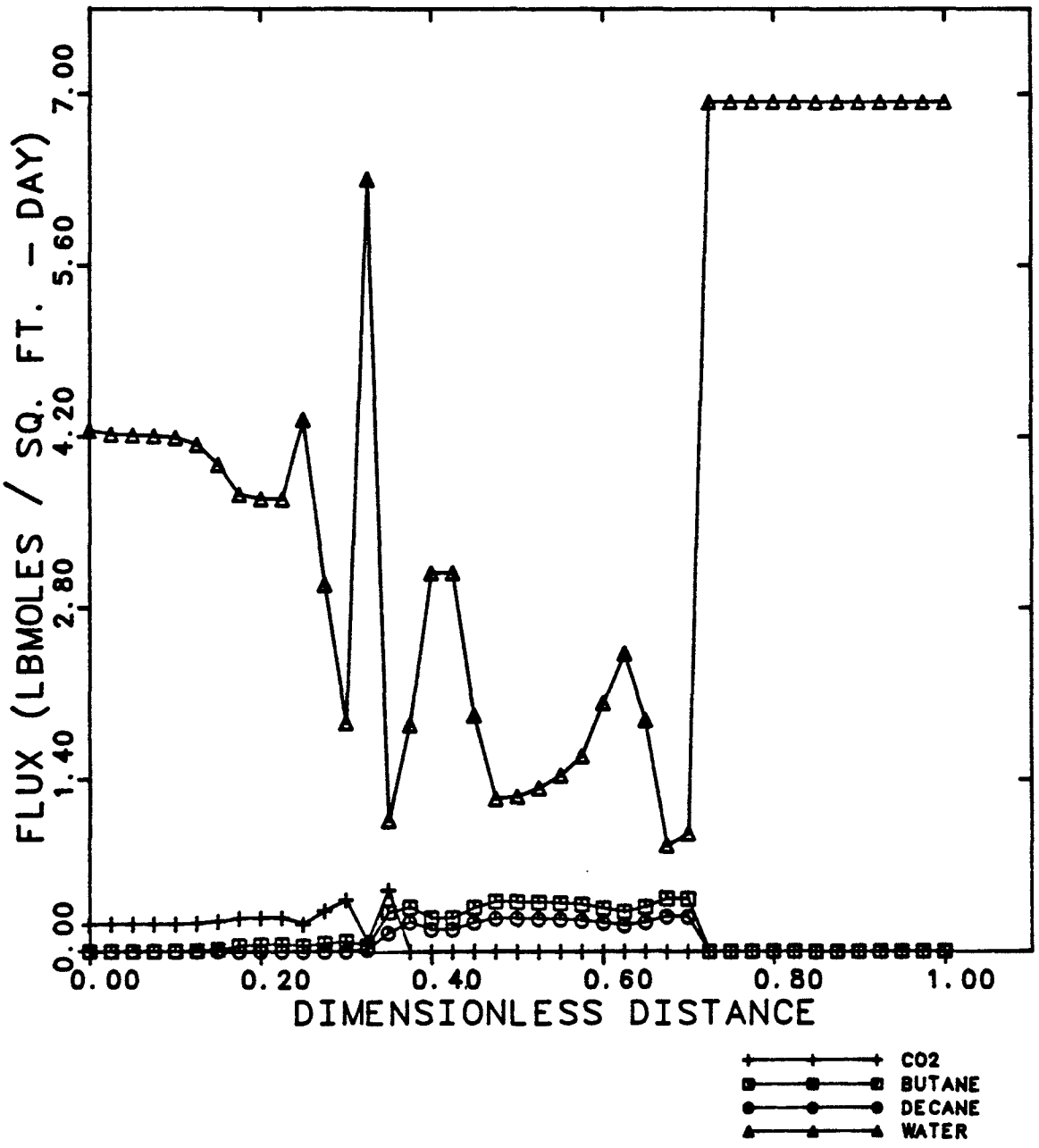

Fig. 5.2-18 Molar flux profiles for Run # 4TD1 at 0.4 DPV.

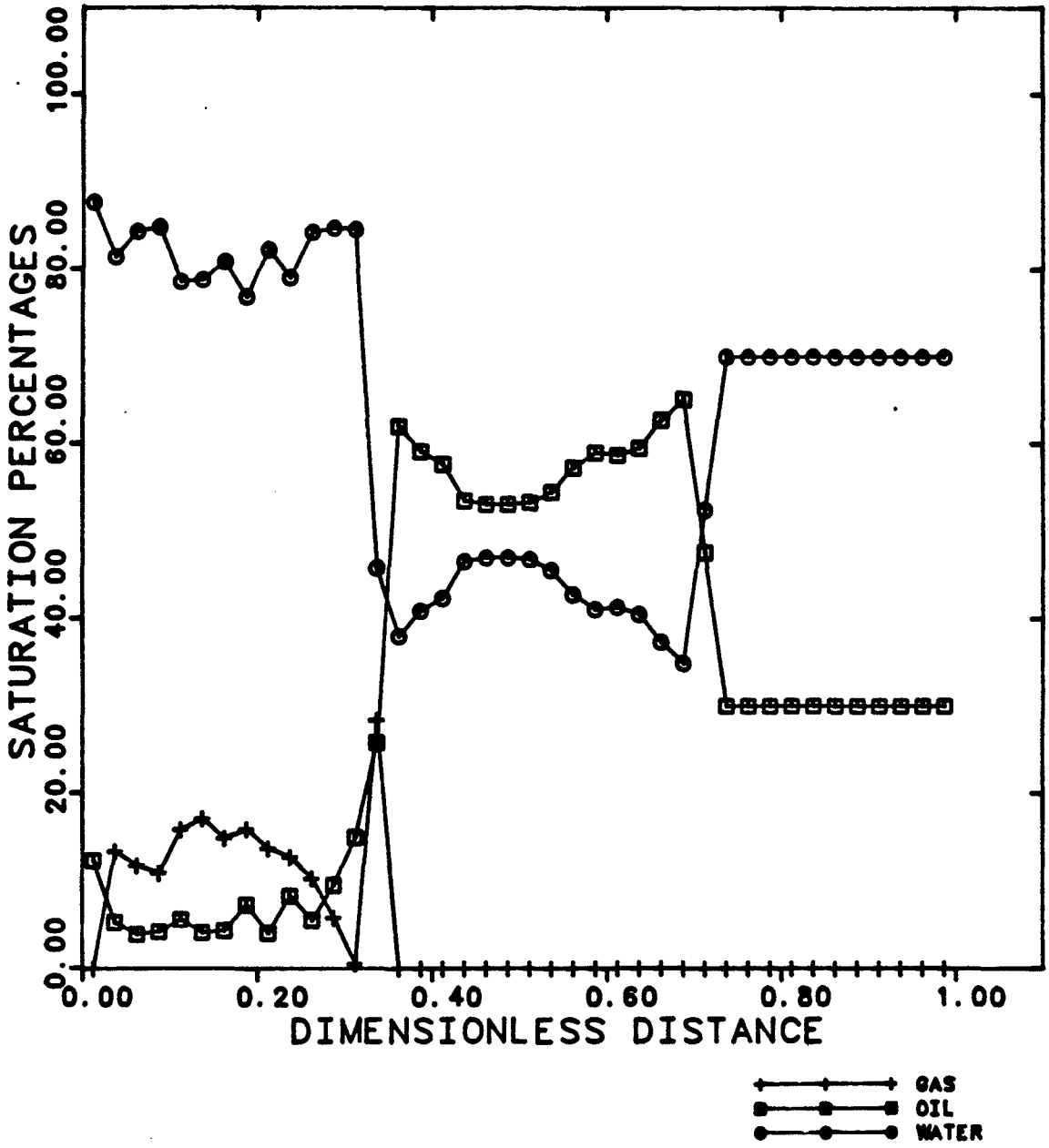

Fig. 5.2-19 Saturation profiles for Run # 4TD3 at 0.4 DPV.

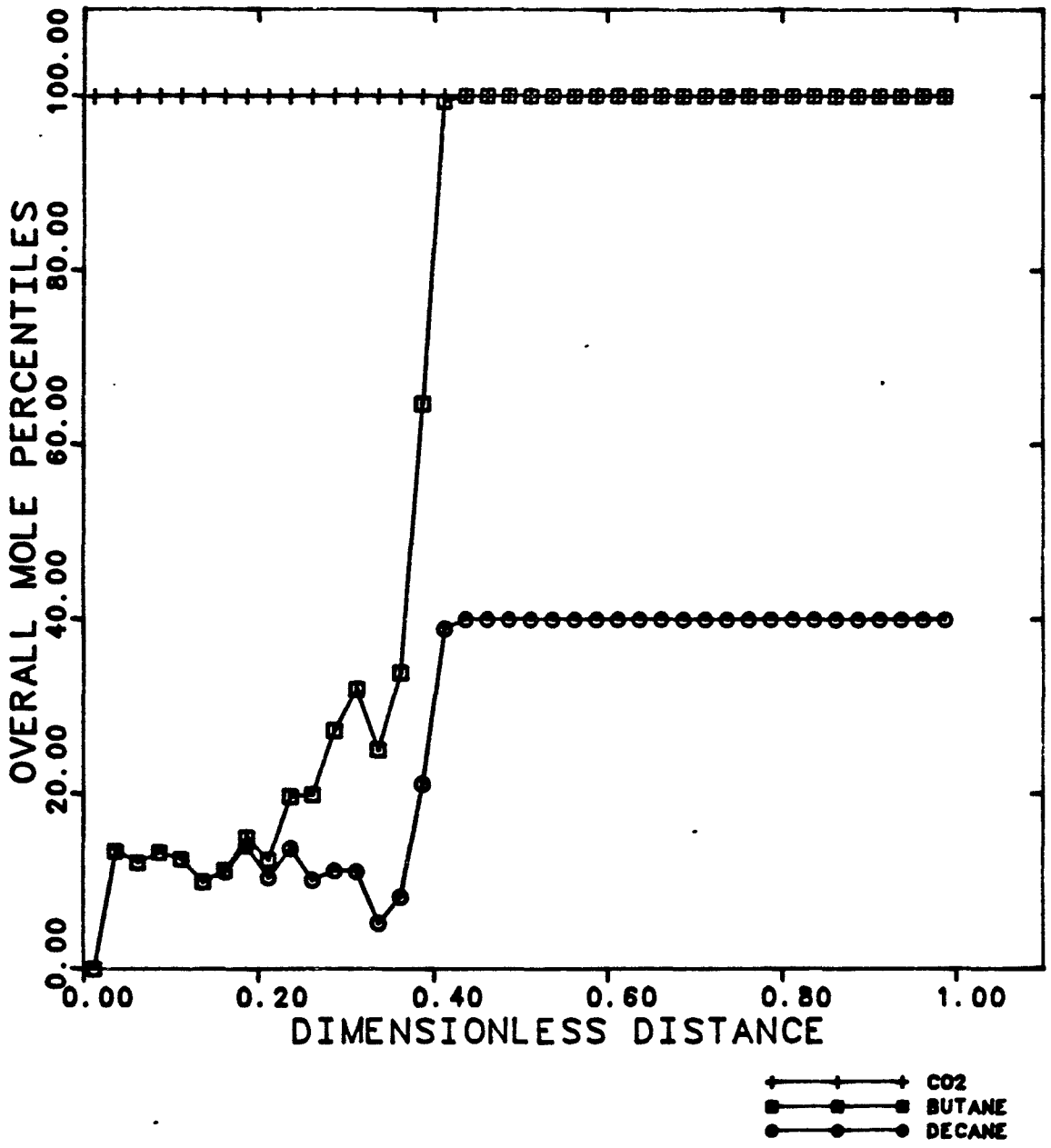

Fig. 5.2-20 Overall composition profiles for Run # 4TD3 at 0.4 DPV.

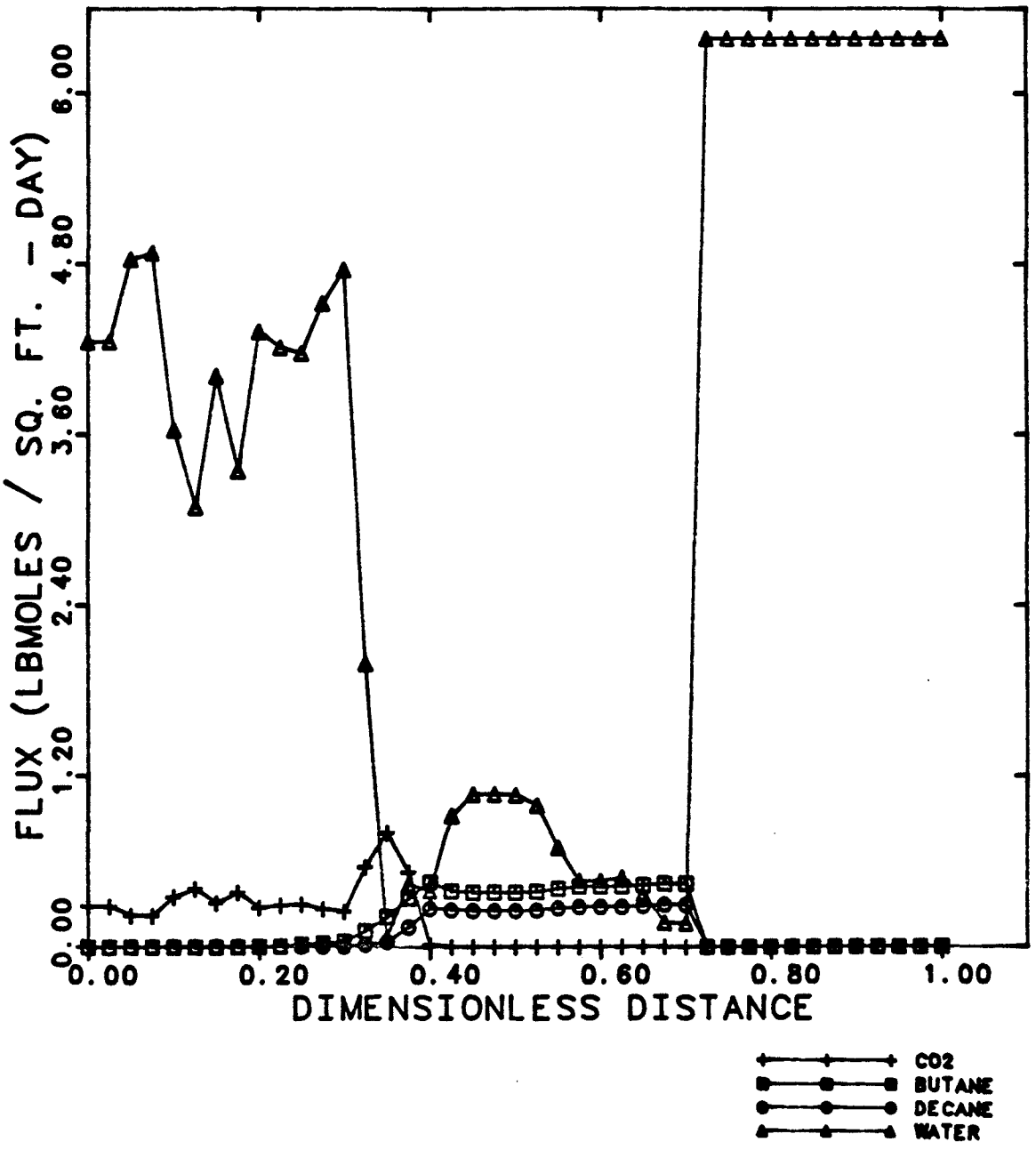

Fig. 5.2-21 Molar flux profiles for Run # 4TD3 at 0.4 DPV.

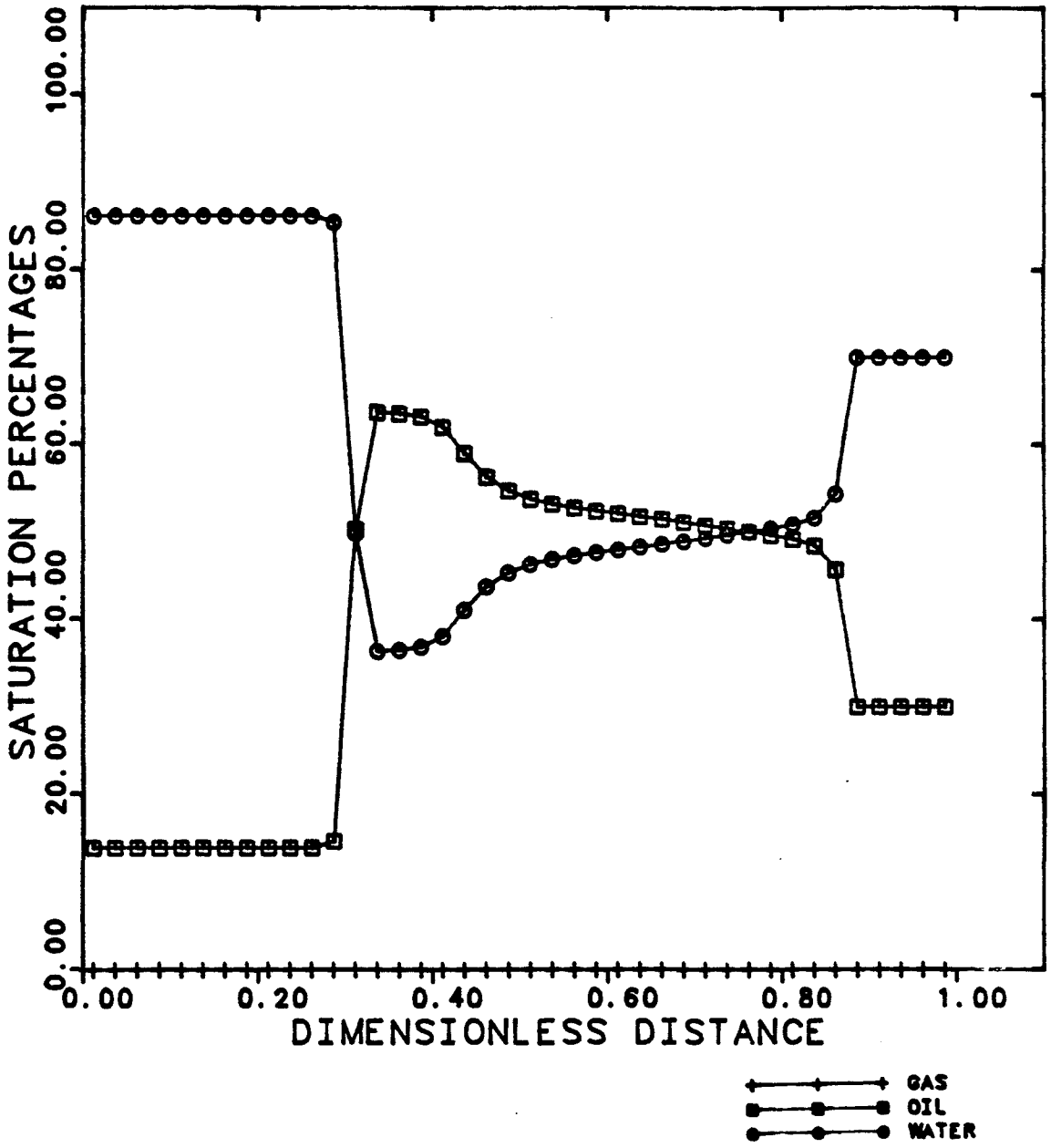

Fig. 5.2-22 Saturation profiles for Run # 4TD6 at 0.4 DPV.

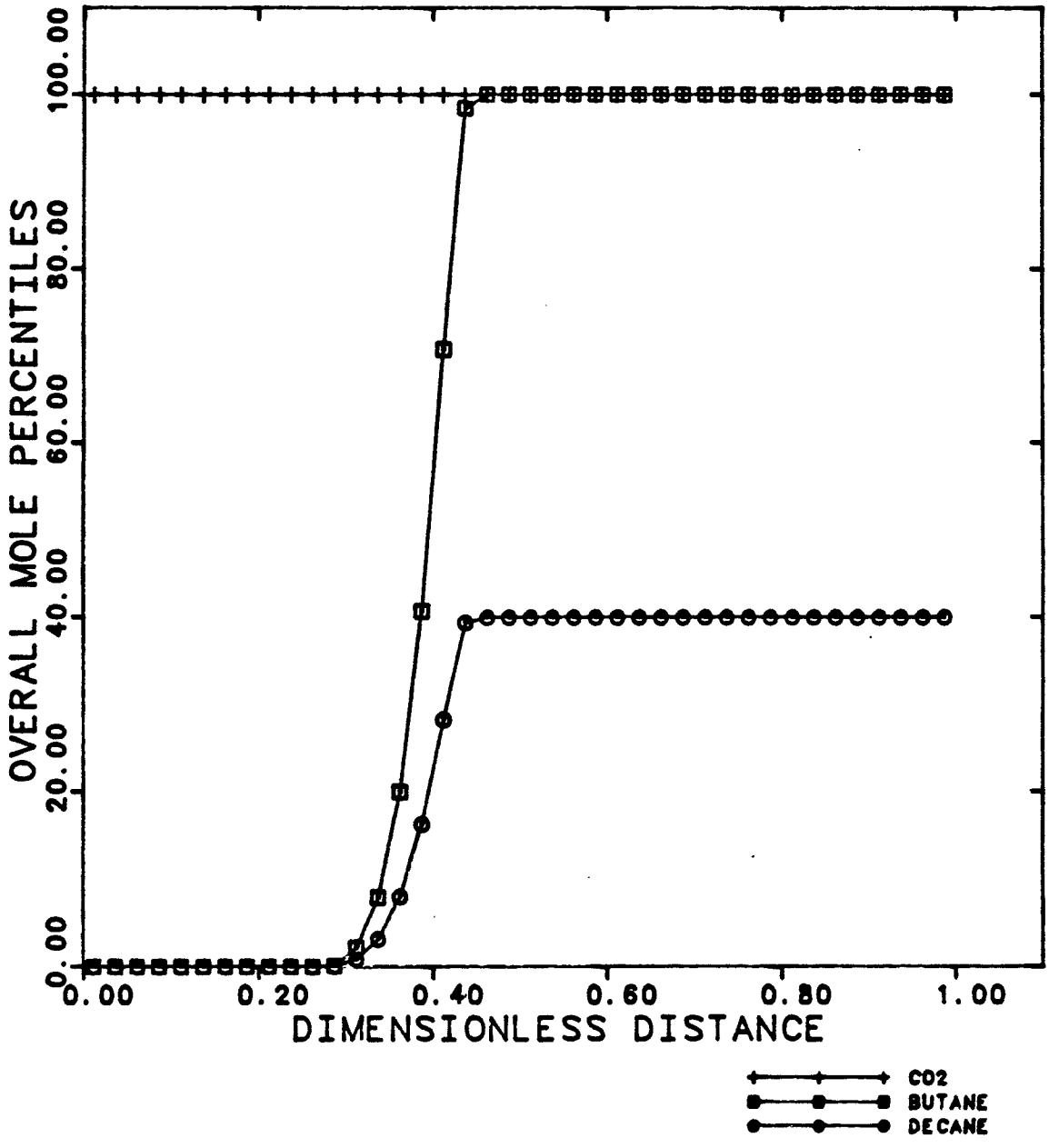

Fig. 5.2-23 Overall composition profiles for Run # 4TD6 at 0.4 DPV.

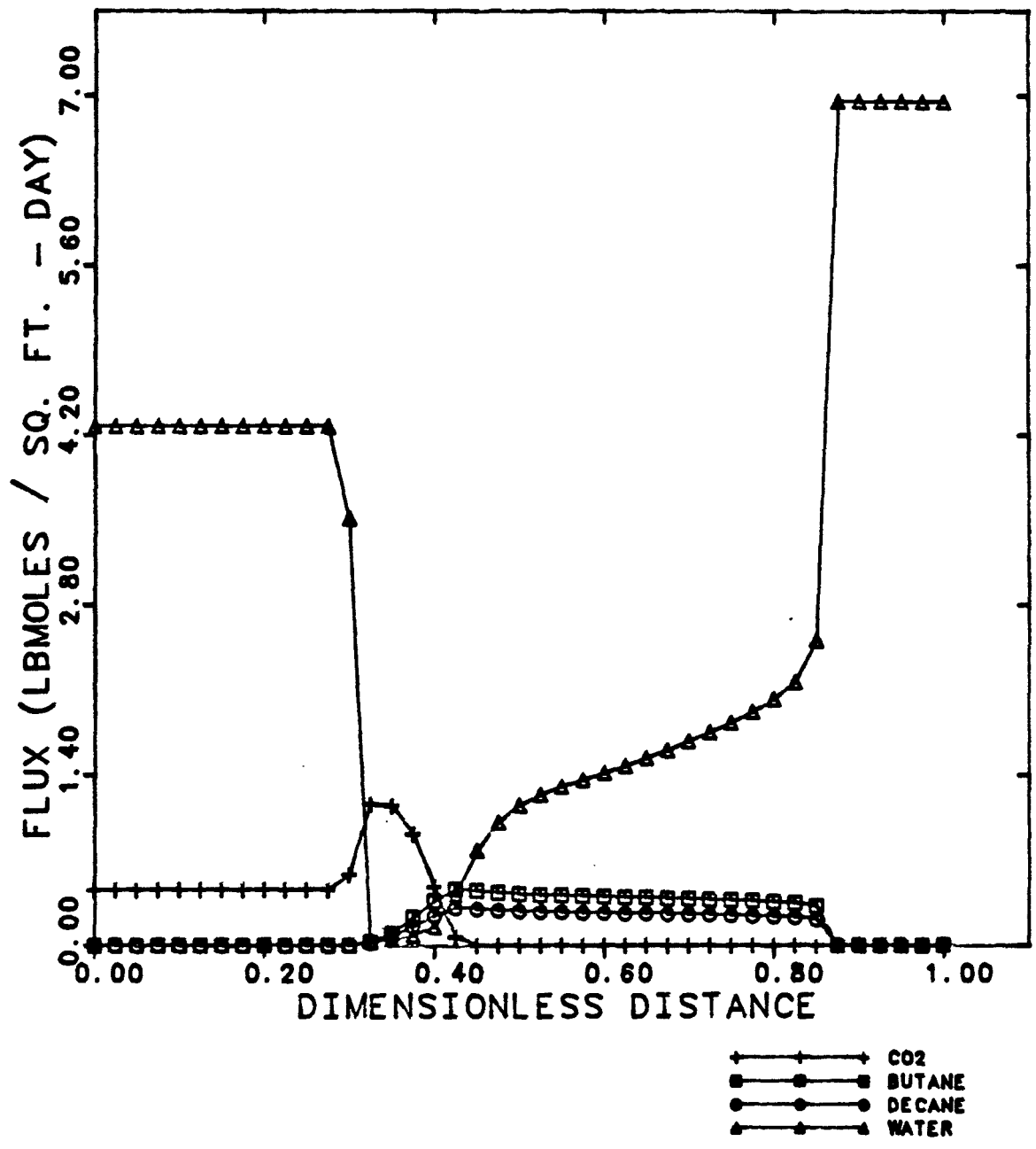

Fig. 5.2-24 Molar flux profiles for Run # 4TD6 at 0.4 DPV.

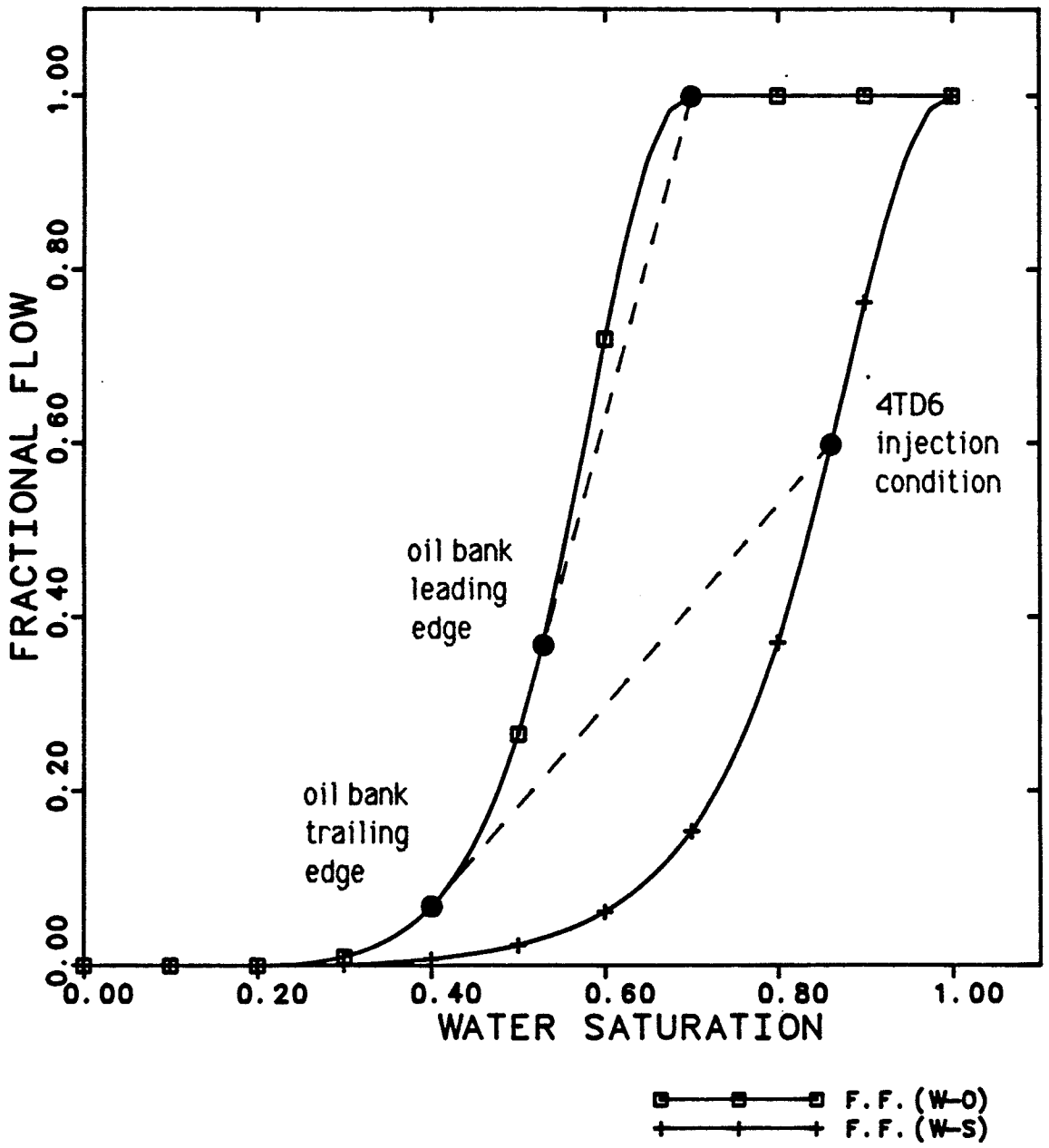

Fig. 5.2-25 Fractional flow curve construction for Class-4 FCM runs at 2400 psia.

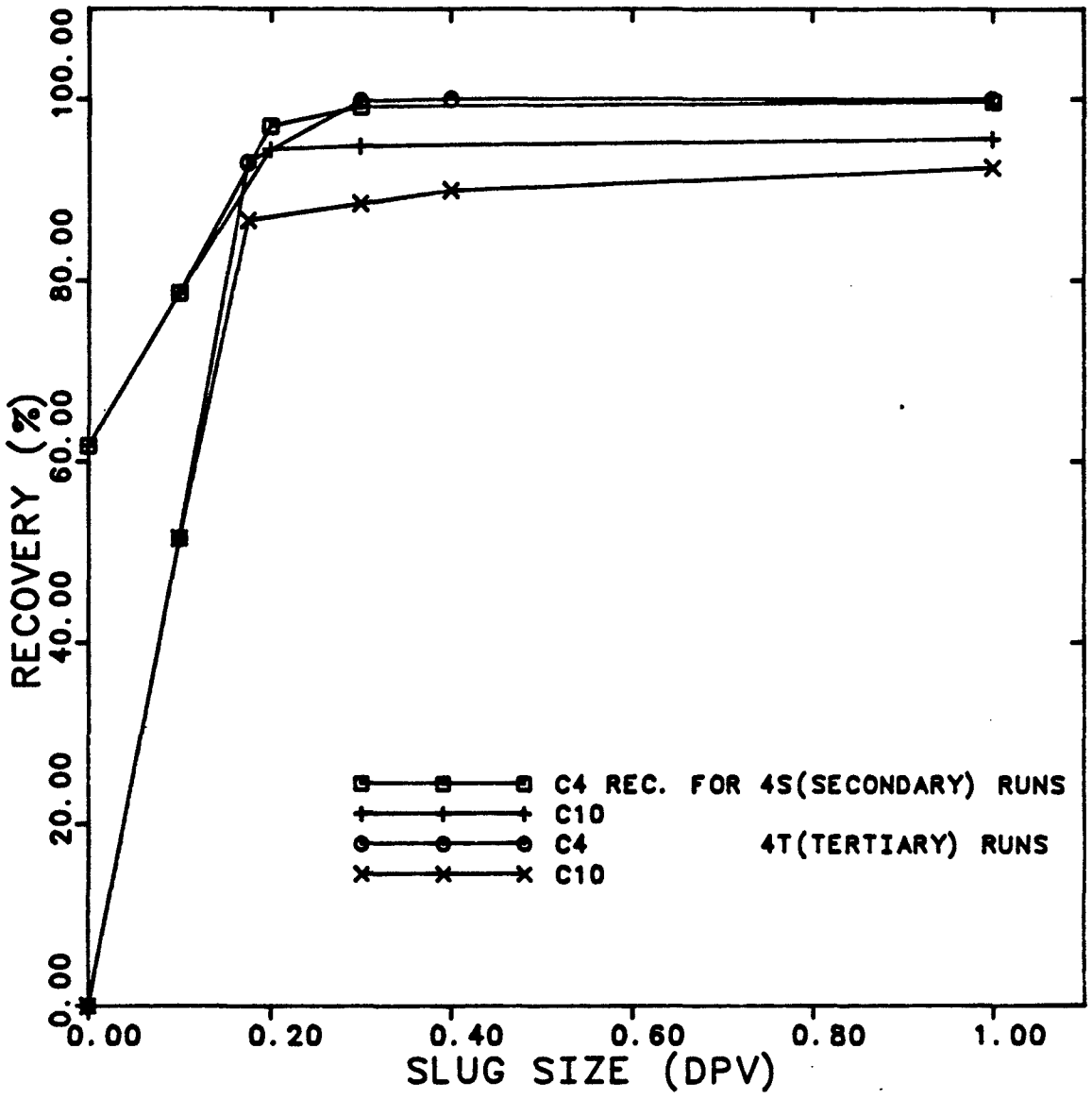

Fig. 5.2-26 Butane and decane recovery at 1700 psia and 1.2 DPV versus slug size.

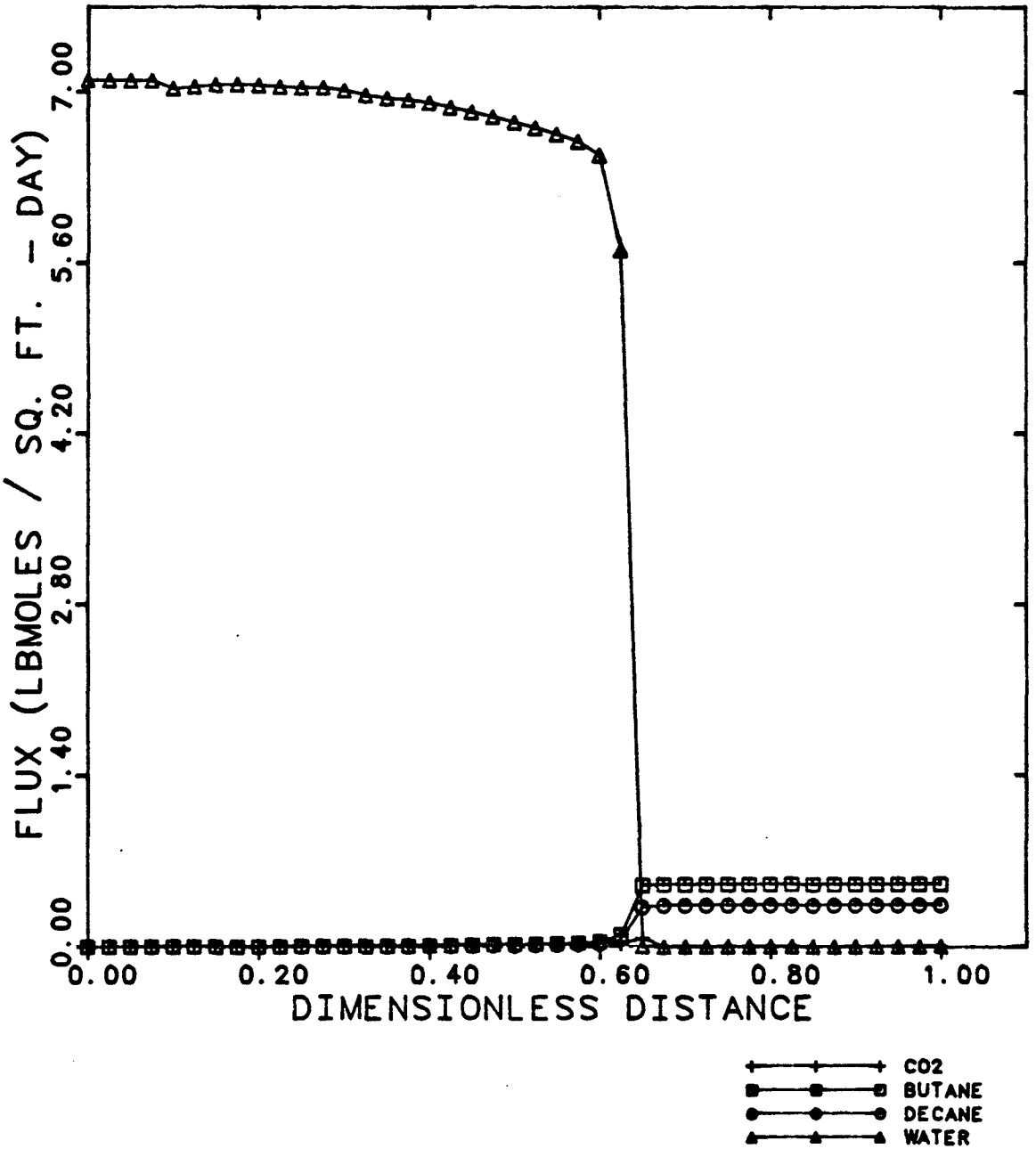

Fig. 5.2-27 Molar flux profile for Run # 4SLG1 at 0.6 DPV.

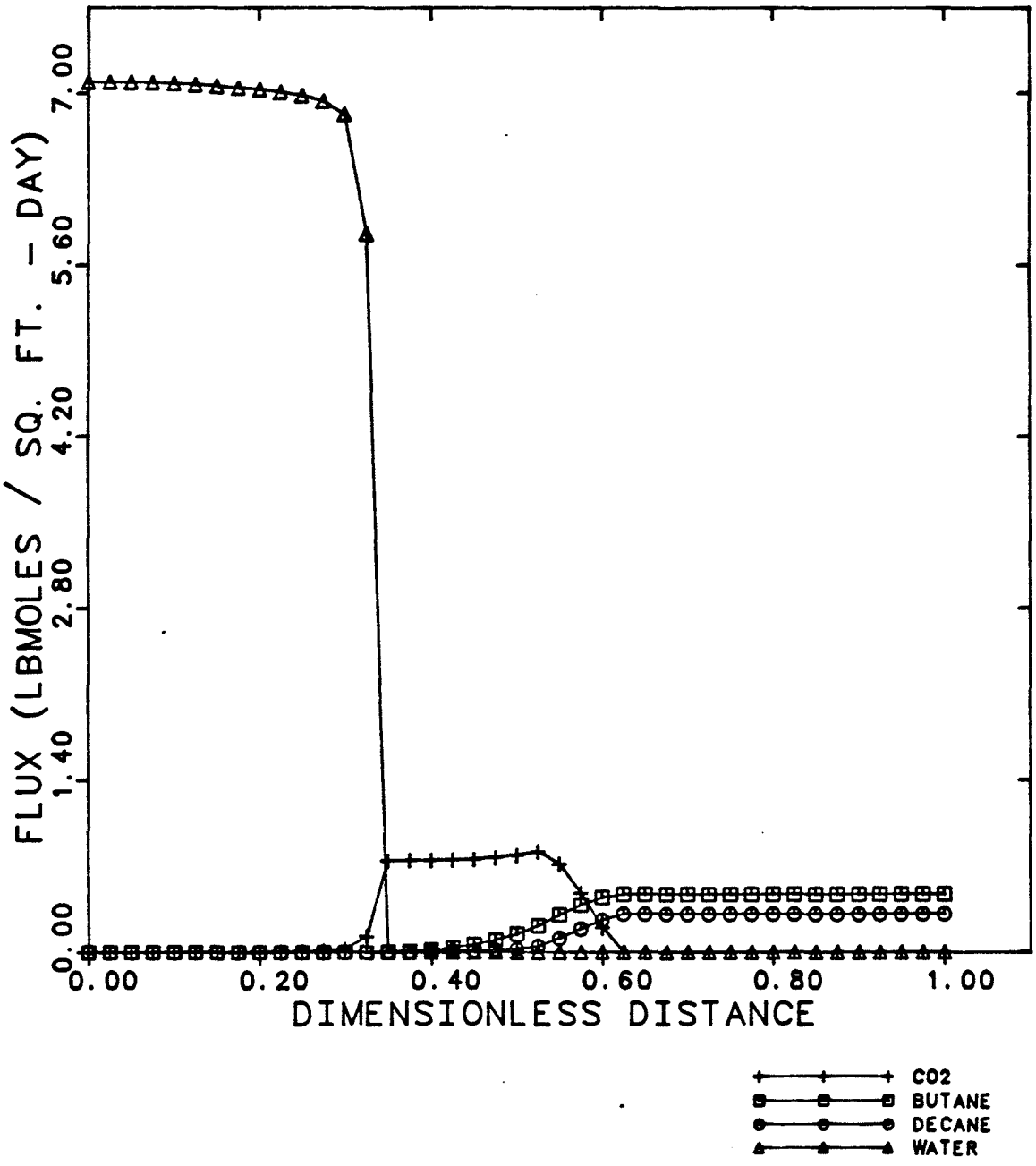

Fig. 5.2-28 Molar flux profile for Run # 4SLG3 at 0.6 DPV.

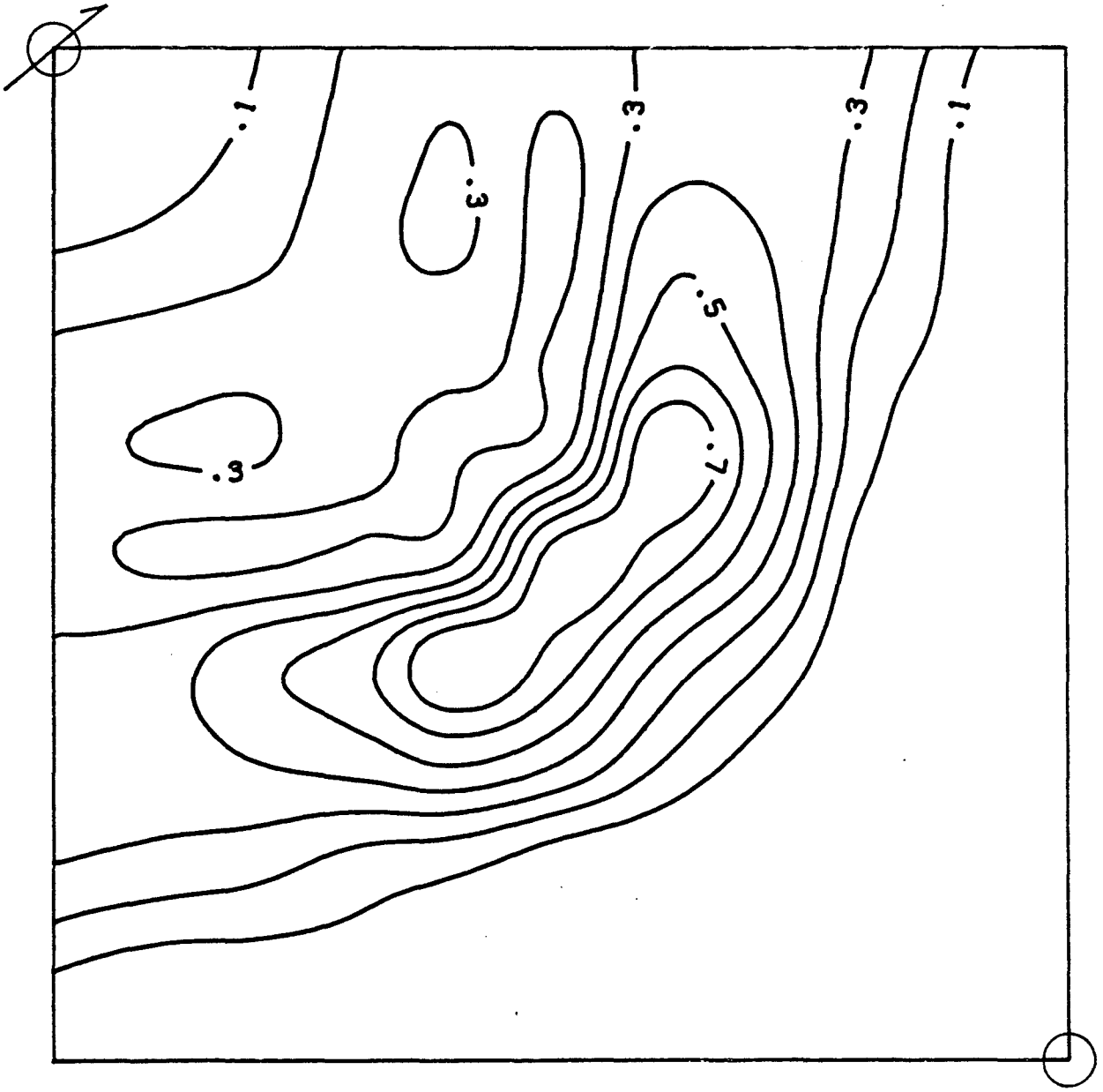

Fig. 5.3-1 CO_2 dimensionless concentration contour for Run # 5.3 at 0.5 DPV. (α_l = 0.1, α_t = 0.01 ft)

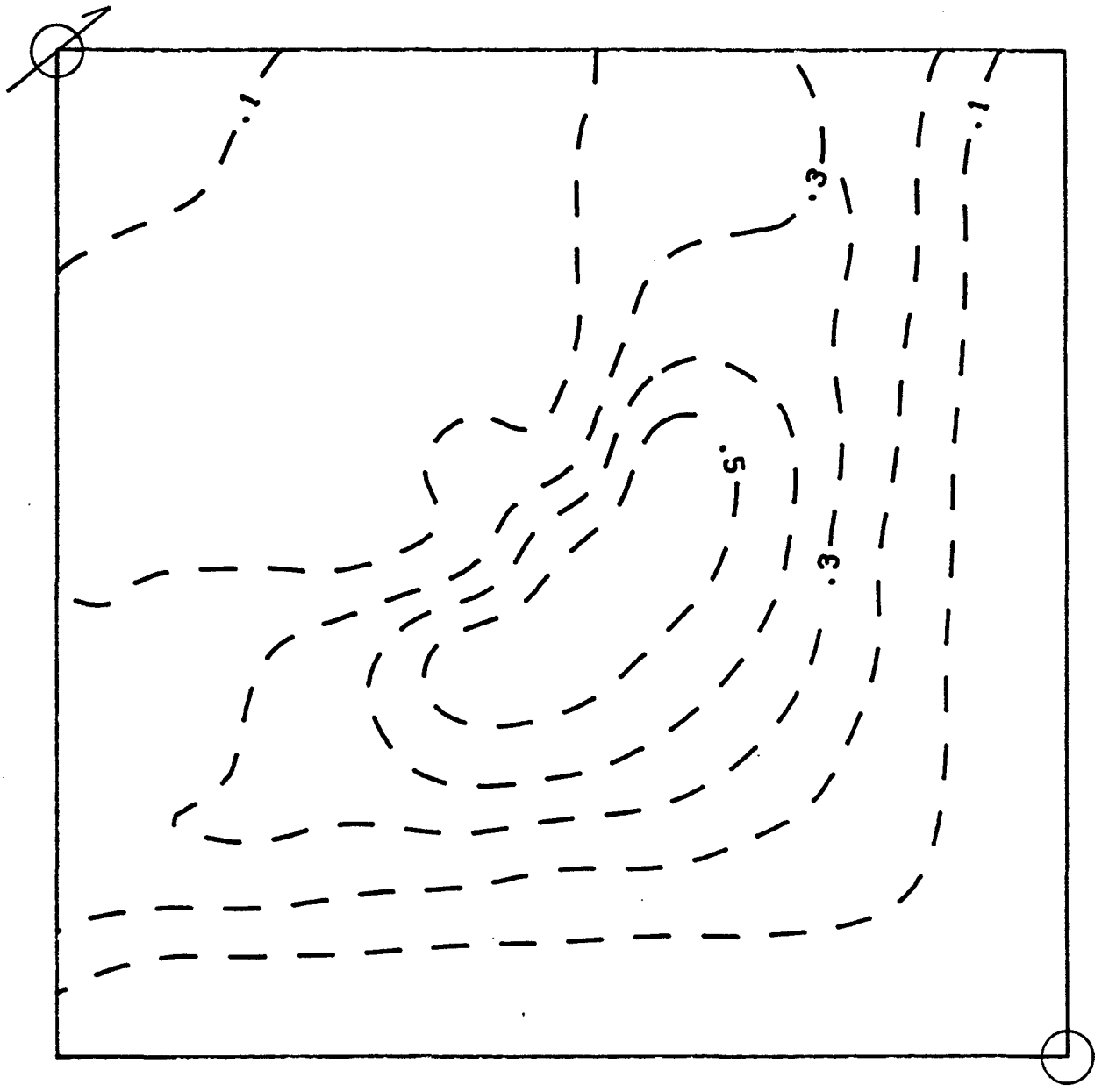

Fig. 5.3-2 CO_2 dimensionless concentration contour for Run # 5.2 at 0.5 DPV. (α_l = 5.0, α_t = 0.5 ft)

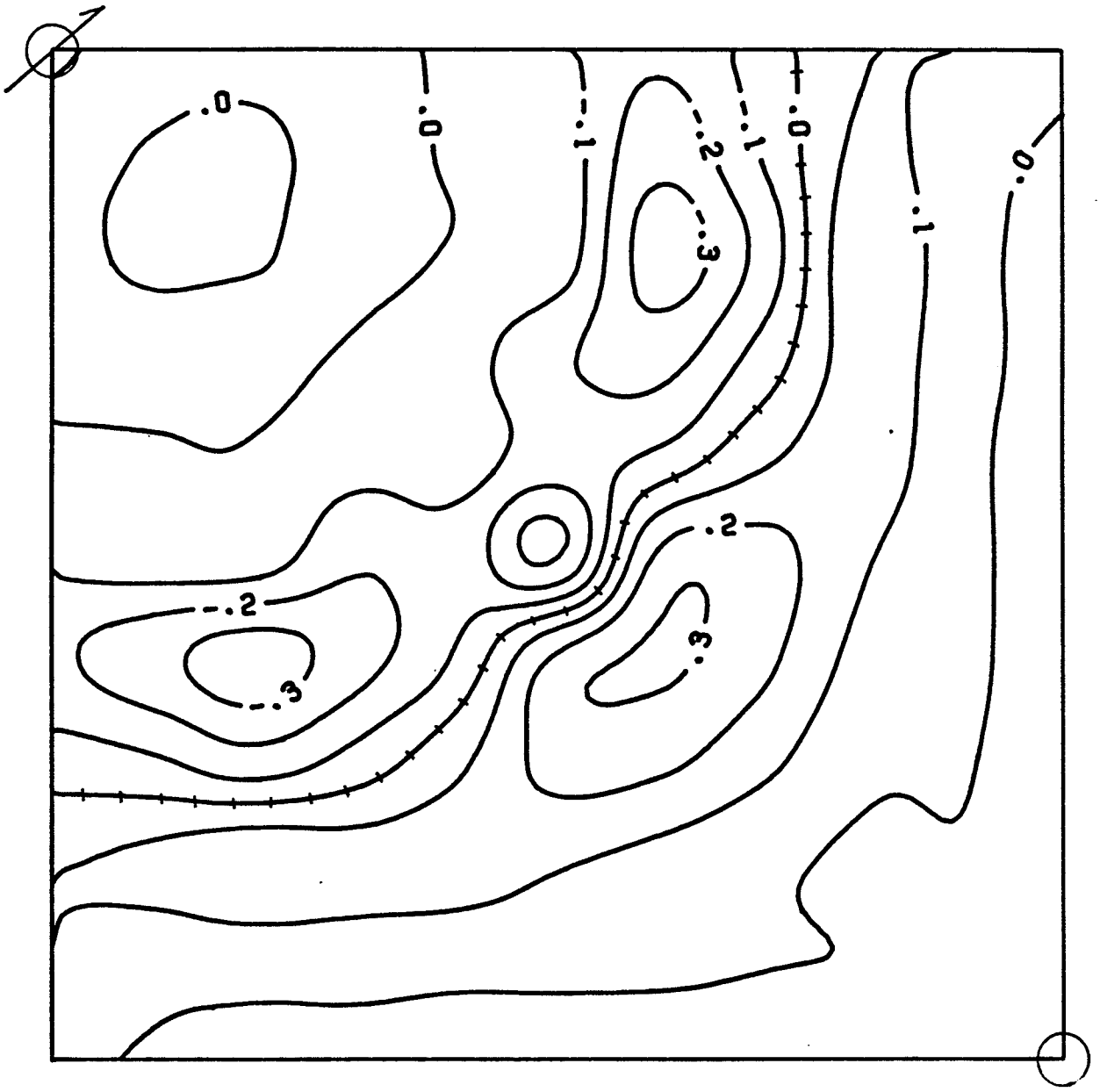

Fig. 5.3-3 CO_2 net flux (moles/time step) contour for Run # 5.3 at 0.5 DPV.
(α_l = 0.1, α_t = 0.01 ft)

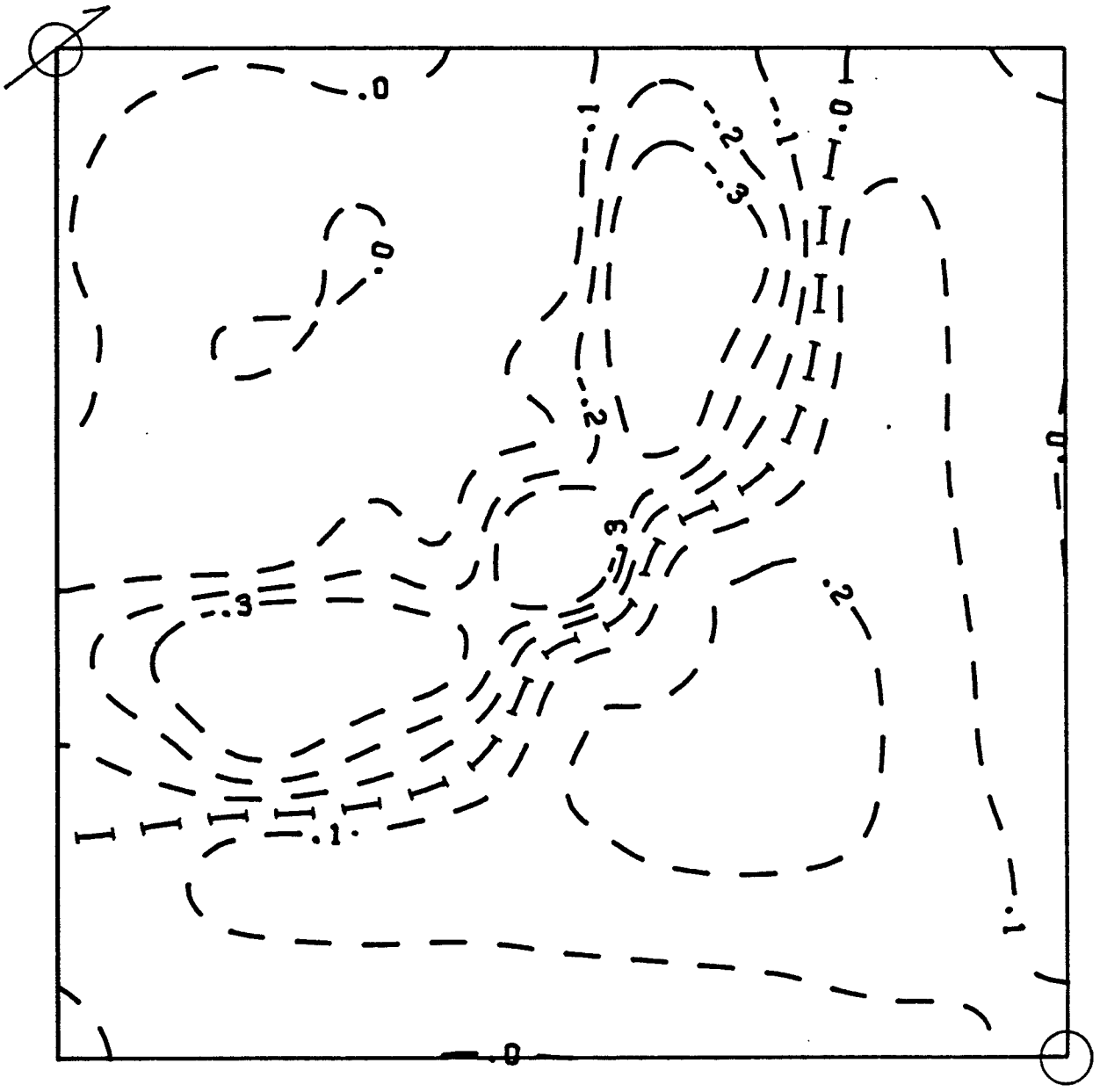

Fig. 5.3-4 CO_2 net flux (moles/time step) contour for Run # 5.2 at 0.5 DPV.
(α_l = 5.0, α_t = 0.5 ft)

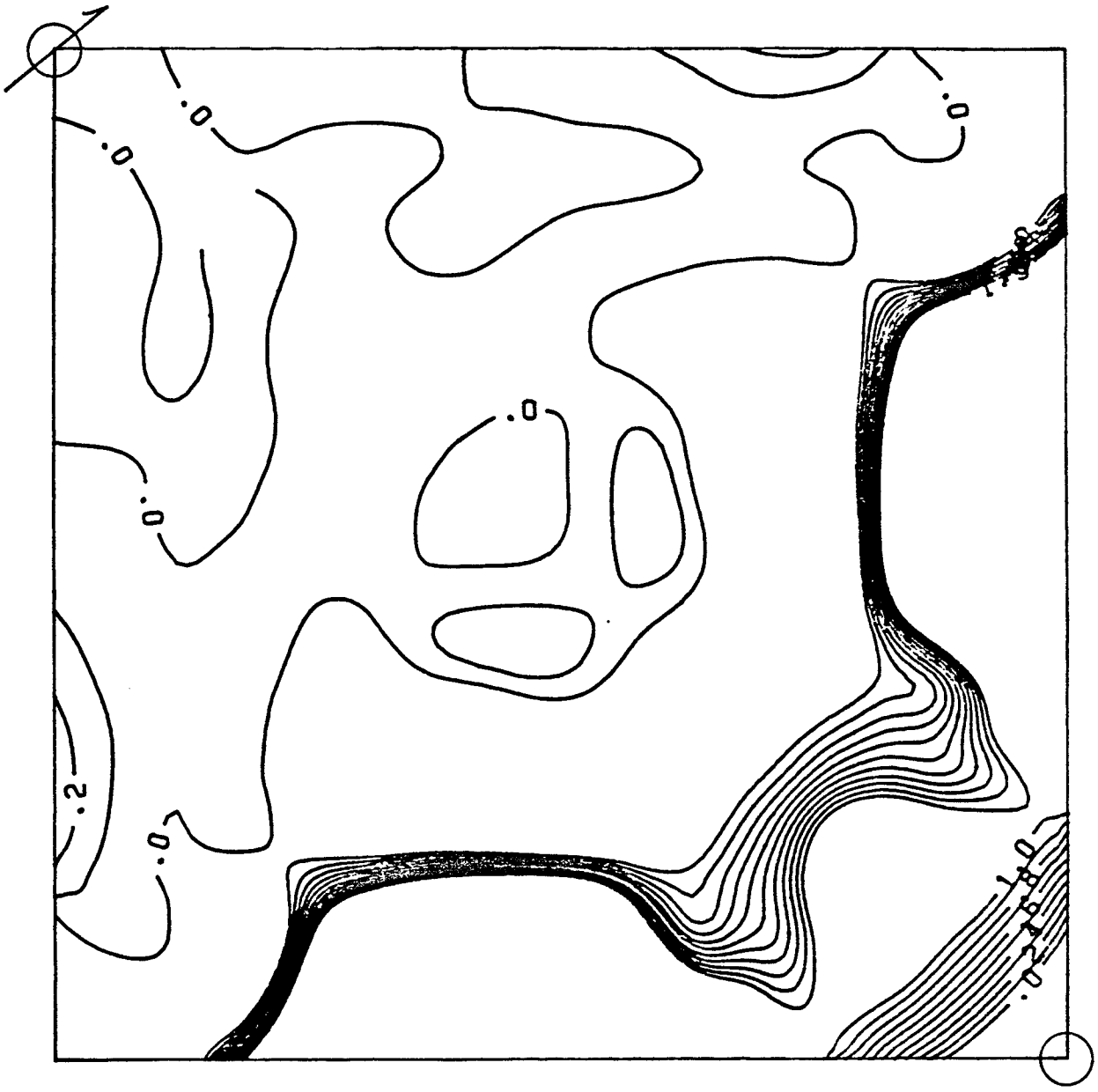

Fig. 5.3-5 CO_2 dispersive accumulation ratio for Run * 5.3 at 0.5 DPV.
(α_l = 0.1, α_t = 0.01 ft)

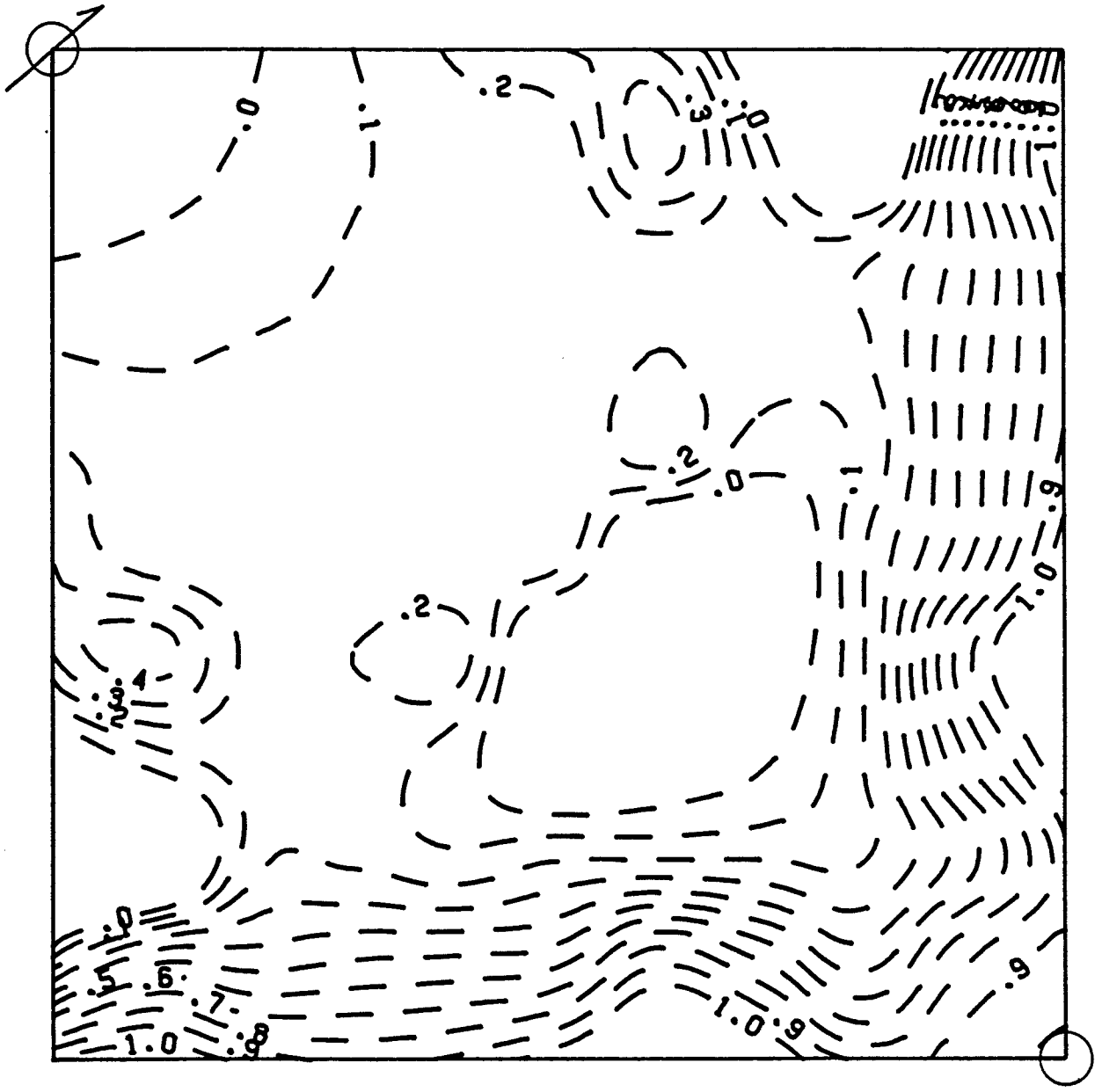

Fig. 5.3-6 CO_2 dispersive accumulation ratio for Run # 5.2 at 0.5 DPV.
(α_l = 5.0, α_t = 0.5 ft)

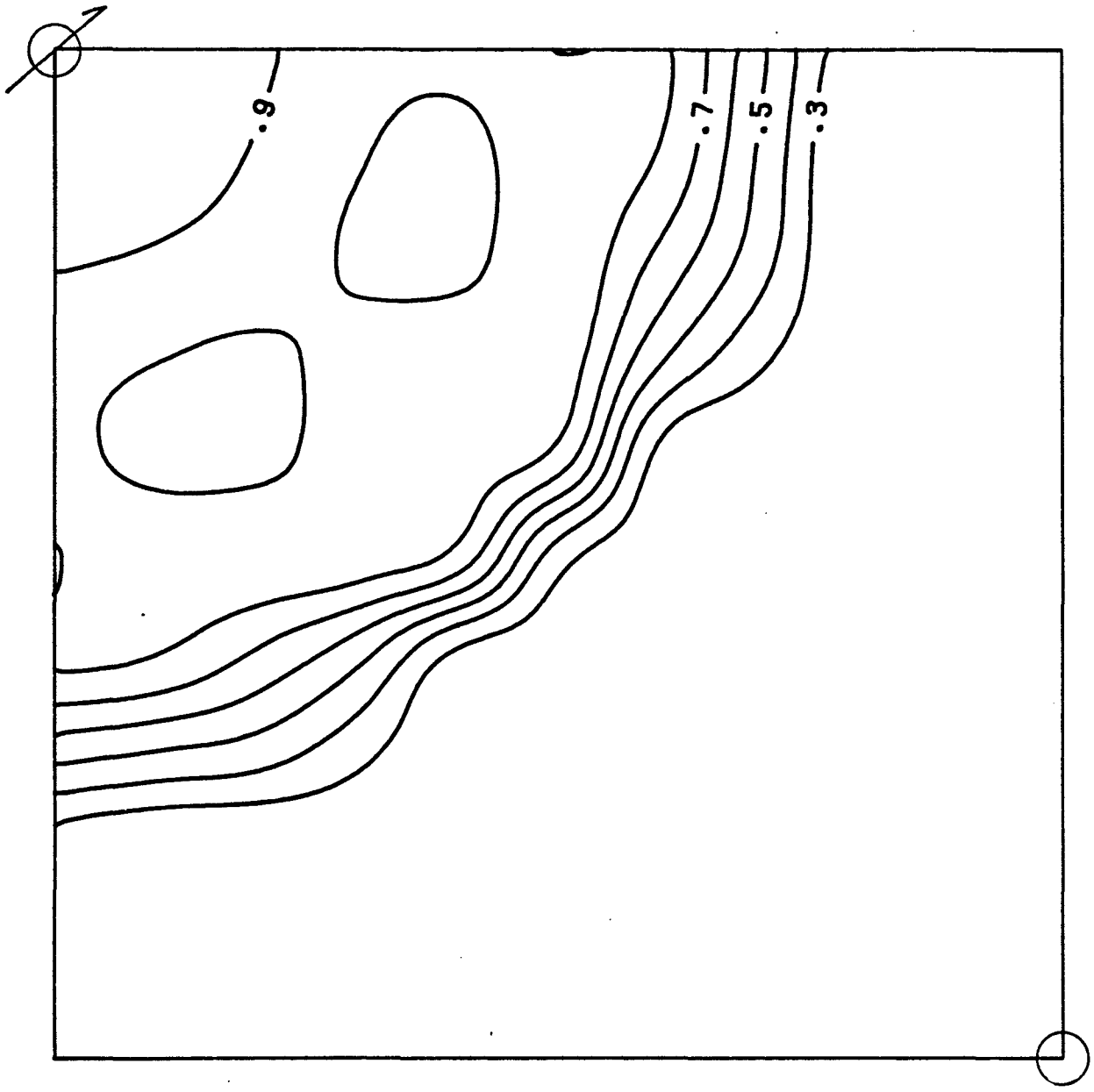

Fig. 5.3-7 Water saturation contour for Run # 5.3 at 0.5 DPV.
(α_l = 0.1, α_t = 0.01 ft)

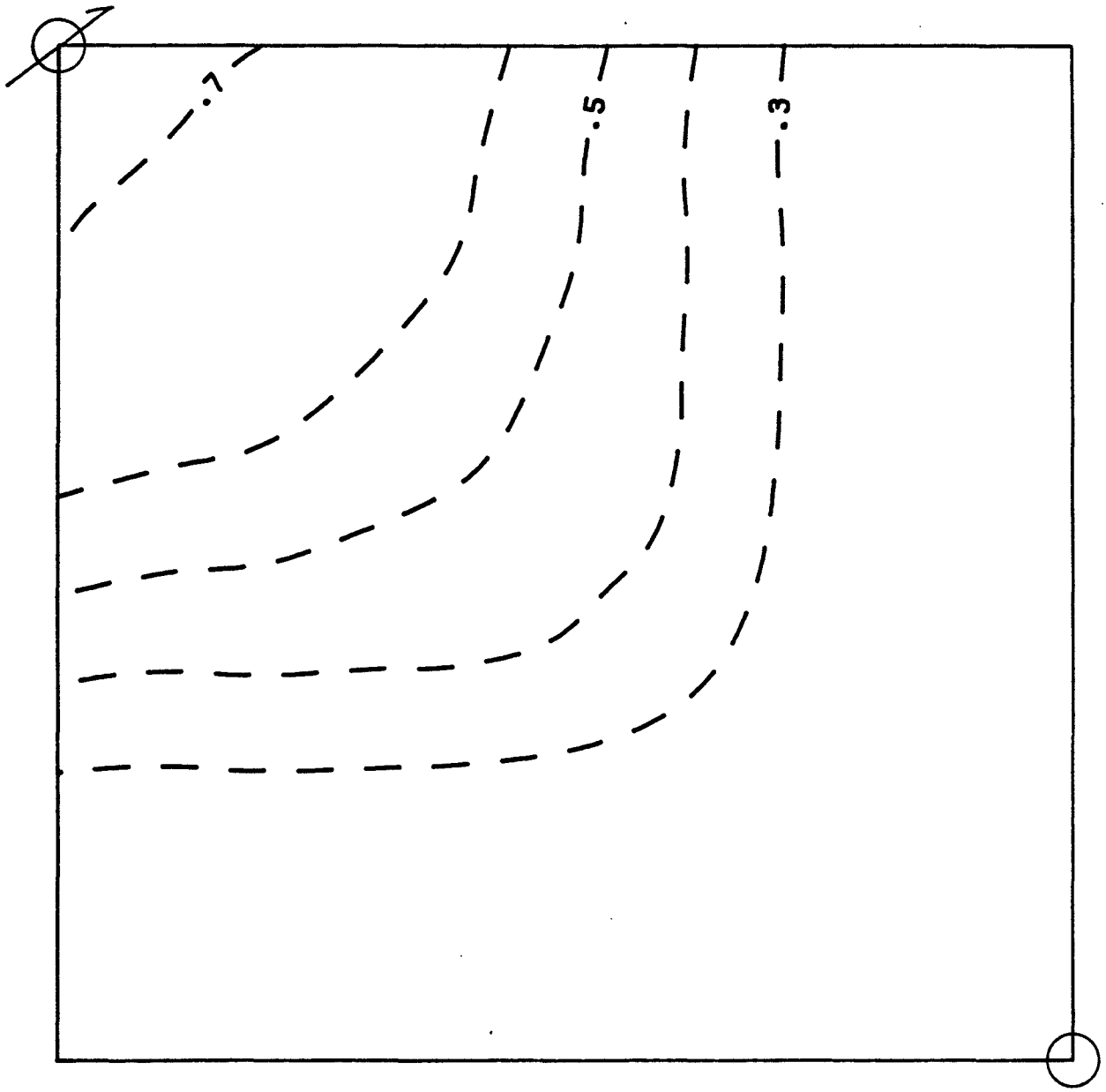

Fig. 5.3-8 Water saturation contour for Run # 5.2 at 0.5 DPV.
(α_l = 5.0, α_t = 0.5 ft)

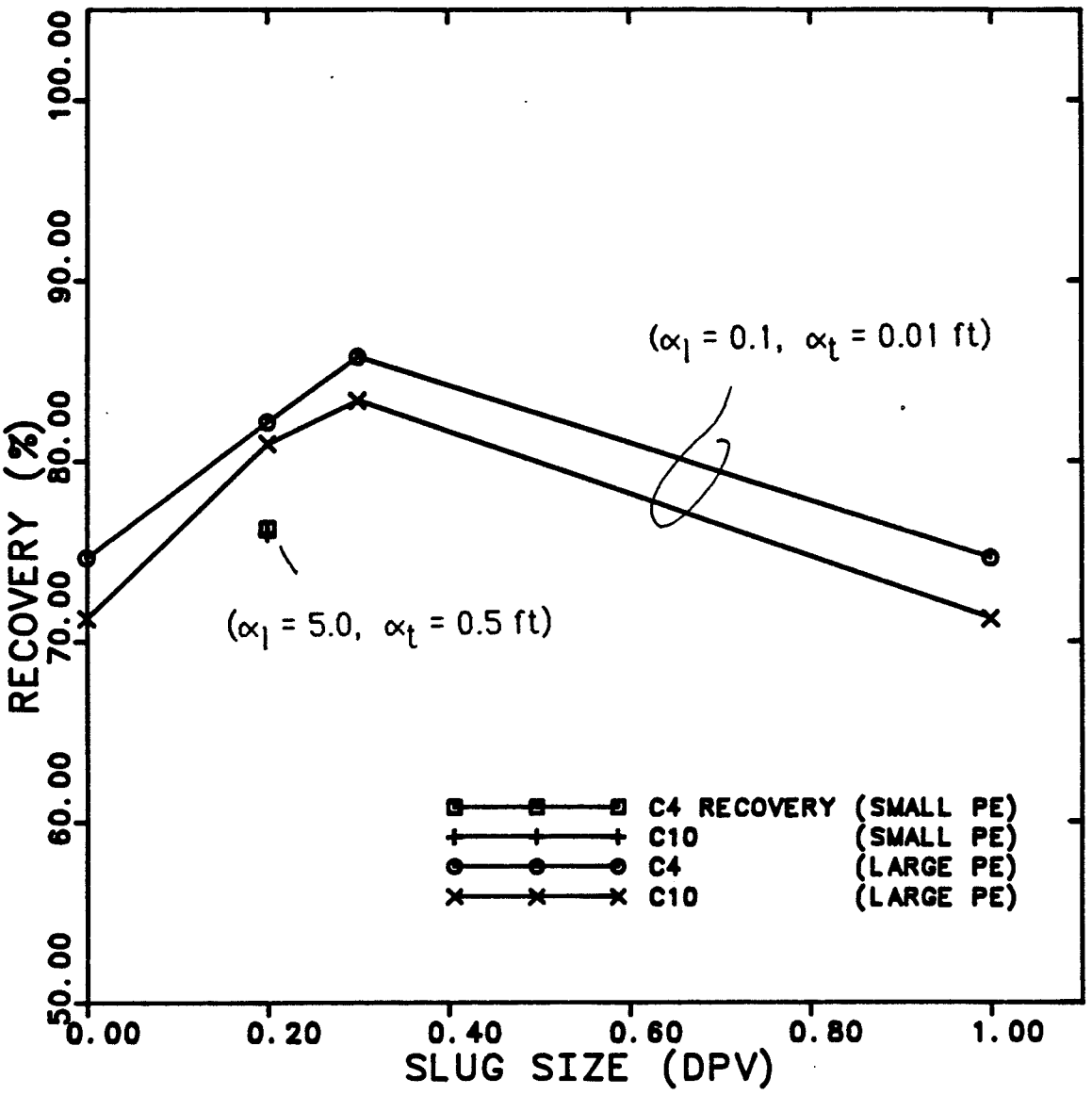

Fig. 5.3-9 Butane and decane recovery versus slug size.

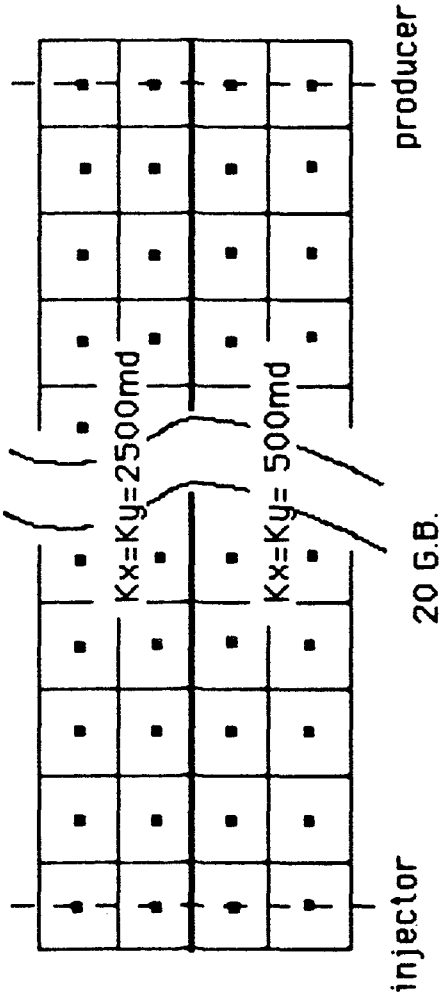

Fig. 5.4-1

Grid System for Class-6 Runs (20x4)

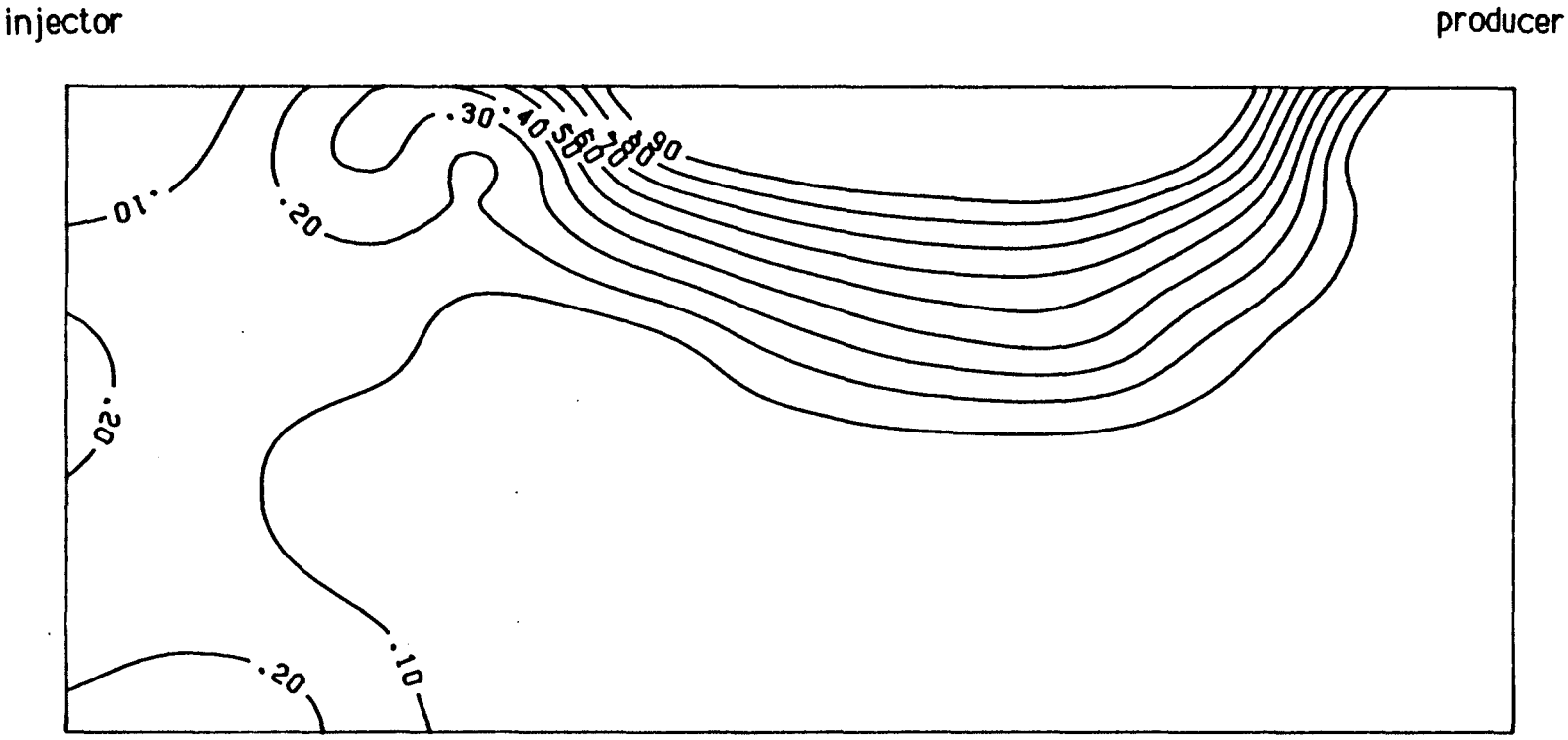

Fig. 5.4-2 CO_2 dimensionless concentration contour for Run * 6.1 at 0.4 DPV. (α_l = 0.1, α_t = 0.01 ft)

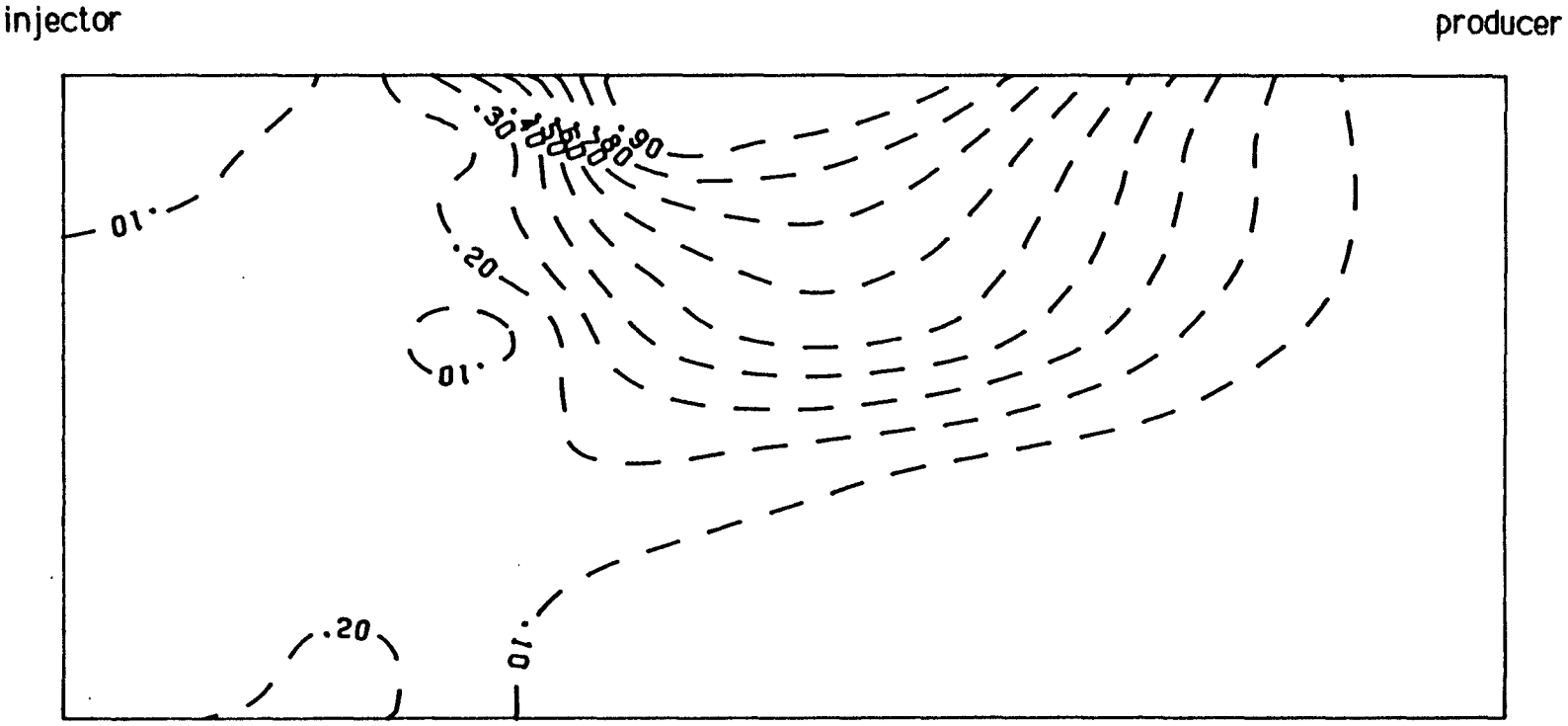

Fig. 5.4-3 CO_2 dimensionless concentration contour for Run # 6.3 at 0.4 DPV. (α_l = 5.0, α_t = 0.5 ft)

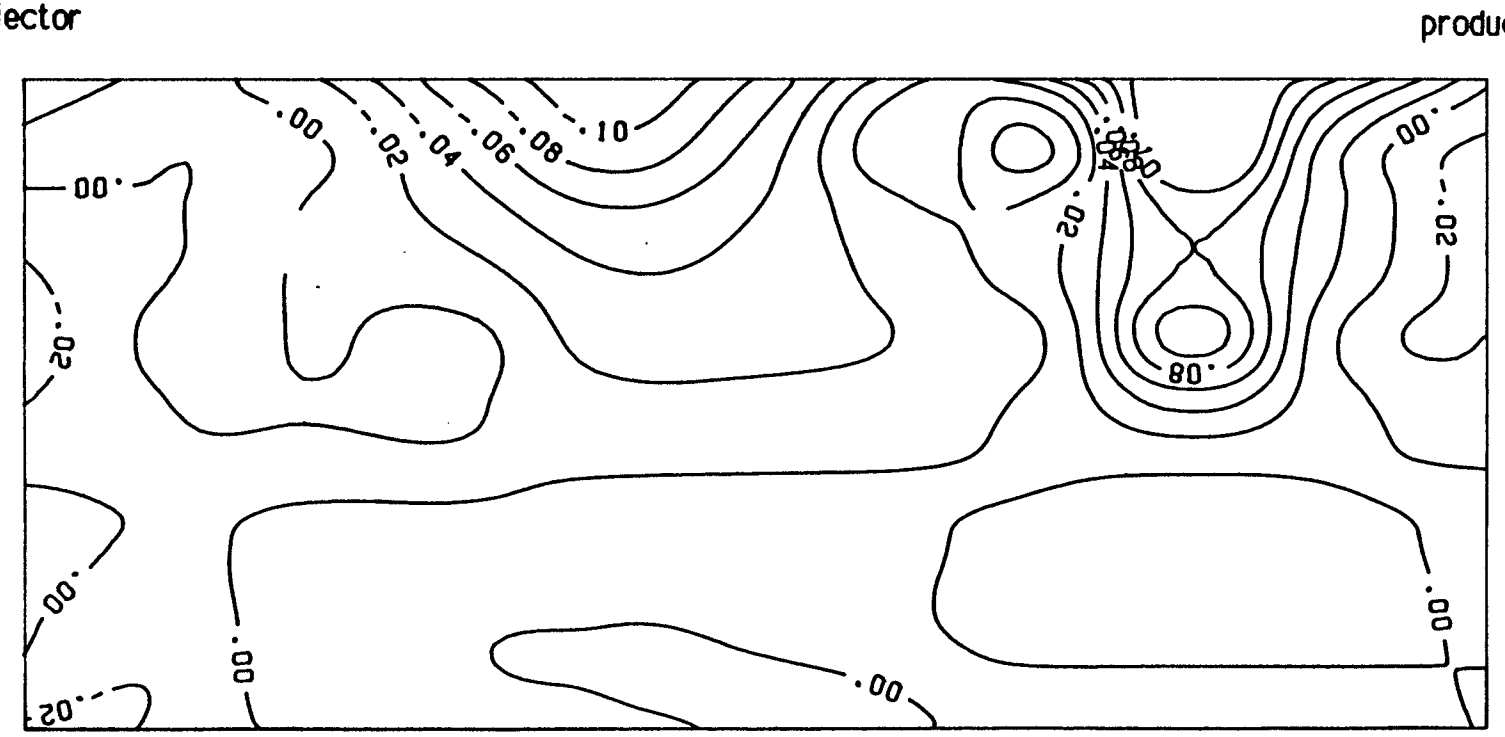

Fig. 5.4-4 CO_2 net flux (moles/time step) contour for Run # 6.1 at 0.4 DPV.
(α_l = 0.1, α_t = 0.01 ft)

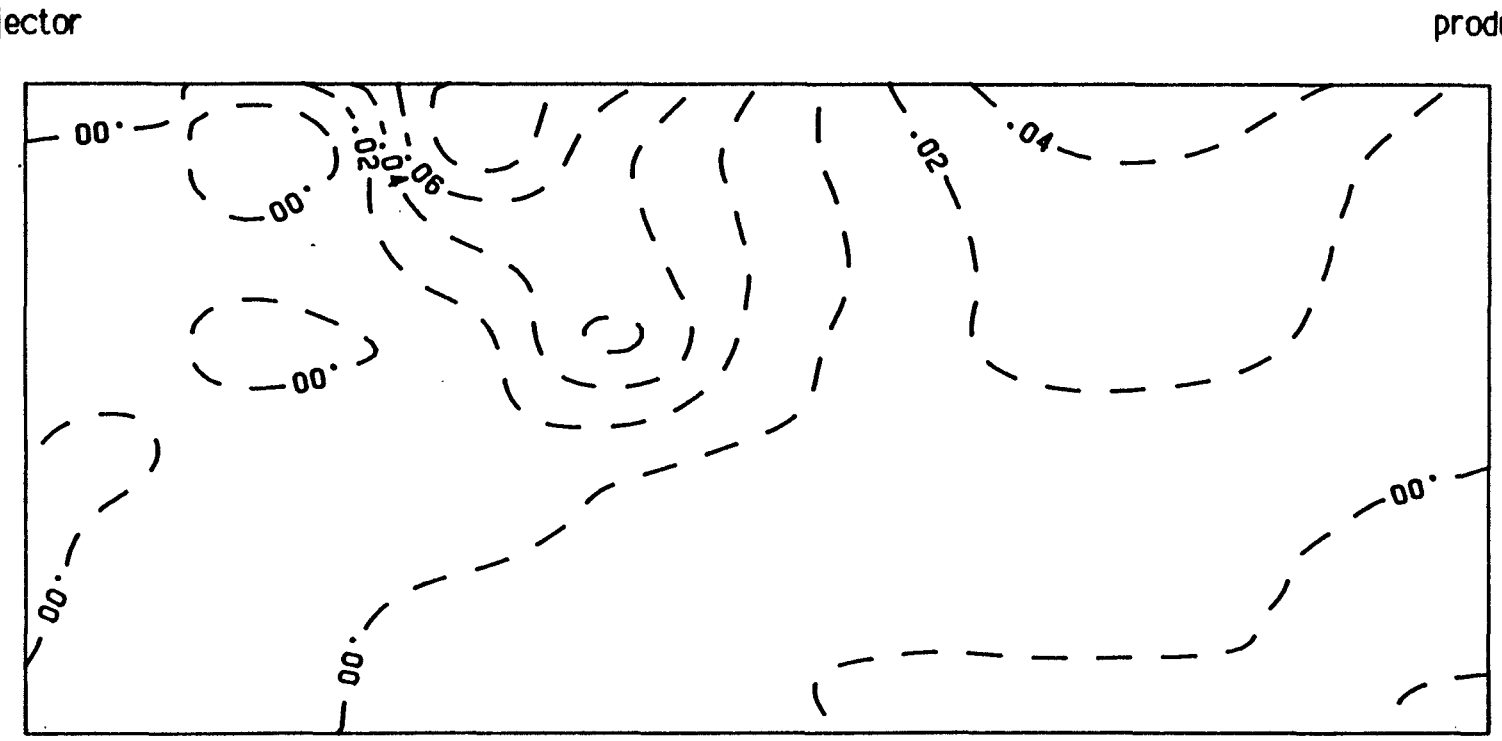

Fig. 5.4-5 CO_2 net flux (moles/time step) contour for Run # 6.3 at 0.4 DPV.
(α_l = 5.0, α_t = 0.5 ft)

injector producer

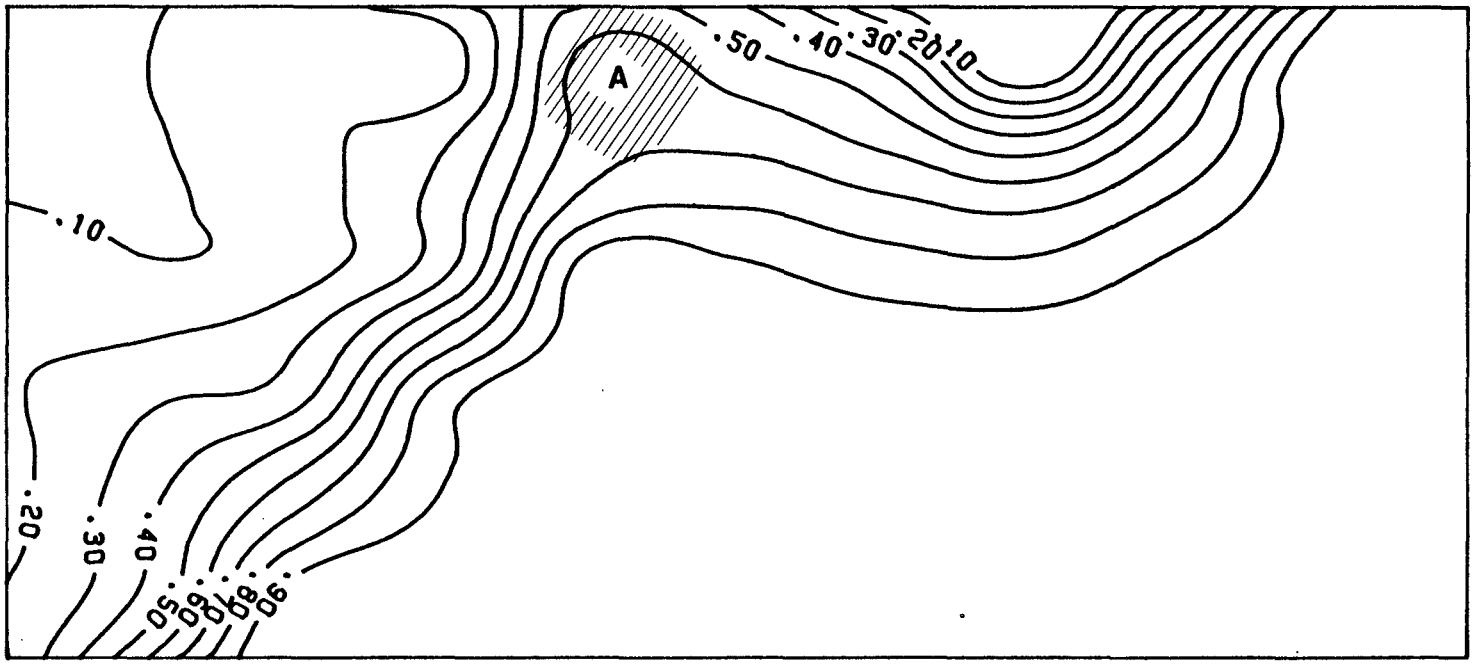

Fig. 5.4-6 C_{10} dimensionless concentration contour for Run # 6.1 at 0.4 DPV.
(α_l = 0.1, α_t = 0.01 ft)

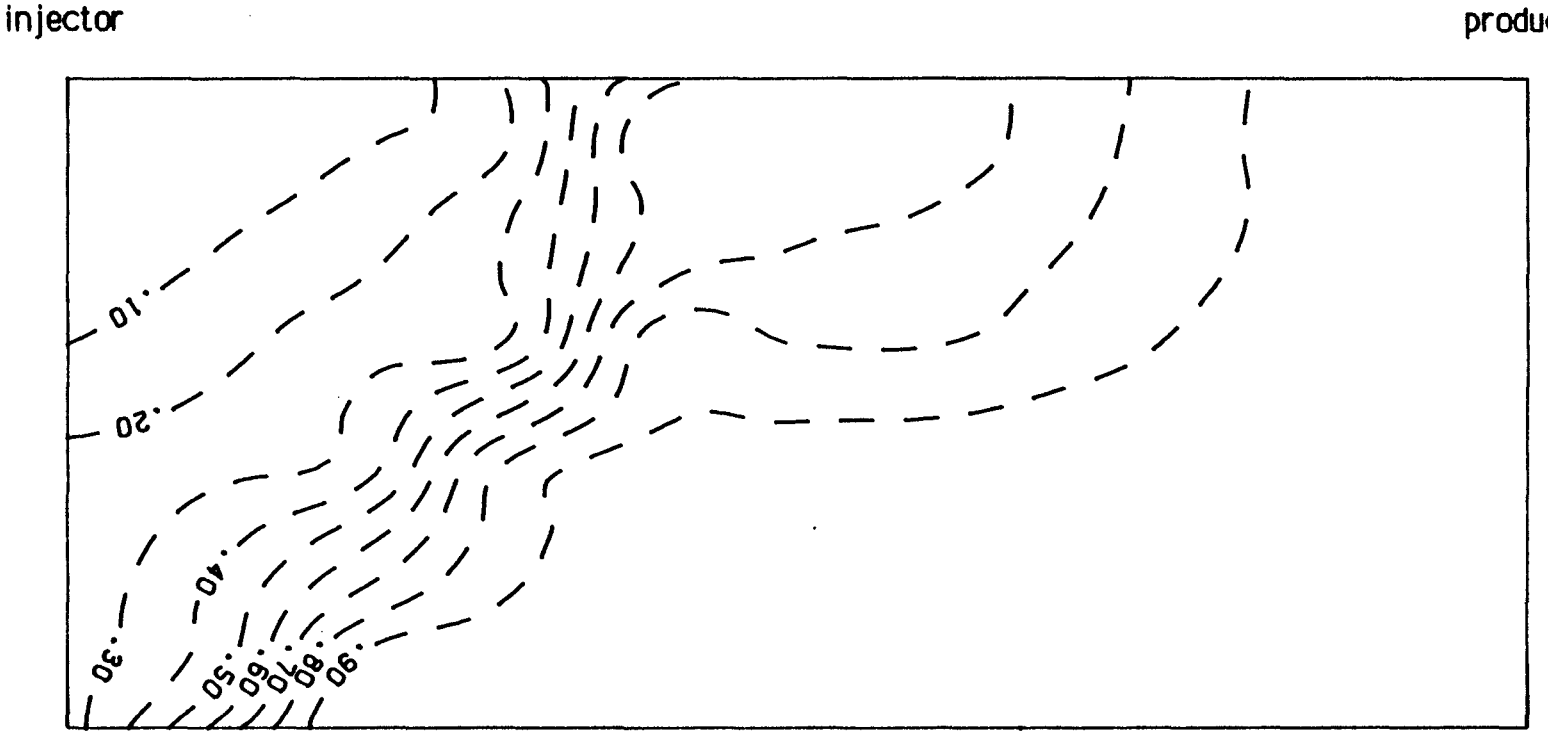

Fig. 5.4-7 C_{10} dimensionless concentration contour for Run # 6.3 at 0.4 DPV.
(α_l = 5.0, α_t = 0.5 ft)

injector producer

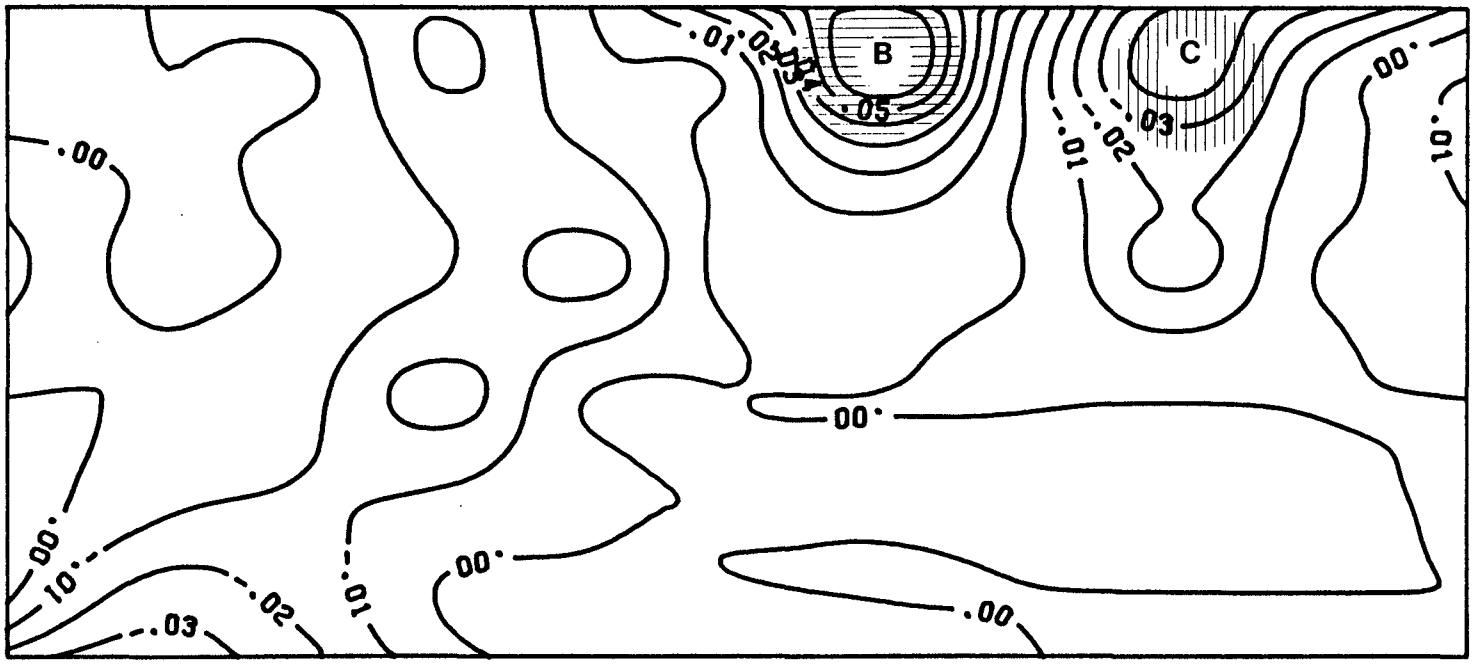

Fig. 5.4-8 C_{10} net flux (moles/time step) contour for Run # 6.1 at 0.4 DPV.
(α_l = 0.1, α_t = 0.01 ft)

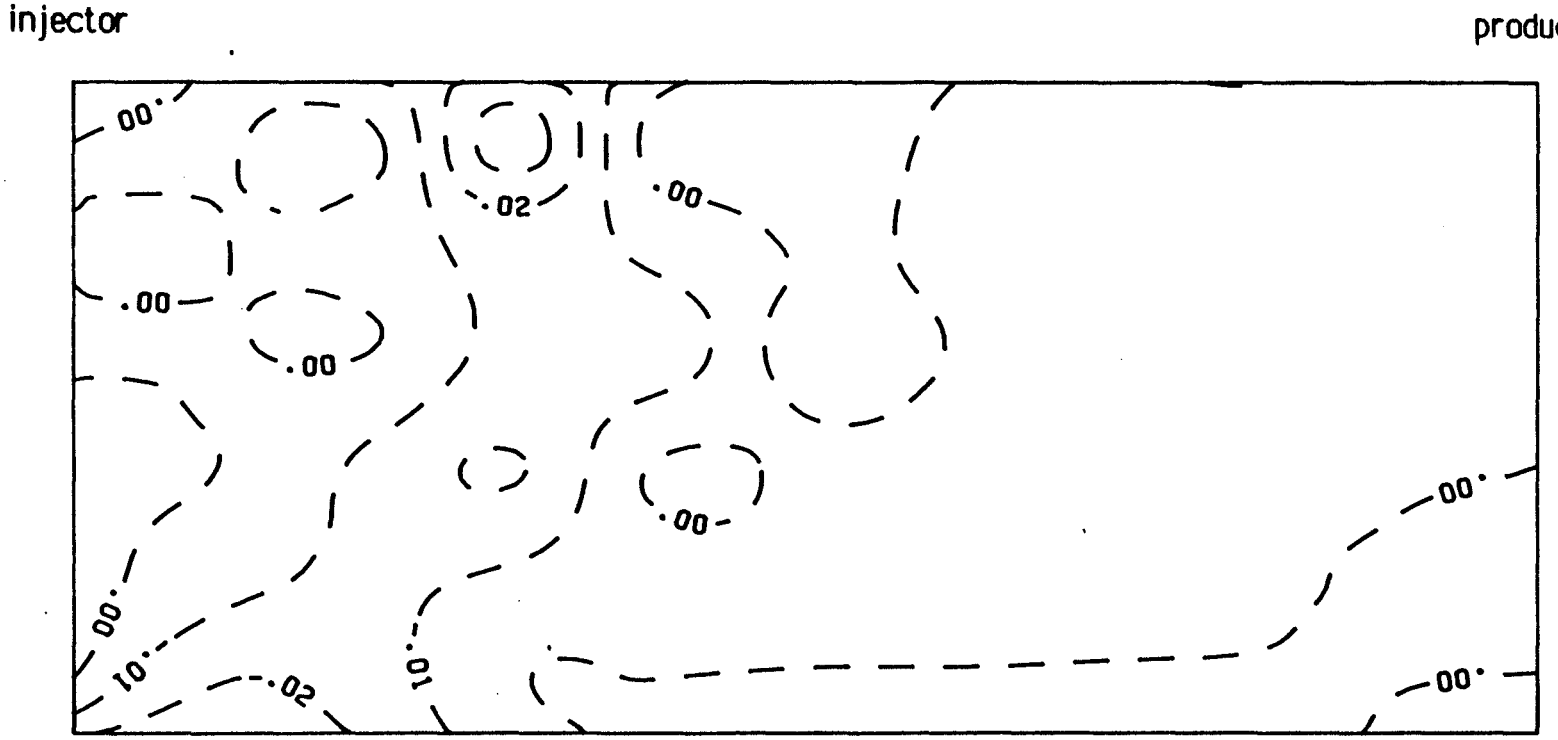

Fig. 5.4-9 C_{10} net flux (moles/time step) contour for Run # 6.3 at 0.4 DPV.
(α_l = 5.0, α_t = 0.5 ft)

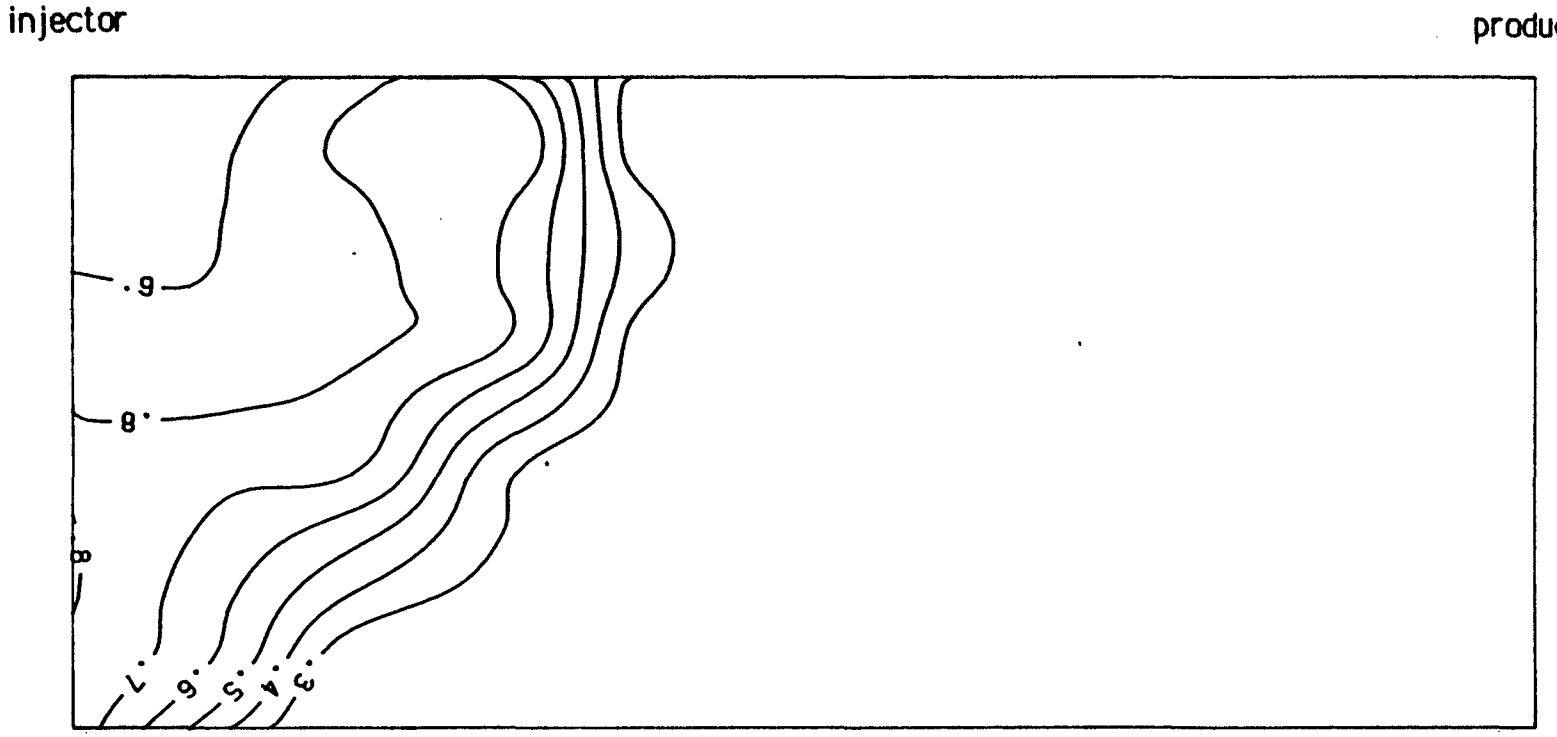

Fig. 5.4-10 Water saturation contour for Run # 6.1
at 0.4 DPV.
(α_l = 0.1, α_t = 0.01 ft)

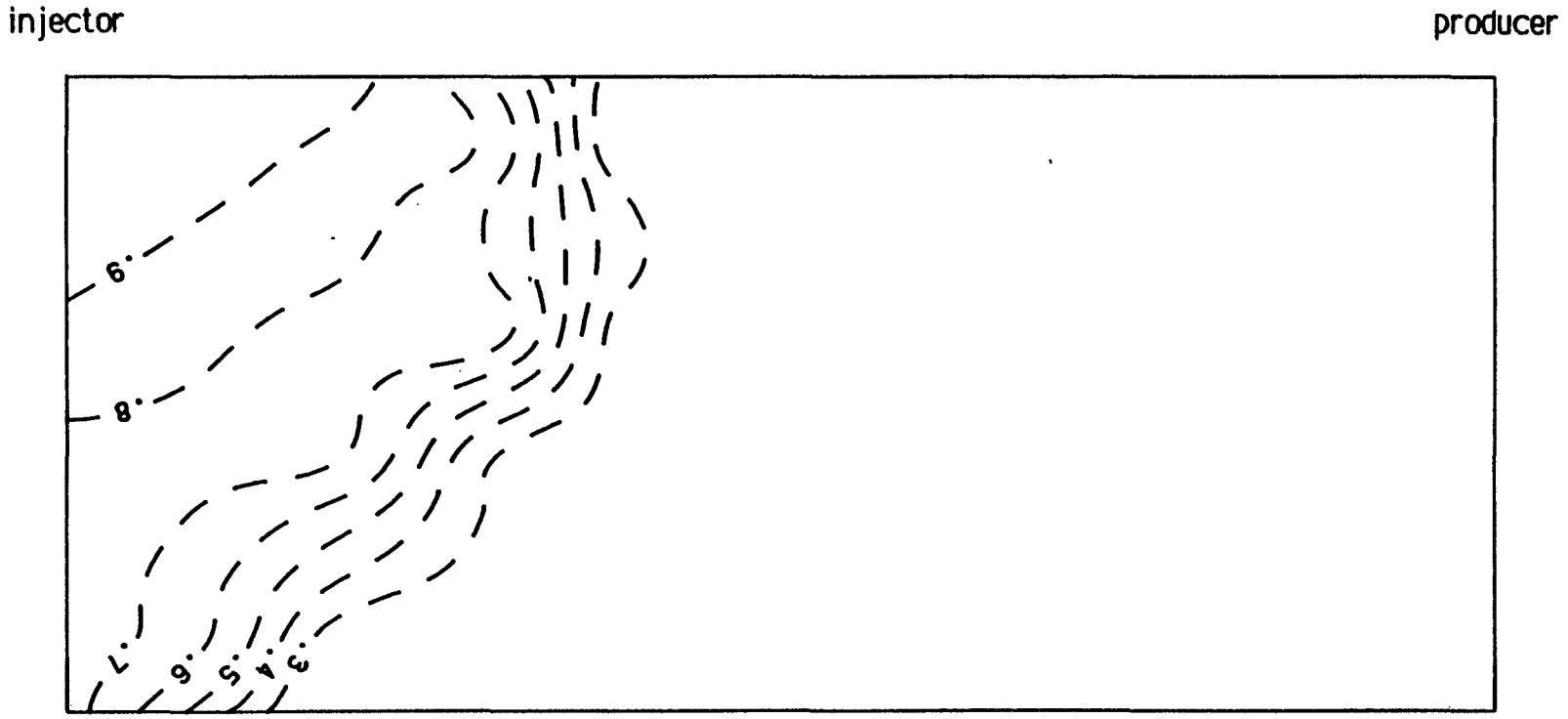

Fig. 5.4-11 Water saturation contour for Run # 6.3
at 0.4 DPV.
(α_l = 5.0, α_t = 0.5 ft)

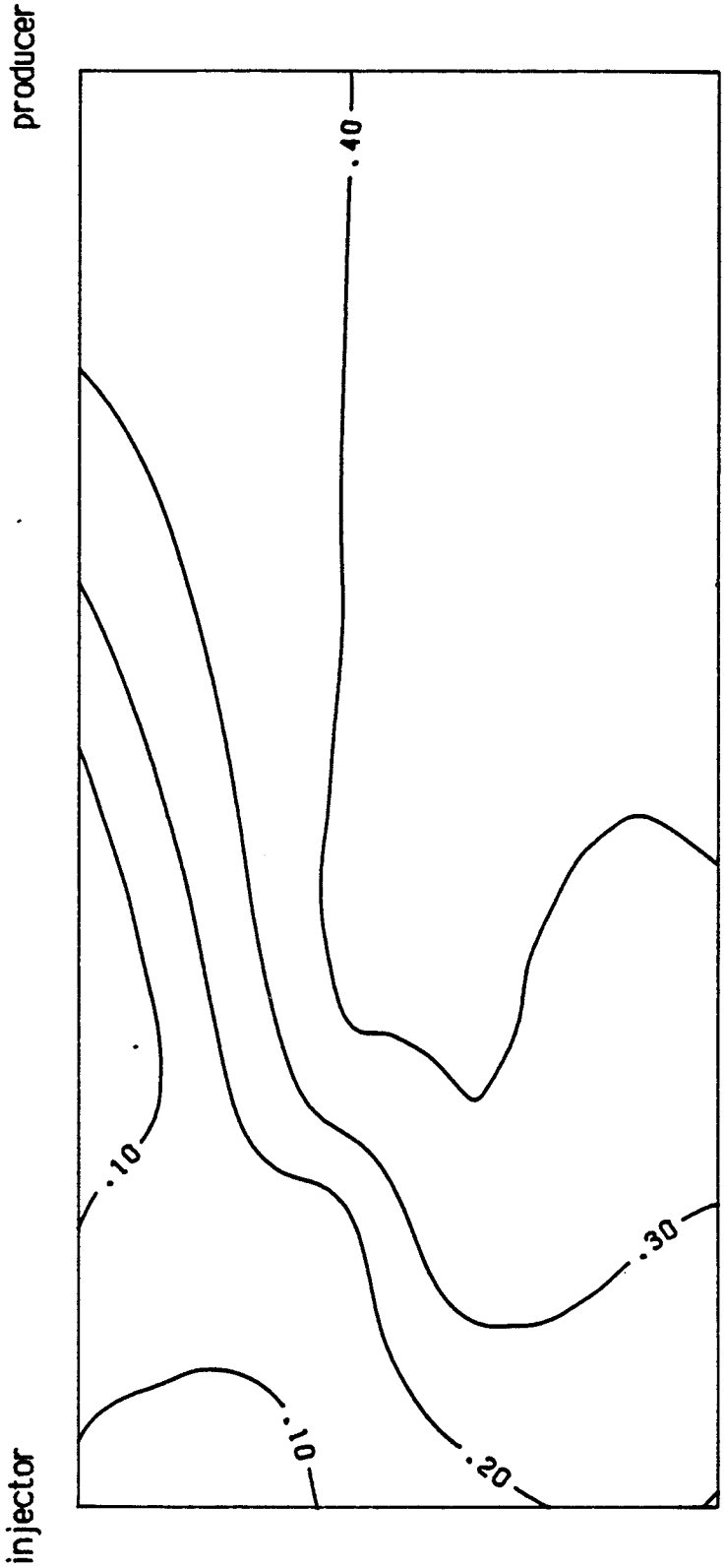

Fig. 5.4-12 C_{10} dimensionless concentration contour for Run # 6.1 at 1.2 DPV. ($\alpha_l = 0.1$, $\alpha_t = 0.01$ ft)

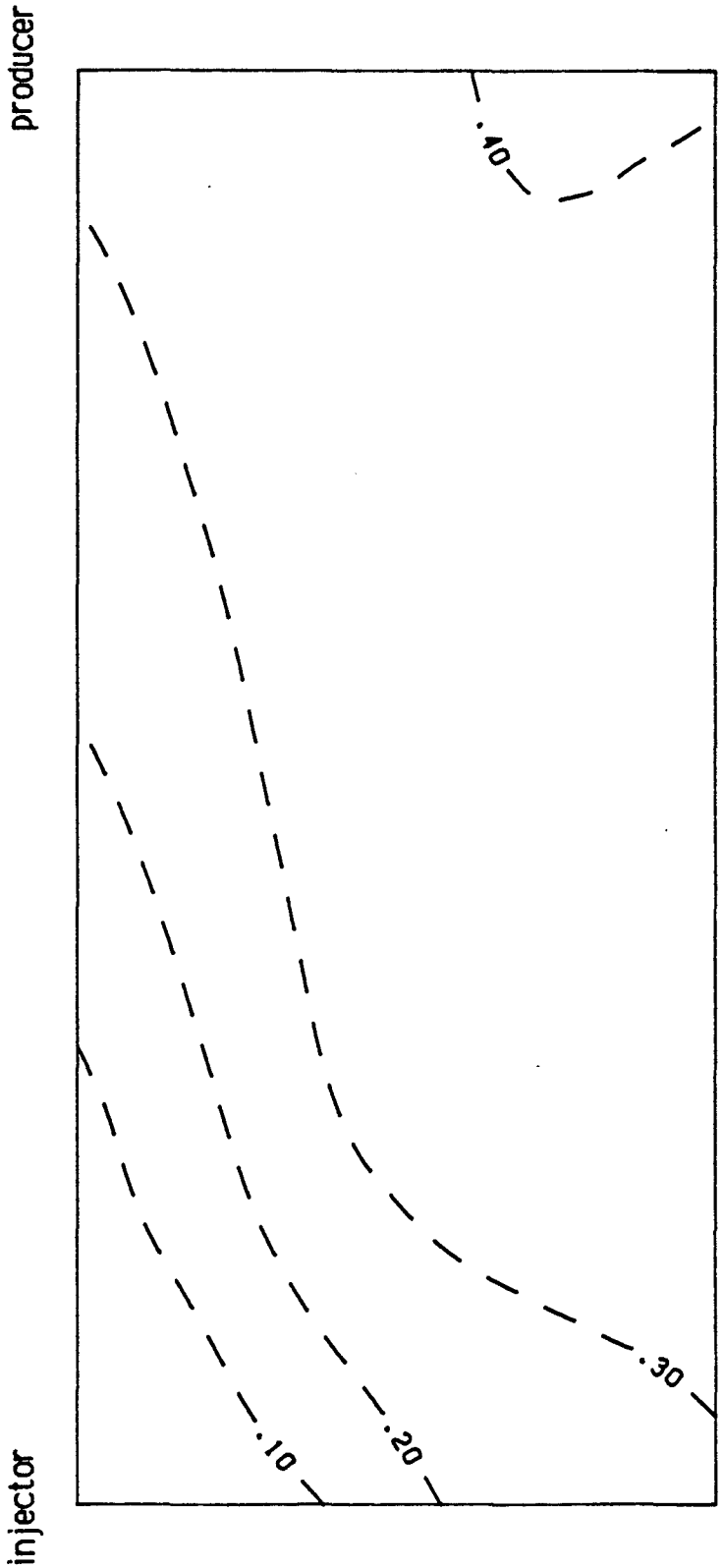

Fig. 5.4-13 C_{10} dimensionless concentration contour for Run # 6.3 at 1.2 DPV. ($\alpha_l = 5.0$, $\alpha_t = 0.01$ ft)

CHAPTER VI

CONCLUSIONS AND RECOMMENDATIONS

6.1 Conclusions

The conclusions from this work are itemized as follows:

1. The displacement process which causes large concentration gradients of components in a certain phase, such as first-contact and multiple-contact miscible processes or immiscible displacements with large interphase mass transfer is significantly affected by dispersion (both physical and numerical). Hence, numerical dispersion must be reduced to a reasonable level in those cases in order to understand correctly the physical flow.
2. As shown in Sec. 5.3.2 and Sec. 5.4.2, equal amounts of the physical dispersivity can affect displacement differently (adversely or favorably), depending on the reservoir system. This simply implies that physical dispersion is one of the most important mechanisms and that accurate modeling, including both longitudinal and transverse dispersion, must be required.
3. MMP is largely affected by dispersion. This fact

should be taken into account when a simulation of slim tube experiment is made.

4. The minimum requirement of solvent slug size to make an efficient displacement is related to the residual oil saturation.
5. Without the presence of dendritic and/or trapped hydrocarbon fraction, the mobile water phase has little effect on the miscible displacement process. For instance, MMPs for the secondary and tertiary displacements were almost the same, and the change of the volume fraction of water in the injecting fluid didn't affect the recovery significantly.
6. Two-point upstream weighting is a valuable practical tool to reduce numerical dispersion. Its implementation is fairly easily done with carefully checked constraints, and the excution of these additional lines in the program causes only a minor increase in computation time (less than five percent). However, as presented through simulations of slim tube displacements, the composition routes remained close to the binodal curve, the region where flash calculations are very difficult and time consuming, when numerical dispersion is reduced. This caused the computation times to increase also. In addition to this, in 2-D runs, some stability difficulties may

occur when a sharp concentration front, which results from a reduction in numerical dispersion, is propagated from a well block to adjacent blocks. A very small time step size is required in this event.

7. Chaudhari's technique can not model a physical dispersion if it is smaller than the numerical dispersion which arises from an ordinary first-order accurate finite difference formulation.
8. Grid orientation effects are very significant for unfavorable mobility ratio miscible displacements. The use of parallel grids with two-point upstream weighting is one of the practical ways to get realistic results.
9. The "All 2-Point" scheme didn't show the difficulty, which was predicted in Sec. 5.1, through the application runs. However, if such kind of situations were met, "Composition 2-Point" should be used.

6.2 Recommendations

Recommendations for further study are listed below:

1. The mixing parameter approach should be implemented to account for viscous fingering.
2. The dendritic and the trapped hydrocarbon fraction,

and the solubility to water should be modeled.

3. The effect of mixing due to the molecular diffusion, which was always set to zero in this study, should be investigated.
4. The third and the fourth hydrocarbon phases, which are probably a second liquid phase and the precipitate, should be included for low temperature miscible applications.
5. After the modifications mentioned above are done, the application runs reported in this study should be repeated or extended, using actual data from experiments and field operations. However, to do this, especially for a field scale simulation, the following improvements are further required.
6. An automatic time step size selector should be incorporated.
7. Some kind of partial solution technique should be very useful to save computation time.
8. Using the in-house machine, the CDC Dual CYBER 170/750, for example, for a 6-component run, the approximate limitation of number of grid blocks may be (13x13). This number can be increased slightly by optimizing the program and by changing the direct matrix solver to one of the iterative methods such as SOR or SSOR, but probably it is still far from what

is requied for a field scale study. To relax the storage limitation and speed up the solution, the use of a supercomputer may be required. Several example runs, using the same simulator as was used in this study, on a CRAY machine were given by Rood [R3].

NOMENCLATURE

$\bar{B}_f$ = diagonal submatrix composed of elements b_{fk} ; k = 1, 2, ... N_b (L^3/t).

$\bar{B}_i$ = diagonal submatrix composed of elements b_{ik} ; k = 1, 2, ... N_b (L^3/t).

$\bar{B}_w$ = diagonal submatrix composed of elements b_{wk} ; k = 1, 2, ... N_b (L^3/t).

$\bar{B}_Z$ = diagonal submatrix composed of submatrices $\bar{B}_{Zi}$; i = 1, 2, ... N_c-1 (moles/t).

$\bar{B}_{Zi}$ = diagonal submatrix composed of elements b_{Zik} ; k = 1, 2, ... N_b (moles/t).

b_{fk} = partial derivative of overall hydrocarbon balance with respect to F appearing as element (k, k) of submatrix $\bar{B}_f$ (L^3/t).

b_{ik} = partial derivative of balance on component i with respect to F appearing as element (k, k) of submarix $\bar{B}_i$ of submatrix $\bar{B}$ (L^3/t).

b_{wk} = partial derivative of water balance with respect to W appearing as element (k, k) of submarix $\bar{B}_w$ (L^3/t).

b_{zik} = partial derivative of balance on component i with respect to overall mole fraction of component i appearing as element (k, k) of submatrix $\bar{B}_{zi}$ of submatrix $\bar{B}_z$ (moles/t).

C = factor in radial form of productivity index to account for location of well in grid block.

$\bar{C}_f$ = originally, diagonal submatrix composed of elements c_{pk} ; k = 1, 2, ... N_b (L^2/F). After forward elimination, this matrix takes on the structure of submatrices $\bar{T}_f$, $\bar{T}_w$, and $\bar{T}_i$, i = 1, 2, ... N_c-1.

$\bar{C}_v$ = diagonal submatrix composed of elements c_{vk} ; k = 1, 2, ... N_b (dimensionless).

$\bar{C}_w$ = diagonal submatrix composed of elements c_{wk} ; k = 1, 2, ... N_b (L^2/F).

$\bar{C}_{yj}$ = diagonal submatrix composed of elements c_{yjk} ; k = 1, 2, ... N_b (dimensionless).

c_f = formation compressibility factor (L^2/F).

c_{fk} = partial delivative of saturation constraint with respect to F appearing as element (k, k) of submatrix $\bar{C}_f$ ($moles^{-1}$).

c_{jk} = partial derivative of saturation constraint with respect to overall mole fraction of component j appearing as

element (k, k) of submatrix $\bar{C}_j$ of submatrix $\bar{C}$ (dimensionless).

c_{pk} = partial derivative of saturation constraint with respect to pressure appearing as element (k, k) of submatrix $\bar{C}_p$ (L^2/F).

c_{vk} = partial derivative of saturation constraint with respect to total mole fraction in vapor phase appearing as element (k, k) of submatrix $\bar{C}_v$ (dimensionless).

c_w = water compressibility factor (L^2/F).

c_{wk} = partial derivative of saturation constraint with respect to W appearing as element (k, k) of submatrix $\bar{C}_w$ ($moles^{-1}$).

c_{yjk} = partial derivative of saturation constraint with respect to vapor mole fraction of component j appearing as element (k, k) of submatrix $\bar{C}_y$ (dimensionless).

C_D = dimensionless concentration of displacing fluid = $(C-C_I)/(C_J-C_I)$.

D = depth relative to some datum to center of grid block; positive downward (L).

D_{ij} = effective molecular diffusion coefficient of component i in phase j (L^2/t).

f_{ji} = component fugacity for component i of phase j, j=o, g (F/L^2).

F = overall hydrocarbon molar concentration, = $S_o\xi_o + S_g\xi_g$ (moles / L^3).

$\bar{\bar{G}}_{pi}$ = diagonal submatrix composed of elements g_{pik} ; k = 1, 2, ... N_b (dimensionless).

$\bar{\bar{G}}_{vi}$ = diagonal submatrix composed of elements g_{vik} ; k = 1, 2, ... N_b (F/L^2).

$\bar{\bar{G}}_{yij}$ = diagonal submatrix composed of elements g_{yijk} ; k = 1, 2, ... N_b (F/L^2).

$\bar{\bar{G}}_{zij}$ = diagonal submatrix composed of elements g_{zijk} ; k = 1, 2, ... N_b (F/L^2).

g = gravitational acceleration (L/t^2).

g_{pik} = partial derivative of fugacity constraint of component i with respect to pressure appearing as element (k, k) of submatrix $\bar{\bar{G}}_{pi}$ of submatrix $\bar{\bar{G}}_p$ (dimensionless).

g_{vik} = partial derivative of fugacity constraint of component i with respect to total vapor mole fraction appearing as element (k, k) of submatrix $\bar{\bar{G}}_{vi}$ of submatrix $\bar{\bar{G}}_v$ (F/L^2).

g_{yijk} = partial derivative of fugacity constraint of component i with respect to vapor mole fraction of component j appearing as element (k, k) of submatrix $\bar{G}_{yij}$ of submatrix $\bar{G}_y$ (F/L^2).

g_{zijk} = partial derivative of fugacity constraint of component i with respect to overall mole fraction of component j appearing as element (k, k) of submatrix $\bar{G}_{zij}$ (F/L^2).

h = height or thickness or width of reservoir (L).

II = injectivity index (moles $L^2/F \cdot t$).

k_{rj} = relative permeability to phase j; j = w, o, g (dimensionless).

k_{roiw} = oil relative permeability at irreducible water saturation.

k_X = absolute permeability in X-direction (L^2).

k_Y = absolute permeability in Y-direction (L^2).

$\bar{k}$ = permeability tensor (L^2).

K_i = equilibrium K-value for component i, = y_i/x_i (dimensionless).

$\bar{K}_{ij}$ = dispersion tensor for component i in phase j (L^2/t).

K^N = inverse of numerical Peclet number ($1/N_{pe}^N$),

(dimensionless).

K^P = inverse of physical Peclet number ($1/N_{pe}^P$), (dimensionless).

L = system length (L).

L = mole fraction of hydrocarbon volume in liquid phase.

M = mobility ratio (mobility of displacing fluid / mobility of displaced fluid).

M_i = molecular weight of component i (a.m.u.).

N_b = number of grid blocks.

N_c = number of non-aqueous components.

$\vec{N}_i$ = flux of component i (including water) in general mass balance equations (moles/L^2).

N_l = number of layers.

N_p = number of phases.

N_{pe} = Peclet number (dimensionless).

N_X = number of grid blocks in X-direction.

N_Y = number of grid blocks in Y-direction.

P = gas phase pressure -- also denoted as P_g (F/L^2).

P_{bh} = bottomhole pressure (F/L^2).

P_{ci} = critical pressure of pure component i (F/L^2).

P_{cog} = oil/gas capillary pressure, $= P_g - P_o$ (F/L^2).

P_{cwo} = water/oil capillary pressure, $= P_o - P_w$ (F/L^2).

P_f^o = reference pressure for porosity correlation (F/L^2).

P_j = pressure of phase j ; j = w, o, g (F/L^2).

PI = productivity index (moles $L^2/F/t$).

P_w^o = reference pressure for water density correlation (F/L^2).

$[P_i]$ = parachor for component i -- used to compute interfacial tensions ($F^{1/4} L^{11/4}$ /moles).

Q_i = volumetric rate of component i ; positive for injection (L^3/t).

Q_w = volumetric rate of water (L^3/t).

Q_T = total volumetric rate (L^3/t).

q_h = overall hydrocarbon rate (moles/t).

q_i = rate of component i (moles/t).

q_T = total rate (moles/t).

q_w = water rate (moles/t).

$\vec{R}_{ci}$ = residual vector of molar balance on component i composed of elements R_{cik} ; k =1, 2, ...N_b (moles/t).

$\vec{R}_{fi}$ = residual vector of fugacity constraint on component i composed of elements R_{fik} ; k =1, 2, ...N_b (F/L^2).

$\vec{R}_h$ = residual vector of overall hydrocarbon molar balance composed of elements R_{hk} ; k = 1, 2, ...N_b (moles/t).

R_i = source term of component i (including water) in general mass balance equations (moles/t).

$\vec{R}_s$ = residual vector of saturation constraint (dimensionless).

$\vec{R}_{sfi}$ = scaled residual vector of fugacity constraint on component i composed of elements R_{sfik} ; k = 1, 2, ...N_b (F/L^2).

r_{eq} = equivalent radius for radial form of well model (L).

r_w = wellbore radius (L).

r_{ij} = homogeneous reaction rate in general mass balance equations (mass i /L^3 j-t).

r_{is} = homogeneous reaction rate in stationary phase in general mass balance equations (mass i /L^3 j-t).

S = skin factor in radial well model (dimensionless).

S_{grw} = residual gas saturation to water.

S_j = saturation of phase j ; j = w, o, g (fraction).

S_{org} = residual oil saturation to gas.

S_{orw} = residual oil saturation to water.

S_{wr} = irreducible water saturation.

$\overline{T}$ = submatrix composed of submatrices $\overline{T}_i$; i= 1, 2, ...N_c-1 (moles $L^2/F \cdot t$).

T_{ci} = critical temperature of component i (T).

$\overline{T}_f$ = banded submatrix composed of elements $t_{fk(k\pm1)}$ where k = 1, 2, ...N_b and (k±1) represents two values for 1-D applications and four values for 2-D (moles $L^2/F/t$).

$\overline{T}_i$ = banded submatrix composed of elements t_{ikk} and $t_{ik(k\pm1)}$ where k = 1, 2, ...N_b and (k±1) represents either two or four values (moles $L^2/F/t$).

T_{ri} = reduced temperature for component i, = T/T_{ci} (dimensionless).

$\overline{T}_w$ = banded submatrix composed of elements t_{wkk} and $t_{wk(k\pm1)}$ where k = 1, 2, ...N_b and (k±1) represents

two values for 1-D applications and four values for 2-D (moles $L^2/F/t$) .

t = time (t) .

t_D = dimensionless time, = $ut/\phi L$.

t_{fkk} = partial derivative of the overall hydrocarbon balance on block k with respect to pressure of block k appearing on the main diagonal of submatrix $\bar{T}_f$ (moles $L^2/F/t$) .

$t_{fk(k\pm1)}$ = partial derivative of the overall hydrocarbon balance on block k with respect to pressure of an adjacent grid block appearing as an off-diagonal element of submatrix $\bar{T}_f$ (moles $L^2/F/t$) .

t_{ikk} = partial derivative of the balance on component i on block k with respect to pressure of block k appearing on the main diagonal of submatrix $\bar{T}_i$ of submatrix $\bar{T}$ (moles $L^2/F/t$) .

$t_{ik(k\pm1)}$ = partial derivative of the balance on component i on block k with respect to pressure of an adjacent grid block appearing as on off-diagonal element of submatrix $\bar{T}_i$ of submatrix $\bar{T}$ (moles $L^2/F/t$) .

t_{wkk} = partial derivative of the water balance on block k with respect to pressure of block k appearing on the main diagonal of submatrix $\bar{T}_w$ (moles $L^2/F/t$) .

$t_{wk(k\pm1)}$ = partial derivative of the water balance on block k with respect to pressure of adjacent grid block appearing as an off-diagonal element of submatrix $\bar{T}_w$ (moles $L^2/F/t$) .

u_j = superficial velocity of phase j (L/t) .

V = mole fraction of hydrocarbon volume in vapor phase .

V_b = grid block bulk volume (L^3) .

V_{ci} = critical volume of component i (L^3) .

W = overall water molar concentration (moles /L^3) .

W_i = accumulation of component i (including water) in general mass balance equation (moles /L^3) .

X_D = dimensionless length , = X/L .

x_i = mole fraction of component i in oil phase.

x_{ji} = mole fraction of component i in phase j ; j = o, g .

y_i = mole fraction of component i in gas phase.

z_i = overall mole fraction of component i in the hydrocarbon phases.

Z_j = compressibility factor of phase j (dimensionless) .

α_{lj} = longitudinal dispersivity in phase j (L).

α_{tj} = transverse dispersivity in phase j (L).

α_D = dimensionless dispersivity, = α_{lj}/L or α_{tj}/L.

γ_j = specific weight of phase j (F/L^3).

δ_{ij} = binary interaction coefficients between components i and j (dimensionless).

ρ_j = mass density of phase j (mass of j $/L^3$).

ω_{ij} = mass fraction of component i in phase j (mass of i in j / mass of j).

Δt = time step (t).

ΔX = grid block length (L).

ΔY = grid block width (L).

$\vec{\nabla}$ = gradient operator (1/L).

ϵ_b = convergence tolerance on molar balances.

ϵ_K = convergence tolerance on vapor-liquid equilibrium calculations.

ϵ_s = convergence tolerance on saturation constraints.

ϵ_V = convergence tolerance on V calculations.

μ_j = viscosity of phase j ; j = w, o, g $(F \cdot T/L^2)$.

μ^* = low pressure, gas mixture viscosity $(F \cdot T/L^2)$.

ξ_j = molar density of phase j ; j = w, o g $(moles/L^3)$.

ξ_r = reduced molar density (dimensionless) .

$\xi_w{}^o$ = molar density of water at reference pressure, $P_w{}^o$ $(moles/L^3)$.

ϕ = porosity (fraction).

ϕ^o = porosity at reference pressure, $P_f{}^o$ (fraction).

Φ_j = flow potential of phase j (F/L^2).

σ = interfacial tension between oil and gas phases (F/L).

τ = tortuosity factor (dimensionless).

Superscripts :

act = actual (or output)

ℓ = iteration level

N = numerical

n = time level

o = reference state

P = physical

' = modified form

Subscripts :

D = dimensionless

g = gas

I = initial condition

i = component index

J = injection condition

j = phase index except in matrices where it is used as a second component index

k = block index

l = layer index

l = longitudinal

o = oil

r = relative

s = stationary

T = total

t = transverse

w = water

X = X-direction

Y = Y-direction

APPENDIX - A

DERIVATION OF CHAUDHARI'S EXPRESSION FOR A COMPONENT CONSERVATION EQUATION

Chaudhari neglected several terms in his derivation[C4, C5]. He mentioned that the effect of these neglected terms were usually small but it should be checked. Here, the system is more general, and, hence, more terms have to be neglected. Some of these terms probably will be important in some cases.

A.1 Time Truncation Error Treatment

Consider a conservation equation of component i in phase j (interphase mass transfer is negligible) without the dispersion term.

$$\partial/\partial t\,(\phi S_j \xi_j x_{ji}) = \partial/\partial X\,(u_{Xj} \xi_j x_{ji}) + \partial/\partial Y\,(u_{Yj} \xi_j x_{ji}) \qquad \text{(A.1-1)}$$

The discretized time derivative will be second-order correct if the second-order derivative in Eq. A.1-2 is evaluated accurately :

$$\partial/\partial t\,(\phi S_j \xi_j x_{ji}) \approx (1/\Delta t)\,[(\phi S_j \xi_j x_{ji})_k^{n+1} - (\phi S_j \xi_j x_{ji})_k^{n}] - (\Delta t/2)\,\partial^2/\partial t^2 (\phi S_j \xi_j x_{ji}) \qquad \text{(A.1-2)}$$

Differentiating Eq. A.1-1 with respect to t, X, and Y, the following

equations can be obtained :

$$\partial^2/\partial t^2\ (\phi S_j \xi_j x_{ji}) = \partial^2/\partial X \partial t\ (u_{Xj} \xi_j x_{ji}) + \partial^2/\partial Y \partial t\ (u_{Yj} \xi_j x_{ji}) \quad \text{(A.1-3)}$$

$$\partial^2/\partial X \partial t\ (\phi S_j \xi_j x_{ji}) = \partial^2/\partial X^2\ (u_{Xj} \xi_j x_{ji}) + \partial^2/\partial X \partial Y\ (u_{Yj} \xi_j x_{ji}) \quad \text{(A.1-4)}$$

$$\partial^2/\partial Y \partial t\ (\phi S_j \xi_j x_{ji}) = \partial^2/\partial X \partial Y\ (u_{Xj} \xi_j x_{ji}) + \partial^2/\partial Y^2\ (u_{Yj} \xi_j x_{ji}) \quad \text{(A.1-5)}$$

Expand these equations and neglect the derivatives of (ϕS_j), (u_{Xj}), and (u_{Yj}) :

$$(\phi S_j)\partial^2/\partial t^2\ (\xi_j x_{ji}) \approx u_{Xj} \cdot \partial^2/\partial X \partial t\ (\xi_j x_{ji}) + u_{Yj} \cdot \partial^2/\partial Y \partial t\ (\xi_j x_{ji}) \quad \text{(A.1-3')}$$

$$(\phi S_j)\partial^2/\partial X \partial t\ (\xi_j x_{ji}) \approx u_{Xj} \cdot \partial^2/\partial X^2\ (\xi_j x_{ji}) + u_{Yj} \cdot \partial^2/\partial X \partial Y\ (\xi_j x_{ji}) \quad \text{(A.1-4')}$$

$$(\phi S_j)\partial^2/\partial Y \partial t\ (\xi_j x_{ji}) \approx u_{Xj} \cdot \partial^2/\partial X \partial Y\ (\xi_j x_{ji}) + u_{Yj} \cdot \partial^2/\partial Y^2\ (\xi_j x_{ji}) \quad \text{(A.1-5')}$$

From Eqs. A.1-3' --- A.1-5', the following relationship may be derived :

$$(\phi S_j)\partial^2/\partial t^2\ (\xi_j x_{ji}) \approx u_{Xj}^2/(\phi S_j)\ \partial^2/\partial X^2\ (\xi_j x_{ji}) + 2u_{Xj}u_{Yj}/(\phi S_j)\ \partial^2/\partial X \partial Y\ (\xi_j x_{ji}) + u_{Yj}^2/(\phi S_j)\ \partial^2/\partial Y^2\ (\xi_j x_{ji}) \quad \text{(A.1-6)}$$

Substitute Eq. A.1-6 into Eq. A.1-2 (neglect again $\partial/\partial t(\phi S_j)$ in Eq. A.1-2) :

$$\partial/\partial t\,(\phi S_j \xi_j x_{ji}) \approx (1/\Delta t)\,[(\phi S_j \xi_j x_{ji})_k^{n+1} - (\phi S_j \xi_j x_{ji})_k^{n}\,]$$

$$- (\Delta t/2)\,\{\, u_{Xj}{}^2/(\phi S_j)\,\partial^2/\partial X^2\,(\xi_j x_{ji})$$

$$+ 2u_{Xj}u_{Yj}/(\phi S_j)\,\partial^2/\partial X\partial Y\,(\xi_j x_{ji}) + u_{Yj}{}^2/(\phi S_j)\,\partial^2/\partial Y^2\,(\xi_j x_{ji})\,\} \qquad \text{(A.1-2')}$$

Then, the numerical dispersion tensor due to time truncation error may be expressed as :

$$\bar{\bar{K}}_{j,time}{}^{N} = \begin{vmatrix} -(\Delta t/2)\,[u_{Xj}/(\phi S_j)]^2 & -(\Delta t/2)\,[u_{Xj}u_{Yj}/(\phi S_j)^2] \\ -(\Delta t/2)\,[u_{Xj}u_{Yj}/(\phi S_j)^2] & -(\Delta t/2)\,[u_{Yj}/(\phi S_j)]^2 \end{vmatrix} \qquad \text{(A.1-7)}$$

From the derivation descrived above, these elements should be evaluated at the block center, however, in our code, to satisfy the boundary conditions (Eq. 3.2.2-9 and 3.2.2-10) they were calculated at the block face.

A.2 Space Truncation Error Treatment

The first-order space derivative may be discretized with second-order accuracy : (assume constant grid block size and positive X-direction of flow for simplicity).

$$\partial/\partial X\,(u_{Xj}\xi_j x_{ji}) \approx (1/\Delta X)\,[(u_{Xj}\xi_j x_{ji})_{k+1/2} - (u_{Xj}\xi_j x_{ji})_{k-1/2}\,]$$

$$\approx (1/\Delta X)\,\{\,[\,(u_{Xj}\xi_j x_{ji})_k + (\Delta X/2)\,(\partial/\partial X\,(u_{Xj}\xi_j x_{ji}))_{k+1/2}]$$

$$- [\,(u_{Xj}\xi_j x_{ji})_{k-1} + (\Delta X/2)\,(\partial/\partial X\,(u_{Xj}\xi_j x_{ji}))_{k-1/2}\,]\,\}$$

$$=(1/\Delta X)\,[\,(u_{Xj}\xi_j x_{ji})_k - (u_{Xj}\xi_j x_{ji})_{k-1}]$$

$$-(1/\Delta X)\,\{(\Delta X/2)\,[\,(\partial/\partial X\,(u_{Xj}\xi_j x_{ji}))_{k+1/2} - (\partial/\partial X\,(u_{Xj}\xi_j x_{ji}))_{k-1/2}\,]\,\}$$

,neglecting $\partial u_{Xj}/\partial X$,

$$\approx (1/\Delta X)\,[\,(u_{Xj}\xi_j x_{ji})_k - (u_{Xj}\xi_j x_{ji})_{k-1}]$$

$$+ (1/\Delta X)\,\{(\Delta X/2)\,[\,(u_{Xj}\partial/\partial X(\xi_j x_{ji}))_{k+1/2} - (u_{Xj}\partial/\partial X(\xi_j x_{ji})_{k-1/2}\,]\,\}$$

(A.2-1)

The diagonal physical dispersion term (Eq. 3.1.2-1) may be written in a similar finite difference form :

$$\partial/\partial x \{\phi S_j K_{xxij} [\partial/\partial x(\xi_j x_{ji})] \}$$

$$\approx (1/\Delta x)\{ [\phi S_j K_{xxij}(\partial/\partial x(\xi_j x_{ji}))]_{k+1/2} - [\phi S_j K_{xxij}(\partial/\partial x(\xi_j x_{ji}))]_{k-1/2}\} \quad \text{(A.2-2)}$$

Comparing Eqs. A.2.-1, A.2-2, and A.1-7, it suggests that the numerical dispersion tensor will have the following form :

$$\overline{K}_j^N = \begin{vmatrix} -[u_{xj}/(2\phi S_j)][\Delta t \cdot u_{xj}/(\phi S_j) - \Delta x] & -(\Delta t/2)\cdot u_{xj}u_{yj}/(\phi S_j)^2 \\ -(\Delta t/2)\cdot u_{xj}u_{yj}/(\phi S_j)^2 & -[u_{yj}/(2\phi S_j)][\Delta t \cdot u_{yj}/(\phi S_j) - \Delta y] \end{vmatrix} \quad \text{(A.2-3)}$$

APPENDIX - B

STABILITY ANALYSIS OF CHAUDHARI'S TECHNIQUE BY THE MATRIX METHOD

Consider a convection-diffusion equation in the dimensionless form :

$$\partial C_D/\partial t_D = - \partial C_D/\partial X_D + K^P \cdot \partial^2 C_D/\partial X_D^2 \qquad (B\text{-}1)$$

Discretize Eq. B-1, using forward difference in time, backward difference for the first-order space derivative, and three-point central difference for the second-order space derivative.

$$(C_{Di}^{n+1} - C_{Di}^{n})/\Delta t_D = - (C_{Di}^{n} - C_{Di-1}^{n})/\Delta X_D + K\,(C_{Di+1}^{n} - 2C_{Di}^{n} + C_{Di-1}^{n})/\Delta X_D^2 \qquad (B\text{-}2)$$

This is the second-order correct discretization, and K is a sum of the physical dispersion coefficient K^P and the negative numerical dispersion coefficient K^N.

$$K = K^P + K^N = K^P - (\Delta X_D - \Delta t_D) / 2 \qquad (B\text{-}3)$$

Let,

$$a = \Delta t_D/\Delta X_D \ , \ b = K^P/\Delta X_D \ , \ a > 0 \ , \ b \geq 0 \qquad \text{(B-4)}$$

Substitute Eqs. B-3 and B-4 into B-2, and solve for C_{Di}^{n+1}.

$$C_{Di}^{n+1} = [(a+1)/2 + b]a \cdot C_{Di-1}^{n} + [1-(a+2b)a]C_{Di}^{n} + [(a-1)/2 + b]a \cdot C_{Di+1}^{n} \qquad \text{(B-5)}$$

This can be solved with the initial and boundary conditions :

$$C_D(X_D, 0) = 0 \ , \quad 0 < X_D < 1 \qquad \text{(B-6)}$$

$$C_D(0, t_D) = 1 \ , \quad \partial C_D/\partial X_D(1, t_D) = 0 \ , \quad t_D > 0 \qquad \text{(B-7)}$$

In a matrix form :

$$[\, C_{Di}^{n+1} \,] = [\ A \ ][\, C_{Di}^{n} \,] + [\, B \,] \qquad (i = 1 \ldots N_b) \qquad \text{(B-8)}$$

,where

$$B = [\, ((a+1)/2+b), 0 \ldots\ldots 0 \,]^T$$

$$A = \begin{pmatrix} [1-(a+2b)a] & [(a-1)/2+b]a & & & \\ [(a+1)/2+b]a & [1-(a+2b)a] & [(a-1)/2+b]a & & 0 \\ & \ddots & \ddots & \ddots & \\ & & [(a+1)/2+b]a & [1-(a+2b)a] & [(a-1)/2+b]a \\ 0 & & & (a+2b)a & [1-(a+2b)a] \end{pmatrix} \quad \text{(B-9)}$$

There are two criteria for regulating the error growth of Eq. B-8 :

1. the spectral radius condition.

$$\text{Max}|\lambda_i| \leq 1 \qquad (i = 1...N_b) \quad \text{(B-10)}$$

where λ_i is a eigenvalue of A.

2. the norm condition.

$$\| A \| \leq 1 \quad \text{(B-11)}$$

The norm condition is more severe than the spectral radius condition, and it guarantees no growth of the initial error. On the other hand, the spectral radius condition guarantees that the error becomes zero when n goes infinity, however, the error can grow significantly for finite n [S2, M6, G5].

From Gerschgorin's "circle theorem",

$$|\lambda_i - [1-(a+2b)a]| \leq |(a^2+a+2ab)/2| + |(a^2-a+2ab)/2| \quad \text{(B-12)}$$

This means that all the eigenvalues must be located in a circle whose center is $[1-(a+2b)a,\ 0]$ and radius is $[\ |(a^2+a+2ab)/2| + |(a^2-a+2ab)/2|\ ]$. If this circle is completely inside the unit circle, both conditions (Eqs. B-10 and B-11) will be satisfied, provided that the maximum norm is used.

$$\| A \|_\infty = \mathrm{Max}_i(\Sigma_j |A_{ij}|) \qquad (i,j = 1...N_b)$$

$$= |[(a+1)/2+b]a| + |1-(a+2b)a| + |[(a-1)/2+b]a| \qquad \text{(B-13)}$$

There are three cases to be checked :

1. $1-(a+2b)a \geq 0$ and $a^2-a+2ab \geq 0$ (region A in Fig. B-2)

   Then, Eq. B-10 and B-11 may be satisfied if,

   $$1-[1-(a+2b)a] \geq (a^2+a+2ab)/2 + (a^2-a+2ab)/2$$
   $$a^2+2ab \geq a^2+2ab$$

   This is always true. (Fig. B-1a)

2. $1-(a+2b)a \geq 0$ and $a^2-a+2ab < 0$ (region B in Fig. B-2)

   $$1-[1-(a+2b)a] \geq (a^2+a+2ab)/2 - (a^2-a+2ab)/2$$
   $$(a+2b)a \geq a$$
   $$a^2-a+2ab \geq 0$$

   This can't happen in this case. (Fig. B-1b)

3. $1-(a+2b)a < 0$ and $a^2-a+2ab \geq 0$ (region C in Fig. B-2)

$$[1-(a+2b)a]-(-1) \geq (a^2+a+2ab)/2 + (a^2-a+2ab)/2$$

$$2-(a+2b)a \geq (a+2b)a$$

$$1-(a+2b)a \geq 0$$

This can't happen in this case. (Fib. B-1c)

As summarized in Table B.1, only region A satisfies both conditions, hence the solution must be stable and the initial error never grows in this region. However, the main region which is required to be modeled in a EOR process may be region B, since the straight line $b = (1-a)/2$ represents the magnitude of numerical dispersion for the first-order correct finite difference scheme (forward in time and two-point backward for the first-order space derivative), and usually the level of physical dispersion is lower than this numerical dispersion. Unfortunately, as shown in Table B.1, the stability in this region is not known from Gerschgorin's theorem, but at least we can say that the initial error will grow for finite n and it can be significant [H5].

TABLE B.1

Summary of Stability Analysis

	Region (Fig. B-1)		
	A	B	C
Spectral Radius Condition	Satisfied	Unknown	Unknown
Norm Condition	Satisfied	Not Satisfied	Not Satisfied

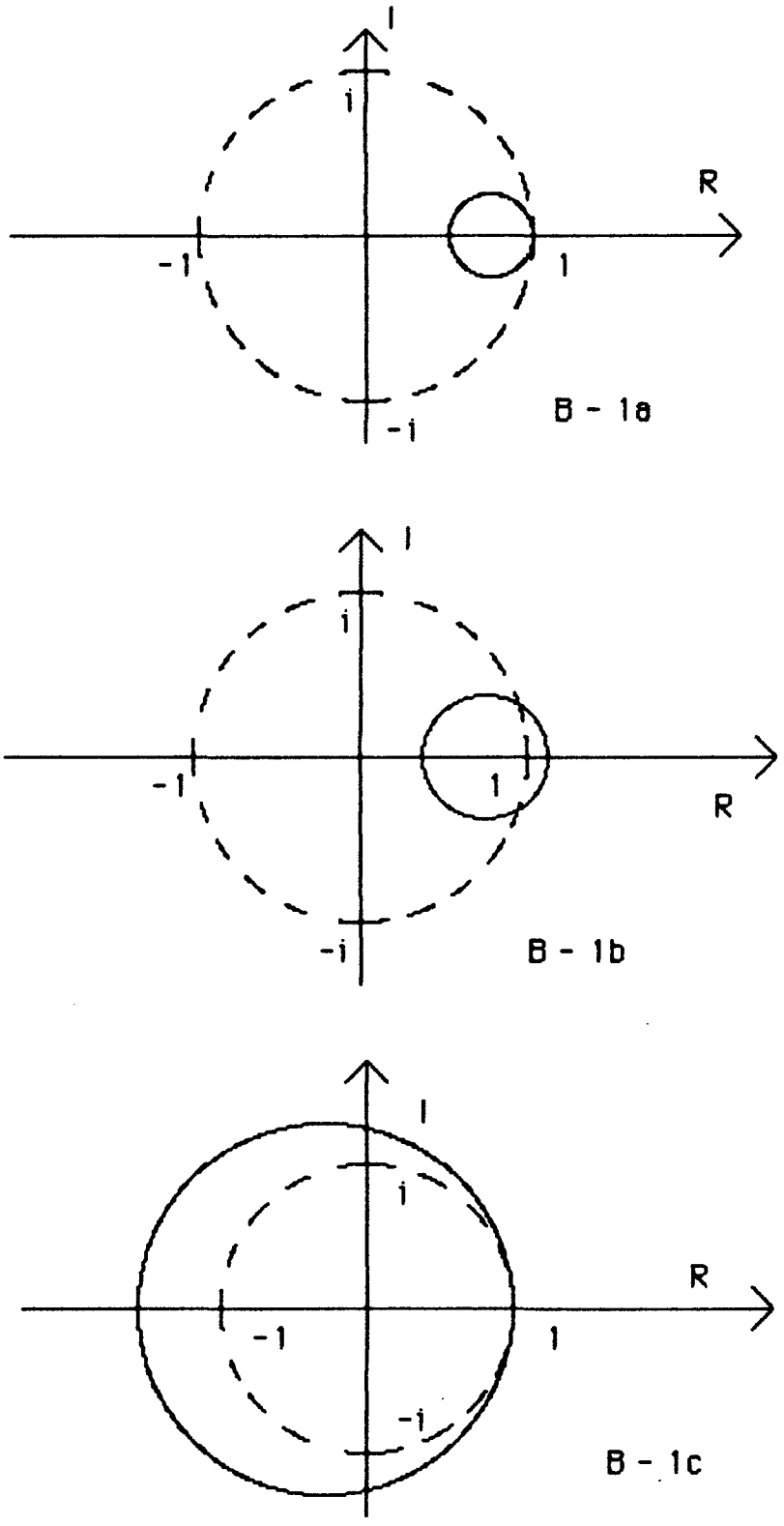

Fig. B-1 Gerschgorin's circle for three possible cases.

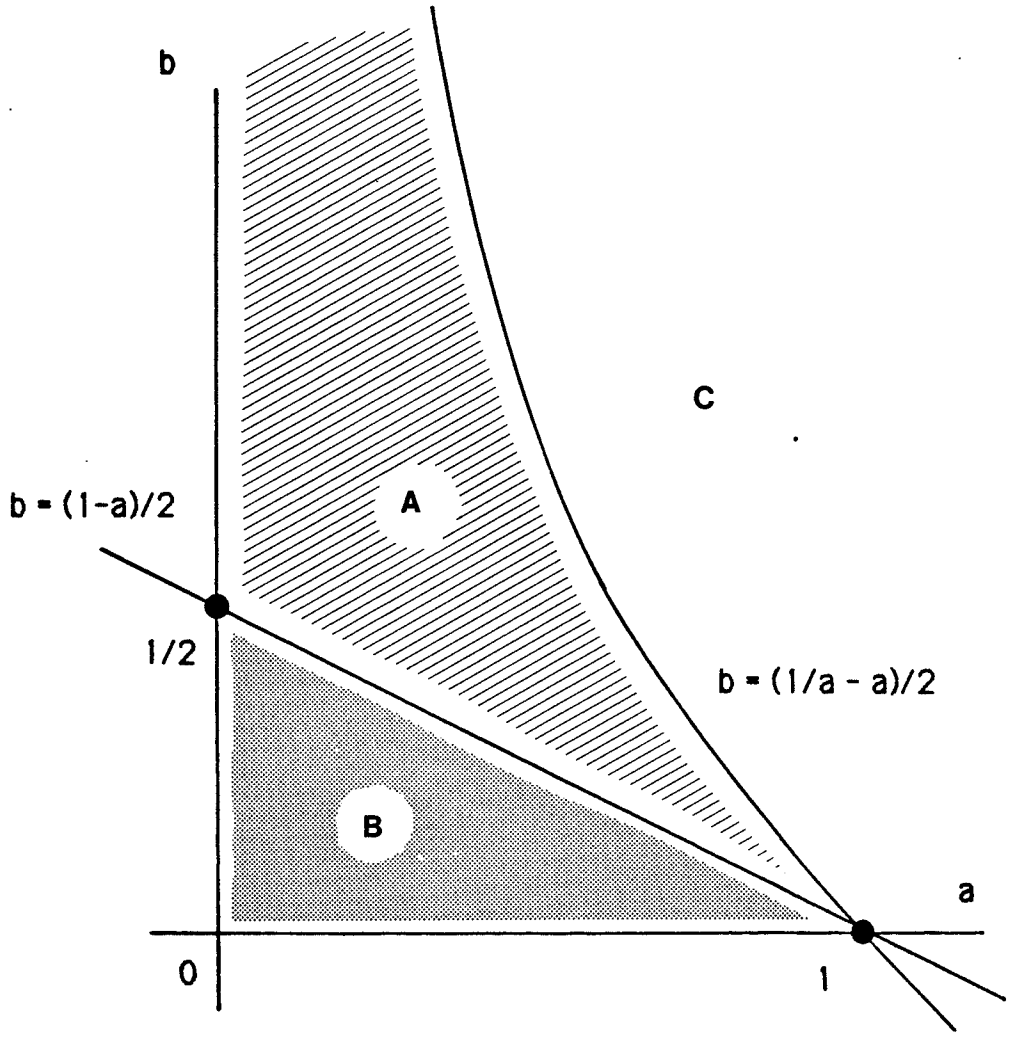

Fig. B-2 Results of stability analysis for Chaudhari's technique.

APPENDIX - C

RUN-STATISTICS AND SPECIFICATIONS FOR CLASS-1, 2, AND 3 RUNS

The reservoir data and the hydrocarbon data were already given in each sections. Here, the additional miscellaneous data, which may be required to reproduce runs, are tabulated with Run-Statistics such as CPU time, and material balance error. All runs were made by CDC Dual CYBER 170/750 machine. The following tolerances were used to check for convergence :

Equilibrium K-value

$$\Sigma_i \{ [K_i^{\ell} - K_i^{\ell-1}]^2 / (K_i^{\ell} K_i^{\ell-1}) \}_k \leq \epsilon_k$$

$$(i = 1...N_c) \quad (k = 1...N_b) \qquad (C\text{-}1)$$

Local Molar Balance

$$|R_{ci}|_k / (\Delta t \cdot \mathrm{Max}_i |q_i^{\ell+1}|) \leq \epsilon_b$$

$$(i = 1...N_c, \text{ water}) \; (k = 1...N_b) \qquad (C\text{-}2)$$

Saturation

$$|R_S|_k \leq \epsilon_S \qquad (k = 1...N_b) \quad (C\text{-}3)$$

And the global material balance errors were calculated as:

$$E_i = (W_{Ii} + N_{Ji} - N_{Pi} - W_i) / W_{Ii} \quad (i=1...N_C) \qquad (C\text{-}4)$$

,where

W_{Ii} : initial-in-place

N_{Ji} : cumulative injection

N_{Pi} : cumulative production

W_i : currently-in-place

The same items are listed for the application runs (Class-4, 5, 6) in Appendix-D.

TABLE C.1

Common Miscellaneous Informations for All Runs

(including the application runs)

: Accelerated succesive substitution was always used in the flash routine.	
: acceleration parameter	3
: ϵ_V tolerance for V calc.	10^{-10}
: ϵ_K tolerance for K-value	
initially 2 H.C. phase block	10^{-16}
elsewhere	10^{-8}
: ϵ_b tolerance for local molar balance	10^{-4}
: ϵ_S tolerance for saturation	10^{-4}
: τ tortuosity	1.0
: D_{ij} molecular diffusion coefficient	
($i=1...N_C$, j=o or g)	0.0

TABLE C.2

Informations for Class-1 Runs

q_T = 0.0016302 moles/day

P.I. = 23.9 ft^3-cp/day-psi (20 G.B.)
47.8 (40 G.B.)
95.6 (80 G.B.)

P_{bh} = 5000 psia

Run #	N_x	Δt days (frac. of 1G.B.P.V.)	t_{Max} days (DPV)	Longi. Dispersivity (ft)	Numerical Dispersion Reduction	CPU time sec per 1G.B. 1 step	CPU time sec per 1G.B. Total	Global Component M.B.E. %
1.1	20	0.4 (0.8)	4.0 (0.4)	0.0	-----	0.0075	1.5	0.137×10^{-4}
1.2	20	0.2 (0.4)	4.0 (0.4)	0.0	-----	0.0068	2.7	0.686×10^{-5}
1.3	20	0.1 (0.2)	4.0 (0.4)	0.0	-----	0.0065	5.2	0.343×10^{-5}
1.4	20	0.05 (0.1)	4.0 (0.4)	0.0	-----	0.0063	10.0	0.171×10^{-5}
1.5	40	0.025(0.1)	4.0 (0.4)	0.0	-----	0.0051	32.5	0.871×10^{-6}
1.6	80	0.0125(0.1)	4.0 (0.4)	0.0	-----	0.0045	116.2	0.439×10^{-6}
1.7	40	0.025 (0.1)	4.0 (0.4)	0.104	-----	0.0053	35.4	0.871×10^{-6}

TABLE C.2 (Continued)

Run #	N_x	Δt days (frac. of I.G.B.P.V.)	t_{Max} days (DPV)	Longi. Dispersivity (ft)	Numerical Dispersion Reduction	CPU time sec per I.G.B. 1 step	CPU time sec per I.G.B. Total	Global Component M.B.E. %
1.8	40	0.025 (0.1)	4.0 (0.4)	0.104	2-pt.*	0.0058	37.0	0.234×10^{-5}
1.9	40	0.025 (0.1)	4.0 (0.4)	0.104	Ch.**	0.0055	35.3	0.853
1.10	40	0.1 (0.4)	4.0 (0.4)	0.104	2-pt.	0.0059	9.5	0.934×10^{-5}
1.11	40	0.1 (0.4)	4.0 (0.4)	0.104	2-pt.+Ch.(t)***	0.0060	9.6	0.192
1.12 (slug)	40	0.025 (0.1)	14.0 (1.4)	0.26	-----	0.0054	121.9	0.140×10^{-5}
1.13 (slug)	40	0.025 (0.1)	14.0 (1.4)	0.26	2-pt.	0.0057	128.4	0.309×10^{-5}
1.14 (slug)	40	0.025 (0.1)	14.0 (1.4)	0.26	Ch.	0.0055	123.0	0.205
1.15	40	0.025 (0.1)	4.0 (0.4)	0.65	2-pt.	0.0057	36.7	0.234×10^{-5}
1.16	40	0.025 (0.1)	4.0 (0.4)	2.6	2-pt.	0.0057	36.7	0234×10^{-5}

TABLE C.2 (Continued)

Run *	N_x	Δt days (frac. of I.G.B.P.V.)	t_{Max} days (DPV)	Longi. Dispersivity (ft)	Numerical Dispersion Reduction	CPU time sec per I.G.B. 1 step	CPU time sec per I.G.B. Total	Global Component M.B.E. %
1.17	40	0.025 (0.1)	4.0 (0.4)	0.65	Ch.	0.0055	35.3	0.632×10^{-1}
1.18	40	0.025 (0.1)	4.0 (0.4)	2.6	Ch.	0.0055	35.4	0.604×10^{-1}

* 2-pt. upstream weighting
** Chaudhari
*** 2-pt. plus Chaudhari (time truncation cancel)

TABLE C.3

Informations for Class-2 Runs

q_T = 0.60299×10^{-3} moles/day (#2.1-2.4) (C_1:0.9, C_4:0.1)

0.90066×10^{-3} (#2.5-2.8) (0.6, 0.4)

P.I. = 47.8 ft^3-cp/day-psi

P_{bh} = 1500 psia

N_X = 40

Δt = 0.025 days (0.1 G.B.P.V.)

t_{Max} = 14.0 days (1.4 DPV)

Run#	Longitudinal Dispersivity (ft)	Numerical Dispersion Reduction	CPU time sec per 1 G.B. 1 step	CPU time sec Total	Global Component M.B.E. %
2.1	0.0	-----	0.0126	282.4	0.817×10^{-2}
2.2	0.0	C.2-pt.*	0.0129	289.3	0.238×10^{-2}
2.3	0.0	A.2-pt.**	0.0132	294.7	0.198×10^{-2}
2.4	0.0	Ch.	0.0132	-----	----------
				(stop at 0.97 DPV)	
2.5	0.0	-----	0.0230	515.6	0.580×10^{-4}

TABLE C.3 (Continued)

Run*	Longitudinal Dispersivity (ft)	Numerical Dispersion Reduction	CPU time sec per 1 G.B. 1 step	CPU time sec per 1 G.B. Total	Global Component M.B.E. %
2.6	0.0	C.2-pt.	0.0233	521.9	0.721×10^{-4}
2.7	0.0	A.2-pt.	0.0239	536.4	0.827×10^{-4}
2.9	0.0	Ch.***	0.0468	-----	----------
				(stop at 0.085 DPV)	
2.11	0.65	Ch.	0.0231	517.4	5.57

* "Composition 2-Point"
** "All 2-Point"
*** "Chaudhari"

TABLE C.4

Informations for Class-3 Runs

q_T =	1248	moles/day/well	("A" runs)
	454.89		("B" runs)
P.I. =	4.0×10^5	ft^3-cp/day-psi	
P_{bh} =	6000	psia	
N_X, N_Y =	7		(odd # runs)
	10		(even # runs)
t_{Max} =	11.76	days (1.2 DPV)	(odd # runs)
	12.0	(1.2 DPV)	(even # runs)

Run#	Δt days (frac. of 1 G.B.P.V)	Longitudinal Dispersivity (ft)	Transverse Dispersivity (ft)	Numerical Dispersion Reduction	CPU time sec per 1 G.B. 1 step	CPU time sec per 1 G.B. Total	Global Component M.B.E. %
3A.1	0.1 (0.5)	0.0	0.0	-----	0.0103	59.7	0.453×10^{-1}
3A.2	0.1 (0.5)	0.0	0.0	-----	0.0128	153.2	0.344×10^{-3}
3A.3	0.1 (0.5)	0.0	0.0	2-pt.*	0.0105	60.9	0.528×10^{-1}
3A.4	0.1 (0.5)	0.0	0.0	2-pt.	0.0129	154.3	0.109×10^{-1}

TABLE C.4 (Continued)

Run*	Δt days (frac. of 1 G.B.P.V)	Longitudinal Dispersivity (ft)	Transverse Dispersivity (ft)	Numerical Dispersion Reduction	CPU time sec per 1 G.B. 1 step	CPU time sec per 1 G.B. Total	Global Component M.B.E. %
3A.5	0.1 (0.5)	0.0	0.0	Ch.**	0.0076	-----	----------
(local molar balance tolerance=0.0, saturation tolerance=0.01, stop at 0.99 DPV)							
3A.6	0.1 (0.5)	0.0	0.0	Ch.	0.0093	-----	----------
(local molar balance tolerance=0.0, saturation tolerance=0.01, stop at 0.39 DPV)							
3A.9	0.1 (0.5)	0.0	0.0	2-pt.+Ch.(t)***	0.0112	64.9	2.09
3A.10	0.1 (0.5)	0.0	0.0	2-pt.+Ch.(t)	0.0087	104.0	2.31
3A.11	0.02 (0.1)	0.0	0.0	2-pt.	0.0098	282.0	0.176×10^{-1}
3A.12	0.02 (0.1)	0.0	0.0	2-pt.	0.0102	612.5	0.251×10^{-1}
3A.13	0.01-0.05 (0.05-0.25)	1.46	-2.54	-----	0.0106 (stop at 0.894 DPV)	-----	----------
3A.14	0.01-0.05 (0.05-0.25)	1.46	-2.54	-----	0.0117	700.5	$0.773 \times^{-1}$
3B.1	0.1 (0.5)	0.0	0.0	-----	0.0113	65.1	0.869×10^{-3}
3B.2	0.1 (0.5)	0.0	0.0	-----	0.0123	147.4	0.839×10^{-3}

* 2-pt. upstream weighting
** Chaudhari
*** 2-pt. plus Chaudhari (time truncation cancel)

APPENDIX-D

RUN-STATISTICS AND SPECIFICATIONS FOR CLASS-4, 5, AND 6 RUNS

The data listed in Table C.1 are also valid for the application runs. The "All 2-Point" scheme was used consistently for all runs except for 4K runs (the single-point scheme was used).

TABLE D.1

Informations for Class-4 Runs

P.I. = 47.8 ft^3-cp/day-psi
N_X = 40
Physical Dispersivity = 0.0 ft
t_{Max} = 9.6 days (1.2 DPV)
Δt = 0.05 days (0.2 G.B.P.V.) for 4SA, 4SK, 4SF, 4TA runs
0.0125 days (0.05 G.B.P.V.) for all other runs

	P_{bh} (psia)						
	(1)	(2)	(3)	(4)	(5)	(6)	
	1400	1600	1700	1800	2000	2400	
A,K	0.6713	0.8055	0.8761	0.9487	1.0978	1.3958	
	0.0	0.0	0.0	0.0	0.0	0.0	
B	2.2619	2.3709	2.4283	2.4872	2.6082	2.8501	
	1.7148	1.7265	1.7274	1.7282	1.7300	1.7334	
C	3.8524	3.9363	3.9804	4.0257	4.1186	4.3043	
	3.4496	3.4530	3.4547	3.4565	3.4599	3.4668	$\frac{q_T(\times 10^{-3}\text{mol/d})}{q_W(\times 10^{-3}\text{mol/d})}$
D	5.4429	5.5017	5.5326	5.5642	5.6290	5.7585	
	5.1744	5.1795	5.1821	5.1847	5.1899	5.2002	
E	7.0334	7.0671	7.0847	7.1027	7.1394	7.2128	
	6.8992	6.9061	6.9095	6.9129	6.9198	6.9336	
EF	8.2263	8.2412	8.2488	8.2565	8.2722	8.3034	
	8.1928	8.2009	8.2050	8.2091	8.2173	8.2336	
F	8.6240	8.6326	8.6369	8.6412	8.6498	8.6670	
	8.6240	8.6326	8.6369	8.6412	8.6498	8.6670	

TABLE D.1 (Continued)

Run #	CPU time sec per 1 G.B. 1 step	CPU time sec per 1 G.B. Total	Global Component M.B.E. %
4SK1	0.0176	135.1	0.119×10^{-2}
2	0.0177	135.6	0.944×10^{-3}
3	0.0186	142.8	0.866×10^{-3}
4	0.0195	149.4	0.406×10^{-3}
5	0.0143	110.0	0.163×10^{-3}
6	0.0136	104.4	0.610×10^{-3}
4SA1	0.0183	140.8	0.671×10^{-2}
2	0.0227	174.6	0.254×10^{-2}
3	0.0280	214.3	0.442×10^{-3}
4	0.0288	221.5	0.597×10^{-3}
5	0.0141	108.5	0.852×10^{-2}
6	0.0133	101.9	0.245×10^{-2}
4SB1	0.0168	514.4	0.245×10^{-2}
2	0.0177	545.0	0.528×10^{-2}
3	0.0181	555.0	0.734×10^{-2}
4	0.0182	558.8	0.573×10^{-2}
5	0.0182	559.4	0.598×10^{-2}
6	0.0104	318.3	0.265
4SC1	0.0168	514.2	0.549×10^{-4}
2	0.0178	546.0	0.378×10^{-4}
3	0.0182	559.8	0.471×10^{-4}
4	0.0185	566.5	0.757×10^{-4}
5	0.0137	420.8	0.186×10^{-2}
6	0.0106	326.6	0.231

TABLE D.1 (Continued)

Run #	CPU time sec per 1 G.B. 1 step	CPU time sec Total	Global Component M.B.E. %
4SD1	0.0159	486.9	0.774×10^{-2}
2	0.0177	544.1	0.342×10^{-4}
3	0.0184	565.3	0.119×10^{-3}
4	0.0189	581.0	0.231×10^{-3}
5	0.0137	420.0	0.151×10^{-2}
6	0.0111	340.0	0.173
4SE1	0.0110	337.3	0.858×10^{-1}
2	0.0110	337.3	0.858×10^{-1}
3	0.0177	543.4	0.135×10^{-1}
4	0.0179	549.3	0.401×10^{-2}
5	0.0138	424.0	0.643×10^{-2}
6	0.0130	399.9	0.116×10^{-1}
4SEF3	0.0170	521.3	0.199×10^{-1}
6	0.0078	238.8	0.273
4SF1	0.0079	60.8	0.797×10^{-6}
6	0.0080	61.1	0.865×10^{-6}
4TA1	0.0200	153.8	0.157×10^{-1}
2	0.0245	187.8	0.554×10^{-4}
3	0.0272	208.9	0.454×10^{-2}
4	0.0255	195.9	0.695×10^{-2}
5	0.0132	100.9	0.608×10^{-1}
6	0.0126	96.5	0.157×10^{-1}

TABLE D.1 (Continued)

Run #	CPU time sec per 1 G.B. 1 step	Total	Global Component M.B.E. %
4TB1	0.0171	524.2	0.179×10^{-1}
2	0.0175	537.4	0.831×10^{-3}
3	0.0170	523.0	0.402×10^{-1}
4(Δt=0.01d)	0.0173	664.1	0.539×10^{-1}
5	0.0126	386.5	0.249×10^{-2}
4TC1	0.0151	462.2	0.984×10^{-1}
2	0.0176	541.5	0.514×10^{-2}
3	0.0186	569.7	0.123×10^{-3}
5	0.0126	387.5	0.218×10^{-2}
4TD1	0.0150	459.7	0.483×10^{-1}
2	0.0174	535.5	0.109×10^{-1}
3	0.0182	558.1	0.107×10^{-1}
4(Δt=0.01d)	0.0178	683.5	0.290×10^{-1}
5	0.0201	615.9	0.247×10^{-1}
4TE1	0.0112	343.5	0.192
2	0.0164	504.4	0.317×10^{-1}
3	0.0175	535.8	0.181×10^{-2}
4	0.0178	546.5	0.104×10^{-1}
5	0.0125	385.3	0.912×10^{-2}
4TEF1	0.0084	256.3	0.485×10^{-1}
3	0.0109	417.1	0.407×10^{-1}
5	0.0081	248.7	0.807

TABLE D.1 (Continued)

Run #	CPU time sec per 1 G.B. 1 step	Total	Global Component M.B.E. %
4SLG1(Δt=0.01d)	0.0098	377.7	0.308×10^{-1}
2(")	0.0163	626.3	0.448×10^{-1}
3(")	0.0177	679.7	0.130×10^{-1}
4(")	0.0116	446.5	0.885×10^{-1}
5(")	0.0201	769.8	0.482×10^{-1}
6(")	0.0168	644.7	0.290×10^{-2}
7(")	0.0184	707.4	0.127×10^{-2}

TABLE D.2

Informations for Class-5 Runs

q_T = 534.275 moles/day

q_w =(chase water) 5267.0

P.I. = 1.0×10^4 ft^3-cp/day-psi

P_{bh} = 1700 psia

N_X , N_Y = 7

Δt = 0.01 - 0.001 days (0.05 - 0.005 G.B.P.V.)

t_{Max} = 9.8 days (1.25 DPV)

Run*	Slug Size(DPV)	Longi. Dispersivity (ft)	Transe. Dispersivity (ft)	CPU time sec per 1 G.B. 1 step	CPU time sec per 1 G.B. Total	Global Component M.B.E.%
5.1	0.2	0.0	0.0	0.0250	2778.5	0.375×10^{-3}
5.2	0.2	5.0	0.5	0.0172	828.9	0.272×10^{-4}
5.3	0.2	0.1	0.01	0.0236	2623.0	0.275×10^{-3}
5.5	continuous	0.1	0.01	0.0303	1454.4	0.313×10^{-4}
5.6	0.3	0.1	0.01	0.0260	2869.9	0.222×10^{-4}
5.7	waterflood	0.1	0.01	0.0090	432.3	0.784×10^{-4}

TABLE D.3

Informations for Class-6 Runs

q_T =	134.67	moles/day
q_w(chase water)	1316.9	
P.I. and I.I.	1.582×10^2	ft^3-cp/day-psi (layer 1,2)
	3.164×10^1	(layer 3,4)
Δt =	0.001 - 0.005	days (0.01 - 0.05 G.B.P.V.)
t_{Max} =	7.68	days (1.2 DPV)

Run#	Slug Size(DPV)	Longi. Dispersivity (ft)	Transe. Dispersivity (ft)	CPU time sec per 1 G.B. 1 step	CPU time sec per 1 G.B. Total	Global Component M.B.E.%
6.1	0.2	0.1	0.01	0.0250	4339.0	0.107×10^{-7}
6.3	0.2	5.0	0.05	0.0199	2441.5	0.148×10^{-7}
6.4	waterflood	0.1	0.01	0.0152	1862.2	0.369×10^{-7}

REFERENCES

[A1] Alston,R.B., Kokolis,G.P., and James,C.F, :"CO_2 Minimum Miscibility Pressure : A Correlation for Impure CO_2 Streams and Live Oil Systems", Soc. Pet Eng. J. (April 1985)

[A2] Aziz,K, and Settari,A, :"Petroleum Reservoir Simulation", Applied Science Publishers Ltd. London (1979)

[B1] Baker,L.E., :"Effects of Dispersion and Dead-End Pore Volume in Miscible Flooding", Soc. Pet. Eng. J. (June 1977)

[B2] Bear,J., :"Dynamics of Fluids in Porous Media", American Elsevier Publishing Co. Inc., Newyork (1972)

[B3] Benham,A.L., Dowden,W.E., and Kunzman,W.J., :"Miscible Fluid Displacement - Prediction of Miscibility", Trans. AIME Vol.219 pp229-237 (1960)

[B4] Bird,R.B., Stewart,W.E., and Lightfoot,E.N., :"Transport Phenomena", John Wiley & Sons, Inc. (1960)

[C1] Cere,A., and Zanotti,F.,:"Sharpening Behavior and Dispersion in a Chemical Flooding", 3rd European Meeting on Improved Oil Recovery, Rome, Italy, Vol.2 pp249 (April 1985)

[C2] Chase,Jr.C.A., and Todd,M.R., :"Numerical Simulation of CO_2 Flood Performance", SPE 10514, 6th Reservoir Simulation Symposium, New Orleans (1982)

[C3] Chappelear,J.E., and Williamson,A.S., :"Representing Wells in Numerical Reservoir Simulator : Part 2 - Implementation", Soc. Pet. Eng. J. (June 1981)

[C4] Chaudhari,N.M., :"An Improved Numerical Technique for Solving Multidimensional Miscible Displacement Equation", Soc. Pet. Eng. J. (Sep. 1971)

[C5] Chaudhari,N.M, :"A Numerical Solution with Second-Order Accuracy for Multicomponent Compressible Stable Miscible Flow", Soc. Pet. Eng. J. (April 1973)

[C6] Chien,M.C.H., :"A New Fully Implicit Compositional Simulator", SPE 13385, 9th Reservoir Simulation Symposium, Dallas (1985)

[C7] Coats,K.H., and Smith,B.D., :"Dead-End Pore Volume and Dispersion in Porous Media", Soc. Pet. Eng. J. (June 1964)

[C8] Coats,K.H., George,W.D., and Marcum,B.E., :"Three Dimensional Simulation of Steamflooding", Trans AIME Vol.257 pp573-592 (1974)

[C9] Coats,K.H., :"An Equation of State Compositional Model", Soc. Pet. Eng. J. (Oct. 1980)

[D1] Dai,K.K., and Orr,Jr.F.M., :"Prediction of CO_2 Flood Performance : Interaction of Phase Behavior with Microscopic Pore Structure Heterogeneity", SPE 13115, 59th Annual Fall Meeting, Houston (1984)

[E1] Ewing,R.E.(Editor), :"The Mathematics of Reservoir Simulation", Frontiers in Applied Mathematics Series, SIAM Philadelphia (1983)

[F1] Fanchi,J.R., :"Multidimensional Numerical Dispersion", Soc. Pet. Eng. J. (Feb. 1983)

[F2] Fayers,F.J., and Matthews,J.D., :"Evaluation of Normalized Stone's Methods for Estimating Three-Phase Relative Permeability", Soc. Pet. Eng. J. (April 1984)

[F3] Fried,J.J., :"Ground Water Pollution", Developments in Water Science 4, Elsevier

[G1] Gardner,W.J., Orr,Jr.F.M, and Patel,P.D., :"The Effect of Phase

Behavior on CO_2-Flood Displacement Efficiency", J. Pet. Tech. (Nov. 1981)

[G2] Giordano,R.M., and Salter,S.J., :"Comparison of Simulation and Experiments for Compositionally Well-Defined Corefloods", SPE/DOE 12697, 4th Enhanced Oil Recovery Symposium, Tulsa (1984)

[G3] Giordano,R.M., and Salter,S.J., :"The Effects of Dispersion and Phase Behavior on Unfavorable Mobility Ratio Displacements", SPE 13165, 59th Annual Fall Meeting, Houston (1984)

[G4] Goggin,D.J., :"Development of a Moving Grid Point Method for the Solution of Multicomponent, Mutiphase Flow Problem in One Dimension", M.S. Thesis, The University of Texas at Austin (1984)

[G5] Griffith,D.F., Christie,I., and Mitchell,A.R. :"Analysis of Error Growth for Explicit Difference Schemes in Conduction-Convection Problems", International Journal for Numerical Methods in Engineering, Vol.15 pp1075-1081 (1980)

[H1] Helfferich,F.G., :"Theory of Multicomponent, Multiphase Displacement in Porous Media", Soc. Pet. Eng. J. (Feb. 1981)

[H2] Hirasaki,G.J., and O'Dell,P.M., :"Representation of Reservoir Geometry for Numerical Simulation", Trans. AIME Vol.249 pp393-404 (1970)

[H3] Holm,L.W., and Josendal,V.A., :"Mechanisms of Oil Displacement by Carbone Dioxide", J. Pet. Tech. (Dec. 1974)

[H4] Holm,L.W., and Josendal,V.A., :"Effect of Oil Composition on Miscible-Type Displacement by Carbone Dioxide", Soc. Pet. Eng. J. (Feb. 1982)

[H5] Hong,C.H., :"Development of a 2-D Micellar/Polymer Simulator", Ph.D. Dissertation, The University of Texas at Austin (1981)

[J1] Jensen,O.K., :"A Numerical Technique for Tracking Sharp Fronts in Studies of Tertiary Oil Recovery Pilots", SPE 12240, 7th Reservoir Simulation Symposium, San Francisco (1983)

[K1] Klins,M.A., :"Carbon Dioxide Flooding : Basic Mechanisms and Project Design", IHRDC Boston (1984)

[K2] Kuniansky,J., and Hillestad,J.G., :"Reservoir Simulation Using Bottom-Hole Pressure Boundary Conditions", Soc. Pet. Eng. J. (Dec. 1980)

[L1] Lake,L.W., and Pope,G.A., :"Enhanced Oil REcovery", publication work still in progress.

[L2] Lake,L.W., Pope,G.A., Carey,G.F., and Sepehrnoori,K., :"Isothermal, Multiphase, Multicomponent Fluid-Flow in Permeable Media Part 1 : Description and Mathematical Formulation", Center for Enhanced Oil and Gas recovery Research, The University of Texas at Austin (1980)

[L3] Lake,L.w., and Hirasaki,G.J., :"Taylor's Dispersion in Stratified Porous Media", Soc. Pet. Eng. J. (Aug. 1981)

[L4] Lantz,R.B., :"Quantitative Evaluation of Numerical Diffusion", Soc. Pet. Eng. J. (Sep. 1971)

[L5] Larson,R.G., :"Controlling Numerical Dispersion by Variably Timed Flux Updating in One Dimension", Soc. Pet. Eng. J. (June 1982)

[L6] Larson,R.G., :"Controlling Numerical Dispersion by Variably Timed Flux Updating in Two Dimension", Soc. Pet. Eng. J. (June 1982)

[L7] Laumbach,D.D., :"A High-Accuracy Finite-Difference Technique for Treating the Convection-Diffusion Equation", Soc. Pet. Eng. J. (Dec. 1975)

[L8] Li,K.M.G., :"Random Choice Method for Treating the Convection-Diffusion Equation", SPE 12237, 7th Reservoir Simulation Symposium, San Francisco (1983)

[L9] Lin,E.C., :"A Study of Micellar/Polymer Flooding Using a Compositional Simulator", Ph.D. Dissertation, The University of Texas at Austin (Dec. 1981)

[L10] Lohrentz,J., Bray,B.G., and Clark,C.R., :"Caluculating Viscosities of Reservoir Fluids from Their Compositions", J. Pet. Tech. (Oct. 1964)

[M1] Mehra,R.K., Heidemann,R.A., and Aziz,K., :"An Accelerrated Successive Substitution Algorithm", The Canadian Journal of Chemical Engineering (Aug. 1983)

[M2] Metcalfe,R.S., and Yarborough,L., :"The Effect of Phase Equilibria on the CO_2 Displacement Mechanism", Soc. Pet. Eng. J. (Aug. 1979)

[M3] Mitchell,A.R., and Griffiths,D.F., :"The Finite Difference Method in Partial Differential Equations", John Wiley & Sons Ltd. (1980)

[M4] Mohanty,K.K., and Salter,S.J., :"Multiphase Flow in Porous Media : II Pore-Level Modeling", SPE 11018, 57th Annual Fall Meeting, New Orleans (1982)

[M5] Mohanty,K.K., and Salter,S.J., :"Multiphase Flow in Porous Media : III Oil Mobilization, Transverse Dispersion and Wettability', SPE 12127, 58th Annual Fall Meeting, San Francisco (1983)

[M6] Morton,K.W., :"Stability of Finite Difference Approximations to a Diffusion-Convection Equation", International Journal for Numerical Methods in Engineering, Vol.15 pp677-683 (1980)

[N1] Naiki,M., :"Numerical Simulation of Polymer Flooding Including the Effects of Salinity", Ph.D. Dissertation, The University of Texas at Austin (1979)

[N2] Nghiem,L.X., Fong,D.K., and Aziz,K., :"Compositional Modeling with an Equation of State", Soc. Pet. Eng. J. (Dec. 1981)

[N3] Nghiem,L.X., Aziz,K., and Li,Y.K., :"A Robust Iterative Method for Flash Calculation Using the Soave-Redlich-Kwong or Peng-Robinson Equation of State", Soc. Pet. Eng. J. (June 1983)

[N4] Nolen,J.S., and Berry,D.W., :"Tests of the Stability and Time-Step Sensitivity of Semi-Implicit Reservoir Simulation Technique", Trans. AIME Vol.253 pp253-266 (1972)

[O1] Orr,Jr.F.M, and Taber,J.J., :"Displacement of Oil by Carbon Dioxide", Prepared for the U.S. Department of Energy, Under Contract No. DE-AS19-80BC10331 (1984)

[P1] Peng,D.Y., and Robinson,D.B., :"A New Two-Constant Equation of State", Ind. Eng. Chem. Fund. Vol.15 pp59-64 (1976)

[P2] Perkins,T.K., and Johnston,O.C., :"A Review of Diffusion and Dispersion in Porous Media", Soc. Pet. Eng. J. (March 1963)

[P3] Ply,J.K., :"A Comparison of Iterative and Direct Methods in Compositional and Geopressured Geothermal Simulators", M.S. Thesis, The University of Texas at Austin (1984)

[P4] Pozzi,A.L., and Blackwell,R.J., :"Design of Laboratory Models for Study of Miscible Displacement", Trans. AIME Vol.228 pp28-40 (1963)

[R1] Reid,R.C., Prausnitz,J.M, and Sherwood,T.K., :"The Property of Gases and Liquids", 3rd Edition, McGraw-Hill Book Co., Newyork (1977)

[R2] Robertson,G.E., and Woo,P.T., :"Grid Orientation Effects and the Use of Orthogonal Curvilinear Coordinate in Reservoir Simulation", SPE 6100, 51st Annual Fall Meeting, New Orleans (1976)

[R3] Rood,J.D., :"A Comparison of Iterative Methods for Compositional Simulators on Scalar and Vector Computers", M.S. Thesis, The University of Texas at Austin (1985)

[S1] Salter,S.J., and Mohanty,K.K., :"Multiphase Flow in Porous Media : I Macroscopic Observation", SPE 11017, 57th Annual Fall Meeting, New Orleans (1982)

[S2] Siemieniuch,J.L., and Gladwell,I., :"Analysis of Explicit Difference Methods for a Diffusion-Convection Equation", International Journal for Numerical Methods in Engineering, Vol.12 pp899-916 (1978)

[S3] Stalkup,Jr.F.I., :"Miscible Displacement", SPE Monograph Vol.8 (1983)

[T1] Thele,K.J., :"A Comparison of Three Equation of State Compositional Simulators", M.S. Thesis, The University of Texas at Austin (1984)

[T2] Thomas,G.W., :"Principles of Hydrocarbon Reservoir Simulation", 2nd Edition, IHRDC Boston (1982)

[T3] Tiffin,D.L., and Yellig,W.F., :"Effects of Mobile Water on Multiple Contact Miscible Gas Displacement", SPE/DOE 10687, 3rd Enhanced Oil Recovery Symposium, Tulsa (1982)

[T4] Todd,M.R., O'Dell,P.M., and Hirasaki,G.J., :"Methods for Increased Accuracy in Numerical Reservoir Simulators", Soc. Pet. Eng. J. (Dec. 1972)

[W1] Williamson,A.S., and Chappelear,J.E., :"Representing Wells in Numerical Reservoir Simulator : Part 1 - Theory", Soc. Pet. Eng. J. (June 1981)

[Y1] Yanosik,J.L., and McCracken,T.A., :"A Nine-Point,Finite Difference Reservoir Simulator for Realistic Prediction of Adverse Mobility Ratio Displacements", Soc. Pet. Eng. J. (Aug. 1979)

[Y2] Yellig,W.F., :"Determination and Prediction of CO_2 Minimum Miscibility Pressures", J. Pet. Tech. (Jan. 1980)

[Y3] Yokoyama,Y., :"The Effects of Capillary Pressure on Immiscible Displacement in Stratified Porous Media", M.S. Thesis, The University of Texas at Austin (1981)

[Y4] Young,L.C., :"A Finite-Element Method for Reservoir Simulation", Soc. Pet. Eng. J. (Feb. 1981)

[Y5] Young,L.C., and Stephenson,R.E., :"A Generalized Compositional Approach for Reservoir Simulation", Soc. Pet. Eng. J. (Oct.1983)

VITA

Hideaki Takeda was born in Tokyo, Japan, on October 11, 1955, the first son of Tokuichi Takeda and Tazuko Takeda. After receiving a Bachelor of Science degree in Petroleum Engineering in 1979 from the University of Tokyo, Tokyo, Japan, he has been working for Teikoku Oil Co., Ltd. In September, 1983, he entered the Graduate School of the University of Texas at Austin to pursue his Master of Science degree in Petroleum Engineering.

Permanent Adress: 1499-24, Ninomiya, Akigawa-shi, Tokyo, Japan

This thesis was typed by the author himself.